MACROMOLECULAR STRUCTURE OF SISAL FIBER AND ITS POTENTIAL APPLICATIONS

Thesis submitted in partial fulfillment of the requirements for the degree of

DOCTOR OF PHILOSOPHY

In

Physics

By

Annapurna Patra

Under the guidance of

Prof. Dillip Kumar Bisoyi

DEPARTMENT OF PHYSICS
NATIONAL INSTITUTE OF TECHNOLOGY
ROURKELA, ODISHA, INDIA-769008

November-2012

Dedicated to

My Loving Family

DECLARATION

I certify that

a. The work contained in the thesis is original and has been done by myself under the general supervision of my supervisor.

b. The work has not been submitted to any other Institute/University for any degree or diploma.

c. I have conformed to the norms and guidelines given in the Ethical Code of Conduct of the Institute.

d. Whenever I have used materials (data, theoretical analysis, and text) from other sources, I have given due credit to them by citing them in the text of the thesis and giving their details in the references.

(Annapurna Patra)

Signature of the Student

CERTIFICATE

This is to certify that the thesis entitled **"Macromolecular structure of sisal fiber and its potential applications"**, submitted by Annapurna Patra to the National Institute of Technology, Rourkela is a record of bonafide research work, carried out by her under my direct supervision and in my opinion, the work fulfills the requirements for which it is being submitted. The contents of the thesis, in full or in parts, have not been submitted to any other Institute or University for the award of any degree.

(Signature of Supervisor)

Dr. Dillip K. Bisoyi
Associate Professor,
Department of Physics,
National Institute of Technology,
Rourkela-769008

ACKNOWLEDGEMENTS

I am highly pleased to express my gratitude to my honorable academic supervisor Dr. Dillip Kumar Bisoyi, Dept. of Physics, NIT Rourkela, Rourkela for his generous guidance, help and useful suggestions.

I express my sincere gratitude to Dr. A.K. Singh, DMRL, Hyderabad, Dr. Pawan Kumar, Dept. of Physics NIT Rourkela, Prof K.C. Patel, Dept. of Chemistry NIT Rourkela for rendering SAXS, LCR meter and FTIR facility respectively in their laboratory for which I could complete major part of my research work.

I am sincerely thankful to Dr. Md. N. Khan for his valuable guidance and useful suggestion on analysis of SAXS data.

Profound appreciation and gratitude is extended to one and all the members of the Department of Physics, NIT Rourkela for their kind cooperation during progress of my research work.

I am grateful to Prof S K Sarangi, Director, NIT Rourkela for allowing me to utilize the computer and other relevant facilities available in the Institute in general and Physics Department in particular.

I must thank Dr. Sitangshu Sarkar, Scientist-in-Charge, Sisal Research Station (ICAR), Bamra, Orissa(INDIA) for his kind cooperation for providing us the sisal fibre for this study.

I am extremely grateful to my DSC members Prof S. Jena, Prof D. Behera, Prof B.C. ray, Prof S. K. Sahu for their insightful comments and constructive suggestions to improve the quality of this research work.

I am especially thankful to Prof B.C. ray for introducing me in the field of fiber reinforced composite and constantly keeps me motivating since my master degree.

I am grateful to Fair & lovely foundation for women studies (2010), Jawaharlal Nehru fellowship for Doctoral studies (2011-13) and CSIR SRF fellowship (2012-14) for part funding and timely support during progress of my research work.

I am thankful to Mr. Barun Kumar Barick, Mr. Prakash Palei, Mr. Biswantha Bhoi, Mrs. Arpita Das, Ms. Sagrika Pashayat, for their valuable suggestion, discussion and help at every step of my research work.

Finally, I am forever indebted to my family members for their understanding and encouragement when it was most required.

ABSTRACT

Among all the natural fibers, sisal is widely used as yarns, ropes, twines, carpets etc. because of its high cellulose content and tensile strength. Several researches have been conducted on this fiber and it is found to be more suitable for the reinforcement applications in polymer composites because of its superior properties such as, low density, high specific strength, environment friendly nature and low cost. As it is the fiber extracted from leaves of a drought resistant plant hence, it can easily be commercially exploited. However, the hydrophilic nature of the fiber hinders its application in the composite field due to the lack of compatibility between hydrophilic fiber and hydrophobic thermosetting matrix. The present study focuses on various surface treatment methods on the sisal fiber to enhance the adhesion, compatibility between the fiber and the matrix in order to improve the mechanical strength as well as electrical properties of the composite for attracting industrial interests for its potential use. Macromolecular structural parameters are evaluated to know the effect of modification on the fiber properties.

Various surface modifications such as Dewaxing, $KMnO_4$, Microwave and Alkali treatments were conducted on the sisal fiber. For dewaxing, the fiber were immerged in ethanol and benzene solution for 12 hr with 2 hr of intermediate heating and cooling of solution in which fibers were soaked. For $KMnO_4$ treatment, the dewaxed fibers were soaked in 0.01%, 0.05% and 0.1% concentered $KMnO_4$ –acetone solution for 1, 2 and 3 mins. Physical modification of the fiber was done by

microwave irradiation at 160W, 320W, 640W for 2, 4 and 8 mins. Alkali treatment on the fiber was carried out for 2hrs at 2%, 4%, 6% and 8% NaOH concentrations. The soaking period of fiber in 6% NaOH solution was varied from 2 hr to 8 hr with a step of 2hr.

The short sisal fiber reinforced polymer composites were fabricated for different fiber volume percentage (5, 10, 15 and 20 %) by hand layup technique. The composite having 15% fiber volume fraction was found to have better mechanical strength and lower loss tangent in comparison to others. Hence, 15% volume fraction of the fiber was kept constant for the fabrication of all composites in the entire study.

Small angle X-ray scattering (SAXS) of the treated fiber showed the change in macromolecular parameters in comparison to the untreated fiber. The enhancement of the macromolecular structural parameters like average periodicity transverse to the layer, volume fraction of matter phase etc. and the reduction of disorderliness of the structure at nano order were observed in each treatment for a particular combination of concentration, soaking period, irradiation power and duration of treatment.

Density of the fibers was determined by Archimedes' principle and varied after the various treatments. It was observed that the density of the surface modified fiber was higher than the untreated one at the optimum condition, which may be due to the removal of natural wax and impurities present in the fiber.

For $KMnO_4$ and Alkali treatment, the observed increment in the structural parameters like periodicity transverse to the layers, volume fraction of matter phase,

transversal length etc. at macromolecular level along with the degree of crystallinity of the fiber may be due to the partial removal and reduction of hemicelluloses, lignin, pectin, wax etc. Microwave irradiation helps in reduction of residual stress in the fiber leading to the increased value of crystallinity of the fiber, confirmed from the XRD studies of the fiber.

Surface roughness of the fiber was achieved after almost all the treatments at optimum treatment condition. It was ascribed to the removal of surface impurities like natural wax, lignin, hemicelluloses and removal of internal constraint from the fiber. Degradation of the fiber was confirmed from the SEM micrograph at higher level of concentration, duration of chemical treatments and irradiation power of microwave.

FTIR study of the fiber helps to assess the structural changes of the fiber by change in absorbed intensity ratio of the different functional groups. The reduction of OH group, hemicellulose was observed for the fiber modified by suitable treatment parameters.

Improved flexural strength and tensile strength was observed after all the treatment at optimized condition. Better wetting of the fiber with the matrix was due to enhanced surface roughness of the fiber as observed in SEM micrographs of the fractured surface of the composites. This may be the possible cause of the improved mechanical strength of the fiber. Degradation of the mechanical strength of the composite was ascribed to the reinforcement of degraded fiber and poor adhesion between fiber and matrix.

Electrical study of the short sisal fiber reinforced epoxy composite revealed that the loss tangent and dielectric constant of the composite were reduced for the suitably modified fiber reinforced composite. However, significant increase in loss tangent for the composite reinforced with degraded fiber was observed. The modulus formalism had been adopted to study the relaxation mechanism in the composite. The advantage of complex electric modulus formalism is that it suppresses the electrode effect. The shifting of relaxation peaks in the temperature dependent modulus plot confirmed the presence of temperature dependent relaxation process in the material.

Key words: Sisal fiber, Composites, Dewaxing, $KMnO_4$, Microwave, Alkali treatment, SAXS, XRD, FTIR, INSTRON 1195, Macromolecule, Dielectric, Tensile strength, Flexural strength.

CONTENTS

List of Figures

CHAPTER-4

CHAPTER-5

CHAPTER-6

CHAPTER-7

List of Tables

LIST OF SYMBOLS AND ABBREVIATIONS

NFRPC	Natrual fiber reinforced Polymer Composite
UT	Untreated Fiber/Raw Fiber
DE	Dewaxed Fiber
UTC	Untreated sisal Fiber reinforced Composite
DEC	Dewaxed sisal Fiber reinforced Composite
KFREC	Potassium permanganate treated sisal Fiber reinforced Composite
MT	Microwaved Treated Fiber
MFREC	Microwave treated sisal Fiber reinforced Composite
ALKC	Alkali treated sisal Fiber reinforced Composite
D	Periodicity Transverse to the layer
$\bar{l}_1$	Transversal length to the matter phase
$\bar{l}_2$	Transversal length to the void Phase
$\bar{l}_r$	Range of inhomogeneity
R	Corrugation at the Phase boundary
E_r	Width of transition layer by Ruland Method
E_v	Width of transition layer by Vonk Method
ε_r	Dielectric Constant
tanδ	Dielectric Loss
RT	Room temperature
SAXS	Small angle X –ray Scattering
XRD	X-ray diffraction
SEM	Scanning Electron Microscope
FTIR	Fourier transform Spectroscopy

Chapter 1

Introduction

1.1 Preamble

The recent environmental concerns on the use of fossil based fibers have resulted in the intensive research in property characteristics of natural fibers with the view of replacing energy intensive synthetic fibers particularly in the composite manufacture [1-3]. Natural fiber reinforced composites are gaining substantial attention as a form of potential application of natural fibers in various field. Natural fiber is defined as the renewable fiber either from plant or animal source that can be transformed into yarn [4]. From ancient time history some of the natural fibers have been exclusively harvested for textile industry like cotton, silk, wool. But from last few decades the scenario has been changed. There are five main points to choose natural fiber over the synthetic fiber [5].

- Healthy choice: Natural fiber creates ventilation through a process called wicking which absorbs perspiration and releases into air. The bends and

wink in natural fiber act as a natural insulator. But the compact molecular structure of synthetic fiber is not having natural ventilation.

- Responsible choice: Its production is generating self-employment through microenterprises. It is acting as nonfood source for the developing countries like India, Pakistan, Bangladesh, Tanzania etc for its economic development.
- Sustainable choice: It is helping in emerging green economy. These are carbon neutral and 100% biodegradable [6].
- High-tech choice: The low density, high specific strength excellent thermal and acoustic insulation, easy processing, environment friendly nature, low cost and light weight have made natural fiber reinforced polymer composite (NFRPC) a smart material with versatile applications in different areas like in automobiles, aerospace, injection molded products, coatings, adhesives, fire-retardants, packaging materials, consumer goods etc. Because of the superior mechanical strength and low density, the particle board made out of it is half the weight of wood board. Growing shortage of wood also favors the natural fiber industry [7, 8].
- Fashionable choice: Natural fiber is emerging as industry because many designers are promoting 100% carbon neutral textile yet soothing and comfortable.

Natural fibers are widely investigated for its tremendous potential applications. The study of NFRPC materials is a fast growing area of research. This rapidly expanding field is generating many exciting new high-performance materials with

novel properties. Lower density of the cellulose-based fibers leads to weight savings in composite manufacture with direct advantages on transportation. The use of plant fibers compared to those of the fossil fuel based reinforcements will result in significant material cost savings as plant fibers are cheaper than the matrices [9]. However, research on the property optimization must continue to compete with the well-established glass and carbon reinforcements, with the substantial cuts in the expenditure in defense and aerospace programs. Therefore because of the tremendous potential use of the natural fiber UN had declared the year 2009 as "The international year of Natural fiber" to facilitate the research and development on this regard. Some multinational companies are re-orienting their product range from high cost and high performance composites towards more environmentally friendly, less energy intensive and lower cost plant fiber reinforced composites. In this regard sisal has attracted good response**.**

1.2 Literature Survey

Sisal (Agave Sisalana) belongs to the Agave Family, a plant group which produces long leaves of 1.2 -1.5 m from which the commercial fibers are extracted. It is the hardest fiber after Manila as far as durability and strength is concerned [10]. Unlike jute, Sisal does not require much water. It is a drought resistance crop and is most commonly used for more practical products e.g. for cordage, rope, mat etc. because of its strength, durability, ability to stretch and its resistance to deterioration in salt water. Among all the natural fibers, sisal fiber in chopped, continuous, and woven forms has been found to be most suitable for application in polymer

composites because of its superior properties like high cellulose content, high tensile strength, and yet cheaper in price [11]. Sisal fiber reinforced polymer composites have high impact strength besides having moderate tensile and flexural properties compared to other lignocellulosics fiber reinforced polymer composites [12]. Table 1.1 shows the comparative illustration of mechanical properties of sisal fiber along with some other natural and synthetic reinforcing fiber. From Table 1.1, it is clear that sisal is having good mechanical strength compare to other natural fiber and lower in density than synthetic fibers like glass and carbon etc. So sisal possesses a good specific strength. Therefore it has attracted attention of scientist of fundamental research and industrialist for energy intensive, durable and biodegradable product either by directly using the fiber itself or reinforcing it in polymer, cements etc. for varied applications.

Table 1.1: Comparison of various physical parameters of natural and synthetic fibers [13].

Fiber	Density (g/cc)	Diameter (μm)	Tensile strength (MPa)	Youngs Modulous (Gpa)	Elongation at break (%)
Jute	1.3-1.5	20-200	393-773	13 -26.5	7-8
Flax	1.5-3	-	45-1100	27.6	2.7-3.2
Hemp	-	-	690	-	1.6
Ramie	1.5	-	400-938	61.4-128	1.2-3.8
Sisal	1.45	50-200	468-640	9.4-22	1.2-3.8
Cotton	1.5-1.6	287-800	-	5.5-12.6	7-8
Coir	1.15-1.6	100-145	131-175	4-6	15-40
E-glass	2.5	-	2000-3500	70	2.5
Carbon	1.7	-	4000	230-240	1.4-1.8

Sisal exhibits high electrical resistance in addition of being thermally and acoustically insulating. Sisal wall covering meets the abrasion and tearing resistance standards of the American Society for Testing and Materials and of the National Fire Protection Association [14]. It can therefore be expected that when these fibers are incorporated in low modulus polymer matrices; they would yield materials with better structural and electrical properties and having higher thermal resistance [15, 16].

According to Lie et al. [17] sisal is the best additive to the asphalter, mixture to improve the antislide performance for the pavement surface. Behera et al. [18] studied the sisal fiber for pulping and paper making and found it suitable for paper making than the rag fiber because of it higher mechanical strength. It also acts as strength giving additive for week and recycled pulp. Hence the study of mechanical properties is important in order to evaluate the strength of the composite and the factors governing it.

Physical and mechanical properties of plant fibers differ from one type to another leading to differences in end use performance. There is a strong relationship between the fine structure of sisal fibers and their mechanical properties. The structure of the fiber has been investigated by several researchers. Such understanding of structure property relationship will not only help to open up new avenues for this fiber but also emphasizes the importance of the agricultural material which forms one of the abundantly available renewable resource in the world. Sisal

fiber is not having fairly uniform dimension. It consists of primary cell wall, secondary cell wall, tertiary cell wall and central hollow lumen as shown in Fig. 1.1. All the cell walls are made of fibrils. The fibrils in the primary wall are arranged in 40^0 from the central longitudinal axis whereas secondary and tertiary wall are 18^0-25^0 from the longitudinal axis. The fibrils which are actually made of micro fibrils are arranged parallel in the tertiary cell wall. The central hollow lumen acts as a sound insulator. These micro fibrils are made up of cellulose chains [19].

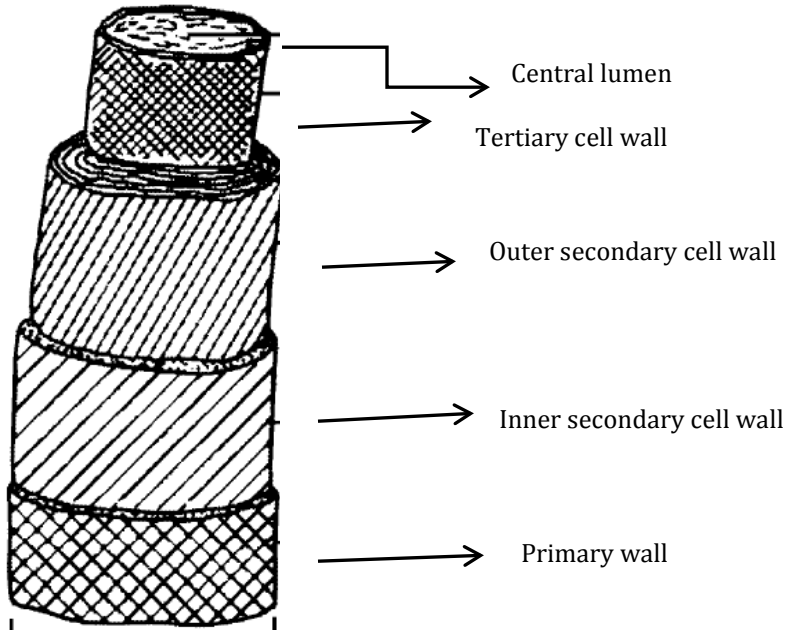

Fig. 1.1: Arrangements of cell walls in Sisal fiber [19].

The composition of the external surface of the cell wall is a layer of lignocellulose material and waxy substances which bond the cell to its adjacent neighbors. Hence, this surface will not form a strong bond with a polymer matrix [20]. Sisal consists of numerous fiber cells which are linked to each other by middle

lamella. Sisal comprises of cellulose (65%), hemicellulose (20%) lignin and waxes (12%), ash (2%), others (1%) [9].

Cellulose, is a linear polymer consisting of 1,4 β-bonded anhydroglucose units having hydroxyl groups which form hydrogen bonds inside the macromolecule itself and between other cellulosic macromolecule as well as with hydroxyl groups from the air. This leads to the hydophilicity of the fiber.

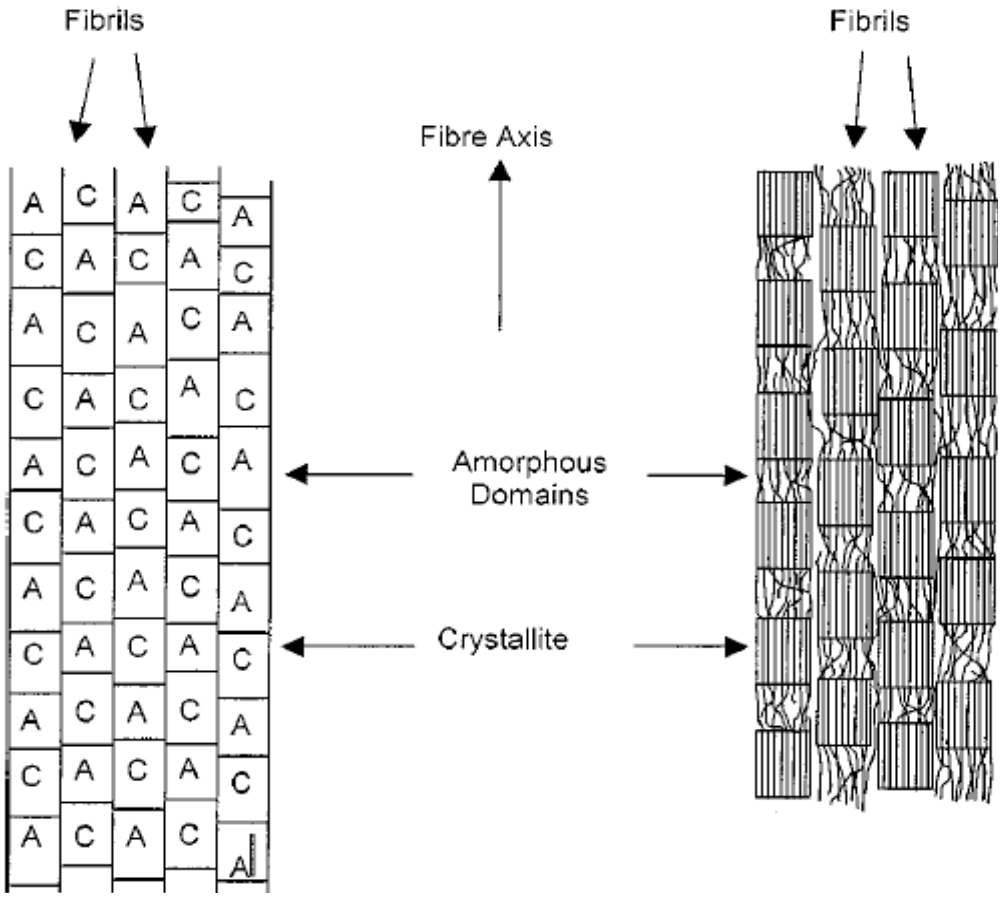

Fig. 1.2: Schematic diagram of (a) the modified series model, (b) possible physical structure of a semi-crystalline cellulose fiber [22].

The moisture content reaches 8%-13% in sisal fiber. So lack of good adhesion, poor resistance to moisture absorption make the use of sisal fiber reinforced composite less attractive [21]. Though cellulose is not crystalline, the micro crystalline structure of high order cellulose produces crystalline region where as low order produces amorphous region. The crystalline region is water insoluble. It provides mechanical strength to the fiber. Fig.1.2 shows the schematic diagram of the crystalline and amorphous arrangement inside the fiber.

Fig.1.3 demonstrates the arrangement of cellulose, hemicellulose and lignin inside the fiber. Inside the fiber cellulose is embedded in matrix of hemicellulose and lignin. It is surrounded by a layer of hemicellulose. In the cell walls the parallel cellulose chains bind together by hydrogen bonds to form micro-fibrils with several nanometers in diameter and millimeter in length.

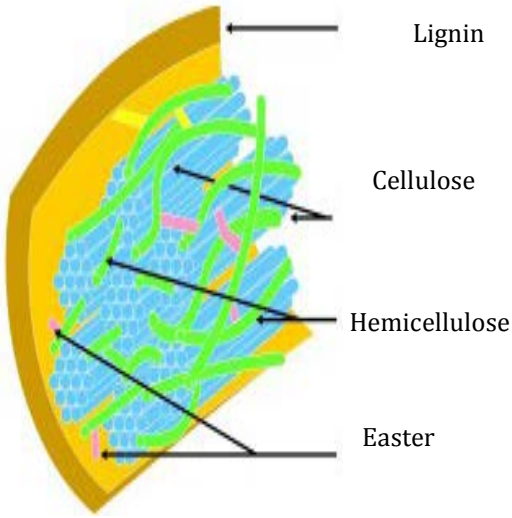

Fig. 1.3: Arrangements of cellulose, hemicellulose and lignin inside the fiber [23].

Table 1.2 summarizes the state and functions of different constituents of the fiber. In the cell walls the parallel cellulose chains bind together by hydrogen bonds to form micro-fibrils with several nanometers in diameter and millimeter in length. These high tensile strength crystalline micro-fibrils are bonded by gel matrix composed by hemicelluloses, lignin and other carbohydrate polymers to form a bio-composite [24]. It is known that that the arrangement and orientation of cellulose micro fibrils in the cell wall has significant effect on the fiber property.

Hemicellulose is highly branched polymer with many sugar units. Its degree of polymerization is much lower than cellulose. It gives a protective sheath to the cellulose and is water soluble.

Table-1.2: State and functions of different constituents of the fiber [25].

Content	**Polymer state**	**Molecular Derivative**	**Function**
Cellulose	Crystalline highly oriented large molecule	Glucose	fiber
Hemicellulose	Semi crystalline smaller molecules	Galactose	Matrix
Lignin	Amorphous large3D molecules	Phenyl propane	Matrix
Extractives	Some polymeric, Others non - polymeric	e.g Terepentes, Polyphenols	Extraneous

Lignin is a polymer containing phenolic groups. It gives the structural support to the fiber by holding the fibrils together. It gives stiffness to the cell wall and provides protective barrier for cellulose [25]. It also influences the structure property, flexibility, hydrolysis rate. Pectin is hetropolyschacharide, provides flexibility to the plant. Wax makes up the last part of the fibers and they consist of different type of alcohols.

The chemical structure of the sisal fiber is well known. However many question on the detail of the super structure still remains open. Even the experimental data growing in literature, there are still many unclear problems of native cellulose super molecular structure due to its variation in origin of cell types and plants. To understand the composition, composition distribution as well as inner surface between different compositions of fibers can absolutely shed some light on preparing man made composite. From the fundamental point of view the deformation of cellulosic fiber is not well understood [26]. This is due to inadequate testing regimes. The compatibility of the fibers and the matrix can also be manipulated if the structural information about the fiber is properly investigated. It is assumed that micro fibrils growing in the cell wall have to push their way through the existing components leading to a number of structural defects which may arise from dislocations at the interface of micro crystalline domains along the micro fibril length. The modification of the fibers by chemical treatment is one of the large areas of research where numbers of researchers are currently investigating to improve the compatibility between fiber and matrix [12]. The modification of the fiber can either

increase or decrease the strength of the fibers and thus an understanding of the structure is paramount [27]. In cellulosic plant fiber cellulose being major constituent remains as a semi crystalline material with both crystalline and amorphous regions whereas void remains across the lamellar cellulosic semi crystals. The macromolecular structure of the plant fibers is hence related with this semi crystalline and void distribution of the glucose chains. These structure can be well understood by evaluating macromolecular parameters like the periodicity transverse to the layer, volume fraction of matter(both crystalline and amorphous phases)and void phase, the transverse length, range of heterogeneity, width of transition layer, the length of coherence, specific surface. These parameters give insight to understand the structure of cellulosic plant fiber and are evaluated using small angle x-ray scattering (SAXS) theory based on the non-ideal two phase structure where the two phases are matter and void [28, 29].

The lignocellulosic fibers show high electrical resistance. As for as mechanical properties are concerned these fibers enhance the mechanical strength of low modulus polymer when reinforced in it. Therefore it also gives the mechanical support to the field carrying conductors. Now a days these natural fiber reinforced polymer composite have been successfully commercialized as insulator, switch boards, terminals, plugs, printed circuit board. In order to improve the mechanical strength of the composite many surface modification of the fibers are proposed. The electrical properties also get affected with these modifications. The electrical properties of the composite greatly depend on the fiber loading, chemical

modification of the fiber, adhesion with the matrix etc. Patania et al. [30] has done a detail review in this regard. Insulation resistance and dielectric strength of lignocellulosic fibers give an indication of their current leakages at certain voltages, moisture content and stability under electric fields [31]. Recently composite as dielectrics are becoming more popular and studies of electrical properties of NFRPC are therefore very important. So keeping in view of the increasing demand of the natural fiber composite in structural and electrical applications, electrical study of the composite is really necessary. Hence many experiments and studies have been conducted on the electrical properties of the natural fibers as well as the natural fiber reinforced composites. The studies of electrical properties of such materials enable us to know the various electrical applications of these materials to attract industrial interest [32, 33]. Natural fiber being biopolymer acts as important segments of dielectric. The dielectric property of polymer depends on the mechanical and thermal properties of the fiber textile [34]. The relaxation processes in natural fiber composite have been studied by many researchers [35, 36]. The relaxation process generally occur in fiber are α, β, γ, δ in order of increasing frequency. As the temperature raised the mobility of the molecules increased making the dipole orientation easier. The relaxation process observed in the natural fiber composite depends on the following factor.

- Primary chain motion of the polymeric chain causing α relaxation
- Side chain motion of the polymeric chain causing β relaxation

- At low temperature the movement of small units of main or side chain is responsible for γ relaxation
- The interface of the non-homogeneous material like fiber and matrix interface also lead to a kind of relaxation known as Maxwell -Wagner relaxation. This interface also acts as charge carrier generation [37].

The electrical properties in terms of dielectric constant, loss, ac conductivity gives a new dimension to find out the polymer structure and its response to different modification, loading etc. The enhancement in the dielectric constant is observed in the well-known adhesive insulator epoxy when mineral filler were added to it [38]. Chand et al. [39] found out the sisal fiber epoxy exhibit electrical anisotropy behavior which means the properties of the composite depends upon the alignment of the fiber in the composite. Dielectric characteristic of sisal–oil palm hybrid bio-fiber reinforced rubber composite found to be suitable in antistatic application when the fibers were undergone through silane treatment. It is due to the increase the retainment of the electrical charge over longer period [40]. The dewaxed sisal fiber reinforced polyester composite is also found to have good antistatic properties [36]. Effects of surface treatment on the electrical properties of the sisal fiber low density polyethylene composite were studied by Paul et al. [41]. Significant change in the dielectric properties, volume resistivity of composite are found to be changed in all the treatment. Higher values of $KMnO_4$ concentration lead to the degradation of cellulose inside the fiber resulting in the formation of more polar groups. This leads to the enhancement of the dielectric constant of the composite [29]. Increase in the

moisture content lead to increase in the conductivity of the matrix [30]. Addition of optimized value of carbon black lead to good antistatic behavior of sisal low density polyetlene composite is also confirmed from the electrical studies [41]. So in order to evaluate the potential applications of the natural fiber composites in specific field electrical characterization is a must. So the present thesis also gives importance on the electrical properties of the sisal fiber composite.

1.3 Surface modification of sisal fiber

Natural fibers are hydrophilic in nature so as sisal fibers, as they are derived from lignocelluloses, which contains strongly polarized hydroxyl groups. The surface of the sisal fiber is coated with waxy substances and having lower surface tension. The major limitations of using these fibers as reinforcements in polymer matrices include poor interfacial adhesion between polar-hydrophilic fiber and non-polar hydrophobic matrix that lead to the poor wetting of fiber with the matrix and lower bond strength. This in turn led to the composites with weak interface. The bond strength can be improved by following operations [8]:

(a) Dissolving the fatty substances and the layer of cuticle from the fiber.

(b) Making the fiber hydrophobic by reacting with some reagents.

(c) Increasing the compatibility of the fiber with the resin by grafting it with some suitable polymers.

(d) Removal of trap air from the resin-fibre mixture by degassing it before cure.

So in order to enhance the compatibility and bond strength of the fiber with its matrix, surface modification of the fiber is essential [42-44]. In this context research has been conducted by several scientists [45, 46]. Surface modifications include

- Chemical modifications.
- Physical treatments, like the use of microwave or any other high energy radiation.

Among various chemical treatment, alkali treatment or mercerization is an old and commercially exploited treatment for improving the texture and softness of the textile fibers [47]. The effect of alkali on cellulose fiber is a swelling reaction, during which the natural crystalline structure of the cellulose relaxes. Native cellulose (i.e. cellulose as it occurs in nature) shows a monoclinic crystalline lattice of cellulose-I, which can be changed into different polymorphous forms through chemical or thermal treatments. The important forms are alkali-cellulose and cellulose-II. The alkali solution influences not only the cellulosic components inside the plant fiber but also the non-cellulosic components (hemicelluloses, lignin and pectin). The type of alkali (KOH, LiOH, NaOH) and its concentration will influence the degree of swelling and hence degree of lattice transformation into cellulose II, which is more stable than Cellulose I. [44].

Permanganate treated fibers improve the tensile strength by increasing the coherence with matrix [48]. Among the various chemical modifications, the $KMnO_4$

treatment on the fiber is known to be very effective in improving the bonding at the interface [13]. $KMnO_4$ is a strong oxidizing agent. George et al. [49] studied the effect of $KMnO_4$ treatment on the pineapple leaf fiber reinforced polyethylene composites and noticed the improvement in the mechanical properties after the treatment. $KMnO_4$ treated banana fiber proved to be responsible for the higher thermal stability due to cellulose-manganet [50].

Heat treatment also influences the structure of the fibers hence its impact on reinforcing efficiency of fiber in the matrix is also important [51]. The ability of certain materials to convert microwaves into heat makes these materials suitable for microwave processing. In microwave heating, the material will absorb microwave energy and then convert it into heat. In recent years many materials are dried and modified under microwave irradiations [52]. Study on the possibility in the reduction of dying time using micro oven dying technique are done by many researchers [53, 54]. Xue et al. [55] have studied the structural and physical properties of microwave irradiated wool fabric. They have found that microwave heating is more efficient than conventional heating. Silk degumming using microwave irradiation was done by Mahmoodi et al. [56]. Their finding supports the potential production of new environment friendly textile fibers using microwave. Microwave irradiation is also found to be suitable on joining of green composite [57].

1.4 Selection of Matrix

Low cost composites are successfully fabricated by reinforcing the natural fiber with the many thermoset hydrophobic matrixes like polyester, phenolic, epoxies. The role of matrix in the composite is to transfer the stress in to the fiber, prevent the fiber-fiber interaction, keeps the position of the fiber intact in the composite to form a stable structure, prevent the fiber from the abrasions. Epoxy resin is found to outperform other resins in mechanical properties, resistance to environmental degradation which leads to their almost exclusive use in air craft. The advantages of using epoxy are

- Cure from 5^0 to 15^0C depending upon the curing agent.
- Low shrinkage during cure
- High electrical insulation
- Good chemical resistance
- High water resistance
- High thermal properties

Epoxy resin is made up of long chain molecular structure with reactive site at the either ends. The absence of ester groups in epoxy is good for water resistance properties. The epoxy group contains two ring groups at its center which are able to absorb both mechanical and thermal shock than the linear groups. Therefore epoxy has good stiffness, toughness and heat resistance [58].

Hence epoxy resin is chosen as the matrix element for the sisal fiber reinforced polymer composite in the present study.

1.5 Problem addressed

From the above literature survey, it is found that the sisal fiber reinforced polymer composites have high impact strength besides having moderate tensile and flexural properties compared to other lignocelluloses fibers and yet cheaper in price. But it suffers from inherent hydrophilicity which does not make it compatible with the hydrophobic polymeric matrix. Therefore, in order to enhance the compatibility of the sisal fiber with its matrix better structural analysis of the fiber is paramount. Modification of the sisal fiber is essential to improve the compatibility between fiber and matrix either physically or chemically in order to get composite with desired properties.

1.6 Proposed modification of the fiber

Following treatments are chosen for the modifications of the sisal fiber in order to enhance the compatibility of sisal fiber with the hydrophobic epoxy matrix.

- Dewaxing
- Permanganate treatment
- Pre-treatment of fiber by high energy microwave radiation
- Alkali treatment

1.7 Main objective

- Study of macromolecular parameters of the untreated and treated sisal fiber to understand the structure and its role in affecting the properties of composite.
- Optimization of the modification process of fiber for its potential use by improving the compatibility between sisal fiber and its matrix.
- Explore the science at the interface between fiber and its matrix.
- Electrical study of the sisal fiber reinforced composite to know its response at various frequency and temperature.
- Studies of Complex Impedance and Modulus spectroscopy.
- Correlation of the structural parameters of the fiber with the electrical and mechanical properties of the composites.

In order to investigate the macromolecular structure of fiber, semi crystalline phase, surface of the fiber, modified structure of the fiber, mechanical and electrical properties of the sisal reinforced composite the following characterizations are performed:

- Macromolecular structure of the raw and modified fiber analysis by SAXS.
- Crystallographic parameters determination by XRD analysis.
- Surface morphology of the fiber and composites by SEM.
- Vibrational studies of the fiber by FTIR.
- Mechanical properties of the composites by 3 pt bending test & tensile test.
- Electrical study of the composite by LCR meter.

References

1. Lopez JP, Mutje P, Peleach MA, Mansouri NEE, Boufi S, Vilaseca F, Analysis of the tensile modulus of polypropylene composites reinforced with stone ground wood fibers. Bio Res, 7, (2012) 1310 -1323.
2. Habibi Y, Zawawyab WKEI, Ibrahimb MM, Dufrense A, Processing and characterization of reinforced polyethylene composites made with lignocellulosic fibers from Egyptian agro-industrial residues. Compos Sci Technol, 68, (2008) 1877-1885.
3. Rahman R, Huue M, Island N, Hasan M, Mechanical properties of polypropylene composites reinforced with chemically treated abaca. Compos Part A –Appl Sci, 40, (2009) 511-517.
4. Environmental benefits of natural fibre production and use. *Jan E.G. van,* Discover natural fibres (Proceedings Of The Symposium On Natural Fibres, Rome, 2008) 56, (2009) 3-17
5. Rijswijk K, Brouwer WD, Beukers A, Application of Natural Fibre Composites in the Development of Rural Societies. (2001).
6. Kalia S, Averous L, Njuguna J, Dufresne A, Cherian BM, Cellulose-Based Bio- and Nanocomposites: A Review. Int J Polym Sci, 2011, (2011) 837-875, doi:10.1155/2011/735932.
7. Shah A N, Lakkad S C, Mechanical properties of jute-reinforced plastics. Fibre Sci Technol, 15, (1981) 41-46.
8. Bisanda E T N, Ansell M P, The effect of saline treatment on the mechanical and physical properties of sisal–epoxy composites. J Compos Sci Techol, 41, (1991) 165 –178.
9. Jayaraman K, Manufacturing sisal-polypropylene composites with minimum fibre degradation. Compos Sci Technol, 63, (2003) 367-374.
10. Weindling L, Long vegetable fibres, University Press, New York: Columbia (1947).

11. Mylsamy K, Rajendran I, Influence of alkali treatment and fibre length on mechanical properties of short Agave fibre reinforced epoxy composites. Mater Des, 32, (2011) 4629–4640.
12. Ganan P, Garbizu S, Liano P, Rodrigo M, Surface modification of sisal fibers: Effects on the mechanical and thermal properties of their epoxy composites. Polym Compos, 26, (2005) 121-127.
13. Kalia S, Kaith B S, Kaur I, Pretreatments of natural fibers and their application as reinforcing material in polymer composites—A review. Polym Engg Sci, 49, (2009) 1253-1272.
14. Chandramohan D, Marimuthu K, Analysis of cutting forces and temperature during turning of materials with different hardness values. Int J Mater Sci, 5, (2010) 399-409.
15. Joseph K, T.Filho RD, James B, Thomas S, Carvalho L H D, A Review on Sisal Fiber Reinforced Polymer Composites. Revista Brasileira de Engenharia Agrícola e Ambiental, 3, (1999) 367-379.
16. Bledzki A K, Gassan J, Composites reinforced with cellulose based fibres. Prog Polym Sci, 24, (1999) 221-274.
17. Lie X, He X, Guan P, Deng P, Effect of Sisal Fiber on Anti-Slide Performance for Asphalt Pavement Surface. Am Soc Civil Engg, 125, (2012) 1310-1319.
18. Behera S, Sahu S, Patel S, Mishra BK, sisal fiber: potential raw material for handmade paper. Ippta, 24, (2012) 37-43.
19. Gram H E, Durability of Natural Fibres in Concrete, Swedish Cement and Concrete Research Institute, 1, (1983) 225-230.
20. Li Y, Mai Y W, Ye L, Sisal fiber and its composites: a review of recent developments. Compos Sci Technol, 60, (2000) 2037-2055.
21. Thew M M, Liao K, Effects of environmental aging on the mechanical properties of bamboo-glass fiber reinforced polymer matrix hybrid composites. Compos Part A: Appl Sci Manuf, 33, (2002) 43-52.
22. Eichhorn S J, BailliE C A, ZafeiropouloS N, Mwaikambo L Y, Ansell M P, Entwistle K M, Herrera-franco P J, Escamilla G C, Groom L, Hughes M, Hill C, Rials T G, Wild P

M, Review: Current international research into cellulosic fibres and composites. J Mater Sci, 36, (2001) 2107–2131.

23. Morrison L, Second-generation biofuels may offer a way forward. 31 Oct 08, http://www.engineeringnews.co.za
24. Sain M, Anthapulkka S P, Green fibre thermoplastic composites, chapter 9, University of Toronto, Canada, (2004) 181 -206.
25. Dinwoodie JM, Timber - its nature and behavior, 1st Edn. Van No strand Reinhold Company, New York, (1981)114-136.
26. Martins MA, Forato LA, Colnago LA, Mattoso LHC, A solid state C-13 high resolution NMR study of raw and chemically treated sisal fibers. Carbohydr. Polym, 64, (2006) 127- 133.
27. Mu Q, Wei C, Feng S, Studies on mechanical properties of sisal fiber/phenol formaldehyde resin in-situ composites. Polym Compos, 30, (2009) 131-137.
28. Mishra T, Bisoyi DK, Patel T, Patra KC, Patel A, Small Angle X-Ray Study of Cellulose in Cotton Using Correlation Functions. Polym J, 20, (1988) 739-749.
29. .the potassium permanganate treated short sisal fiber reinforced epoxy composite in correlation to the macromolecular structure of the reinforced fiber. J Appl Polym Sci, (2012), doi: 10.1002/app.38195.
30. Pathania D, Singh D, A review on electrical properties of fibre reinforced polymer composites. Int J Theor Appl Sci, 1, (2009) 34-37.
31. Kulkarni AG, Satyanarayana K G, Rohtagi P K, Electrical resistivity and dielectric strength of plant fibres. J Mater Sci Lett, 16, (1981) 1719-1726.
32. Dutta AK, Mukherjee PS, Mitra CB, A dielectric study of cellulose fibres. J Mater Sci, 15, (1980) 1856-1860.
33. Patra A, Bisoyi DK, Dielectric and impedance spectroscopy studies on sisal fiber-reinforced polyester composite. J Mater Sci, 45, (2010) 5742–5748.
34. Bal K, Kothari V K, Measurement of dielectric properties of textile materials and their applications. Int J Fiber Text Res, 35, (2009) 191-199.
35. Amor I B, Rekik H, kaddami H, Raihane M, Arous M, Kallel A, Studies of dielectric relaxation in natural fiber-polymer composites. J Electrostat, 67, (2009) 717–722.

36. Patra A, Bisoyi DK, Investigation of the electrical and mechanical properties of short sisal fiber-reinforced epoxy composite in correlation with structural parameters of the reinforced fiber. J Mater Sci, 46, (2011) 7206-7213.
37. Ghallabi Z, Rekik H, Boufi S, Arous M, Kallel A, Effect of the interface treatment on the dielectric behavior of composite materials of unsaturated polyester reinforced by Alfa fiber. J Non-Cryst Sol, 356, (2010) 684–687.
38. Wu SL, Tung IC, Dielectric studies of mineral-filled epoxy. Poym Compos, 16, (1995) 233-239.
39. Chand N, Jain D, Effect of sisal fiber orientation on electrical properties of sisal fiber reinforced epoxy composites. Compos part A, 36, (2005) 594-602.
40. Jacob M, Varughese KT, Thomas S, Dielectric characteristics of sisal–oil palm hybrid biofibre reinforced natural rubber biocomposites. J Mater Sci, 41, (2006) 5538-5547.
41. Paul A, Joseph K, Thomas S, Effect of surface treatments on the electrical properties of low-density polyethylene composites reinforced with short sisal fibers. Compos Sci Technol, 57, (1997) 67- 79.
42. Li Y, Mai YW, Ye L, Effects of fibre surface treatment on the fracture- mechanical properties of sisal-fibre composites. Compos Interfaces, 12, (2005) 141-163.
43. Li Y, Mai Y W, Interfacial characteristics of sisal fiber and polymeric matrices. J Adhes, 82, (2006) 527-554.
44. John K, Naidu SV, Effect of Fiber Content and Fiber Treatment on Flexural Properties of Sisal Fiber/Glass Fiber Hybrid Composites. J Reinforced Plast Compos, 23, (2004) 1601- 1605.
45. Jacob JM, Rajesh A, Recent developments in chemical modification and characterization of natural fiber-reinforced composites. Polym Compos, 29, (2008) 187-207.
46. Zafeiropoulos NE, Baillie CA, Hodgkinson JM, The Effect of Surface Treatment on the Interface. Compos Part A, 33, (2002) 185-1190.
47. Berger PB, Hoven TV, Ramaswamy G N, Kimmel L, Boylston E, Cotton/Kenaf Fabrics: a Viable Natural Fabric. J Cotton Sci, 3, (1999) 60-70.

48. Song JH, Kim Y, Mechanical Properties of Sisal Fiber Reinforced Composites on Surface Treatment and Temperature. J Kor Inst Met Mater, 46, (2008) 471-476.
49. George J, Bhagawan S, Thomas S, Fiber stress analysis in short fiber reinforced composites by means of laser Raman spectroscopy. Compos. Interface, 5, (1998) 201-223.
50. Paul A, Oommen C, Joseph K, Thomas S, The role of interface modification on thermal degradation and crystallization behavior of composites from commingled polypropylene fiber and banana fiber. Polym Compos, 31, (2010) 1113–1123.
51. Manikandanr KC, Thomas S, Groeninckx G, Thermal and dynamic mechanical analysis of polystyrene composites reinforced with short sisal fibres. Compos. Sci. Technol, 61, (2001) 2519-2529.
52. Microwave Processing Of Materials, Washington D.C., National Academy Press, 1994.
53. Murugan R, Senthilkumar M, Ramachandran T. Study on the possibility in the reduction of dying time using micro oven dying technique. J Inst Eng India Inst Eng (India), Part TX: Text Eng Div 87, (2007) 23–27.
54. Li JP, Lin HF, Zhao WF, Chen GH, Instant modification of graphite nanosheets by the grafting of a styrene oligomer under microwave radiation. J Appl Polym Sci, 109, (2008) 1377–1380.
55. Xue Z, Xin HJ, Effect of microwave irradiation on the physical properties and structures of wool fabric. J Appl Polym Sci, 119, (2011) 944–952.
56. Mahmoodi NM, Moghimi F, Arami M, Mazaheri F, Silk degumming using microwave irradiation as an environmentally friendly surface modification method. Fiber Polym, 11, (2010) 234–240.
57. Singh I, Bajpai KP, Malik D, Sharma AK, Kumar P, Feasibility study on microwave joining of 'green'composites. Akademeia, 1, (2011) 1–6.
58. Dogra RK, Sharma AK. Advances in material science, SK Katria publisher, Second edition, (2000) 505-537.

Chapter 2

Experimental Techniques

2.1. Materials

Sisal fibers were obtained from the Sisal Research Station, Indian Council of Agricultural Research, Bamara, Odisha, India having diameter of (170-300) μm. The fibers were extracted from 8 year old Sisal plants' leaves by decortication process. The color of the fiber was pale white and each fiber length varied from 1 meter to 1.5 meters. Fig 2.1 shows the sisal fibers collected from the sisal research station.

Fig.2.1: Sisal fiber collected from the sisal research station.

Unmodified liquid epoxy resin based on Bisphenol A, of grade LY 556 along with hardener HY 951 was provided by B.Mukesh & Co., Kolkata, India. The density of the resin was 1.15 g/cc, whereas the hardener density was 0.97g/cc. The hardener content was kept at a ratio of 1:10 as compare to resin to suit the curing and processing condition. Due to low shrinkage rate the LY 556 /HY 951 gives dimensionally stable laminates with excellent water resistance.

2.2. Modifications of the fiber

2.2.1. Dewaxing

As received fibers were washed with distilled water to remove the surface dirt present in the fibers and then they were dried in an air circulating oven at a temperature of 100°C until it gains a constant weight. Then the fibers are designated as raw sisal fibers or untreated fiber (UT).

For dewaxing the fibers were cooked in a mixture of (1:2) ethanol and benzene, as done earlier by Roy [1], for 12 hrs so that it attains a hohlraum character which, means the substances lying in layers with free spaces in between [2]. During this process the fibers were cooked in the solution under gradual rise and fall of the temperature of the bath from 30°C to 55.5°C. This process of heating and cooling was done intermittently per every 2 hrs for a period of 12 hrs. Finally the fiber bundles were removed from the mixture at a temperature of 30°C. In order to remove excess mixture, the fibers were washed with distilled water. After washing, the fibers were again dried in an air circulating oven at a temperature of 100°C until it gained

constant weight. Then the fibers were designated as dewaxed sisal fibers (DE). The composite fabricated from the reinforcement of untreated and dewaxed fiber were named as untreated sisal fiber reinforced composite(UTC) and dewaxed sisal fiber reinforced epoxy composite (DEC) respectively. The method for fabrication of the composite is described in section 2.3.

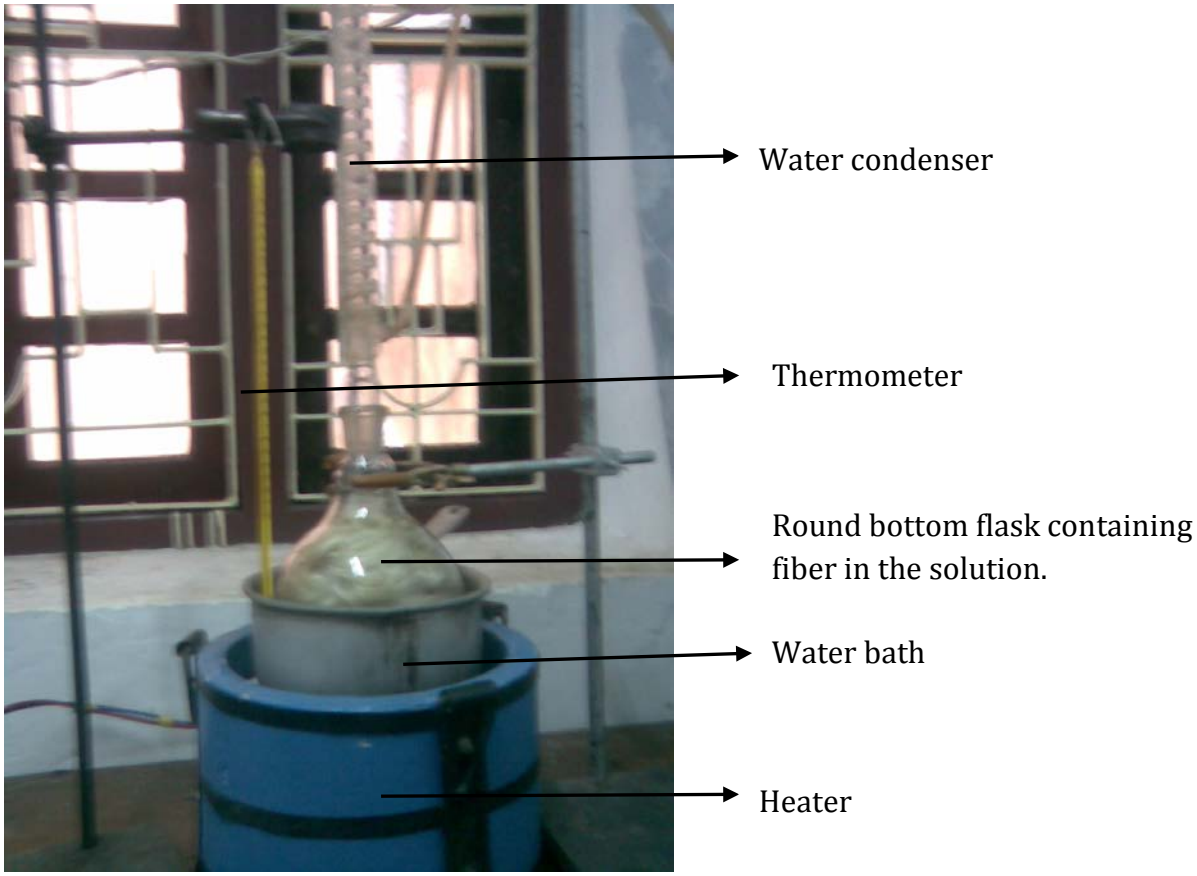

Fig. 2.2: Experimental set up for the Dewaxing treatment.

Fig 2.2 shows the experimental set up for the dewaxing treatment. The fibers were put in a round bottom flask containing desired mixture of the benzene and ethanol solution. The flask was put in the water bath. Heat was supplied from the

electric heater. Temperature of the solution was kept constant by water condenser. The temperature of the water was measured by the thermometer hanging from a stand.

2.2.2. $KMnO_4$ treatment

For the $KMnO_4$ treatment the dewaxed fibers (80g) were soaked in 1liter $KMnO_4$-acetone solution having various concentrations of $KMnO_4$ (0.01%, 0.05%, and 0.1%) for the period of 1, 2 and 3 min. After that the solution was decanted and the fibers were washed with acetone to remove excess solution present in the fiber. Finally fibers were dried at 60°C in the oven for 12 hrs. The $KMnO_4$ treated fibers are designated as 01K1, 05K1, 1K1, 01K2, 05K2, 1K2, 01K3, 05K3 and 1K3 respectively. Here K symbolizes to $KMnO_4$ treatment. The prefixes of K denote the concentration of $KMnO_4$ acetone solution i.e. 01, 05, 1 for 0.01%, 0.05% and 0.1% concentrations respectively. However, the suffixes of K denotes the soaking time for the fiber in the solution in minutes.

Untreated composite and $KMnO_4$ treated sisal fiber reinforced epoxy composites (KFREC) were designated as UTC, 01KC1, 05KC1, 1KC1, 01KC2, 05KC2, 1KC2, 01KC3, 05KC3 and 1KC3 respectively. Here KC symbolizes to the $KMnO_4$ treated sisal fiber reinforced composite. The suffixes and prefixes of KC are same as that as discussed in the earlier paragraph

2.2.3. Microwave treatment

The microwave treatment of the fiber was carried out in a microwave oven (LG electronics) having adjustable power of (160 – 640) W with a microwave

frequency of 2450 MHz. This frequency falls under ISM band (industrial, scientific, medical use) showing that how microwave industry is immerging as a potential market for these above mentioned area. The dewaxed fibers were treated with microwave irradiation at various power setting (160, 320, 640W) for different treatment period (2, 4, 8 min). The fibers were removed from the oven and cooled under vacuum for 24 hours. Now the microwave treated (MT) fibers were designated as 160W2, 160W4, 160W8, 320W2, 320W4, 320W8, 640W2, 640W4, 640W8. The prefixes of 'W' denote the power setting where as the suffixes of it represent the microwave irradiation time on the fiber in minutes.

The composites made out of these treated fibers were designated as 160WC2, 160WC4, 160WC8, 320WC2, 320WC4, 320WC8, 640WC2, 640WC4, 640WC8. Here WC denotes the microwave treated sisal fiber reinforced epoxy composites (MFREC). The suffixes and prefixes of WC are same as that as discussed in the earlier paragraph.

2.2.4. Alkali treatment

The dewaxed fibers were immersed in the solution of 2%, 4%, 6%, 8% of sodium hydroxide (NaOH) solution for 2hrs. The soaking period of 6% fibers were varied from 2hrs to 4, 6, 8 hrs. Then the fibers were taken out from the solution. The fibers were rinsed with distilled water several times and finally washed with very dilute acetic acid (CH_3COOH) to remove the residual alkali. Neutrality of the fibers were checked by PH paper. The fibers were dried at room temperature for 1 day. The fibers were then put in the air circulating oven until the fiber gets the constant weight. Generally in our case it took 16 to 17 hrs to get the constant weight of the

fiber. The fibers were designated as 2N2, 4N2, 6N2, 6N4, 6N6, 6N8, 8N2. The prefixes of 'N' denote the concentration of the NaOH solution whereas the suffixes of 'N' represent the immersion time of the fiber in the solution in hours.

The composites made out of these treated fibers were designated as 2NC2, 4NC2, 6NC2, 6NC4, 6NC6, 6NC8, 8NC2. Here NC denotes the alkali treated sisal fiber reinforced composites (ALKC). The suffixes and prefixes of NC are same as that as discussed in the earlier paragraph.

2.3. Composite fabrication

A handmade indigenous wooden mold was designed for the fabrication of the randomly oriented composites which is shown in Fig. 2.3.

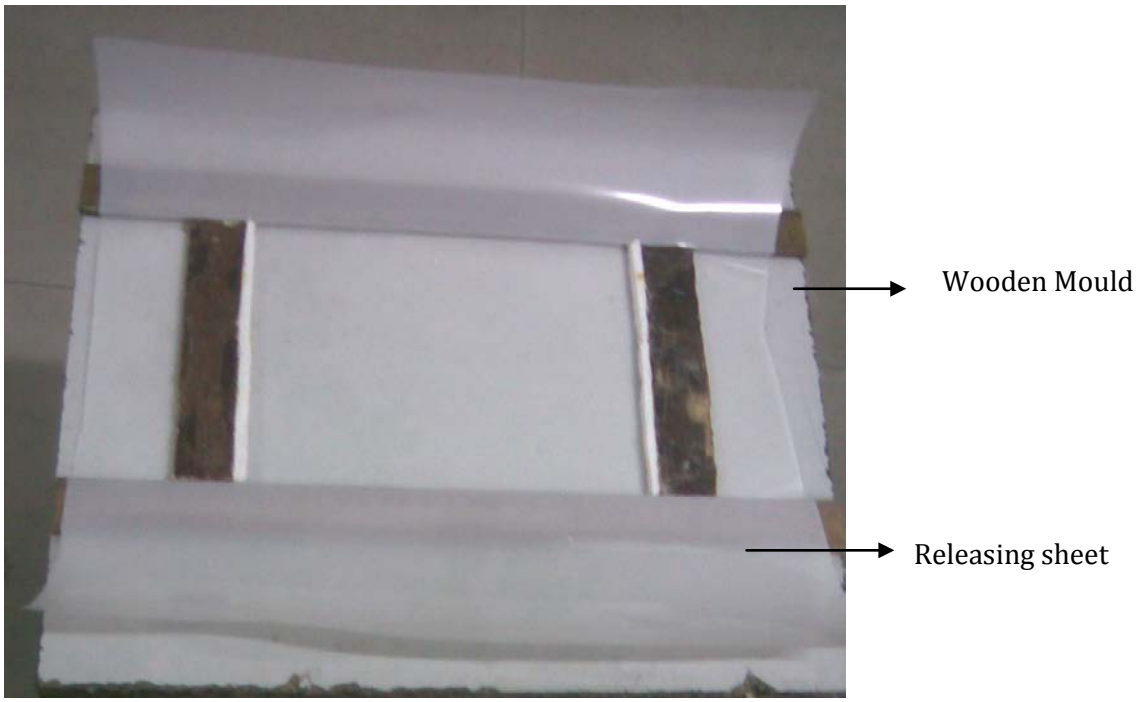

Fig. 2.3: Handmade wooden mould with releasing sheet for the fabrication of composites.

First, a releasing plastic was spread over the bottom of the wooden mold. Heavy duty silicon spray was applied to the plastic sheet for easy removal of the composite plate. The fibers were cut into 20mm length and distributed uniformly at the bottom of the mold which is prepared before. The length of the sisal fiber was kept at ~ 20mm as it was found to have good flexural and mechanical strength when reinforced in epoxy and polyester matrices [3]. Initially epoxy and hardener were mixed together on a weight percentage of 10:1 to form a matrix. The matrix was poured over the fibers evenly then pressed and pushed down with the iron roller to avoid and eliminate the air bubbles. Finally load was given to it in order to remove excess matrix and left for curing at room temperature for 24 hrs.

2.4. Characterization

2.4.1 Small angle X-Ray Scattering (SAXS)

SAXS measurements were carried out by the small wide angle X-ray scattering (SWAXS) equipment. The basic components of this equipment are a source, focusing multilayer optics, collimation system, sample stage and sample holder, semitransparent beam stop, image plate, CCD(for detection), wide angle extension and pinhole option. X-rays are produced with conventional X-ray tubes having target materials such as Cu, Co, Fe, Mo etc. Focusing multilayer optics (line and point) is employed to produce high flux of monochromatic X-rays. The collimation system makes the beam narrow and defines the zero-angle position. In addition, it also results in high resolution and lower background. Pinhole option is used for oriented and the fiber samples. Three different types of sample holders are used in SWAXS

experiment depending upon the type of sample. These are for solid, powder and liquid samples. Low and high temperature attachments are also attached with sample stage. A typical temperature range of these sample holders is –30 to 300 ^{0}C. The beam stop prevents the high intensity of the incoming beam, which can damage the detector. Apart from this, it also indirectly indicates the location of the starting point of scattering in the vicinity of the direct beam. The detector is used to measure the scattering from the sample over a range. The image plates and CCD camera are generally used for X-ray detection. The wide-angle extension is employed to measure the scattering data simultaneously from 0.1^0 to 40^0 for WAXS application.

The room temperature, smeared out, SAXS data of the untreated and treated sisal fiber were obtained from SAXS 896986 (Anton -Paar, Austria) which was mounted on PANalytical X-ray generator (PW3830), using CuK_α radiation with a wavelength of 1.5406Å and keeping voltage and current 40KV and 50mA respectively system. The sample to detector distance 'a' was 310 mm. These samples were exposed for 5 minutes. Data were obtained in the form of scattered X-ray intensity *I* as a function of the scattering vector *q* [1/nm],

$$q = \frac{4\pi \sin\theta}{\lambda} \qquad (2.1)$$

where θ is half the scattering angle (SAXS (angles 0.1 to 5°)) and λ is the wavelength of the radiation.

X-ray Scattering takes place due to the difference in the electron density inside the particle. SAXS is a form scattering that occurs at small angle. Small angle contains the information about the large object such as particles, macromolecules, and

micelles and govern by the relation 2.1. Scattering vector (q) reflects to the process in which X-ray photon transfer energy to the electron with which they interact. Larger the angles if the electrons are close to each other as shown, in particle 'a'. Smaller will be the angles if the distances between electrons are greater as shown in the particle 'b' in Fig. 2.4.

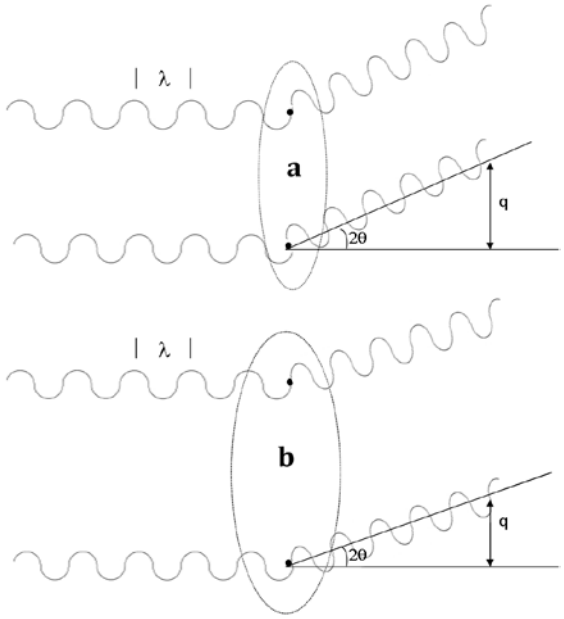

Fig.2.4: X-ray interaction with the particle [4].

The electron density map tells about the defects in the crystal system in the sample. Due to the little difference in the electron density ($\Delta\eta$) between crystalline phase and amorphous phase, these two are taken as one phase i.e. matter phase whereas void is as another phase. The electron density difference between these two phases is high enough to scatter. The idea of taking sisal fiber as a two phase system is due to the difference in electron density between matter phase and void phase [5]. In the present study we have treated the sisal fiber as a non-ideal two- phase system,

which is a realistic approach and are also justified. The samples are isotropic as proved by the applications of Vonk theory (relation 2.3) and the computed three dimensional correlation functions from the slit smeared intensity data of the samples (5).

The evaluation and analysis of all the macromolecular parameters in the present study are based on the Vonk [6] and Ruland [7] theory according to which the sample are non-ideal two-phase system with isotropic structure. A useful parameter in characterizing the structure of the fiber sample when absolute intensity is not available is given below

$$R = \frac{\left\langle \left| \, grad\eta \, \right|^2 \right\rangle}{\left\langle \eta^{\,2} \right\rangle} = 4\pi^2 \frac{\int_0^\infty s^4 I(s)ds}{\int_0^\infty s^2 I(s)ds} = 6\pi^2 \frac{\int_0^\infty s^3 \tilde{I}(s)ds}{\int_0^\infty s\ \tilde{I}(s)ds} \qquad (2.2)$$

where *I(s)* and $\tilde{I}$ *(s)* are desmeared and smeared out intensities respectively in arbitrary units, η is deviation of electron density from its mean value, *s* is a vector in a reciprocal (Fourier) space which was later modified by Mishra et al. [8] is as follows:

$$R = \frac{3}{2}\left(\frac{2\pi}{\lambda a}\right)^2 \frac{\int_0^\infty x^3 \tilde{I}(x)dx}{\int_0^\infty x\tilde{I}(x)dx} \qquad (2.3)$$

Where '*R*' is the corrugation at the phase boundary, '*a*' is the sample to detector distance, '*x*' is the position co-ordinate of the scattered intensity from the center of primary beam and $s = 2\theta/\lambda = x/\lambda a$, 2θ is the scattering angle. If *R* goes to ∞, the system is ideal i.e. the gradient at phase boundary is infinity. But if it has some

finite value, the system becomes non-ideal two phase suggesting that corrugation at the phase boundary exists. The change of electron density from matter phase to void phase is not sudden but a continuous process through a transitional layer '*E*' know as width of transition layer. In the present study, the width of transition layers (*E*) is calculated by Ruland and Vonk method and is designated as E_r and E_v accodrdingly. The width of transition layer, E_v (Vonk method) is calculated by normalizing $C(r)$ to unity at the start of the real space. According to Vonk method,

$$\mathrm{E}=-\frac{4}{R}\left[\frac{dC(r)}{d(r)}\right]_r=E_v \qquad (2.4)$$

where *C(r)* is the three-dimensional correlation function of a sample normalized to unity at the origin in real space and expressed in terms of '*x*' by Patel et al. [9].

The 3D correlation function $C(r)$ which contains the valuable information regarding macromolecular structural parameters is defined as the ratio of the average of the product of the electron density across the two ends of a virtual rod moving inside the particle to the average of the product when the length reduces to zero at the origin. It gives information about the nature of the phases present in the particle. The function $C(r)$ was originally coined by Mering and Tchoubar [10]. The function then modified by Patel et al. [9] in terms of '*x*' as per following relation for convince.

$$C(r)=\frac{\int_0^\infty x\tilde{I}(x)J_0\left(2\pi rx/\lambda a\right)dx}{\int_0^\infty x\tilde{I}(x)dx} \qquad (2.5)$$

Here J_0 is the Bessel function of Zero order first kind. The value of $C(r)$ normalizes to unit at the origin and decreases to zero when r attains the phase boundary of the particle i.e. $r=R$, corresponding to the maximum displacement. This correlation function contains the information about the particle in three dimensions hence known as 3D correlation function.

The one-dimensional correlation function $C_1(y)$ can be visualized as a measuring rod of length 'y' perpendicular to the layers which moves along the y-direction. In the present study there is significant contribution of $C_1(y)$ as sisal is having the lamellar structure. The expression for the one-dimensional correlation function $C_1(y)$ for layer structure in terms of x is expressed by Misra et al. (8) as

$$C_1(y) = \frac{\int_0^\infty x\tilde{I}(x)[J_0(z) - zJ_1(z)]dx}{\int_0^\infty x\tilde{I}(x)dx} \qquad (2.6)$$

where $z = 2\pi xy/\lambda a$ and J_1 is the Bessel function of first order of first kind.

According to Vonk [11] the position of first subsidiary maximum in the one-dimensional correlation function $C_1(y)$, gives the value of the average periodicity transverse to layers (D). Inside the fiber, the matter phase and void phase are thought to be arranged in terms of lamellar stack and each lamellar having some periodicity displays information about the specific inner surface area (S/V) of those lamellar stacks. It is also defined as phase boundary per unit volume of the dispersed phase.

$$S/V=2/D \qquad (2.7)$$

The extent of matter and void phase inside the fiber are represented by $\bar{l}_1$ and $\bar{l}_2$ respectively whereas the volume fractions of matter and void phase are denoted by φ_1 and φ_2 respectively. Here, $\bar{l}_1$ and $\bar{l}_2$ are calculated by using the relations $\bar{l}_1 = 4\varphi_1(V/S)$ and $\bar{l}_2 = 4\varphi_2(V/S)$. It is obvious that

$$\phi_1 + \phi_2 = 1 \tag{2.8}$$

The transversal lengths of matter and void phases for a two-phase three-dimensional system were derived by Mittelbach and Porod [12] and are given by the relation

$$1/\bar{l}_r = 1/\bar{l}_1 + 1/\bar{l}_2 \tag{2.9}$$

where $\bar{l}_r$ is the range of inhomogeneity which has same meaning with that of reduced mass in mechanics.

Another important parameter that is derived from the $C(r)$ is the length of coherence (l_c) which gives the information about the distribution of electron across the phase boundary of the particle.

$$l_c = 2\int_0^\infty C(r)dr \tag{2.10}$$

In order to find out the width of transition layer E as given by Ruland [7] for a non-ideal two phase system the functional relationship between $\tilde{I}(x)\cdot x$ and x^{-2} takes the form of

$$\tilde{I}(x)\cdot x = \frac{\pi C}{2\cdot(\lambda a)^3\cdot x^{-2}} - \frac{\pi^3 C}{3\cdot(\lambda a)\cdot E^2} \qquad (2.11)$$

where *C* is the probability constant

Tail end of the $\tilde{I}(x)$. *x* versus x^{-2} is known as Ruland plot**.** It is calculated by taking the 15 extreme points at the tail region of the corresponding curve.

2.4.2. X-Ray diffraction (XRD)

The bending of a wave around an obstacle of comparable size of the wave length is called diffraction. The periodic array of atom in crystal acts as a coherent scatterer. The interplanner spacing(d) between the atomic planes is comparable to the wavelength of the X-rays . Thus it can diffract the X-rays at some particular angle (θ) satisfying the Bragg's law of diffraction[13].

$$2d\sin\theta = n\lambda \qquad (2.12)$$

Where *n* is the order of diffraction, *d* is interplanner spacing. These diffracting planes contain the information about the atomic arrangement within the crystal. Peak positions signify the space between diffracting planes of atoms. The number of atoms in the diffracting plane determines the peak intensity.

.

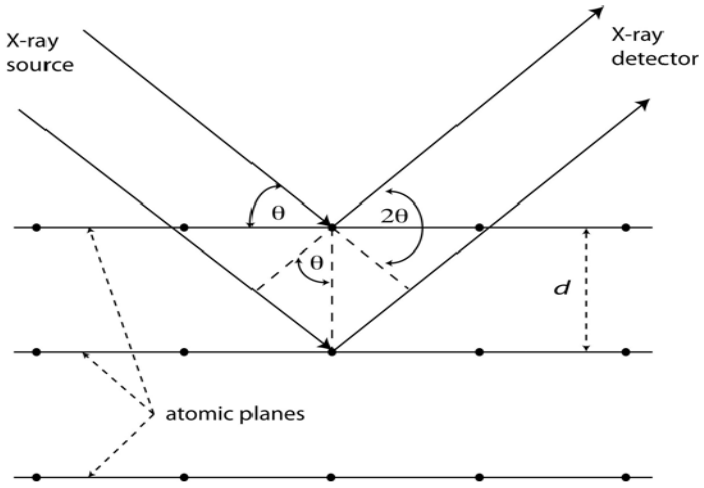

Fig. 2.5: X-Ray diffraction from the lattice planes with inter planner spacing d.

In order to identify the effect of treatment on the crystallographic structures of sisal fiber, wide angle x-ray diffraction (WAXD) spectra were collected by PHILIPS PANalytical PW1830 with Cu-K_α radiation from 5^0 to 45^0 with a scan speed of 0.04 degree/sec. The crystallite sizes of the fibers were determined by modified Scherer's formula whereas the degree of crystallinity was computed by Segal's empirical method [14].

$$CrI(\%) = \left(\frac{I_{002} - I_{001}}{I_{001}} \right) \times 100 \qquad (2.13)$$

Where I_{002} corresponds to the cellulose peak which appears to be ~ 22.5^0 whereas I_{001} is the intensity of the amorphous material.

2.4.3. Fourier transmission infrared (FTIR) spectroscopy

The structure of a compound can be evaluated from the infra-red spectrum by the quantized absorption of the infrared radiation by various bands in a molecule. As

each material has unique combination of atoms like that no two compounds produce same spectrum. The absorption peak in infrared spectrum corresponds to the bonds of constituting atom of the material. So it is generally called as the finger print of the material.

The differences of charges in the electric fields of atoms in a molecule are the cause of the dipole moment of the molecule. These molecules absorb the infrared photons causing excitation to higher vibrational states. Strength of absorption of infrared light depends on the size of deformation of the dipole moment due to the vibration. As the vibrations are quantized the absorption of the infrared energy occurs at specific region of the spectrum for a compound [15].

Chemical compositions of the raw and treated sisal fibers were investigated by the Perklin Elmer FTIR spectrometer spectrum RX-1 in the mid IR range i.e. from 400 cm^{-1} to 4000 cm^{-1}. The fibers were cut into very fine pieces by a pair of scissor and then shivered with a fine mess to get fine fiber powder. The fiber powder were mixed with KBr powder and made into almost a transparent pellet for the FTIR measurement.

2.4.4. Density measurement of the fiber

The density measurements of the fibers were done as per ASTM D3800-99. The bundle of fibers were weighed and denoted as W_a. Then the bundle of fiber was immersed in benzene having a density (ρ_b) 0.875 g/cc. The immersed fiber's weight is denoted as W_i. The bulk density (ρ) of the fiber was calculated by the following equation [16].

$$\rho = \frac{\rho_b - W_a}{(W_a - W_i)} \tag{2.14}$$

2.4.5. Scanning electron Microscopy (SEM)

SEM is a nondestructive analysis technique. It uses highly focused beam of high energy electron on the sample. The interactions of electron with the sample produce different signals which are known as secondary electron (SE), backscattered electron (BSE), X-rays etc. Out of all the signals the SE comes from the few layer of the sample surface where as the BSE comes from the deeper layer of the sample thus having lower contrast than the SE. SE helps in getting the information of topography and BSE gives the information compositional variation in the sample by the contrast [17, 18]. Fig 2.6 demonstrates the interaction of electron beam with the sample. The selected sample areas are focused by the electron beam and the scanned image of the area gives the information about the chemical composition, defects in the sample, crystallite orientation of the various phases of the sample. So SEM helps in quality analysis for the morphology of the sample.

In the present study the surfaces of sisal fibers and fractured surfaces of the composites are examined by SEM (JEOL JSM-6480 LV) at 20 kV. It proves to be an essential tool to find out the bonding of the fiber with the matrix.

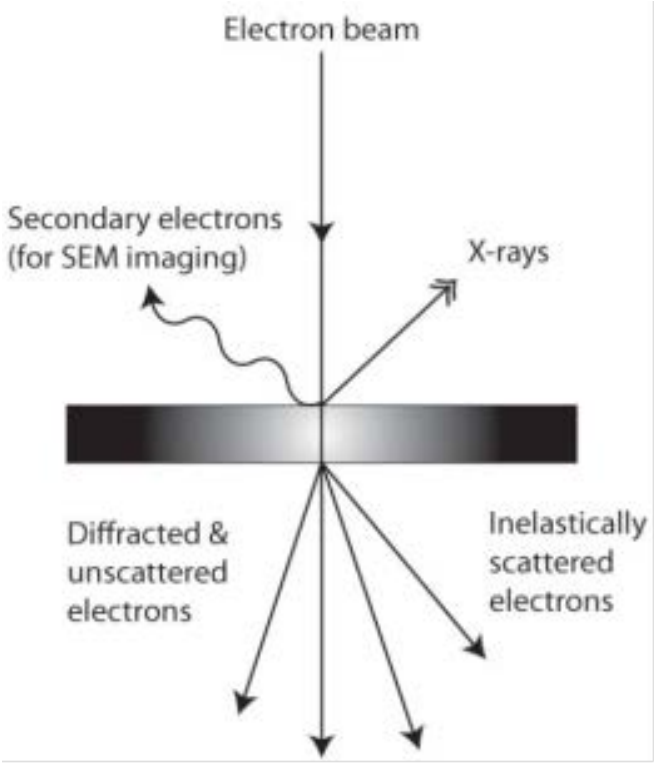

Fig. 2.6: Interaction of electron beam with the sample.

2.5. Mechanical Properties of the composite

The mechanical properties of the composites were calculated by two methods (a) 3 point bending test (b) tensile test.

2.5.1. Three point bending test

It is a very popular bending test for plastic, ceramics, fiber reinforced polymer composite as their failure behaviors are linear. In this method the sample is supported by two ends and loaded at the center. The flexural strength of the sample is calculated by applied load to the corresponding strain. This indicates that the maximum load that the sample can withstand before it breaks. The flexural modulus

of the sample was calculated by the slope of the stress-strain curve. So it defines the sample how stiffer it is.

2.5.2. Tensile test

It is done to find out the tensile strength of the material. It determines the toughness of the material by measuring the elongation at the fracture of the sample. The test is performed by holding the sample in longitudinal direction so that monoaxial stress will develop. The loading of the sample is slowly and continuously increased until it breaks. Elongation at the fracture determines the change in length to the original length. The maximum tensile strength is calculated by maximum tensile force to the initial cross section.

In order to evaluate the flexural strength and tensile strength of the composites three point bending test and tensile test are carried out by INSTRON1195 respectively. The randomly oriented composites were cut as per the ASTM D790 and ASTM D3039 to measure the flexural strength and tensile strength respectively. The sample size for flexural measurement was (13×30×5) mm^3 with a crosshead speed of 2 mm/min with a gauge length of 50mm whereas for tensile measurement the sample size was (200×30×5) mm^3 with crosshead speed of 1mm/min with gauge length of 120mm [19]. The reported data are the average of the five successful tests.

2.6. Electrical Properties of the composite

2.6.1. Dielectric Spectroscopy

Dielectric and impedance spectroscopy are important characterizing tool for electrical properties of material both fundamental and application oriented research. It is the study of response of the material to the varying frequency and temperature.

With the help of sample dimensions, intrinsic electric material properties like the complex permittivity $\varepsilon^*(\omega)$ or conductivity $\sigma^*(\omega)$ spectra are easily evaluated from $Z^*(\omega)$.

When electric field is applied to a parallel plate capacitor containing dielectric then separation of charges takes place. This is called polarization. Dielectric study of the materials generally deals with four major kind of polarizations [20].

1. Electronic polarization
2. Atomic or ionic polarization
3. Dipolar polarization
4. Interface or space charge polarization.

Out of the above mentioned polarization electronic and atomic polarization's resonant frequency falls in the realm of vibrational spectroscopy. So they are instantaneous in the dielectric spectroscopy. These two polarizations are also temperature independent whereas the dipolar and space charge polarizations are temperature dependent. A relaxation effect is associated with the orientation polarization (10^2-10^{10}) Hz [21].

The dielectric measurements are done by applying the electric voltage at the electrode interface. The ratio of the resulting current and its phase shift to the applied voltage is called impedance of the system. In an ideal dielectric the resulting current should be 90^0 out of phase to the applied voltage but practically it never happens because of the two reasons.

1. Dissipation of energy due to inertia of the moving species.

2. The long range hopping of charged species.

The total current in a non ideal dielectric will lead the voltage by an angle (90-δ), where δ is called the loss angle and $\tan\delta$ is the electrical loss due to resonance and called as tangent loss which is shown in Fig. 2.7 [20]. Loss tangent can be expressed as:

$$\tan\delta = \frac{\varepsilon_r''}{\varepsilon_r'} \qquad (2.15)$$

Where ε_r' and ε_r'' are real and imaginary part of relative permittivity

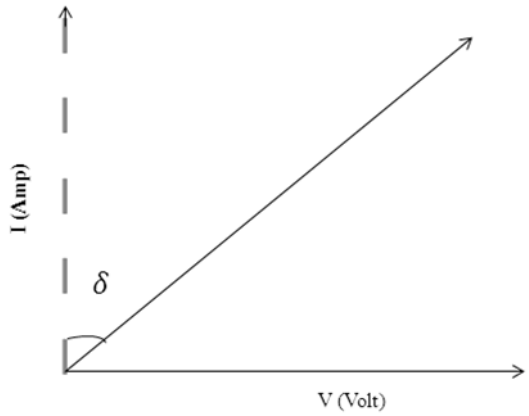

Fig. 2.7: Response of out put current to the input voltage in non-ideal dielectric.

2.6.2. Impedance and Modulus spectroscopy

The impedance sepctroscopy enables us to evalute and separate the contribution of the electrode reaction to the overall electrical properties. Baurley was first to propose the generalised impedance and admittance plot to extract the bulk conductivity from the sample. In impedance spectroscopy technique, a sinusoidal signal is applied across a solid elctrolyte cell and the response to the output is compared with the input signal inorder to determine the impedance modulous $|Z|$ and phase shift (θ). The results of complex impedance measurment of a cell as a function of the applied signal freuency can be displayed conventionally in a complex plane in terms of any of the follwing form [22].

Complex impedance $Z^* = Z' - jZ''$ (2.16)

Complex admittance: $Y^* = (Z^*)^{-1}$ (2.17)

Complex permittivity: $\varepsilon^* = (j\varpi C_0 Z^*)^{-1} = \varepsilon' - j\varepsilon''$ (2.18)

Complex electric modulus: $M^* = j\omega C_0 Z^* = M' + jM''$ (2.19)

Where (Z', M', ε') and $(Z'', M'', \varepsilon'')$ are the real and imaginary components of impedance, modulus, and permittivity, respectively. j=-1, ω=2πf is the angular frequency and C_0=$\varepsilon_0 A\ell^{-1}$ in which C_0 is the vacuum capacitance of the cell without the sample, ε_0 the permittivity of free space (8.854×10^{-14} F·cm^{-1}), ℓ, A are the thickness and area of the sample respectively.

For electrical measurements, disk shaped samples having ~15 mm diameter were cut out of the composites and polished to make thickness of 2mm. The surfaces of the test samples were polished and coated with conductive silver paste. The electrical measurements in this study were performed by using a computer interfaced LCR meter supplied by HITESTER. Two sets of electrical measurements were carried out. One was from room temperature room temperature (RT) to 200^0C at various frequencies with a heating rate of 2^0C/min and another was from 100 Hz to 1 MHz frequency at various temperatures for the evaluation of electrical properties of both untreated and treated composites.

The dielectric constant (ε_r) was calculated from the capacitance using the equation:

$$\varepsilon_r = Ct/\varepsilon_0 A \qquad (2.20)$$

Where ε_r is the relative dielectric constant of the material, ε_0 is the permittivity of air, C is the capacitance, A is the area of cross section, and t is the thickness of the sample.

References:

1. Roy SC. An X-ray study of acetylated jute. Text Res J, 30, (1960) 451-456.
2. Ratho T, Torasia S, Mohanty JC, X-ray method of determining the amplitude factors of organic liquids. Ind J Phy, 38, (1964) 28–30.
3. Joseph K, Varghese S, Kalaprasad G, Thomas S, Prasannakumari L, Koshyh P, Pavithran C, Influence of interfacial adhesion on the mechanical properties and fracture behaviour of short sisal fibre reinforced polymer composites. Eur. Polym J, 32, (1996) 1243-1250.
4. Langenbucher G. Small-Angle X-ray Scattering for Pharmaceutical Applications. Pharmaceutical Technology, 34, (2010) 32-37
5. Khan MD, Small angle X-ray scattering study of sisal fiber using correlation function. Ph. D Thesis: 16, (1991) 71–72.
6. Vonk CG, Investigation of non-ideal two-phase polymer structures by small-angle X-ray scattering, J Appl Crystallogr, 6, (1973) 81-86.
7. Ruland W, Small-Angle Scattering of Two-Phase Systems: Determination and Significanceof Systematic Deviations from Porod's Law. J Appl Cryst, 4, (1971) 70-73.
8. Mishra T, Patra KC, Patel T, One-Dimensional Correlation Functions Obtained from Slit-smeared Intensity Colloid. Polym Sci, 262, (1984) 611-616.
9. Mishra T, Bisoi DK, Patel T, Patra KC, Patel A, Small angle x-ray study of cellulose in cotton using correlation functions. Polym J, 20, (1988) 739-749.
10. Mering J, Tchoubar D, Interprétation de la diffusion centrale des rayons X par les systèmes poreux. I, J Appl Crystallogr, 1, (1968) 153-165.
11. Vonk CG, A procedure for desmearing X-ray small-angle scattering curve, J Appl Crystallogr, 4, (1971) 340-342.
12. Mittelbach P, Porod G, Zur Rontgenkleinwinkelstreuung verdunnter kolloider Systeme, Kolloid Z Z Polym, 202, (1965) 40-49.
13. Smart LE, Moore EA, Solid State Chemistry. Taylor & Francis, London (2005).

14. Segal L, Creely J, Martin AE, Conrad CM, An empirical method for estimating the degree of crystallinity of native cellulose using the X-ray diffractomerter. Text Res J, 29, (1959) 786-794.
15. Nakamoto K, Infrared and Raman spectra of inorganic and coordination compounds. Fourth edition, John Wiley and Sons, (1986).
16. ASTM D3800-99, Standard test method for density of high–modulous fiber. ASTM International:Pennsylvania
17. Suzuki E, High-resolution scanning electron microscopy of immunogold-labelled cells by the use of thin plasma coating of osmium, J Microscopy, 208, (2002) 153-157.
18. Goldstein GI, Newbury DE, Echlin P, Joy DC, Fiori C, Lifshin E, Scanning electron microscopy and x-ray microanalysis. Plenum Press, New York 1981
19. Rosa IMD, Santulli C, Sarasini F, Mechanical and thermal characterization of epoxy composites reinforced with random and quasi-unidirectional untreated Phormium tenax leaf fibers. Mater Des, 31, (2010) 2397–2405.
20. Hippe RV, Dielectric materials and applications. Cambridge technology press of MIT, (1995).
21. Kao KC, Dielectric phenomena in solids with emphasis on physical concepts of electronic processes. Elsevier Academic Press, (2004).
22. Barsoukov E, Macdonald JR, Impedance spectroscopy: theory, experiment, and applications. John Wiley and Sons, (2005).

Chapter 3

Effect of Fiber Volume Fraction on the Mechanical & Electrical Properties of the Short Sisal Fiber-Reinforced Epoxy Composites

3.1 Introduction

The reinforcement of the natural fiber in the thermoset and thermoplastic material created new class of material which is mechanically superior to the non-fibrous filler matrix [1]. Applications of these materials have covered almost all the area of fundamental research like aerospace, automobile, marine, structural engineering, pharmaceutical etc. [2]. However, there are several factors that affect the durability and strength of the natural fiber composite like critical length of the fiber, volume fraction of the fiber in the matrix, compatibility between the polymer and the fiber etc. [3]. The effect of volume fraction of fiber on the mechanical strength of the composite has been an exciting area of research since last few decades. There are many reports on the effect of volume fraction of fiber on the various properties of composite. Kristina et al. [4] studied the effect of fiber loading on the stiffness,

strength and morphology of unidirectional sisal–epoxy composites manufactured by resin transfer molding (RTM). They found that the real fracture mechanism of the composite depends upon the inhomogeneous fiber stress distribution, wide distribution of individual fiber, technical fiber strength and poor interfacial adhesion. According to Monette et al. [5] the strength of viscoelastic aligned short-fiber composites with a homogeneous fiber dispersion displays a higher value at high fiber volume fractions, as compared to a perfectly brittle matrix, which suggests that matrix toughness plays a key role in the strengthening of short-fiber composites. At lower volume fractions of banana fiber, the strength of the composite specimen reduced compared to the virgin resin. At 35% of the fiber volume fraction, the tensile strength was increased by 38.6% whereas tensile modulus increased to 65%. The improvement in the mechanical properties is owed to the improvement in the bonding at the fiber matrix interface [6]. The inter-laminar and interfacial strength parameters affect the composite fracture toughness [7]. The study of the mechanical properties of sisal fiber reinforced urea-formaldehyde resin composites showed the optimal charpy impact strength and it reached ~ 9.42 kJ/m^2 with 50 weight percentage sisal fiber loading. At 30% of fiber loading, the resin was more than sufficient for the fiber which led to the increase in interfacial friction stress and chemical bonding between the fibers. This ultimately caused drop in the toughness of the sample and explained why impact strength was lower whereas the flexural, wear resistance and water absorption properties were proved to be excellent in the composite with 30 weight percentage. Homogeneous distribution of the fiber in the matrix due to better mixing was supposed to be the key factor for improved

mechanical strength. As the sisal fiber itself has higher wear resistance the composite made out of it was found to have higher mechanical strength and minimal water resistance which is suitable in fiber board applications [8].

Due to the potential applications of the NFRPC in dielectrics, insulators, antistatic fields etc., the investigation of electrical properties of these composite has become an interesting area of research. The electrical conductivity of the composites was found to depend on several factors out of which fiber loading in the matrix is a major one. Pothan et al. [9] demonstrated that the dielectric constant increased with increase of fiber loading in the composite. Fiber surface modification decreased the dielectric constant values due to the induced hydrophobicity by the chemical modification on the fiber surface. The overall polarity of the surface modified fibers was decreased and gave lower dielectric constant values. Volume resistivity decreased with fiber loading while the electrical conductivity increased.

Though many studies have been carried out on the effect of fiber loading on different properties of the composites but the fabrication process of the composites were different. Our present study focuses on the effect of volume fraction of short sisal fiber on the overall morphological, mechanical and electrical properties of the fiber reinforced epoxy composites which were fabricated by hand layup technique. The volume fraction of the fiber in the matrix has been optimized in order to have better mechanical and electrical properties of the composites.

The morphological studies of the fabricated composites were carried out by SEM. Electrical and mechanical studies were conducted to know the effect of fiber

volume percentage in these composites. The composites were fabricated with different volume percentages of fiber such as 5, 10, 15 and 20. The composites were named accordingly 5UTC, 10UTC, 15UTC and 20UTC. Here UTC refers to the untreated sisal fiber reinforced composites. The prefixes of UTC are the different volume percentage of the fiber used for reinforcement in the epoxy matrix.

3.2. **Results and Discussion**

3.2.1 Morphological Study

The mechanical properties of the fiber reinforced composites expected to depend upon the fiber content in the composite. Slight change in the physical condition of the fiber may also affect the overall properties of the composite. The SEM micrographs of the fractured surfaces of the composites with different volume percentage of fiber are shown in Fig. 3.1. 5UTC composite shows unevenly distributed fibers in the composite. The fibers seem to come out of the composite due to poor bonding between the fiber and matrix. At lower volume fraction of fibers, packing of fibers in the matrix is not sufficient to provide better reinforcing effect to the matrix, hence result in lower mechanical properties of the corresponding composites. At 10UTC, though the distribution of the fibers in the composite is little better but still significant amount of fiber comes out from the composite after the sample had gone through the three point bending test. Whereas, out of all the samples, 15UTC had minimum fiber pull out. This may be due to the uniform distribution of the fibers in the matrix which transfer the load from the matrix and comes out to be a better composite as compared to the other. It can be clearly observed that 20UTC composite possesses lots of void and cracks. It shows significant amount of fiber pull out from

the composite resulting in a very weak structure since, higher volume fraction of fiber often results in more defects owing to fiber contacts [10].

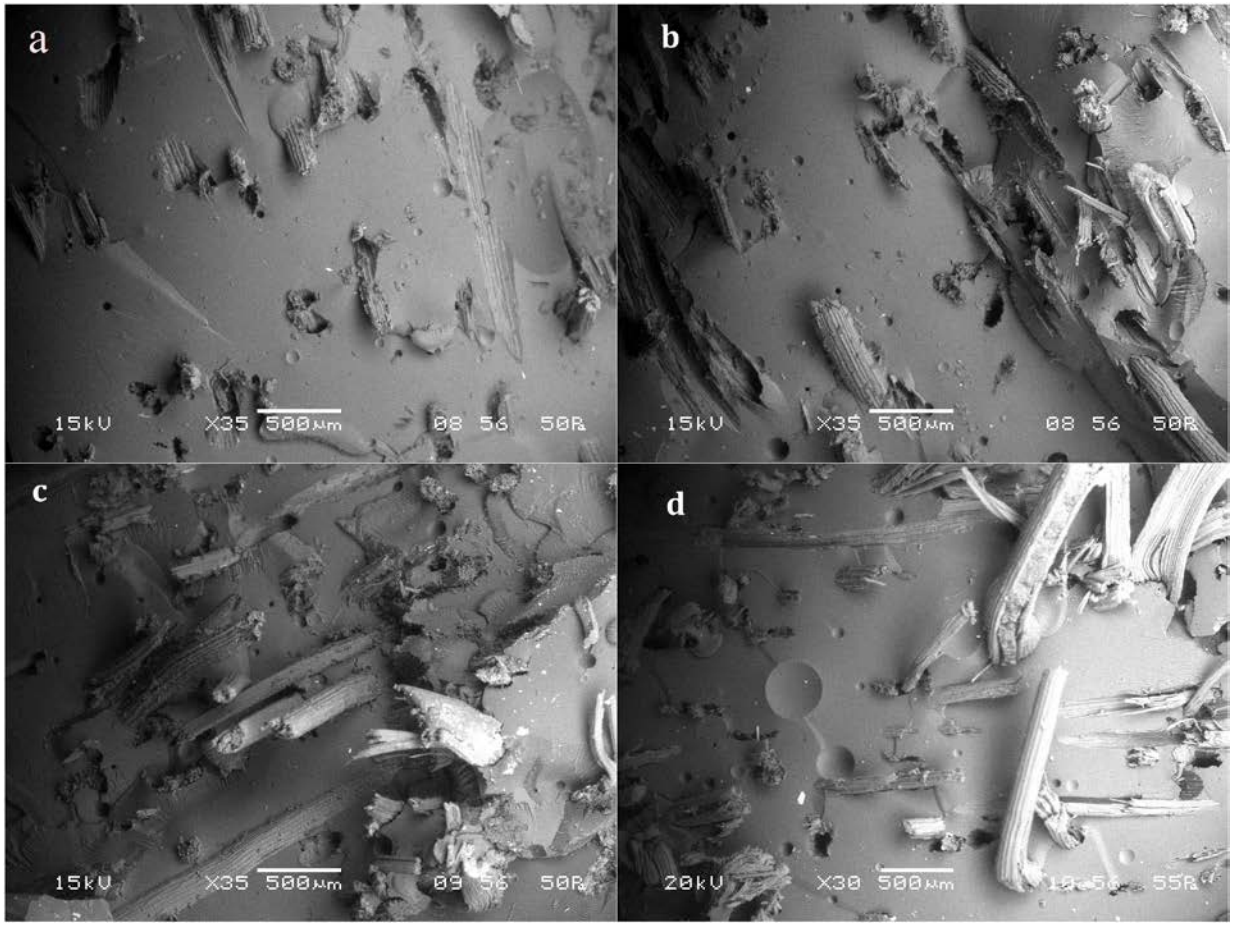

Fig. 3.1: (a, b, c, d) Distribution of fibers in 5UTC, 10UTC, 15UTC, 20UTC composites, respectively.

3.2.2 Mechanical Study

Fig. 3.2 depicts the variation of flexural strength of the composites with the increase in percentage of fiber volume fraction. At lower fiber loading flexural strength tends to decrease than the cured epoxy. The increase in flexural strength of the composite can be observed from 5% volume fraction of fiber to 15 %. But sudden

decrease in the flexural strength of the composite was observed at 20% volume fraction of fiber. During the initial stage of fiber loading, the load was not properly transmitted to the fibers due to the lower packing of the fiber hence the sole purpose of reinforcement was not properly served. At lower volume fractions, the fiber packing inside the matrix was ineffective for the load transfer. This causes failure of bonding at the interface. However, as the fiber volume percentage increased from 5% to 15%, increment in the flexural strength was observed. This may be due to the increased bonding between the fiber and the matrix due to the uniform and optimal distribution of the fiber in the matrix. Thus the load sharing was easily transmitted to the fibers [6]. At 20% fiber loading the flexural strength of the composite was found to decrease. This might be due to the poor interfacial adhesion and non-uniform distribution of fiber in the matrix. The over packing of the fiber inside the composite might have created friction between the individual fibers leading to the degradation of individual fiber and ultimately lowering the mechanical strength of the composite. The inhomogeneous fiber distribution creates negative effect in the composite. As local load concentrations were experienced by the fibers, the failure process continued and became catastrophic [4]. The partial spaces generated between the fiber and matrix material due to poor interfacial bonding resulted in a weak structure [11, 12].

The tensile strength of the 15UTC was significantly increased compared to the matrix and other composites which are shown in Fig. 3.3. Decrement in tensile strength was observed for the 20UTC sample. This might be due to the development

of local stress resulting from the non-uniform distribution of fibers and excess fiber reinforcement.

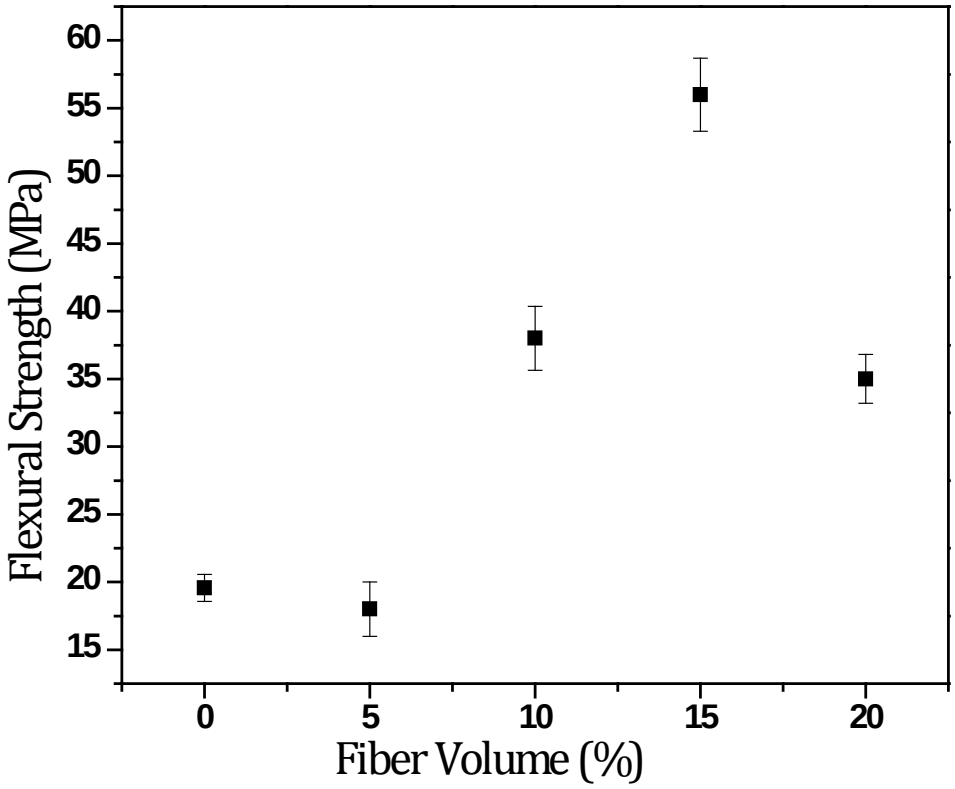

Fig. 3.2: Variation of the flexural strength of the composites for different volume fractions of fiber.

It can be noticed that with the increase in fiber volume fraction beyond 15% the thermoset epoxy matrix becomes more brittle and the strength reduced [3]. The lower values of the mechanical properties for 20UTC might also be due to the presence of large number of fiber ends in the composites. This can initiate cracks and propagation of it in the fiber reinforced composites. The fiber-to-fiber interaction hinders the effective stress transfer from matrix to fiber and become responsible for potential failure of the composites [13]. Though according to Brahmakumar et al.

[14], the young's modulus of the matrix should increase theoretically but practically the bonding mechanism at the interface plays a major role which has significant effect on the composite mechanical properties [15].

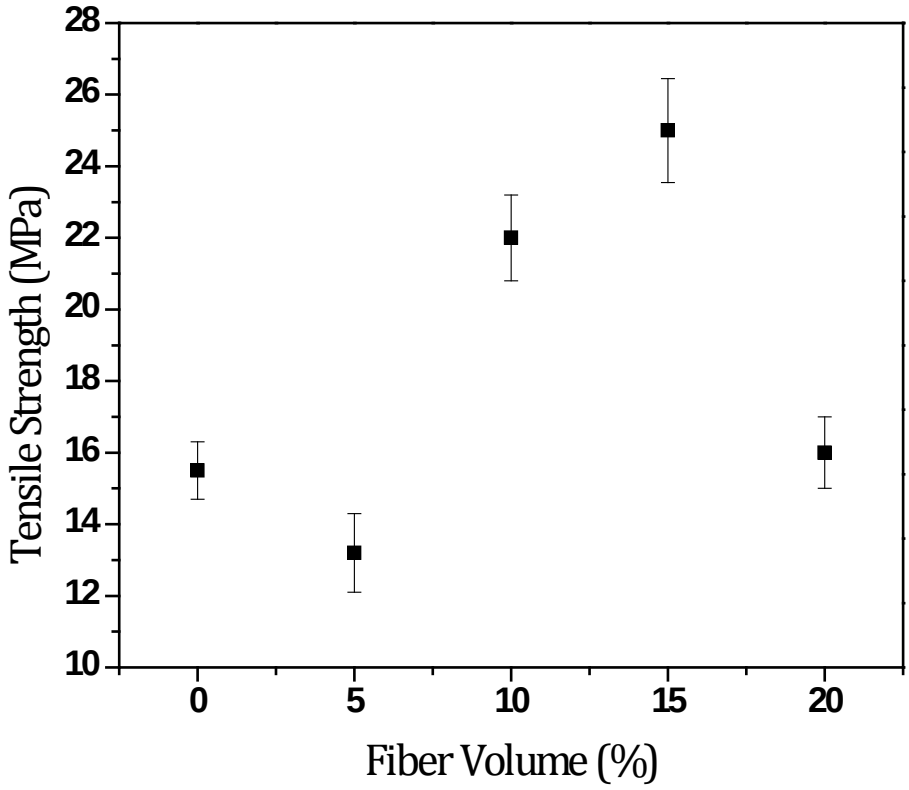

Fig. 3.3: Variation of the tensile strength of the composites for various volume fractions of fiber.

3.2.3 Dielectric Study

The variation of dielectric constant (ε_r) for different fiber loading as a function of frequency along with cured epoxy are shown in Fig. 3.4. The dielectric constants for all the samples were higher at lower frequency region. As a composite is

regarded as a heterogeneous material, the enhanced dielectric constant might be due to the presence of interfacial polarization at lower frequency.

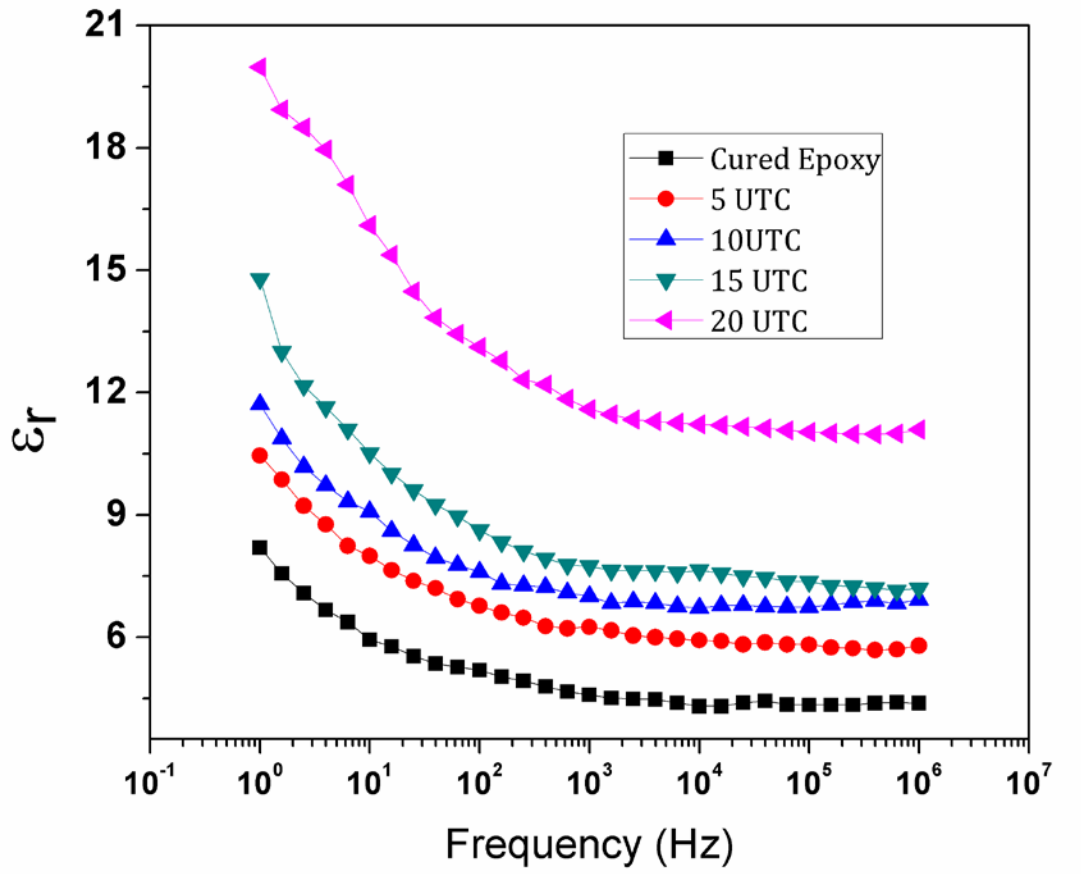

Fig. 3.4: Variation of dielectric constant with frequency at different fiber loading.

Composites consist of different phases with different conductivities so interfacial polarization dominates other polarization mechanism at lower frequency. Apart from interfacial polarization, dipolar polarization also affects the dielectric constant of the composites because of the presence of the polar groups in the fiber. At low frequency region, both dipolar and interfacial polarization contributes to the net dielectric constant of the material. However, with the increase in frequency the contribution

from both these polarization decreases and which in turn reduces the value of dielectric constant. Hence, for all the composites the value of dielectric constant tends to fall at higher frequency region.

The dielectric constant was found to increase linearly with the increase in fiber content in the composite which might be due to the availability of more number of polar groups at higher fiber loading in the composite. But there is a point to note that the dielectric constant of 5UTC, 10UTC, 15UTC samples were found to increase with the fiber loading but the increment in the values of ε_r was not so high where as for 20UTC it increased significantly compared to other three composites. This might be due to the trapped air in the central lumen of the fiber which decreased the dielectric constant of the composites. This did not allow substantial increase in the values of ε_r in case of the lower volume fraction of the fiber in the composites [9, 16]. However, beyond certain fiber loading the effect of trapped air in the central lumen of the fibers faded away. Here, the role of impurities and catastrophic increment of the polar groups of the fiber in the epoxy matrix becomes dominant. Hence, sudden rise in the dielectric constant was observed in 20 UTC.

The variation of loss tangent ($\tan\delta$) with the frequency as a function of fiber loading is presented in Fig. 3.5. The value of $\tan\delta$ in both cured epoxy matrix and SFREC at low frequency region became very high due to free motion of dipoles within the material and was connected to a.c. conductivity relaxation. It can be seen that dissipation factor also increased with the increase in fiber loading.

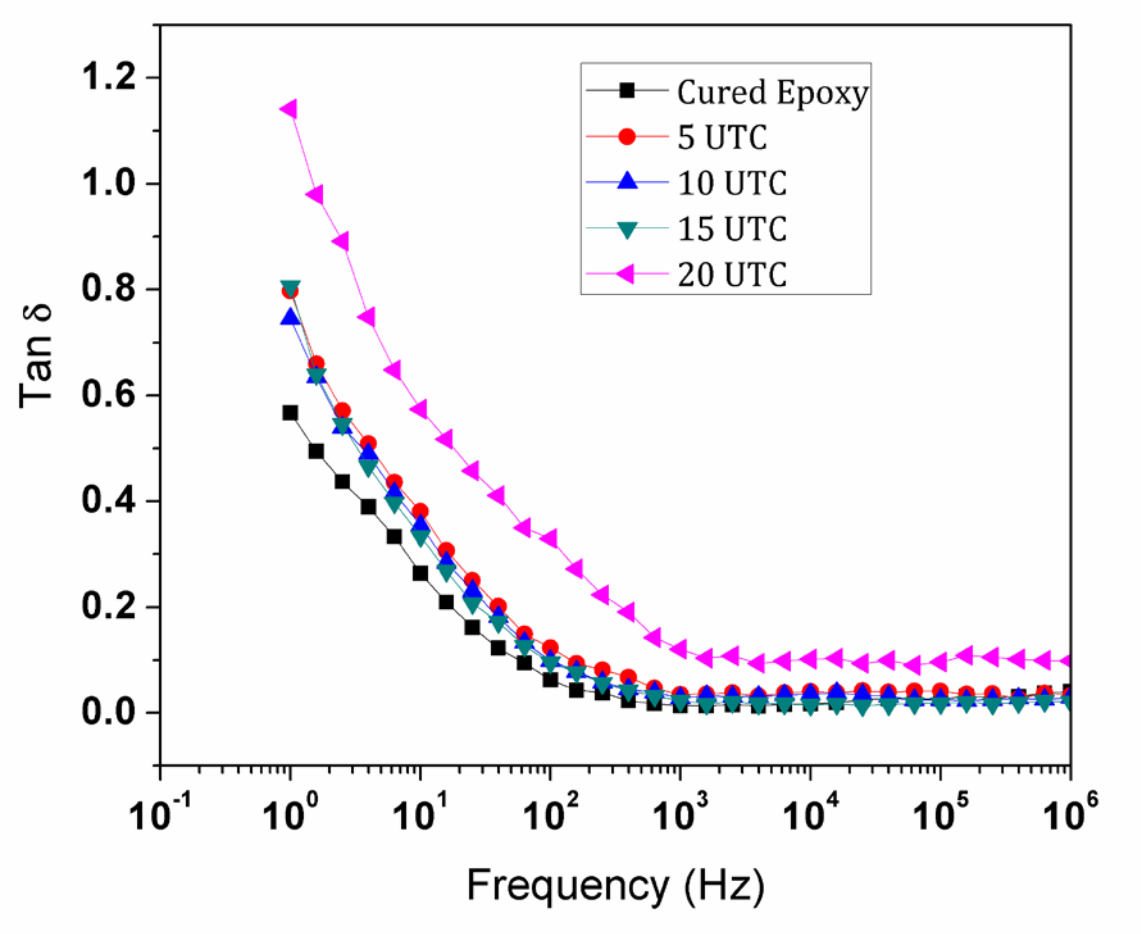

Fig 3.5: Variation of tanδ with frequency at room temperature with different fiber loading.

The loading of fiber adds amorphous part in the matrix [17]. More over the raw fibers are inherently hydrophilic in nature which allows the flow of current in the composite through amorphous phase. This led to the higher amount of loss in the composite owing to the amorphous phase relaxation [18]. The dissipation factor can be associated with the amount of electrical energy converted to heat energy in a dielectric or insulator. It is inherent dissipation of electromagnetic energy. The term tanδ refers to the tangent of the angle in a complex plane between the resistive (lossy) component of an electromagnetic field and its reactive (lossless) component.

Increase in fiber loading facilitates more storage of electric current due to the presence of polar fiber in the composite [9].

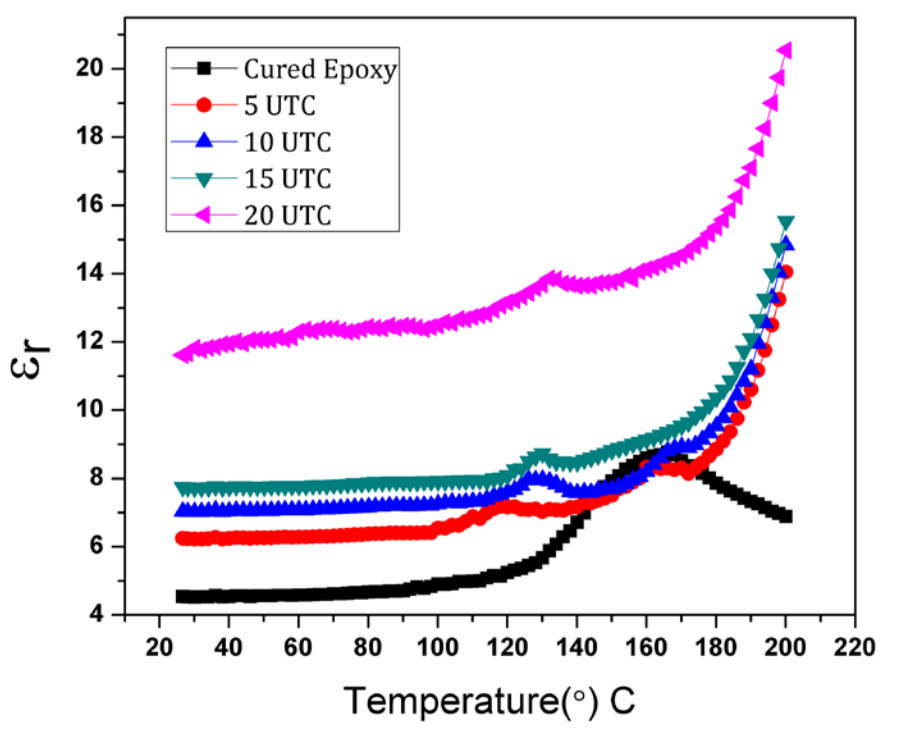

Fig. 3.6: Variation of dielectric constant at 1 kHz frequency with temperature at different fiber loading.

Fig. 3.6 depicts the temperature dependence of dielectric constant of 5UTC, 10UTC, 15UTC, 20UTC along with epoxy at 1kHz whereas the Fig. 3.7 shows the temperature dependence of $\tan\delta$ at the same specified frequency. The room temperature (RT) ε_r values of 5UTC, 10UTC, 15UTC, 20UTC at 1 kHz frequency were found to be 6.24, 7.04, 7.81 and 11.67 whereas for cured epoxy it came out to be 4.54.

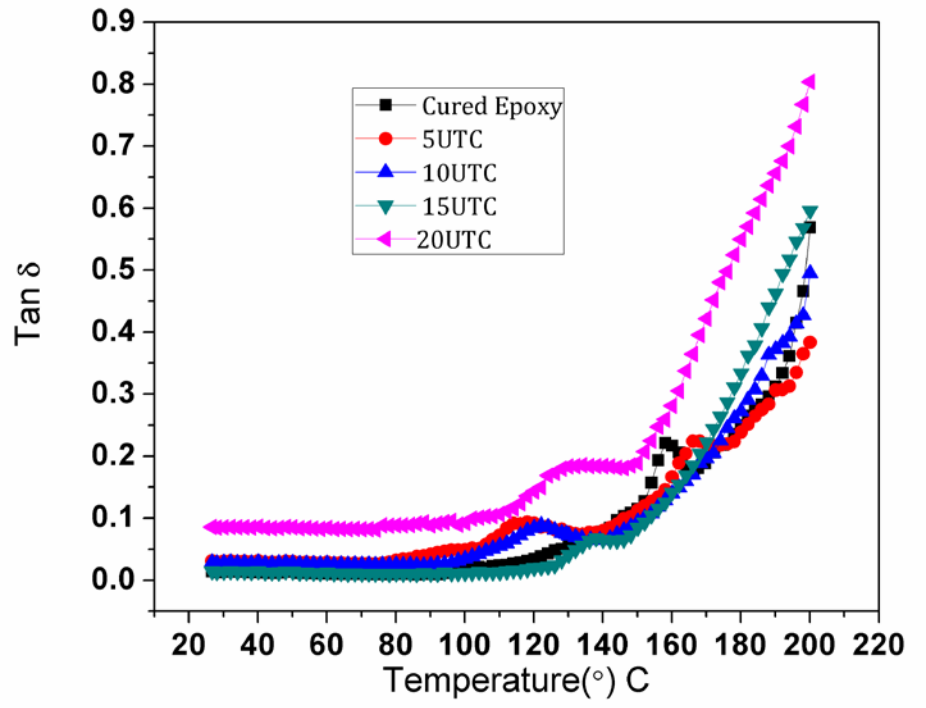

Fig. 3.7: Variation of tanδ at 1 kHz with temperature at different fiber loading.

Higher values of ε_r in case of SFREC in comparison to the cured epoxy matrix may be due to the incorporation of fiber, presence of water and impurities. The values of tanδ were found to be 0.014, 0.030, 0.028, 0.015, 0.086 for cured epoxy, 5UTC, 10UTC, 15UTC and 20UTC respectively. It was observed that with the rise in temperature, ε_r and tanδ values for all the investigated composites were increased. An exothermic peak was observed in the plot of ε_r vs temperature ~130^{o}C at 1 kHz frequency in all the samples which confirms the presence of a relaxation process. This relaxation is associated with glass-rubbery transition of the polymer. The relatively high values of ε_r and tanδ at high temperature were attributed to the enhanced mobility of large parts of the polymer chains and the co-operating contribution of inter-face polarization [weak Maxwell–Wagner–Sillars (MWS)] effect in the

composite systems which aroused due to additives, plasticizers etc. in polymer composite.

3.3. Conclusions

The effect volume fraction of fiber on the electrical and mechanical properties of the composites was well studied. The morphological study of the 15UTC composite was shown to have better adhesion and least fiber pullout than 5UTC, 10UTC and 20UTC. The composite with 15% fiber volume fraction was found to have maximum flexural strength and tensile strength. At lower volume fraction like 5%, the fibers were not sufficient to give the reinforcing effect to the matrix. Hence, reduction in mechanical strength was observed. At higher volume fraction of the fiber, tremendous increase of fiber ends in the matrix caused crack initiation which led to weak structure and drop in mechanical strength of the composites. The dielectric constant of 15UTC was not very high as compared to the 10UTC. This may be due to the air present in the central lumen and the better contact with the matrix. The sudden increase of dielectric constant and loss values in the 20UTC was due to the catastrophic increase in the polar groups and introduction of amorphous phase in the matrix which increased the conductivity in the composites. From the above study, it can be concluded that the composite containing 15% volume fraction of fiber provides the best combination for mechanical strength and electrical properties. Therefore 15% fiber volume fraction in the epoxy matrix has been taken into consideration for further study.

References

1. Lightsey G R, Organic fillers for thermoplastics. Polym Sci Technol, 17, Plenum Press, New York (1983).
2. Prasad MS, Venkatesha CS, Jayaraju T, Experimental Methods of Determining Fracture Toughness of Fiber Reinforced Polymer Composites under Various Loading Conditions. J Miner Mater Char Engg, 10, (2011) 1263-1275.
3. Varghese S, Kalaprasad G, Thomas S, Prasannakumari L, Koshyh P, Pavithran C, Influence of interfacial adhesion on the mechanical properties and fracture behaviour of short sisal fiber reinforced polymer composites. Eur Polym J, 32, (1996) 1243-1250.
4. Kristiina O, Lennart W M, Lars A. Berglund, Romildo DTF, Morphology and Mechanical Properties of Unidirectional Sisal–Epoxy Composites. J Appl Polym Sci, 84, (2002) 2358–2365.
5. Monette L, Anderson M, Grest GS, Effect of volume fraction and morphology of reinforcing phases in composites. J Appl Phys, 75, (1994) 1155.
6. Ghosal R, Reena G, Krishna RA, Raju BHL, Effect of fiber volume fraction on the tensile strength of Banana fiber reinforced vinyl ester resin composites, Int J Adv Engg Sci Technol, 4, (2011) 89-91.
7. Mishra S, Mohanty A K, Drzal LT, Misra M, Parija S, Nayak S K, Tripathy SS, Studies on mechanical performance of biofibre/glass reinforced polyester hybrid composites. Compos Sci Technol, 63, (2003) 1377–1385.
8. Zhong JB, Lv J, Wei C, Mechanical properties of sisal fibre reinforced urea-formaldehyde resin composites. Express Polymer, 1, (2007) 681–687.
9. Pothan LA, George CN, Jacob M, Thomas S, Effect of Chemical Modification on the Mechanical and Electrical Properties of banana fiber polyester composite J Compos Mater, 41, (2007) 2371-2386.
10. Ghali L, Msahli S, Zidi M, Sakli F, Effects of Fiber Weight Ratio, Structure and Fiber Modification onto Flexural Properties of Luffa-Polyester. Adv Mater Phys Chem, 1, (2011) 78-85.

11. Ismail H, Edyham MR, Wirjosentono B, Bamboo fibre filled natural rubber composites: the effects of filler loading and bonding agent. Polym Test, 21, (2002) 139–144.
12. Yao W, Li Z, Flexural behavior of bamboo-fiber-reinforced mortar laminates. Cem Concr Res, 33, (2003) 15–19.
13. Inul AN, Ishak A, Prasanna K L, Koshyh P, Pavithran C, Effect of Fiber Loading and Compatibilizer on Rheological, Mechanical and Morphological Behaviors. Opn J Polym Chem, 2, (2012) 31-41.
14. Brahamakumar M, Pavithran C, Pillai RM, Coconut fiber reinforced polyethylene composites: effect of natural waxy surface layer of the fiber on fiber/matrix interfacial bonding and strength of composites. Compos Sci Technol, 65, (2005) 563-569.
15. Zaman I, Ismail AI, Awang MK, Influence of fiber volume fraction on the tensile properties and dynamic characteristics of the coconut fiber reinforced composites. J Sci Technol, 1, (2010) 55-71.
16. Hong CK, Wool RP, Development of a bio-based composite material from soybean oil and keratin fibers. J Natural Fibres, 1, (2004) 83–92.
17. Folk MJ, Hardwick ST, The mechanical properties of glass/polypropylene multilayer laminates. J Mater Sci, 52, (1990) 2598-2606.
18. Jacob M, Varugese KT, Thomas KT, Dielctric characterstics of sisal–oil palm reinforced natural rubber biocomposites. J Mater Sci, 41, (2006) 5538-5547.

Chapter 4

Influence of Dewaxing

4.1. Introduction

The study of natural fiber reinforced polymer composite (NFRPC) materials is a fast growing area of research. This rapidly expanding field is generating many exciting new high-performance materials with novel properties. Easy processing, environment friendly nature, low cost, excellent insulation properties, light weight have made NFRPC a smart material with versatile applications like in automobiles, aerospace, injection molded products, coatings, adhesives, fire-retardants, packaging materials, consumer goods etc. [1, 2]. Insulation resistance and dielectric strength of ligno-cellulosic fibers give an indication of their current leakages at certain voltages, moisture content and stability under electric fields [3]. Now days composite as a dielectric is becoming more popular and studies of electrical properties of natural fiber reinforced polymer composites are therefore very important. The study of electrical properties of such materials enable us to know the various electrical applications of these materials such as in suspension insulators, switch boards,

antistatic applications etc. [4, 5]. Among all the natural fibers, Sisal fiber in chopped, continuous and woven forms has been found to be most suitable for application in polymer composites because of its superior properties like high cellulose content, high tensile strength and yet cheaper in price [6].

Sisal like any other lingo-cellulosic fibers acts as a reinforcing material in the polymer composites. Surface of sisal fiber can be modified chemically and physically with an aim to reduce moisture sensitivity so as to increase the adhesion between fiber and matrix [7, 8]. Chemical treatment of Natural fiber often causes defibrillization, which also contributes to the increased reinforcing efficiency of the fibers in the composite [9]. The removal of surface impurities which is a part of purification is advantageous for fiber-matrix adhesion as it facilitates both mechanical interlocking and the bonding reaction at the interface. In this regard dewaxing is a very suitable conventional technique [10].

The present chapter investigates the effect of dewaxing on the structural, vibrational properties of sisal fiber including electrical and mechanical properties of short sisal fiber reinforced epoxy composite. An attempt has also been made to correlate the macro molecular parameters, structural, vibrational properties of the fiber to the mechanical and electrical properties of the polymeric composite system.

4.2. Results and Discussions

4.2.1 SAXS Analysis

The slit smeared SAXS intensity data with proper background correction are shown in Fig 4.1. As the intensity data collected are mixed with background scattering, proper background correction is essential for the quality analysis. The SAXS intensity data attain a stable pattern after 0.6 cm, hence the intensity at 0.6 cm is treated as background scattering intensity for untreated (UT) and dewaxed (DE) fiber samples which is subtracted from the observed intensity. Five background corrected intensities near the origin are fitted to the following Gaussian curve by least square technique.

$$\tilde{I}(x \to 0) = p \cdot \exp(-qx^2) \qquad (4.1)$$

Here, $\tilde{I}(x)$ is the smeared out intensity and x is the positions co-ordinate of the scattered intensity from the centre of the primary beam, where x=2$a\theta$ and 2θ is the scattering angle. The values of constants p and q are used to extrapolate the scattering curve up to x=0. The extrapolation is necessary as it is practically impossible to get the scattering curve up to x=0. The extrapolated points are indicated by hollow symbols in the inset graph of Fig.4.1. These background corrected intensities are required to find out the macromolecular parameters in subsequent analysis. The method of extrapolation is shown in Fig. 4.1(inset) does not disturb the position and height of the 1st subsidiary maxima of the one dimensional correlation function $C_1(y)$ [11]. The symmetry of the intensity pattern confirms the isotropic behavior of the sisal fiber. Previous works on the lignocellulosic fiber suggest that the areas of cellulose production near the protoplasm are related to each other in some

order. Hence form the cellulose molecules with some order to each other with high degree of orientation. This leads to the kind of isotropic lamellar structure.

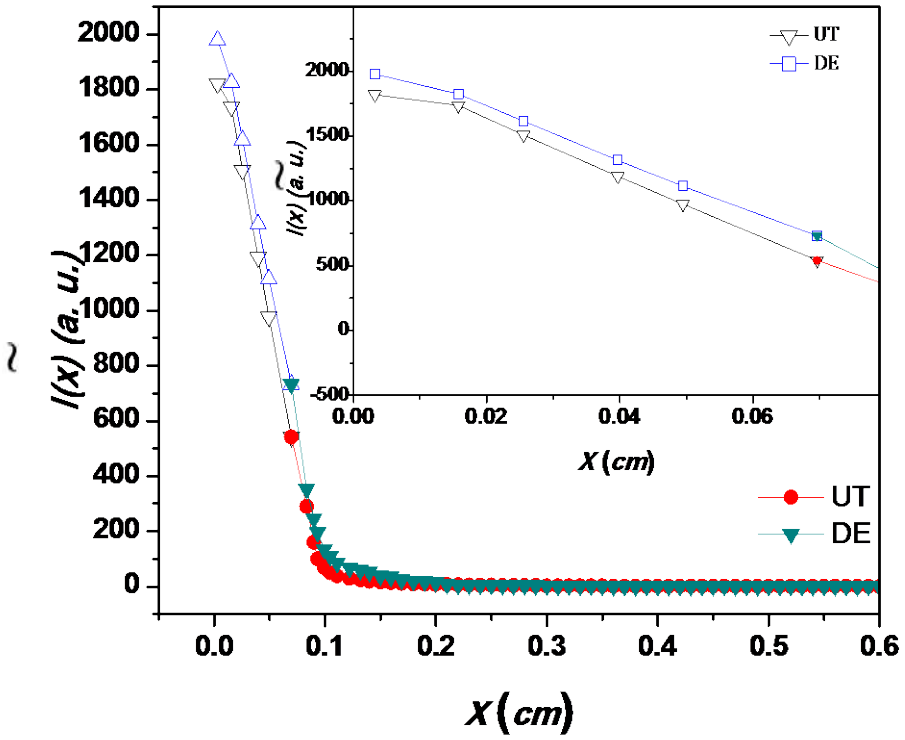

Fig. 4.1: Background-corrected, smeared-out scattering curves for raw and dewaxed sisal fibers. **Inset:** Magnified view of the initial scattering curves to show the extrapolated data.

The 3D correlation function $C(r)$ which contains the valuable information regarding macromolecular structural parameter is defined as the ratio of the average of the product of the electron density across the two ends of a virtual rod moving inside the particle to the average of the product when the length reduces to zero at

the origin. It gives information about the nature of the phases present in the particle. The above function $C(r)$ is governed by the following relation.

$$C(r) = \frac{\int_0^\infty x\tilde{I}(x) J_0\left(2\pi r x / \lambda a\right) dx}{\int_0^\infty x\tilde{I}(x) dx} \qquad (4.2)$$

Here J_0 is the Bessel function of Zero order first kind. The value of $C(r)$ normalizes to unit at the origin and decreases to zero when r attains the boundary of the particle i.e. $r=R$, corresponding to the maximum displacement. This correlation function contains the information about the particle in three dimensions hence known as 3D correlation function.

The one-dimensional correlation function $C_1(y)$ can be visualized as a measuring rod of length 'y' perpendicular to the layers which moves along the y-direction. In the present study there is significant contribution of $C_1(y)$ as sisal is having the lamellar structure. The expression for the one-dimensional correlation function $C_1(y)$ for layer structure in terms of x is expressed as

$$C_1(y) = \frac{\int_0^\infty x\tilde{I}(x)[J_0(z) - zJ_1(z)] dx}{\int_0^\infty x\tilde{I}(x) dx} \qquad (4.3)$$

Where J_1 is the Bessel function of first order first kind. The isotropic lamellar structure of all the investigated fiber samples justifies taking of one dimensional correlation, $C_1(y)$ function [10]. $C_1(y)$ of all the fibers for various values of y are computed and the plots are given in the Fig. 4.2. According to Vonk [12] the position

of first subsidiary maximum in the one-dimensional correlation function, gives the value of the average periodicity transverse to layers (D).

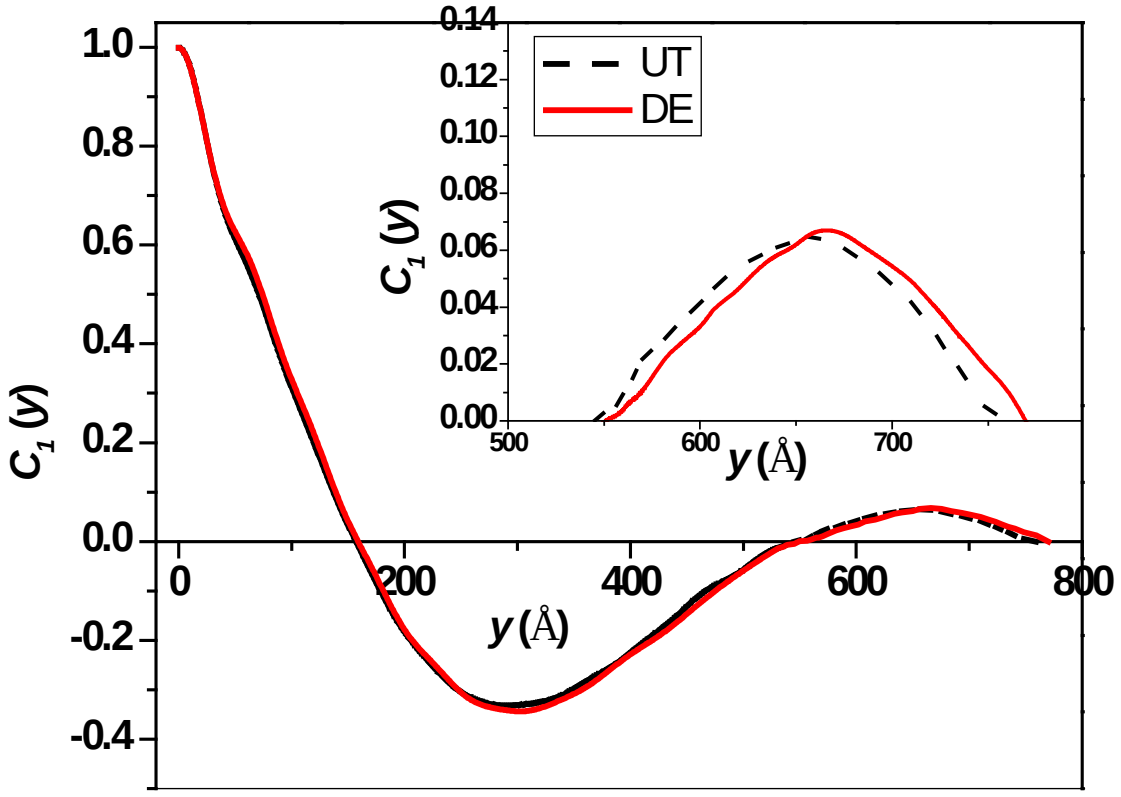

Fig. 4.2: Variation of one dimensional correlation function C_1 (y) against y for the raw and dewaxed fibers. **Inset:** First subsidiary maximum of the one-dimensional correlation functions.

Inside the fiber, the matter phase and void phase are thought to be arranged in terms of lamellar stack and each lamellar having some periodicity displays information about the specific inner surface area (S/V) of those lamellar stacks. It is also defined as phase boundary per unit volume of the dispersed phase.

$$S/V=2/D \qquad (4.4)$$

The values of D (average periodicity transverse to the layer correspond), specific inner surface area (S/V) calculated from each curve of the Fig. 4.2 has been listed in Table 4.1. The value of D is found to be higher for the DE fiber sample with lesser specific inner surface area than UT.

The $C(r)$ which has same nature as that of $C_1(y)$ are shown in Fig.4.3. The damping oscillatory behavior of the $C(r)$ for large values of r shows the non-ideal two phase behavior of all the fiber samples. Another important parameter that is derived from the $C(r)$ is the length of coherence (l_c) which gives the information about the distribution of electron across the boundary of the particle.

$$l_c = 2\int_0^\infty C(r)dr \qquad (4.5)$$

According to Ruland [11] and Vonk [12] the information about the non-ideal two phase system can be obtained from the parameter defined as 'R' which was later modified by Mishra et al. [13] is as follows:

$$R = \frac{3}{2}\left(\frac{2\pi}{\lambda a}\right)^2 \frac{\int_0^\infty x^3 \tilde{I}(x)dx}{\int_0^\infty x\tilde{I}(x)dx} \qquad (4.6)$$

Where 'R' is the corrugation at the phase boundary and 'a' is the sample to detector distance. If R goes to infinity the system is the ideal but if it has some finite value i.e. the system is non-ideal two phase. The small but finite positive values of R in Table 4.1 indicate that the electron density gradient is finite for all the investigated samples. Hence all the fiber samples are found to be non-ideal two phase system [12].

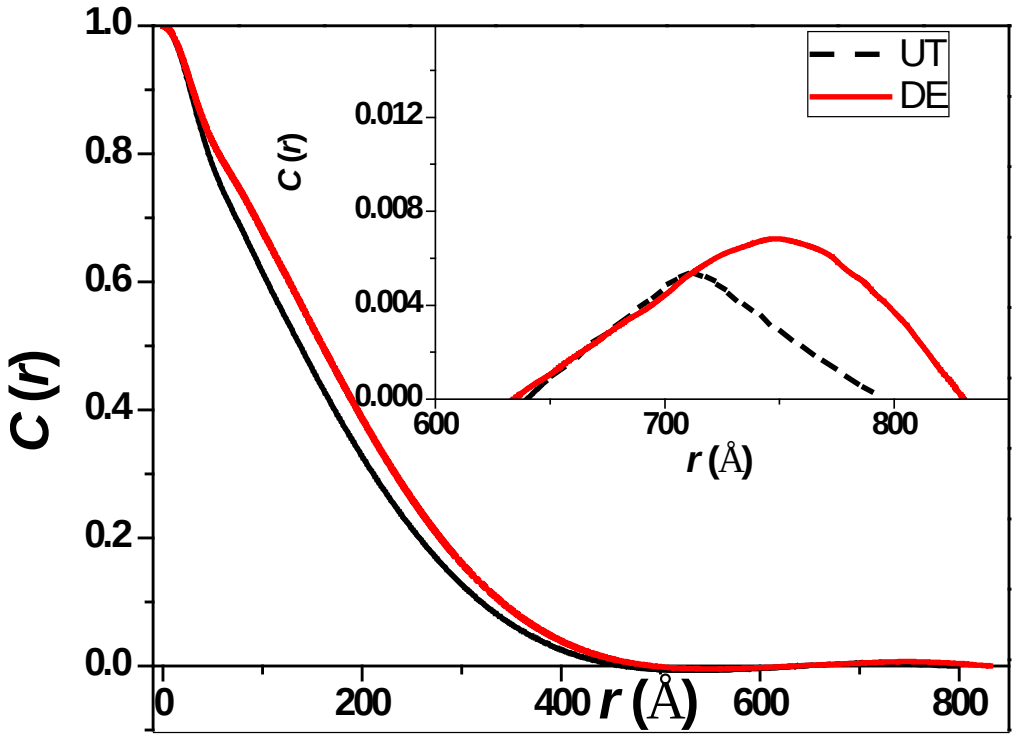

Fig. 4.3: Variation of three dimensional correlation function $C(r)$ against r for raw and Dewaxed fibers. **Inset:** First subsidiary maximum of the three-dimensional correlation functions.

From Table 4.1 it is found that the values of $\bar{l}_1$ and φ_1 are higher for DE fiber samples, but the values of φ_2 and $\bar{l}_2$ are least for the same sample. Where $\bar{l}_1 = 4\varphi_1(V/S)$ and $\bar{l}_2 = 4\varphi_2(V/S)$. The higher value of $\bar{l}_1$ and φ_1 for the sample DE shows the increment in the matter phase. It may be due to the removal of the impurities and the waxy material from the inter-fabrillar regions of the fiber. The cellulose micro fibril gets rearranged properly decreasing the volume fraction of the void content 'φ_2'. The decrease in void content increases the mechanical properties of the fiber

[13-15]. The transversal lengths of matter and void phases for a two-phase three-dimensional system were derived by Mittelbach and Porod, is given by the relation

$$1/\bar{l}_r = 1/\bar{l}_1 + 1/\bar{l}_2 \qquad (4.7)$$

Where $\bar{l}_r$ = the range of inhomogeneity. The decrease in the value of $\bar{l}_r$ in case of DE fiber indicates the decrease in the disorder inside the fiber due to the rearrangement of cellulose chains inside the fiber [10]. In order to find out the nature of the phase of the untreated and the treated fibers, logarithmic plots between the *x* and $\tilde{I}(x)$ values are drawn in Fig 4.4. The slopes of all the plots are found to be negative, which is ~ -3. This suggests that both the untreated and treated samples are non-ideal, two phase system [15].

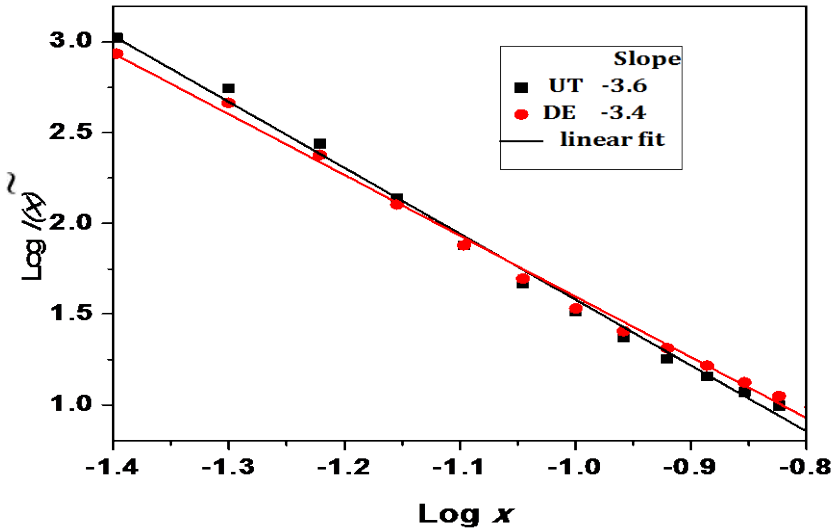

Fig. 4.4: Double logarithmic plots for raw and dewaxed fiber.

In the present study the width of transition layers are calculated by two different methods as described by Ruland and Vonk. Fig. 4.5 displays the typical

Ruland plots for all the investigated fibers, which is a graph of $\tilde{I}(x)\cdot x$ vs. x^{-2}. The Ruland plots are obtained by taking 40 background corrected intensities. Linear fitting of each curves are carried out on 15 extreme points at the tail region of the corresponding curve. The functional relationship between $\tilde{I}(x)\cdot x$ and x^{-2} takes the form of

$$\tilde{I}(x)\cdot x = \frac{\pi C}{2\cdot(\lambda a)^3\cdot x^{-2}} - \frac{\pi^3 C}{3\cdot(\lambda a)\cdot E^2} \qquad (4.8)$$

Where C is the probability constant.

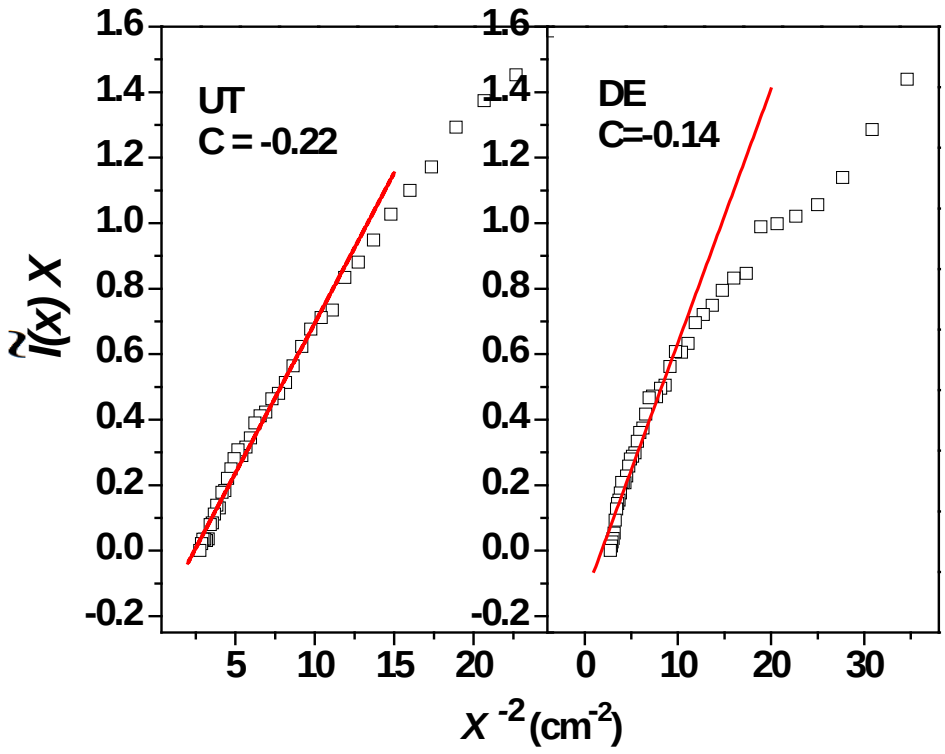

Fig. 4.5: Ruland plots $\tilde{I}(x)x$ vs. x^{-2} for raw and Dewaxed sisal fibers.

The standard deviations (σ) of the intensities are well within the permissible range showing the accuracy of the data collection. The width of transition layer, E_v (Vonk

method) is calculated by normalizing $C(r)$ to unity at the start of the real space. According to Vonk method, $E = -\frac{4}{R}\left[\frac{dC(r)}{d(r)}\right]_r = E_v$

(4.9)

The plot between $-\frac{4}{R}\left[\frac{dC(r)}{d(r)}\right]$ vs. r is shown in Fig. 4.6. The straight line equidistance from both the axes has been drawn and the point of intersection with the curve gives the values of E_v [12] for different fiber which are compiled in Table 4.1. The values of E_r that are calculated from Fig.4.5 are in close agreement with the values of E_v evaluated from Fig. 4.6. Hence, it justifies the accuracy of our analysis.

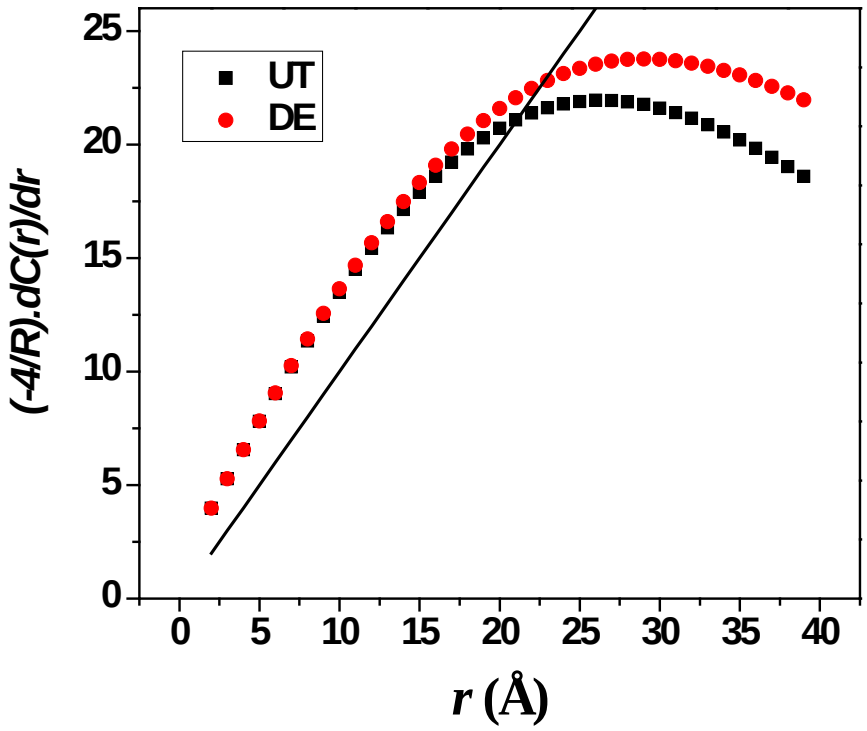

Fig. 4.6: The curves showing the variation of $\left(-\frac{4}{R}\right)\frac{dC(r)}{dr}$ against r for the raw and dewaxed sisal fibers.

Table 4.1: Various macromolecular parameters of raw and dewaxed sisal fibers

Sample	R (10^{-4} Å^{-2})	D (Å)	S/V (10^{-3} Å^{-1})	E_v (Å)	E_r (Å)	Φ_1	Φ_2	$\bar{l}_1$ (Å)	$\bar{l}_2$ (Å)	$\bar{l}_r$ (Å)	l_c	$2E_v/D$ (%)	σ
UT	8.83	654	3.06	21.08	19.80	82.60	17.40	1080.42	227.58	187.98	351.10	6.45	0.013
DE	8.98	666	3.00	22.79	19.98	83.93	16.07	1117.92	214.08	179.67	330.04	6.84	0.001

derived from SAXS study.

Finally the above SAXS computational analysis on the sisal fiber confirms the fibers to be in the non-ideal two phase system. DE fiber is found to have least void content and disorder.

4.2.2 XRD Study

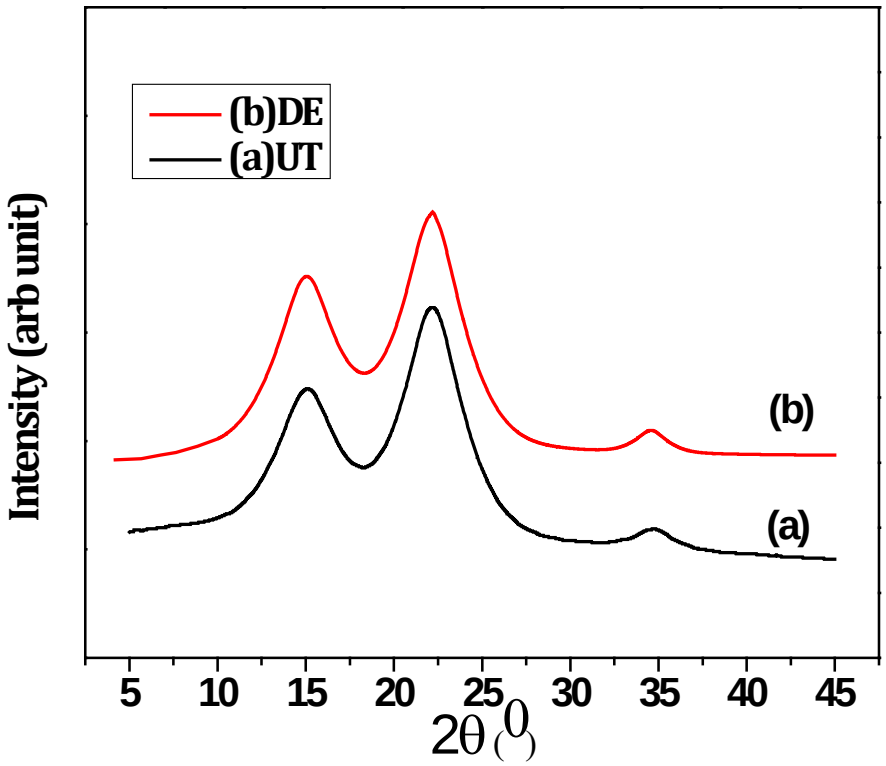

Fig. 4.7: XRD patterns of raw and dewaxed sisal fiber.

The XRD patterns of both dewaxed and raw sisal fibers are shown in Fig. 4.7. The full width at half maximum (FWHM) of the diffraction peaks of both raw and dewaxed samples are analyzed. The $K_{\alpha 2}$ components of the peaks are stripped from the data by Philips Xpert High score software. The diffractograms of both dewaxed and raw sisal fiber display a well-defined main peak around 2θ = 22.5°, which is the characteristic of cellulose I [16]. Table 4.2 shows the crystallite size and degree of crystallinity of dewaxed and raw sisal fibers. It can be seen, after dewaxing the degree of crystallinity of the fiber has been increased, which may be due to the reduction of lignin and hemicellulose content of the sisal fiber and the rearrangement of the cellulose chain. The changes in the crystalline peaks in Fig. 4.7 of dewaxed sample denote the changes in the crystalline region. The increasing percent of crystalline peak area relative to the whole diffraction area suggests an improvement in the degree of crystallinity of the dewaxed fiber. The increase in the dimension and size of the crystallites may be due to the decrease in crystal distortion and defects [17].

Table-4.2: Crystallite size and degree of Crystallinity of raw and dewaxed sisal fibers.

Fiber	Degree of crystallinity (%)	Crystallite size (Å)	Density(g/cc)
UT	52.11	29.19	1.32
DE	53.56	31.05	1.39

4.2.3 FTIR Study

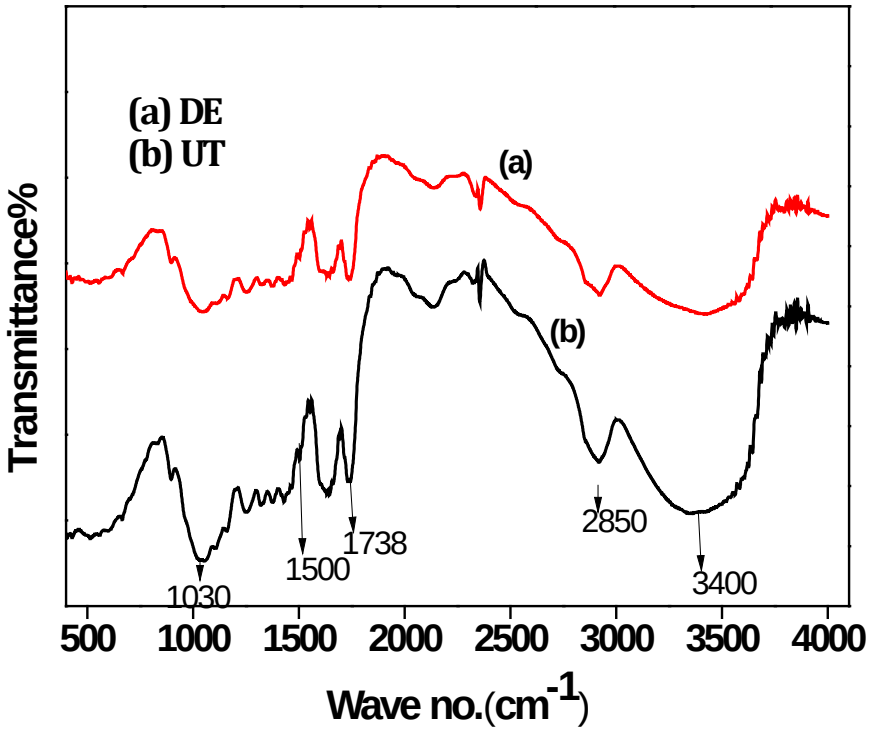

Fig. 4.8: FTIR spectra of raw and dewaxed sisal fiber.

Fig. 4.8 shows the FTIR spectra of dewaxed and raw sisal fiber. The broad intense peak at ~3400 cm^{-1} in raw sisal fiber is due to the O–H stretching for hydrogen-bonded hydroxyl group present in polysaccharide. However, this peak gets narrower and less intense in the case of dewaxed fiber because of the reduction of the O-H group which is further confirmed by the decrease in absorbance intensity ratio. The weak peak which is at ~1738 cm^{-1} in raw sisal fiber is due to the presence of hemicelluloses and can be assigned to the C=O stretching. It is found that the absorbance intensity ratio of this peak decreases after dewaxing, which suggests that

dewaxing is responsible for the partial removal of hemicelluloses in the fiber. Similar is the case for the wax peak observed at ~2850 cm^{-1} in dewaxed fiber which is reduced in comparison to the raw fiber. This indicates that weaving size potato wax has been removed partially from the sisal fiber. It appears that during dewaxing substantial portion of uronic acid, a constituent of hemicelluloses and xylene has been removed, resulting in reduction of this peak. The weak broad peak that occurs in raw sisal fiber ~ 1600–1650 cm^{-1} is associated with water absorbed in cellulose [18]. Here also the absorbance intensity ratio decreases due to dewaxing. The aromatic ring of lignin band (~1505 cm^{-1}) shows a decreased absorbed intensity ratio after dewaxing which confirms the reduction of lignin content in the dewaxed fiber [19].

The density of the raw fiber is found to be ~1.32 g/cc whereas for the dewaxed fiber it came out to be ~1.39 g/cc. The increase in density of the dewaxed fiber may be due to the partial removal of the wax and impurities. The rearrangement of the fibrils in a more compact manner may also be leading to the closer packing of the cellulose chain structure after dewaxing.

4.2.4 Morphological Study

The longitudinal morphologies of raw and dewaxed sisal fibers are shown in the Fig. 4.9 (a) & (b) respectively. It is observed that the surface roughness of the fibers has been increased significantly after dewaxing [20]. Again, because of the removal of the surface impurities and cementing material like lignin and hemicelluloses, separation of the ultimate cells has increased. This leads to the increase in effective surface area of the fiber to become more compatible with the

matrix. The partial removal of waxy material in dewaxed fiber has also increased the inter-fabrillar region and gives a rough morphology. Fig. 4.9 (c) & (d) show the fractured surfaces of both UTC (untreated fiber reinforced composite) and DEC (dewaxed fiber reinforced composite) respectively. The mechanism of failure in case of UTC is clear from the fractured surface of the composite. The adhesion between fiber and matrix is poor, which is shown by gap around the fiber at the interface whereas in DEC the fiber matrix adhesion is shown by fiber breakage rather than fiber pullout.

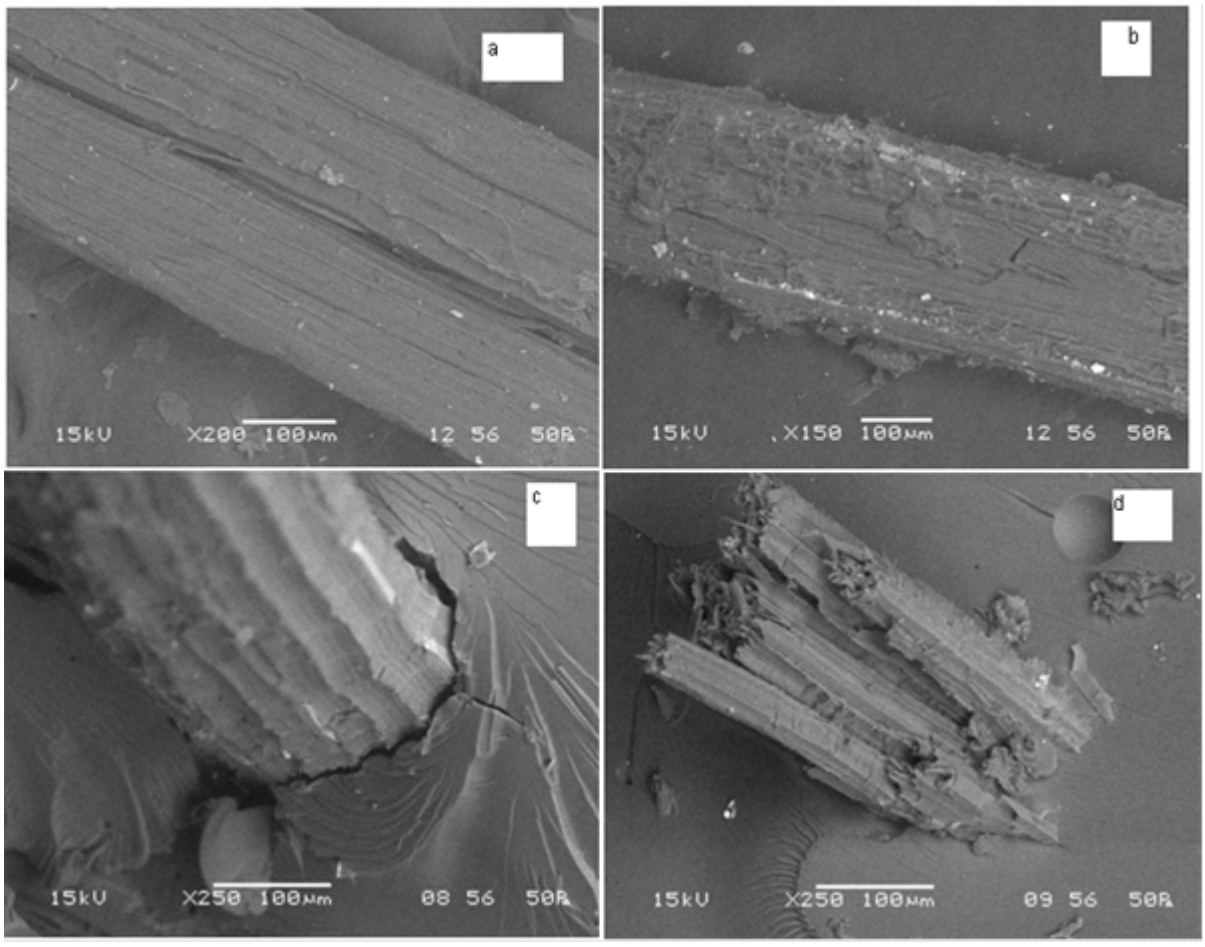

Fig. 4.9(a) & (b): Longitudinal section of Raw sisal fiber and Dewaxed sisal fiber respectively. (c) & (d): Fractured surface of UTC and DEC respectively.

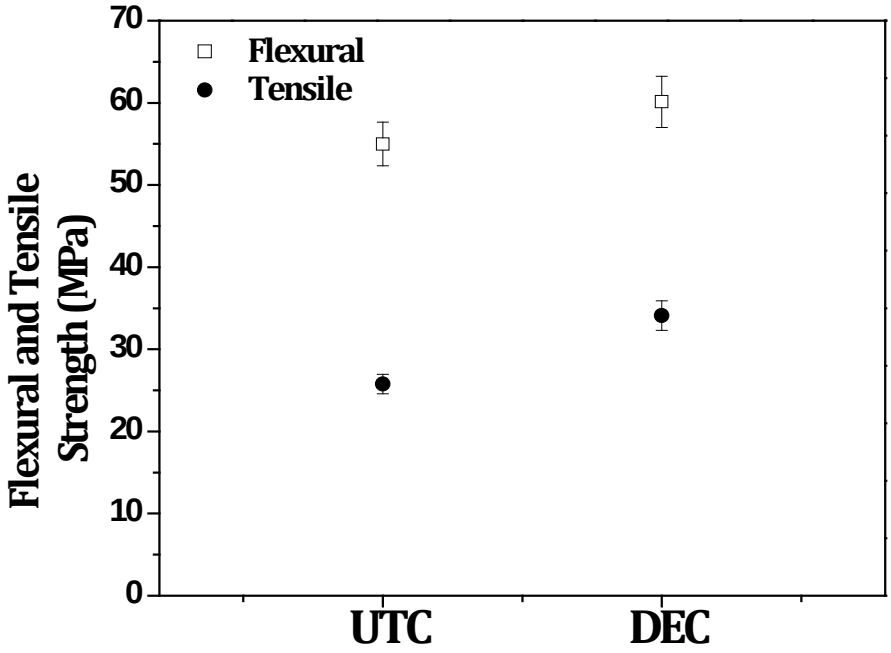

Fig. 4.10: Flexural strength and tensile strength of UTC and DEC.

Fig. 4.10 shows the flexural strength and tensile strength of both UTC and DEC. In both the cases the strength of DEC is found to be higher than the UTC. It is well known that for fiber reinforced composites, the interfacial zone plays a leading role in transferring the load between fiber and matrix which consequently affects the mechanical properties such as strength [21-23]. This finding demonstrates that flexural failure depends mainly on the fiber/matrix adhesion. The increased value of flexural strength and tensile strength in case of DEC may be due to the increase in effective surface area available for contact with the matrix [24]. The removed cementing material of the dewaxed fiber is replaced by epoxy during composite

formation which creates a reactive bond between them with increased static force because of the rough surface of the fiber. Hence, from the mechanical point of view, the dewaxing of fibers is beneficial since it reinforces the fiber/matrix load transfer.

4.2.5 Dielectric Study

Fig. 4.11 & 4.12 shows the frequency dependence of ε_r of both UTC and DEC respectively in a temperature range from 75^0C-200^0C, whereas the inserted plot in the above figures shows the frequency dependence of tanδ in the same specified range of temperature. It is found that in both cases with increase in frequency the value of ε_r as well as tanδ decreases. The change of ε_r and tanδ at lower frequency region is higher than at very high frequency. Generally, the dielectric constant (ε_r) of a polymeric material depends mainly on interfacial and dipole polarization.

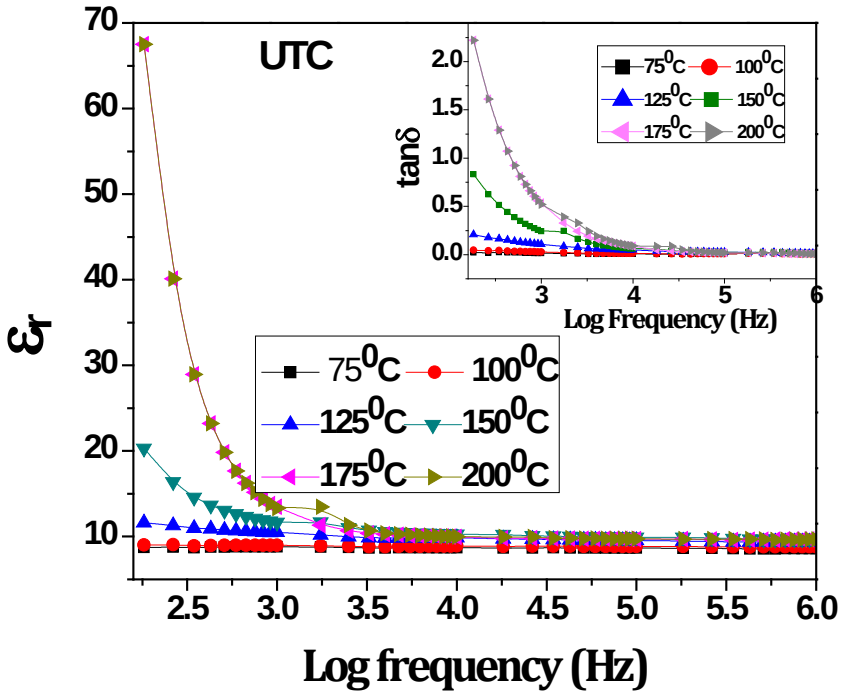

Fig. 4.11: Variation of ε_r with frequency of UTC. **Inset:** Variation of tanδ with frequency of UTC.

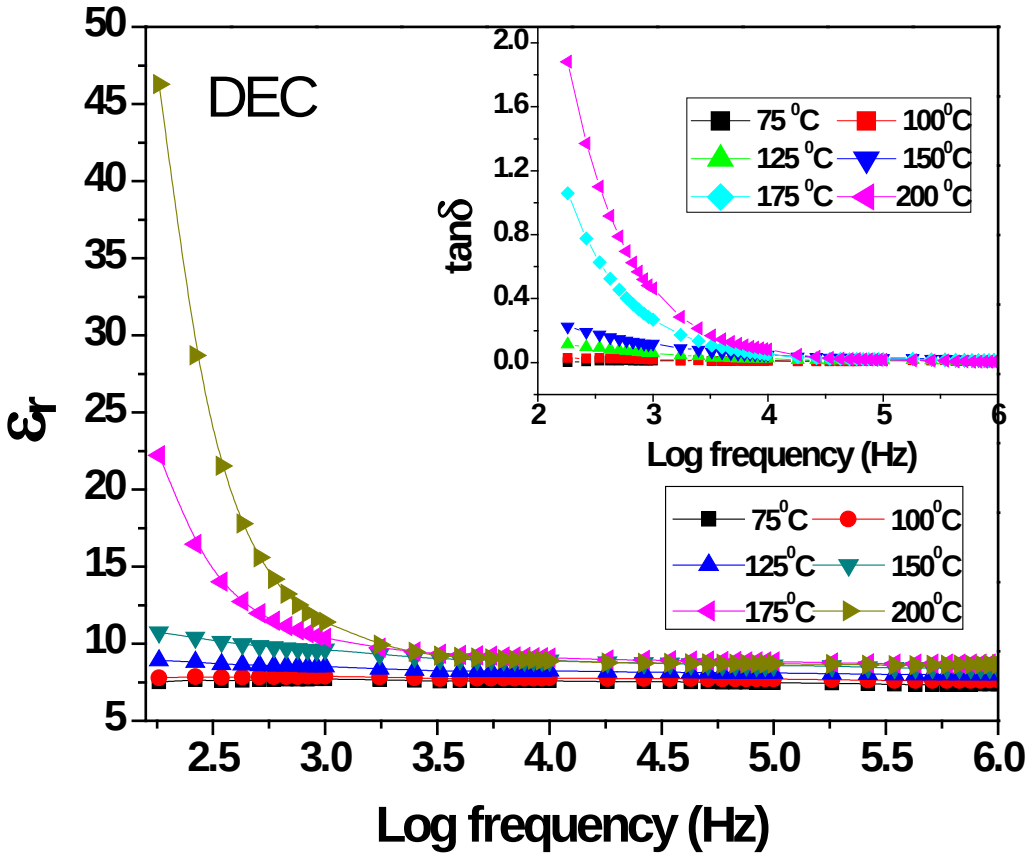

Fig. 4.12: Variation of ε_r with frequency of DEC. **Inset:** Variation of tanδ with frequency of DEC.

The interfacial polarization is prominent in heterogeneous material and is highest at lower frequency. Hence, the higher values of ε_r and tanδ at low frequency can be explained in terms of interfacial polarization and the free motion of dipoles within the material which is connected to ac conductivity relaxation. It is found that the value of ε_r for the DEC has been decreased in comparison to the UTC. The overall dielectric properties in a polymeric composite are the contribution of both the crystalline and amorphous regions. Usually, the amorphous regions makes the major

contribution to both ε_r and tanδ. As a result, ε_r and tanδ decreases with an increasing degree of crystallinity [25].

Fig. 4.13 & 4.14 shows the temperature dependence of ε_r of both UTC and DEC at four different frequencies whereas the inserted plot in the above figures show the temperature dependence of tanδ at specified frequencies.

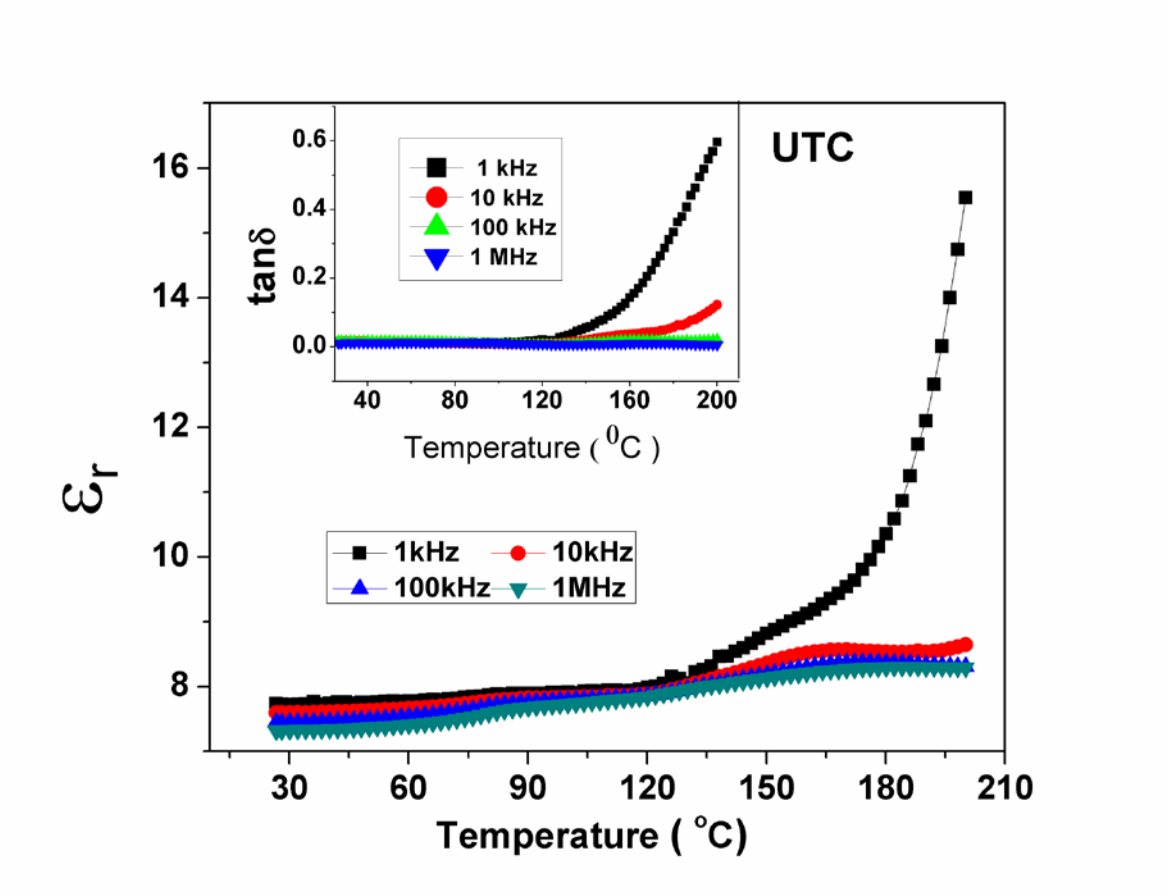

Fig. 4.13: Variation of ε_r as a function of temperature for the UTC. **Inset:** Variation of tanδ as a function of temperature for the UTC.

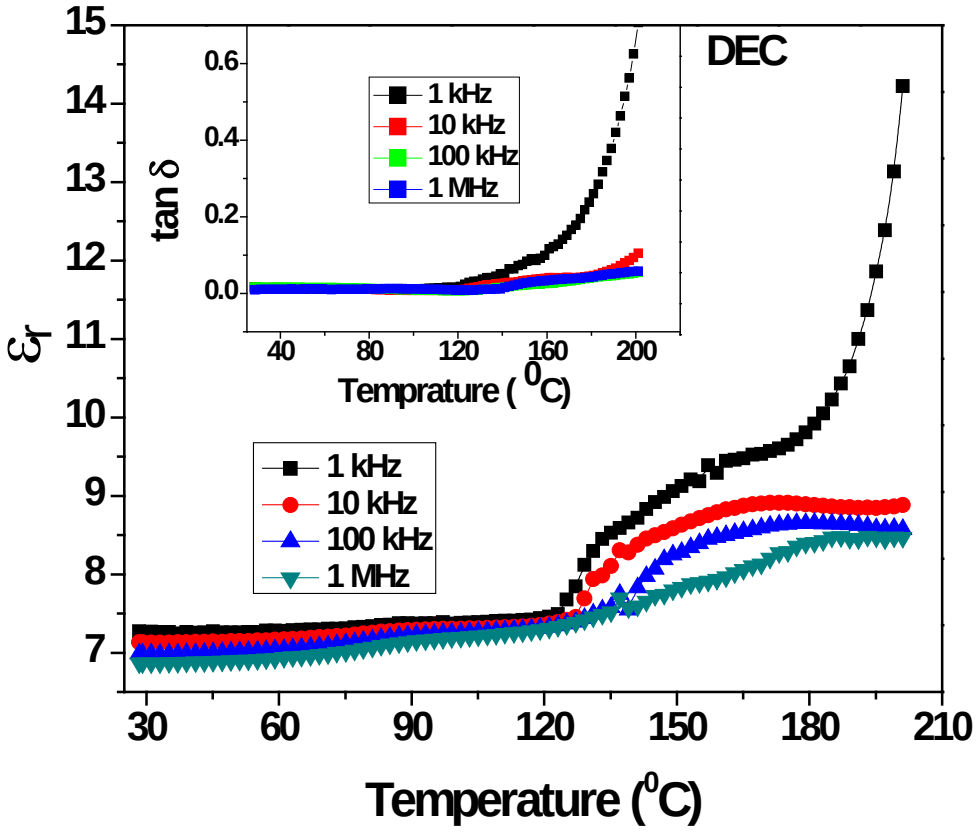

Fig. 4.14: Variation of ε_r as a function of temperature for the DEC. **Inset:** Variation of tanδ as a function of temperature for the DEC.

The room temperature (RT) ε_r values of UTC and DEC at 1 kHz frequency are found to be ~ 7.81 and 7.29, whereas the tanδ values are ~0.015 and 0.013 respectively. It is observed that with the rise in temperature, ε_r and tanδ value for both UTC and DEC increases. An exothermic peak is observed in the plot of ε_r Vs temperature ~ 130^{0}C at 1 kHz frequency in both samples which confirms the presence of a relaxation process. This relaxation is named as α relaxation (glass–rubbery transition). Further with increase in frequency this relaxation shifted towards higher temperature side. The relatively high values of ε_r and tanδ at high

temperature is attributed to the enhanced mobility of large parts of the polymer chains and the co-operating contribution of interface polarization (weak Maxwell-Wagner-Sillars (MWS)) effect in the composite systems which arise due to additives, plasticizers etc. in polymer composite.

4.2.6 Conductivity Study

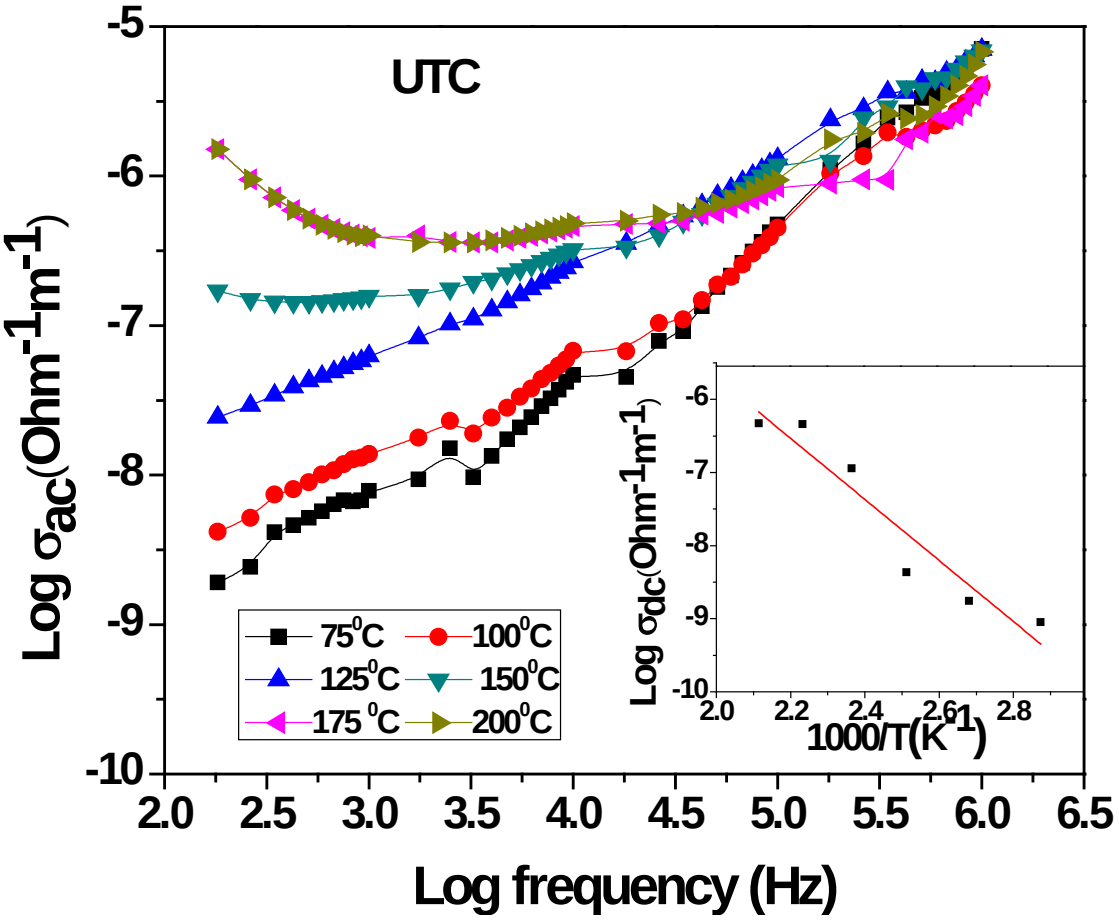

Fig. 4.15: Frequency dependent ac conductivity for the UTC. **Insert:** Variation of dc conductivity against 1000/T for the UTC.

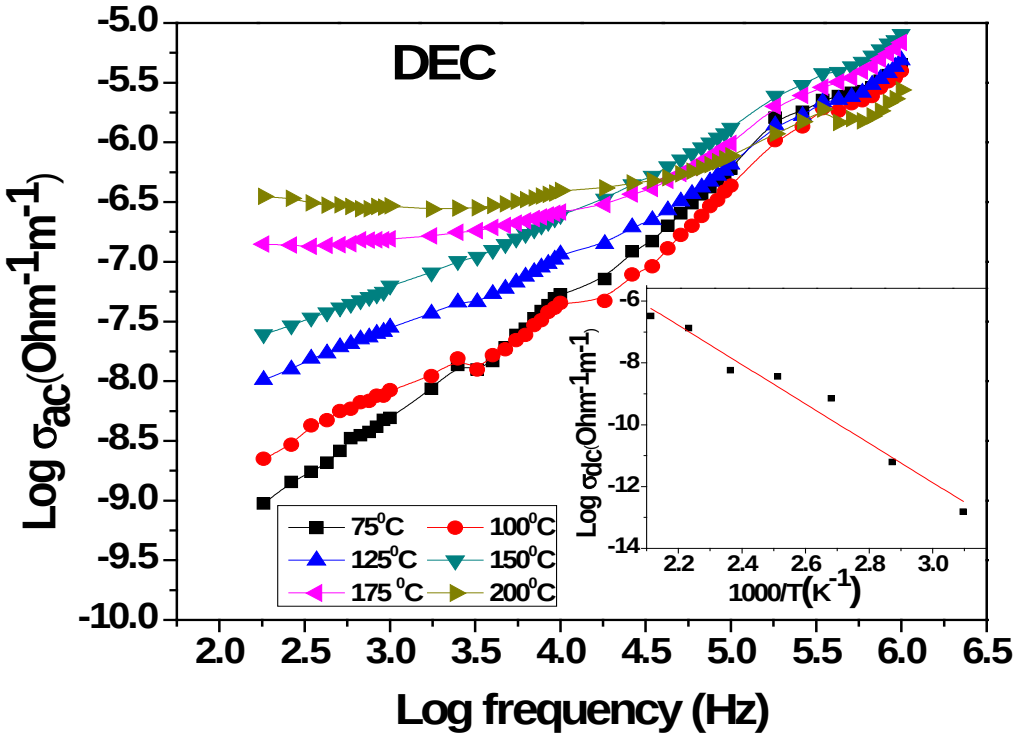

Fig. 4.16: Frequency dependent ac conductivity for the DEC. **Inset:** Variation of dc conductivity against 1000/T for the DEC.

The frequency dependence of ac conductivity ($\log\sigma_{ac}$) of UTC and DEC at different temperatures in a wide range of frequencies in logarithmic scale are shown in Fig. 4.15 & 4.16 respectively. The σ_{ac} was calculated using an empirical relation i.e.

$$\sigma_{ac} = \omega\varepsilon_r\varepsilon_0\tan\delta \qquad (4.10)$$

Where ε_0 is the permittivity of free space, and ω is the angular frequency. The σ_{ac} patterns show a frequency independent behavior in the low frequency region and exhibits dispersion at higher frequencies. This behavior satisfies the universal power law:

$$\sigma(\omega) = \sigma_0 + A\omega^n \qquad (4.11)$$

Where σ_0 is the dc conductivity, A is the pre-exponential factor and n is the fractional exponent, whose value lies in between 0 and 1. It is observed that σ_{ac} for DEC and UTC increases with the increase in temperature and that confirms the negative temperature coefficient of resistance behavior. This behavior also suggests that the electrical conduction in the sample is increasing at the higher temperature which may be due to the increase in the segmental mobility of the polymer molecules. It can also be seen that ac conductivity decreases with decrease in frequency and becomes independent of frequency after a certain limit. Dc conductivity (σ_{dc}) has been calculated by extrapolating this towards the lower frequency side, which follows Arrhenius law given by:

$$\sigma_{dc} = \sigma_0 \exp [-E_a/K_\beta T] \qquad (4.12)$$

Where E_a is the activation energy of conduction and T is the absolute temperature. The inserted plot in Fig. 4.15 & 4.16 shows the variation of dc conductivity ($\log\sigma_{dc}$) against 10^3/T. The nature of variation is almost linear over a wide temperature range. The slope of the linear least squares fitting of the data gives the values of activation energy (E_a) ~ 0.82 eV and 1.41 eV for UTC and DEC, respectively. The lower value of activation energy is obtained in case of UTC may be due to the decrease in the height of the potential barrier between two orientational conformation states. As the potential barrier between two orientational conformation states in case of UTC is lower than the DEC, the movement of the molecules becomes relatively easier, which in turn increases the values of ε_r, tanδ and σ_{dc} in the sample.

4.2.7 Modulus Spectroscopy Study

Impedance spectroscopy has been considered as a powerful technique for characterization of dielectric materials. The use of modulus spectroscopy plot is particularly useful for separating the components with similar resistance but different capacitance. In this study, we have adopted the formalism of electric modulus in order to minimize the effect of σ_{dc} and to suppress the electrode effect [26, 27]. The complex electric modulus (M*) has been calculated from the impedance data using the following relation: $M^* = M' + JM'' = 1/\varepsilon^* = J\omega C_0 Z^*$, where $M' = \omega C_0 Z''$, $M'' = \omega C_0 Z'$, ω (angular frequency) $= 2\pi f$, C_0 = geometrical capacitance of the sample = $\varepsilon_0 (A/t)$, ε_0 = permittivity of free space, A = area of the electrode surface and t thickness of the sample.

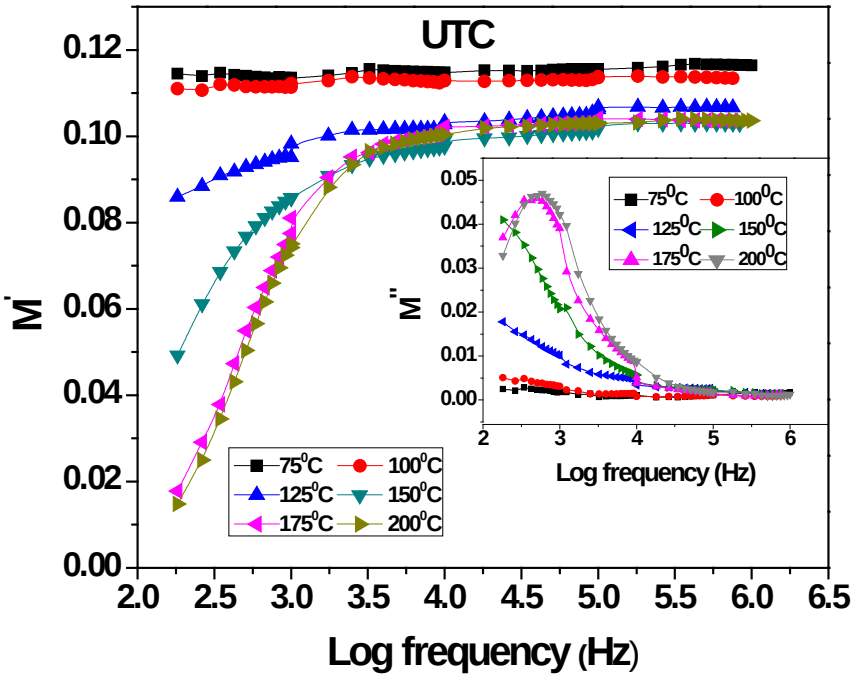

Fig. 4.17: Variation of M' as a function frequency for the UTC. **Inset:** Variation of M'' as a function frequency for the UTC.

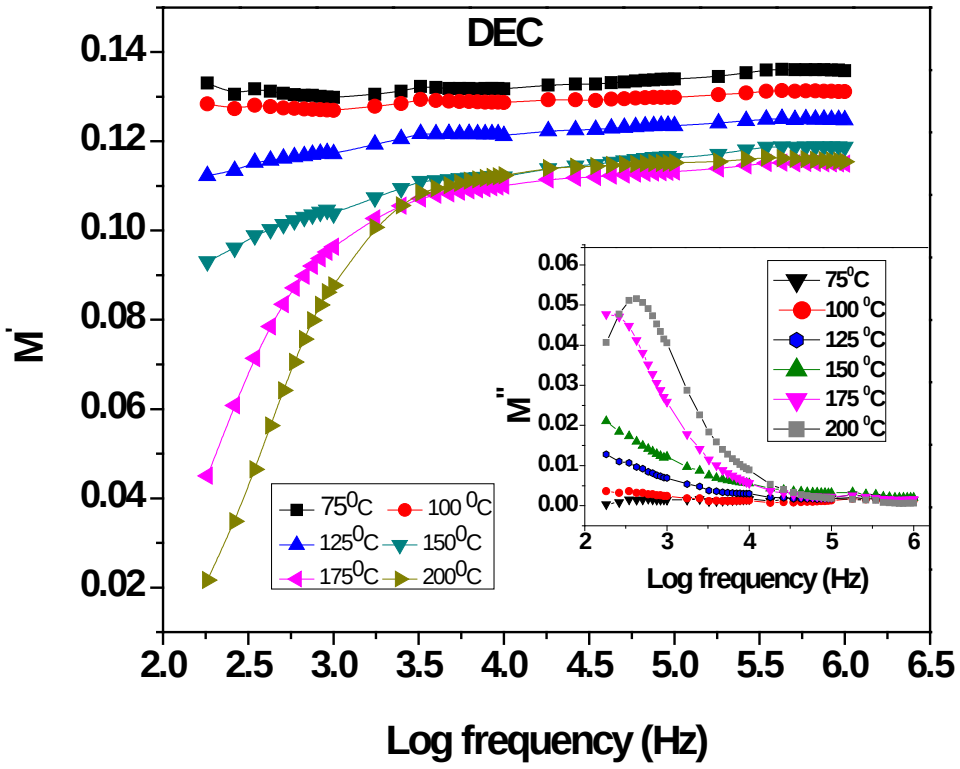

Fig. 4.18: Variation of M' as a function frequency for the DEC. **Inset:** Variation of M'' as a function frequency for the DEC.

Fig. 4.17 & 4.18 respectively show the variation of real parts of the complex modulus (M') of UTC and DEC with frequency over a wide range of temperature. It is found that the values of M' increase with frequency at each temperature and have finally reached a constant value, on the other hand, the frequency variation of ε_r has been decreased almost to a constant value. This behavior is exactly opposite to the variation of ε_r with frequency. The evolution of M' towards a constant value at the high frequency region is due to the fact that polarization becomes ineffective to the applied field at higher frequency. The existence of a step-like transition from low to high values of (M') is evident in all specimens, at temperatures higher than 100°C. The

recorded transitions imply the presence of a relaxation process, which should be accompanied by a loss peak in the diagrams of the imaginary part of electric modulus (M'') versus frequency. Again, it is also observed that the M' value in case of DEC is higher than the UTC, which is in good agreement with the dielectric data.

The variation of the imaginary part of the electric modulus (M'') of both UTC and DEC with frequency at selected temperature are shown in the inserted Fig. 4.17 & 4.18 respectively. The shifting of relaxation peaks with rise in temperature ascribing correlation between motions of mobile ions, which suggests that there is a spread of relaxation times. The relaxation mechanism at lower temperature and lower frequency is different from at higher temperature and higher frequency. The nature of the inserted Fig. 4.17 & 4.18 suggests that there are other relaxations also present at a frequency lower than 100 Hz. It can be explained that the appearance of loss peak ~130^0C is may be due to the presence of glass/rubber transition and after 130^0C, it may be attributed to the presence of interfacial polarization. Hence, it is clear that the behavior of M'' is nearly same in case of both UTC and DEC i.e. different kind of relaxation phenomena are present in both cases.

4.3 Conclusions

Sisal fiber has been modified by dewaxing which results an increment in the degree of crystallinity, crystallite size and the density of the dewaxed fiber. This may be due to rearrangement of cellulose chains and removal of internal constraints. The values of periodicity transverse to the layer D, volume fraction of matter phase Φ_1, transverse length in matter phase l_1 calculated from SAXS data are higher for DE

than UT which is due to the reduction in disorder in dewaxed fiber. Better flexural strength and tensile strength has been reported in case of DEC because of the removal of cementing materials and that may be obviously due to the increased adhesion between fiber and matrix. The observed decrease in the value of ε_r in case of DEC, may be attributed to the reduction in OH group and absorbed water which in turn decreases the orientation polarization. Better interlocking between the fibers and matrix have hindered the free molecular motion of the molecular chain at the composite interface in DEC, which may also lead to the decrease in value of ε_r, tanδ and σ_{dc}, but an increment in the flexural strength and tensile strength. The SEM micrograph of fractured surface of DEC confirms the better wetting of the fiber by the matrix which in turn increases both flexural strength and tensile strength of the composite. The σ_{dc} is found to follow the Arrhenius relation for both DEC and UTC. The activation energy DEC is found to be higher than that of UTC indicating a rigidification of the fiber-matrix interfacial region. Modulus spectra confirm the presence of different relaxation mechanism in the composite.

This work enables us to confirm that there exists a good correlation between dielectric behavior and mechanical properties of epoxy reinforced by sisal fiber. Beside that both electrical and mechanical properties of the composites have also been correlated with the macromolecular and structural parameters of the reinforced fiber.

References:

1. Shah AN, Lakkad SC, Mechanical properties of jute-reinforced plastics. Fiber Sci technol, 15, (1981) 41–46.
2. Bisanda ETN, Ansell MP, The effect of saline treatment on the mechanical and physical properties of sisal–epoxy composites. J Compos sci techol, 4, (1991) 165–178.
3. Kulkarni AG, Satyanarayana KG, Rohtagi PK, Electrical resistivity and dielectric strength of the plant fiber. J mater Sci let, 16, (1981) 1720–1726.
4. Dutta AK, Mukherjee PS, Mitra CB, A dielectric study of cellulose fibers. J Mater Sci, 15 (1980) 1856 –1860.
5. Patra A, BIsoyi DK, Dielectric and impendance spectroscopy studies on sisal fiber reinforeced Polyester composite. J Mater Sci 42, (2010) 4557–5748.
6. Rong MZ, Zhang MQ, Liu Y, Yang GC, Zeng HM, The effect of fiber treatment on the mechanical properties of unidirectional sisal- reinforced epoxy composites. Comp Sci Tech, 61, (2001) 1437–1447.
7. Feng DAAN, Caulfield DF, Sanadi AR, Effect of Compatibilizer on the structure-property relationships of Kenaf-fiber/polypropylene composites. Polym Compos, 22, (2001) 506–517.
8. Nosbi N, Akil HMd, Ishak ZA, Bakar AA, Behaviour of kneaf fiber after immersion in several water condition. Bioresources, 6, (2011) 950– 960.
9. Marcia CB, Alessandra LM, Marcio K, Jose DA, Antonio DN, Wood polymer composites technology supporting the recovery and protection of tropical forests. The Amazonian Phoenix Project Sustainability, 1, (2009) 1431–1443.
10. Khan NMD, Ph.D thesis "Small angle X-ray scattering of sisal fiber using correlation functions". (1991) 71–72.
11. Ruland W, Small-Angle Scattering of Two-Phase Systems: Determination and Significance of Systematic Deviations from Porod's Law. J Appl Cryst, 4, (1971) 70-73.
12. Vonk CG, A general computer program for the processing of small angle X-ray scattering data. J Appl Cryst, 8, (1975) 340-341.

13. Mishra T, Bisoyi DK, Patel T, Patra KC, Patel A, Small Anglex-ray study of cellulose in cotton using correlation function. Polym J, 20, (1988) 739-749.
14. Vilay V, Mariatti M, Taib RM, Todo M, Effect of fiber surface treatment and fiber loading on the properties of bagasse fiber–reinforced unsaturated polyester composites. Compos Sci Technol, 68, (2008) 631–638.
15. Prasad N, Patnaik J, Bohidar N, Mishra T, Effect of temperature on Nylon 6 fibers at different denier values and study of macromolecular parameters by SAXS technique. J Appl Poly Sci, 67, (1998) 1753–1759.
16. Klemm D, Heublein B, Fink H, Bohn A, Cellolose: Fascinating biopolymer and sustainable raw material. Angew Chem, Int. Ed 44, (2005) 3358–3393.
17. Liansong W, Dongling H, Tianyao Z, Lifang Z, Chengdong X, Effect of isothermal annealing on degree of crystallinity and mechanical properties of poly(l-lactide-co-glycolide. Cryst Res Technol, 45, (2010) 275–280.
18. Le TM, Peyratout C, Chotard T, Bonnet JP, Smith, Guinebretiére R, Physico-chemical modifications of the interactions between hemp fibers and alime mineral matrix: Impacts on mechanical proper-ties of mortars. In '10th International Conference of the European Ceramic Society' Berlin, Germany'; (2007) 451–456.
19. Mahato DN, Prasad RN, Mathur BN, Surface morphological band and lattice structural studies of cellulosic fibers coir under mercerization by ESCA, IR, XRD techniques. Indian J Pure Appl Phys, 47, (2009)643-647.
20. Mani GK, Rayappan JBB, Bisoyi DK, 2012. Synthesis and Characterization of Kapok Fibers and its Composites. J Appl Sci, 12, (2012)1661-1665.
21. Trindade WG, Hoareau W, Megiatto JD, Razera IAT, Castellan A, Frollini E, Thermoset phenolic matrices reinforced with unmodified and surface-grafted furfuryl alcohol sugar cane bagasse and curaua fibers: Properties of fibers and composites. Biomacromolecules, 6, (2005) 2485–2496.
22. Georgopoulos ST, Tarantili PA, Avgerinos E, Andreopoulos AG, Koukios EG, Thermoplastic polymers reinforced with fibrous agricultural residues. Polym Degrad and Stabil, 90, (2005) 303–312.
23. Thielemans W, Wool RP, Lignin esters for use in unsaturated thermosets Lignin modification and solubility modeling. Biomacromolecules, 6, (2005) 1895–1905.

24. Bisanda ETN, PhD Thesis "sisal fiber reinforced composites" (1991).
25. Hanna AA, Atef AI, Salwa O, Heikal SO, Some electrical properties of wood pulp treated with sodium hydroxide. J Polym Sci: Polymer Chemistry Edition 18, (2003) 1425–1429.
26. Turnhout JV, Wübbenhorst M, Analysis of complex dielectric spectra. II: Evaluation of the activation energy landscape by differential sampling. J Non-Cryst Solids, 305, (2002) 50–58.
27. Hammami H, Arous M, Lagache M, Kallel A, Experimental study of relaxations in unidirectional piezoelectric composites. Composites Part A, 37, (2006) 1–8.

Chapter 5

Influence of Potassium Permanganate treatment

5.1. Introduction

Recent environmental concern and health hazards associated with the conventional synthetic fibers like glass, carbon, aramid etc. have forced the manufacturing industries and scientists of fundamental research to develop an alternative reinforcing material. In this regard the abundantly available natural plant fiber with low density, low cost, biodegradability, non-toxicity has been proved to be a boon in the present energy crisis situation [1]. Natural fiber reinforced composite not only gaining attention in substituting the synthetic fiber in conventional structural, automotive applications but also found to be suitable in many electrical applications like in suspension insulators, switch boards, anti-static applications etc. [2]. Among all the natural fibers, sisal fiber which is widely used as yarns ropes, twines, carpets is found to be most suitable for the applications in polymer composites because of its superior properties like high cellulose content, high tensile strength and yet cheaper in price [3].

However, the inherent hydrophilic nature of the sisal fiber leads to the poor compatibility with hydrophobic matrix hence creates hindrance for its full exploitation in the composite manufacturing industries [4]. Chemical and physical modifications of the fiber are found to be an effective method to improve the compatibility between the matrix and the reinforcing fiber, either by modifying the surface of the fiber or generating some new functional groups which can form bond with the matrix [5]. The literatures are flooded with the references of many surface modification of the natural fiber by physical and chemical methods.

Among the various chemical modifications, the $KMnO_4$ treatment on the fiber is known to be very effective in improving the bonding at the interface [6]. $KMnO_4$ is well known as a strong oxidizing agent. George et al. [7] studied the effect of $KMnO_4$ treatment on the pineapple leaf fiber reinforced polyethylene composites and noticed the improvement in the mechanical properties after the treatment. $KMnO_4$ treated banana fiber proved to be responsible for the higher thermal stability due to cellulose-manganet [8]. Khan et al. [9] studied the effect of $KMnO_4$ treatment on the photo cure coir fiber which increases the tensile strength due to the strong oxidizing effect of $KMnO_4$ on the cellulose molecules in the fiber. The dependence of the volume resistivity on the concentration of $KMnO_4$ treated sisal fiber reinforced low-density polyethylene was studied by Paul et al. [10]. The strength and stiffness of the fiber provided by the cellulose gets modified during the chemical treatment [11]. Hence, it is essential to know the structural changes caused by chemical modifications. An understanding of the structural parameters of the fiber is also extremely important to

assess the suitability of the fiber as well as the fiber reinforced composite in various potential applications.

SAXS is a powerful technique to characterize the structural changes and strain produced in a polymer along with the changes in the macromolecular parameters [12, 13]. This analysis helps in understanding the structure-property relationship of the polymer and tailor-making the technology for mass production of different polymeric materials, especially fiber and fiber-reinforced composites by having a deeper understanding at the macromolecular level. Moreover, it can estimate the percentage of matter phase, void phase and many more macromolecular parameters of the fiber which can affect the strength, durability and stability of the fiber [14].

Electrical properties and mechanical performance of natural fiber composites were found to depend on the interfacial characteristics as well as the orientation of the fibers. The effect of sisal fiber orientation on the electrical properties of sisal fiber reinforced epoxy composites was studied by Chand et al. [15]. The authors found that dielectric constant and tanδ of the epoxy, for 0^o and 90^o oriented sisal fiber epoxy composites decreased with increasing frequency, and a.c. conductivity increased with increasing frequency. Near the transition temperature of the epoxy matrix, the observed properties showed anomalous behavior. Clear relaxation peaks for tanδ around 169^oC were observed in epoxy resin, shifting to the lower temperature side with increasing frequency. The electrical properties of natural composites are directly related to the adhesiveness between the fiber and matrix. Hong et al. [16] developed a new low dielectric constant material suited to electronic materials applications using

hollow keratin fibers and chemically modified soybean oil. The unusual low value of dielectric constant obtained was due to the air present in the hollow microcrystalline keratin fibers and the triglyceride molecules. The authors were of the opinion that the low cost composite made from avian sources and plant oil has the potential to replace the dielectrics in microchips and circuit boards in the ever growing electronics materials field. In an extension of the above study the authors have also observed that the coefficient of thermal expansion (CTE) of the composite was low enough for electronic applications and similar to the value of silicon materials or polyimides used in printed circuit boards [17].

Therefore, in order to confirm the change of hydrophilicity, the study of electrical properties is required. Though there are few reports which are devoted to study the electrical properties of natural fiber composite, however detail dielectric, ac conductivity and electric modulus spectroscopy study has not been reported anywhere yet.

The literature survey suggests that there is hardly any report on the study of macromolecular parameters of the $KMnO_4$ treated sisal fiber in correlation to the electrical and mechanical properties of the short sisal fiber reinforced epoxy composites. Dewaxing of the sisal fiber is effective in increasing the reinforcing efficiency of the fiber in epoxy [18]. Hence, the present work aims in further improvement in the reinforcing efficiency of the composite system by pretreating the sisal fiber with the combined effect of dewaxing and $KMnO_4$. This work investigates the effect of $KMnO_4$ treatment on the surface morphology, and macromolecular

parameters of the sisal fiber. The mechanical and electrical properties of the short sisal fiber reinforced epoxy composite have also been studied in detail.

5.2. Results and discussion

5.2.1 SAXS Analysis

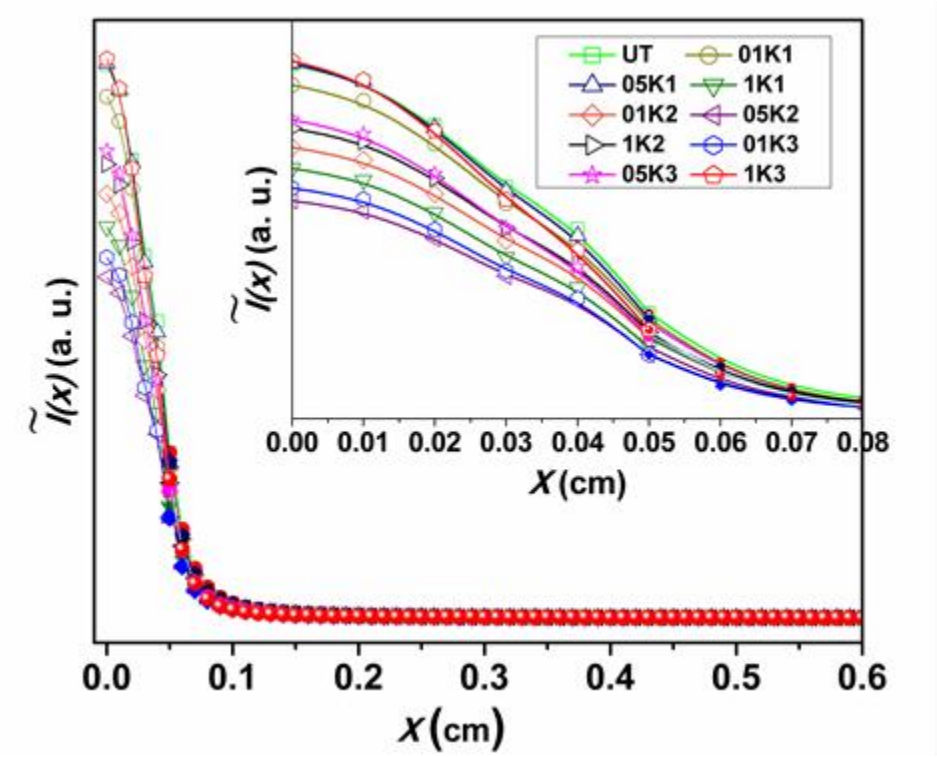

Fig. 5.1: Background-corrected, smeared-out scattering curves for raw and $KMnO_4$ treated sisal fibers. **Inset:** Magnified view of the extrapolated scattering curve.

Fig. 5.1 exhibits the diffuse scattering curves of the untreated fiber and $KMnO_4$ treated fibers. The background corrected intensities are used for the analysis of the SAXS data. Five background corrected intensities near the origin are fitted to the following Gaussian curve by least square technique.

$$\tilde{I}(x \to 0) = p\exp(-qx^2) \qquad (5.1)$$

Here, $\tilde{I}(x)$ is the smeared out intensity and x is the positions co-ordinate of the scattered intensity from the center of the primary beam, where x=2$a\theta$ and 2θ is the scattering angle. The values of constants p and q are used to extrapolate the scattering curve up to x=0. The extrapolation is necessary as it is practically impossible to get the scattering curve up to x=0. The extrapolated points are indicated by hollow symbols in the inset graph of Fig. 5.1. These smeared out intensities and x shown in Fig. 5.1, are required to find out the macromolecular parameters in subsequent analysis. The method of extrapolation shown in Fig. 5.1(inset) does not disturb the position and height of the 1st subsidiary maxima of the one dimensional correlation function $C_1(y)$ [19]. The symmetry of the intensity pattern confirms the isotropic behavior of the sisal fiber. Previous works on the lignocellulosic fiber suggest that the areas of cellulose production near the protoplasm are related to each other in some order. Hence form the cellulose molecules with some order to each other with high degree of orientation. This leads to the kind of isotropic lamellar structure.

The 3D correlation function $C(r)$ which contains the valuable information regarding macromolecular structural parameters is defined as the ratio of the average of the product of the electron density across the two ends of a virtual rod moving inside the particle to the average of the product when the length reduces to zero at the origin. It gives information about the nature of the phases present in the particle.

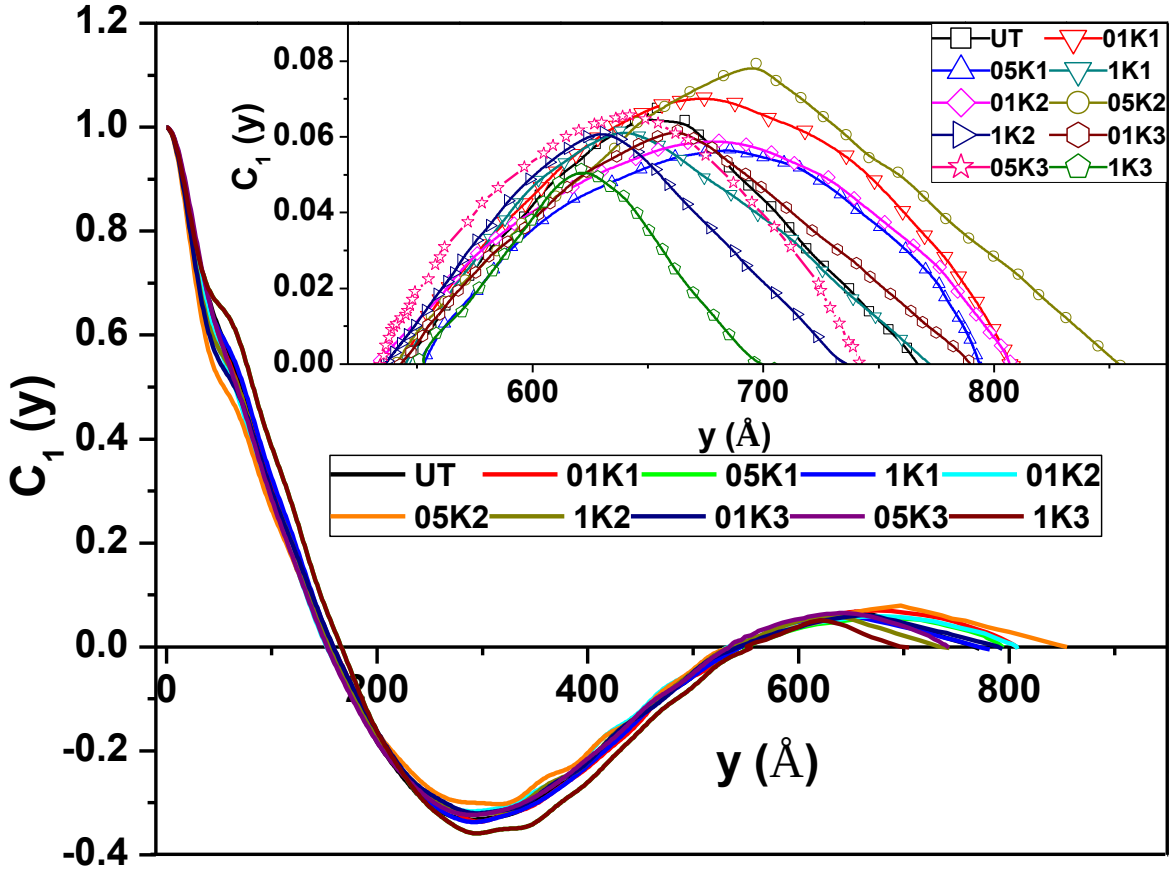

Fig. 5.2: Variation of one dimensional correlation function $C_1(y)$ as a function of y for the raw and $KMnO_4$ treated fibers. **Inset:** Magnified view of first subsidiary maximum of one-dimensional correlation functions.

The above function *C(r)* is governed by the following relation.

$$C(r) = \frac{\int_0^\infty x\tilde{I}(x)J_0\left(2\pi rx/\lambda a\right)dx}{\int_0^\infty x\tilde{I}(x)dx} \qquad (5.2)$$

Here J_0 is the Bessel function of Zero order first kind. The value of $C(r)$ normalizes to unit at the origin and decreases to zero when r attains the boundary of the particle i.e. $r=R$, corresponding to the maximum displacement. This correlation function contains the information about the particle in three dimensions hence known as 3D correlation function.

The one-dimensional correlation function $C_1(y)$ can be visualized as a measuring rod of length 'y' perpendicular to the layers which moves along the y-direction. In the present study there is significant contribution of $C_1(y)$ as sisal is having the lamellar structure. The expression for the one-dimensional correlation function $C_1(y)$ for layer structure in terms of x is expressed as

$$C_1(y) = \frac{\int_0^\infty x\tilde{I}(x)[J_0(z) - zJ_1(z)]dx}{\int_0^\infty x\tilde{I}(x)dx} \qquad (5.3)$$

where J_1 is the Bessel function of first order first kind.

The isotropic lamellar structure of all the investigated fiber samples justifies taking of one dimensional correlation, $C_1(y)$ function [20]. $C_1(y)$ of all the fibers for various values of y are computed and the plots are given in the Fig. 5.2. According to Vonk [21] the position of first subsidiary maximum in the one-dimensional correlation function, gives the value of the average periodicity transverse to layers (D). Inside the fiber, the matter phase and void phase are thought to be arranged in terms of lamellar stack and each lamellar having some periodicity displays information about the specific inner surface area (S/V) of those lamellar stacks. It is also defined as phase boundary per unit volume of the dispersed phase.

$$S/V = 2/D \qquad (5.4)$$

The values of D (average periodicity transverse to the layer correspond), specific inner surface area (S/V) calculated from each curve of the Fig. 5.2 has been listed in Table 5.1. The value of D is found to be highest for the 05K2 sample with least specific inner surface area.

The extent of matter and void phase inside the fiber are represented by $\bar{l}_1$ and respectively $\bar{l}_2$ whereas the volume fractions of matter and void phase are denoted by φ_1 and φ_2 respectively. From Table 5.1 it is found that the values of $\bar{l}_1$ and φ_1 are highest for 05K2 samples, but the values of $\bar{l}_2$ and φ_2 are least for the same sample. The maximum value of $\bar{l}_1$ and φ_1 for the sample 05K2 shows the increment in the matter phase. It may be due to the removal of the lignin, impurities and the waxy material from the inter-fibrillar regions of the fiber. The cellulose micro fibril gets rearranged properly decreasing the volume fraction of the void content 'φ_2 '. The decrease in void content increases the mechanical properties of the fiber [22]. The transversal lengths of matter and void phases for a two-phase three-dimensional system were derived by Mittelbach and Porod and are given by the relation

$$1/\bar{l}_r = 1/\bar{l}_1 + 1/\bar{l}_2 \qquad (5.5)$$

where $\bar{l}_r$ is the range of inhomogeneity which has same meaning with that of reduced mass in mechanics.

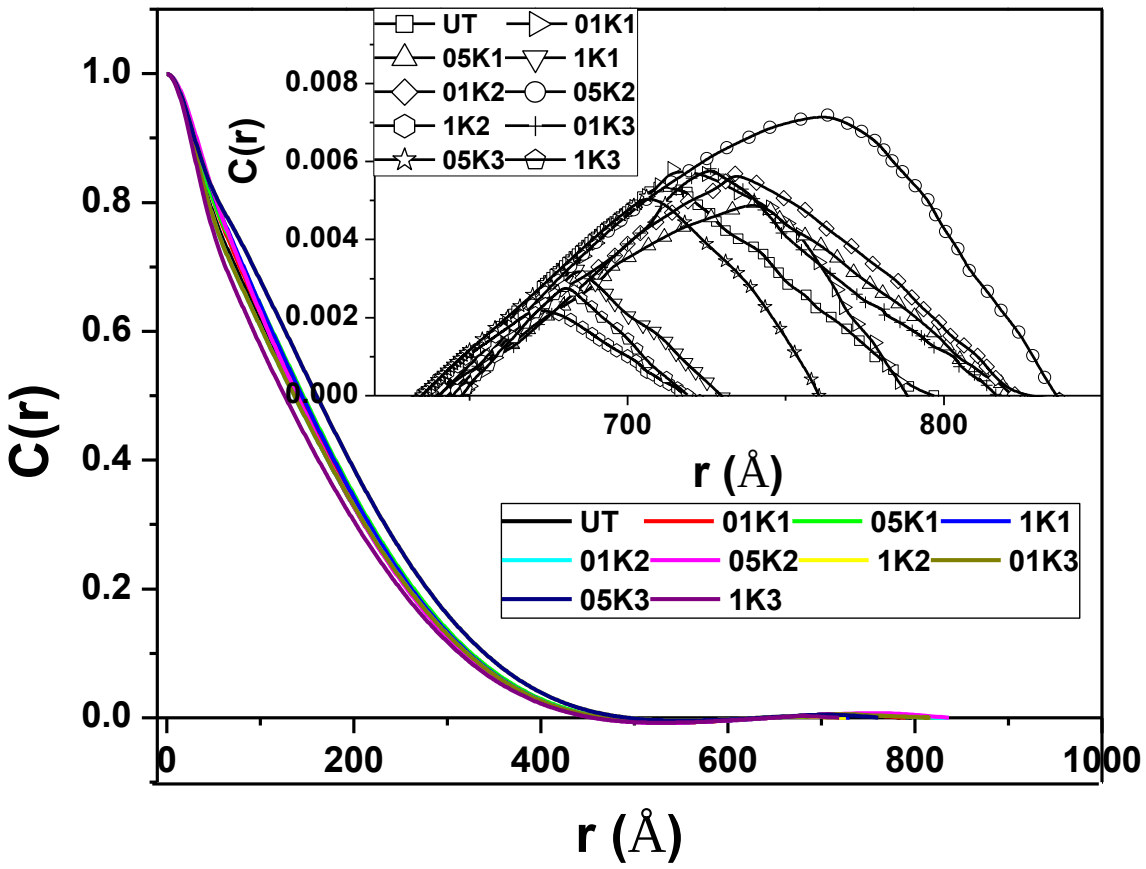

Fig. 5.3: Variation of three dimensional correlation function $C(r)$ as a function of r for raw and $KMnO_4$ treated fibers. **Inset:** Magnified view of first subsidiary maximum of the three-dimensional correlation functions.

The decrease in the value of $\bar{l}_r$ with the increase in soaking period of the fiber in the $KMnO_4$ solution indicates the decrease in the disorderness inside the fiber due to the rearrangement of cellulose chains [20]. Out of all the samples, the fiber treated with 0.05% $KMnO_4$ acetone solution for 2 min (05K2) is found to have least void content i.e. 'φ_2 'and disorderness. However, the sample gets more disordered and void content starts to increase at higher concentrations and it becomes highest for

1K3. It may be due to the degradation of cellulosic material at higher concentrations with higher soaking periods because of the excessive oxidizing effect of $KMnO_4$ acetone solution.

The plots of $C(r)$ of all the investigated fibers are shown in Fig. 5.3. The damping oscillatory behavior of the $C(r)$ for large values of r shows the non-ideal two phase behavior of all the fiber samples. Another important parameter that is derived from the $C(r)$ is the length of coherence (l_c) (given in Table 5.1) which gives the information about the distribution of electron across the boundary of the particle.

$$l_c = 2\int_0^\infty C(r)dr \tag{5.6}$$

According to Ruland [19] and Vonk [21] the information about the non-ideal two phase system can be obtained from the parameter defined as 'R' which was later modified by Mishra et al. [22, 23] is as follows:

$$R = \frac{3}{2}\left(\frac{2\pi}{\lambda a}\right)^2 \frac{\int_0^\infty x^3 \tilde{I}(x)dx}{\int_0^\infty x\tilde{I}(x)dx} \tag{5.7}$$

Where 'R' is the corrugation at the phase boundary and 'a' is the sample to detector distance. If R goes to ∞, the system is ideal but if it has some finite value the system becomes non-ideal two phase. In the present study, the values of R (shown in Table-5.1) are found to be finite for all the investigated fibers which indicate that the electron density gradient is also finite for all the samples. Hence, all the fiber samples are non-ideal two phase system [21].

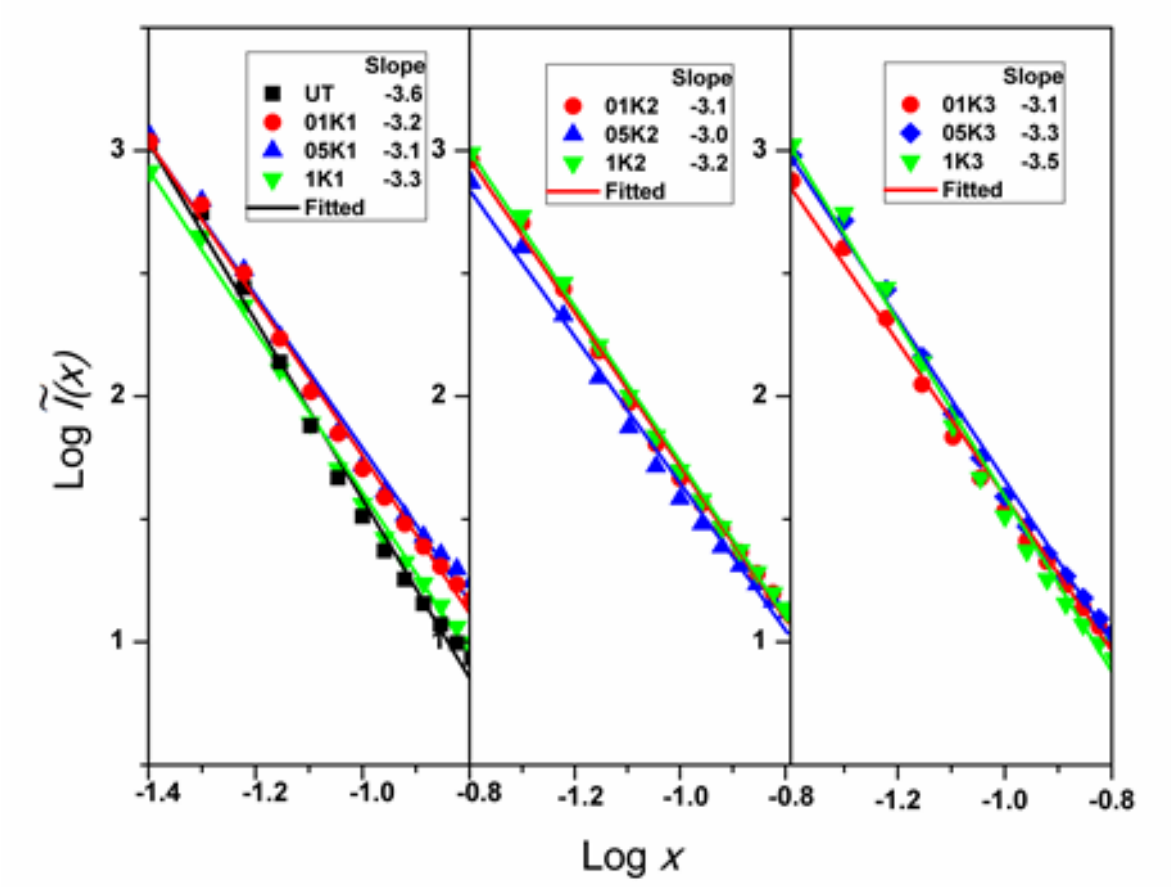

Fig. 5.4: Logarithmic plots between x and $\tilde{I}(x)$ for the raw and $KMnO_4$ treated fibers.

In order to find out the nature of phases of the untreated and treated fibers Logarithmic plots between the *x* and $\tilde{I}(x)$ are drawn (Fig. 5.4). The slopes of all the plots are found to be negative, which is ~ -3. This suggests that both the untreated and treated samples are non-ideal two phase system [24].

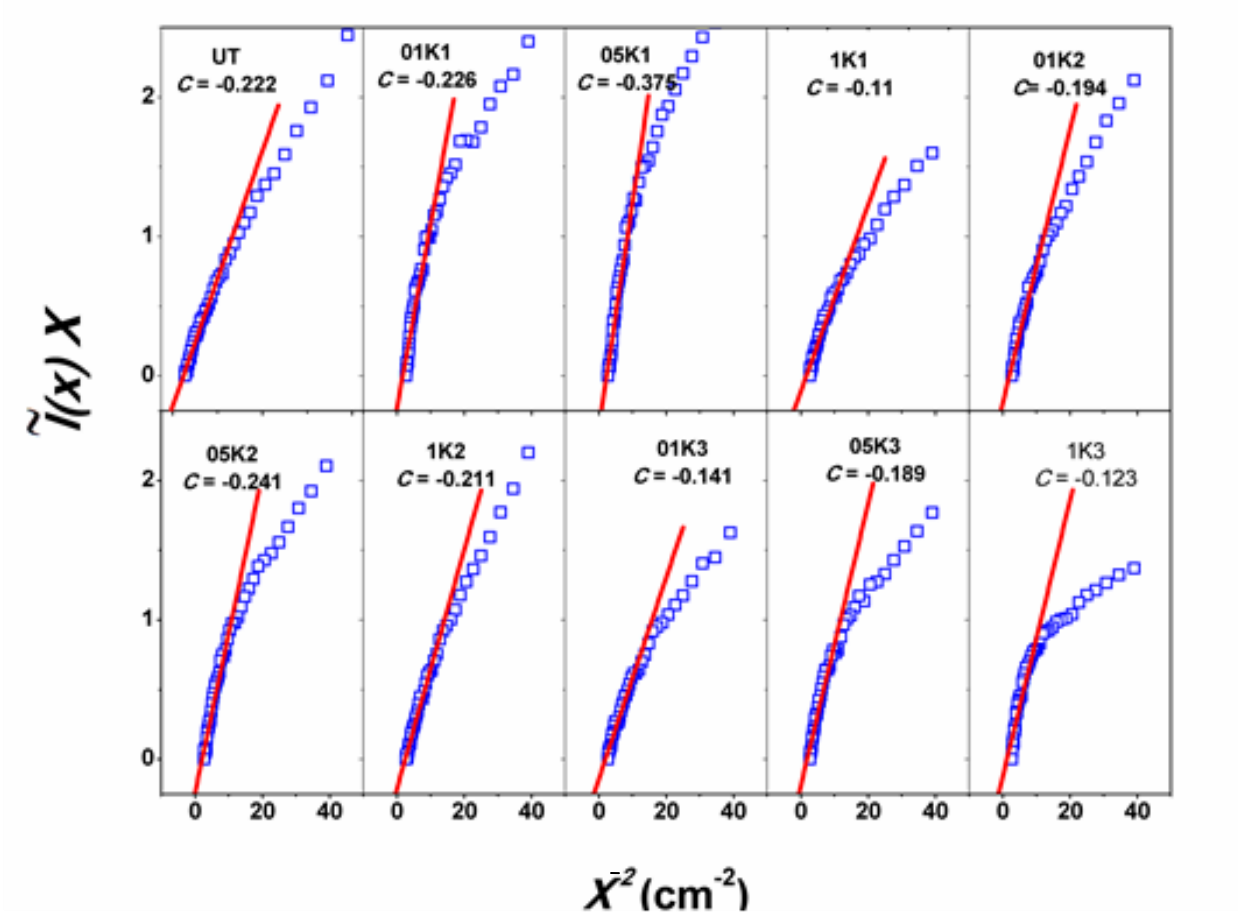

Fig. 5.5: Ruland plots of raw and $KMnO_4$ treated sisal fibers to find out E_r of the respective fibers.

In the present study, the width of transition layers (E) is calculated by Ruland and Vonk method and is designated as E_r and E_v accodrdingly. The width of transition layer gives information about the corrugation at the phase boundary between the matter and void phase. Fig. 5.5 displays the typical Ruland plots for all the investigated fibers, which is a graph of $\tilde{I}(x)\cdot x$ Vs x^{-2}. The Ruland plots are obtained by taking 40 background corrected intensities. Linear fitting of each curves are

carried out on 15 extreme points at the tail region of the corresponding curve. The functional relationship between $\tilde{I}(x)\cdot x$ and x^{-2} takes the form of

$$\tilde{I}(x)\cdot x = \frac{\pi C}{2\cdot(\lambda a)^3\cdot x^{-2}} - \frac{\pi^3 C}{3\cdot(\lambda a)\cdot E^2} \qquad (5.8)$$

where C is the probability constant. The standard deviations (σ) of the intensities are well within the permissible range showing the accuracy of the data collection. The values of E_r obtained from Fig. 5.5 are given in Table 5.1. The width of transition layer, E_v (Vonk method) is calculated by normalizing $C(r)$ to unity at the start of the real space. According to Vonk method,

$$\mathrm{E}=\left(-\frac{4}{R}\right)\frac{dC(r)}{dr} = E_v \qquad (5.9)$$

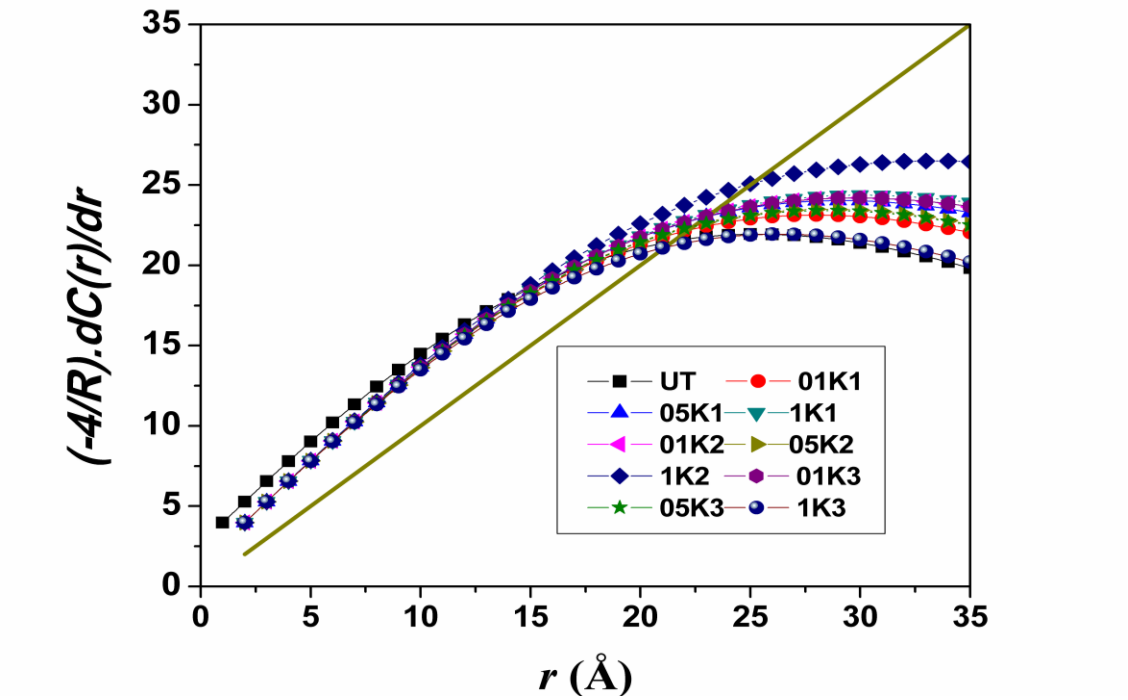

Fig. 5.6: Variation of $\left(-\frac{4}{R}\right)\frac{dC(r)}{dr}$ against r for the raw and $KMnO_4$ treated sisal fibers to find out the E_v of the respective fibers.

Table 5.1: Various macromolecular parameters of raw and $KMnO_4$ treated sisal fibers derived from SAXS study.

Macromolecular parameter	UT	01K1	05K1	1K1	01K2	05K2	1K2	01K3	05K3	1K3
R(10^{-4}Å^{-2})	8.831	10	9.931	8.052	9.002	11.109	7.354	8.573	9.093	6.813
D(Å)	654	674	686	637	680	696	630	664	642	621
S/V(10^{-3} Å^{-1})	3.0581	2.967	2.915	3.139	2.941	2.873	3.174	3.012	3.115	3.220
E_v(Å)	21.081	22.133	23.238	23.152	23.078	22.686	25.073	23.056	22.089	25.22
E_r(Å)	19.792	19.663	19.616	19.251	19.399	19.331	18.867	19.711	19.154	19.466
Φ_1	82.601	84.358	84.646	80.939	84.468	87.339	80.800	83.398	82.55	79.189
Φ_2	17.399	15.642	15.354	19.061	15.532	12.661	19.200	16.602	17.45	20.811
$\bar{l}_1$ (Å)	1080.421	1137.145	1161.343	1031.162	1148.764	1215.758	1018.080	1107.525	1059.942	983.527
$\bar{l}_2$ (Å)	227.578	210.854	210.656	242.837	211.235	176.241	241.9200	220.474	224.058	258.472
$\bar{l}_r$ (Å)	187.982	177.872	178.312	196.549	178.426	153.927	195.471	183.871	184.959	204.681
l_c	351.097	314.736	313.879	325.976	311.374	299.084	318.62	323.666	327.916	322.513
$2E_v/D$ (%)	6.446	6.567	6.774	7.269	6.787	6.518	7.959	6.944	6.881	8.122
σ	0.013	0.014	0.012	0.014	0.013	0.016	0.007	0.008	0.023	0.007

The plot between $\left(-\frac{4}{R}\right)\frac{dC(r)}{dr}$ vs r is shown in Fig. 5.6. A straight line equidistance from both the axes has been drawn and the point of intersection with the curve gives the values of E_v [21] for different fibers which are compiled in Table 5.1. The values of E_r that are calculated from Fig. 5.5 are in close agreement with the values of E_v evaluated from Fig. 5.6. Hence, it justifies the accuracy of our analysis.

Finally the above SAXS computational analysis on all the sisal fibers confirms the fibers to be non-ideal two phase system. Out of all the fibers, 05K2 fiber is found to have least void content and disorderness.

5.2.2 XRD Study

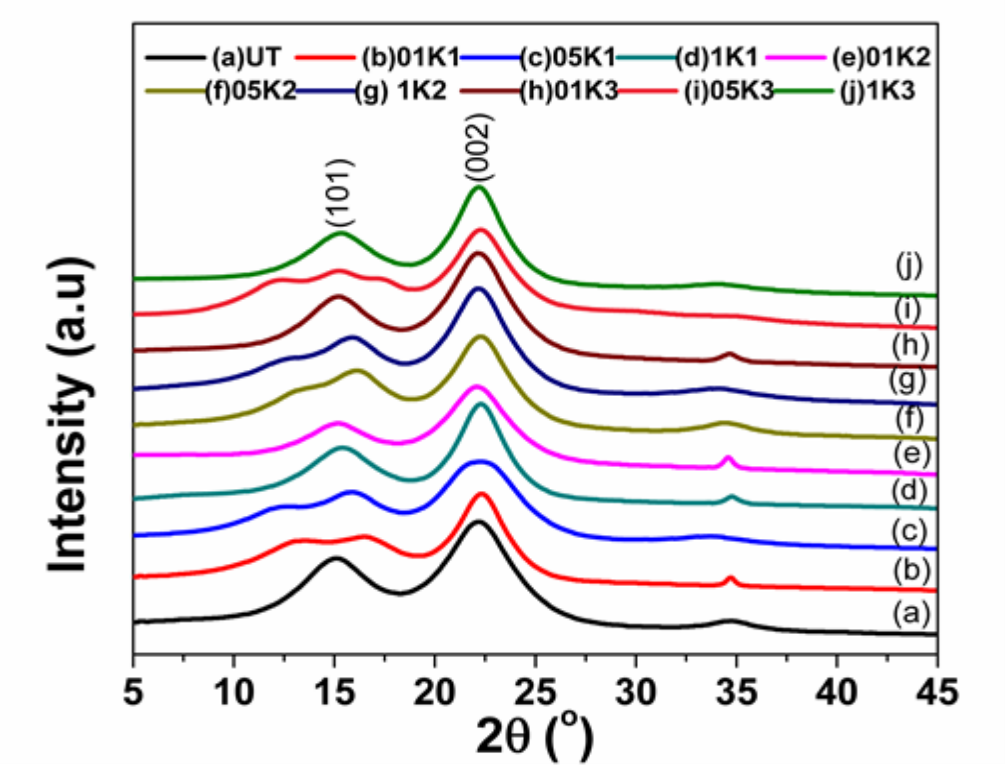

Fig. 5.7: XRD patterns of UT and $KMnO_4$ treated sisal fibers.

Fig. 5.7 shows the XRD patterns of the untreated and $KMnO_4$ treated sisal fibers. The diffraction patterns are profile fitted by standard software. The crystallite sizes of the fibers were determined by modified Scherer's formula whereas the degrees of crystallinity were calculated by Segal's empirical method [25]. All these crystallographic structural parameters are shown in Table 5.2. The highest degree of crystallinity for the 05K2 is shown by maximum increase in the intensity of the crystalline peak at 22.5° followed by 05K1 and is least for 1K3. The particular concentration of $KMnO_4$ at 05K1 and 05K2 may have able to effectively oxidize the sisal fiber surface and etch out lignin binding thousands of micro-fibrils together

inside the fiber [26]. It helps in removing the non-crystalline material from the fiber and making the inter-fibrilar region less dense and less rigid there by allowing cellulose microfibiril to rearrange in a more compact manner. This may have lead to the increment in the degree of crystallinty. Whereas at a higher soaking period and higher concentration of $KMnO_4$ acetone solution, the removal of cellulosic material along with the lignin takes place resulting in decrease of degree of crystallinity and increase in bulk fiber density.

Table 5.2: Various crystallographic and physical parameters of the investigated raw and $KMnO_4$ treated sisal fibers.

Fiber	Degree of Crystallinity (%)	Crystallite size (Å)	Density(g/cc)
UT	52.11	29.19	1.32
O1K1	53.01	31.42	1.39
05K1	58.22	33.18	1.50
1K1	50.01	26.85	1.29
01K2	56.09	32.18	1.43
05K2	59. 93	33.93	1.61
1K2	49.29	25.77	1.25
01K3	52.16	30.47	1.34
05K3	51.22	27.93	1.30
1K3	45.91	22.09	1.20

5.2.2 FTIR Study

Fig. 5.8 exhibits the FTIR Spectra of the untreated and $KMnO_4$ treated sisal fibers. The broad absorbance peak at 3200-3400 cm^{-1} range corresponds to the O-H stretching of hydrogen bond network. This peak tends to decrease with the increment

in the soaking period of the fiber in $KMnO_4$-acetone solution from 1 min to 2 min. It suggests that the hydroxyl stretching vibration decreases due to longer period of treatment. The decrease in intensities becomes prominent in case of 05K2 followed by 05K1. It suggests that at this particular concentration and time the $KMnO_4$ effectively oxidizes the sisal fiber and breaks the hydrogen bond between the O-H groups of cellulose and hemicelluloses. But at higher concentration i.e. at 0.1% the intensities of O-H group tends to increase because of the degradation of cellulose and incorporation of more polar groups [10]. Hence at 1K3 the O-H group is highest.

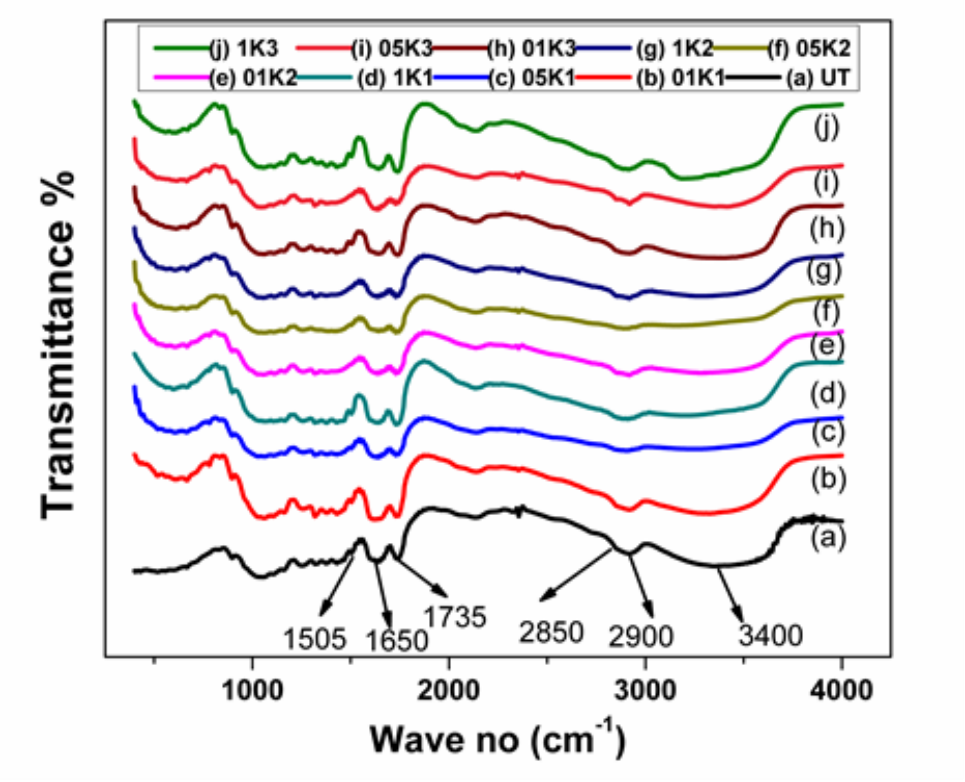

Fig. 5.8: FTIR spectra of UT and $KMnO_4$ treated sisal fibers.

The peaks at 2900 and 2850 cm^{-1} are also seem to be affected by $KMnO_4$ treatment which are the characteristic peak of C-H stretching vibration of methyl group of

methylene and wax respectively. The intensities at these two peaks are found to be least for 05K2 which confirms the substantial removal of wax from the fiber due to the treatment. The peaks at 1735 and 1650 cm^{-1} which correspond to C=O stretching in carbonyl, unsaturated β-keton and absorbed water are found to be decreased remarkably at 05K2. The lignin peak at 1505 cm^{-1} is also decreased showing that $KMnO_4$ has effectively etched out lignin from the fiber surface at this particular concentration and soaking period. But at the higher treating period like 3 min for the same concentration, the degradation of the fiber starts which is due to the excessive oxidation. This may be due to the degradation of cellulose inside the fiber and sedimentation of wax on the fiber by the subsequent reaction for which the peak at 2900 cm^{-1} and 2850 cm^{-1} were appeared again.

5.2.4 Morphological Study

The longitudinal surface morphologies of $KMnO_4$ treated sisal fibers are shown in the Fig. 5.9(a-i). The fiber treated with 0.01% and 0.05% concentration of $KMnO_4$ – acetone solution the fiber roughness increases from 1 min to 2 min period of treatment and degraded roughness is observed for 3 min. The surface morphology of 05K2 fiber showed uniform surface roughness of the sisal fiber. This might be due to the effective oxidation of the fiber surface when it is soaked in 0.05% of concentration of $KMnO_4$ – acetone solution for 2 min which lead to the better roughness of the fiber due to the removal of lignin, waxy material along with the impurities from the fiber [26]

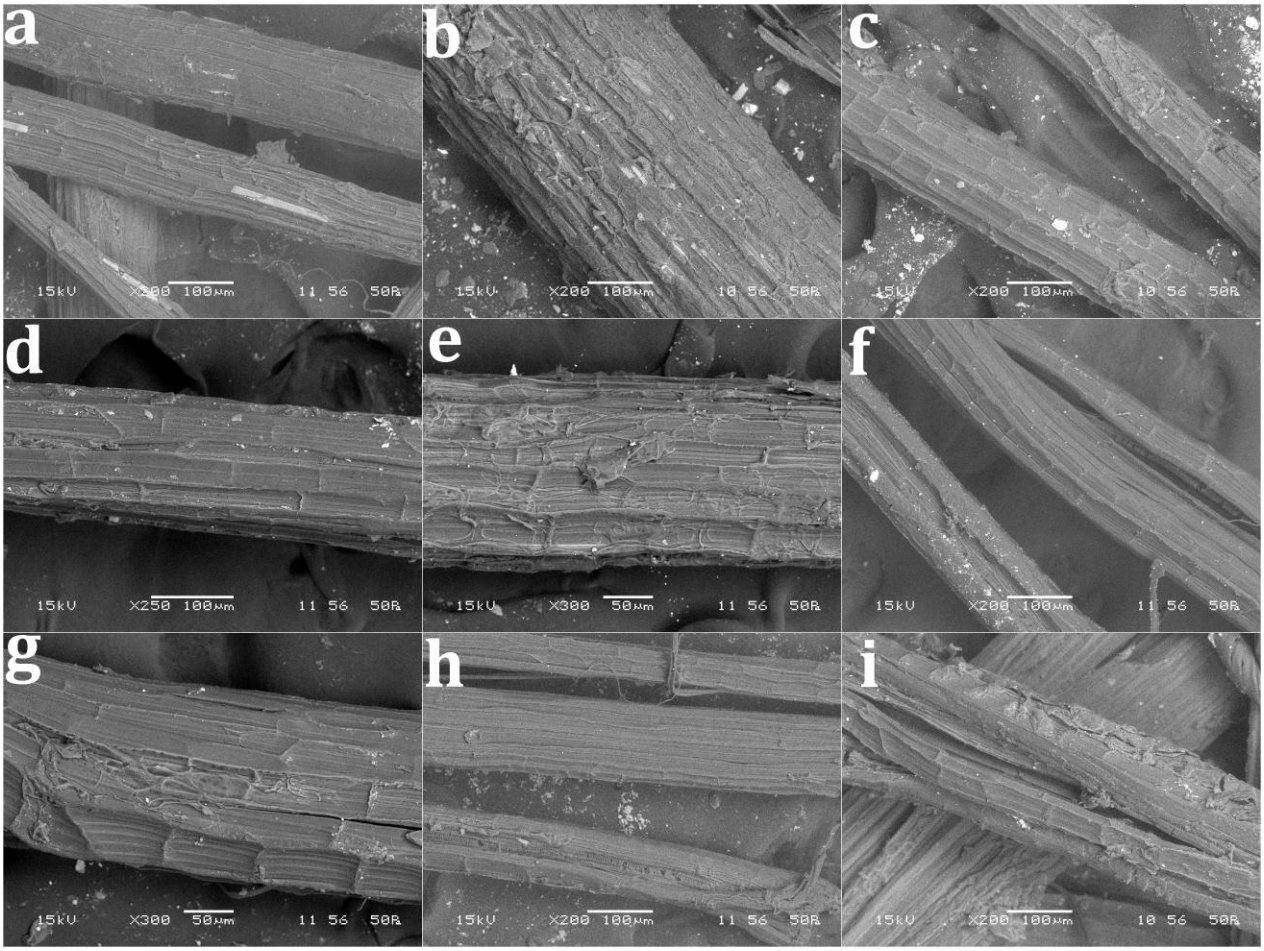

Fig. 5.9 (a-i): Longitudinal morphology of 01K1, 05K1, 1K1, 01K2, 05K2, 1K2, 01K3, 05K3, 1K3 fiber respectively.

Fibers treated with 0.1% of $KMnO_4$ – acetone solution have surface degradation directly proportional with increase in period of treatment i.e. more the period of treatment more is the degradation. So it may be concluded that the permanganate treatment on the sisal fiber has negative effect at higher concentration. The degradation becomes severe with increase in period of treatment at this concentration. But at moderate concentration (0.05%) and moderate period of

immersion (2 min), the oxidation of the fiber surface is properly achieved leading to a uniform surface roughness of the fiber.

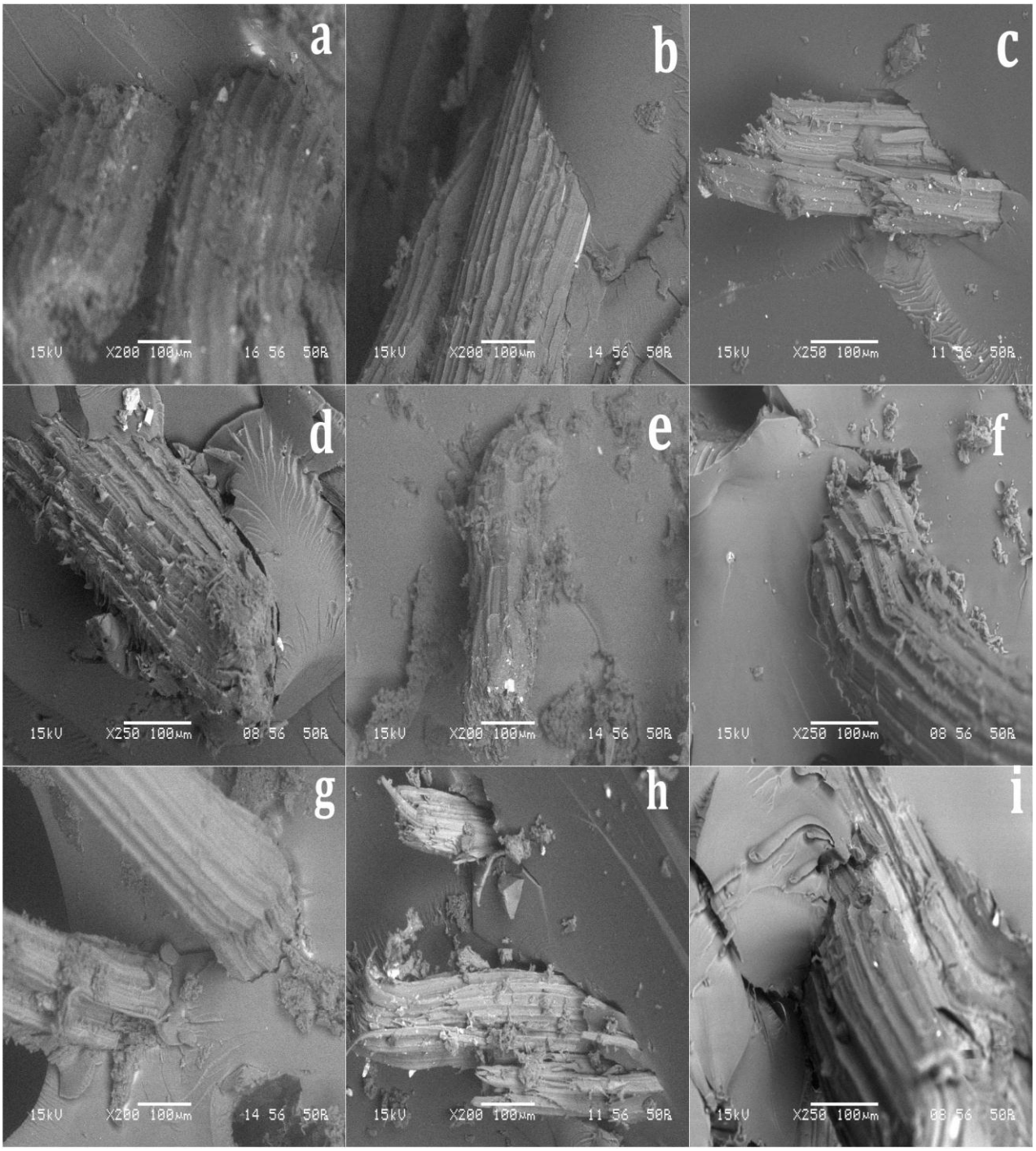

Fig. 5.10 (a-i): Surface Morphology of 01KC1, 05 KC1, 1KC1, 01KC2, 05KC2, 1KC2, 01KC3, 05KC3, 1KC3 composites respectively.

Fig. 5.10 (a-i) shows the fractured surfaces of the (Potassium Permanganate treated sisal fiber reinforced epoxy composite) KFREC. Due to the increased surface area of contact and roughness of the fiber after $KMnO_4$ treatment the adhesion between fiber and the matrix has increased which is very much clear from the SEM micrographs of 05KC2. The adhesion is so strong that it is marked by traces of matrix on the surface of the fiber in the fractured region. This may be due to the initiation of graft co-polymerization by highly reactive MnO^{3-} ion as explained below [27]. Here the OH groups inside the fiber get oxidized.

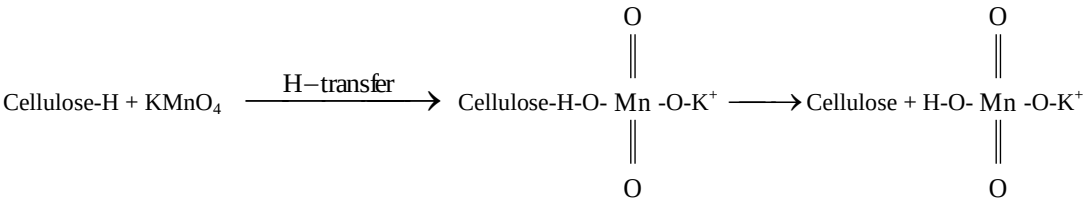

(Georgopoulos et al. [28])

However, the gap around the fiber at the interface for the higher period of treatment at higher concentration of $KMnO_4$- acetone solution depict the poor adhesion between untreated sisal fiber and the matrix. The excessive oxidation of the fiber at higher concentration and longer period of treatment also leads to the composites with weak interface which are shown in Fig. 5.10 (f, i).

5.2.5 Mechanical Study

The flexural strength and tensile strength of UTC and KFREC are shown in Fig. 5.11. It is established that the interfacial zone plays a leading role in transferring the load between fiber and matrix in the fiber-reinforced composite system, which consequently affects the mechanical properties of the composites [28].

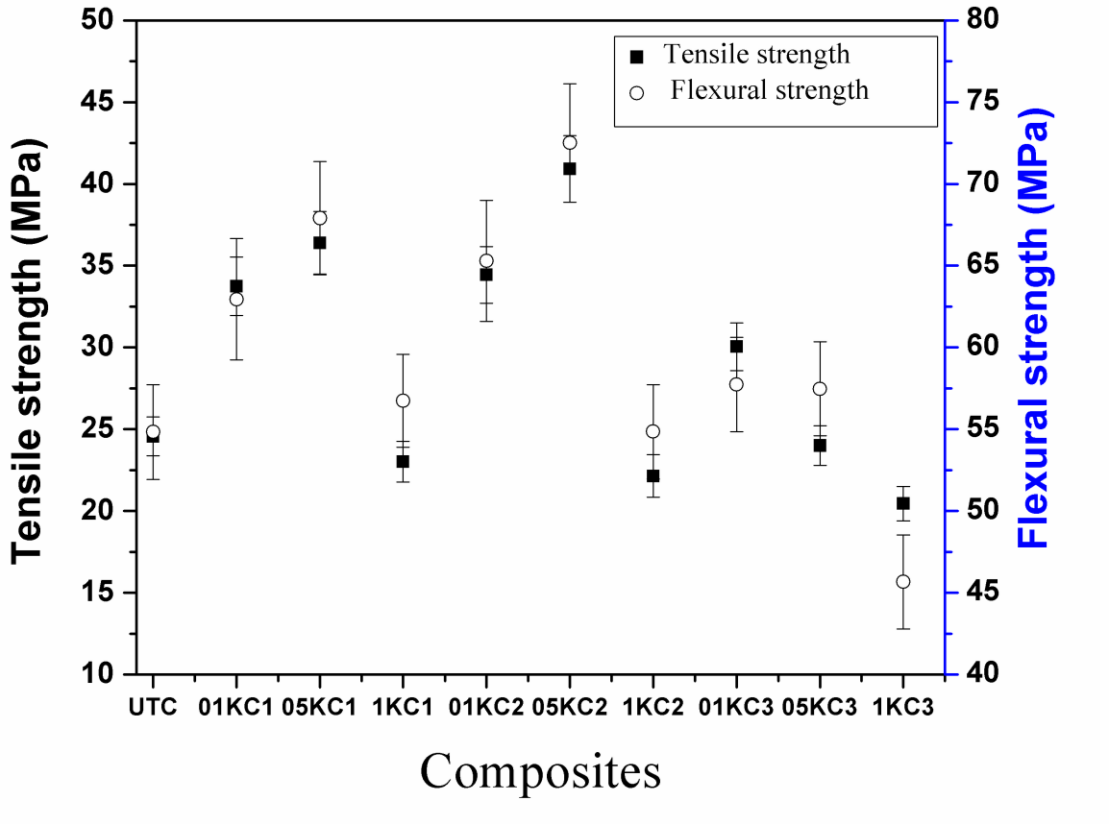

Fig. 5.11: Flexural and tensile strengths of UTC and KFREC.

The flexural failure depends mainly on the fiber-matrix adhesion. The flexural strength and the tensile strength of the 05KC2 are found to be the highest and are followed by 05KC1. The increased surface area and roughness due to the removal of impurities and waxy layer in these samples facilitates the mechanical interlocking between fiber and the resin [29]. This is further confirmed from the SEM micrograph as shown in Fig. 5.9. But at a higher concentration, because of the excessive oxidation of the fiber surface by $KMnO_4$ the strength providing cellulosic gets degraded along with the lignin and waxy material present in fiber. This may have lead to the poor mechanical strength of the composite. It justifies the previous finding that the concentration of $KMnO_4$ has significant effect on the fiber and hence on the fiber

reinforced composites [30]. The degradation of the mechanical strength becomes more intense with increase in soaking period at higher concentration which is clear from the Fig. 5.11.

5.2.6 Dielectric Study

Fig. 5.12 displays the frequency dependence of dielectric constant (ε_r) of both UTC and KFREC. Inset of the above Figure shows the frequency dependence of dielectric loss (tanδ).

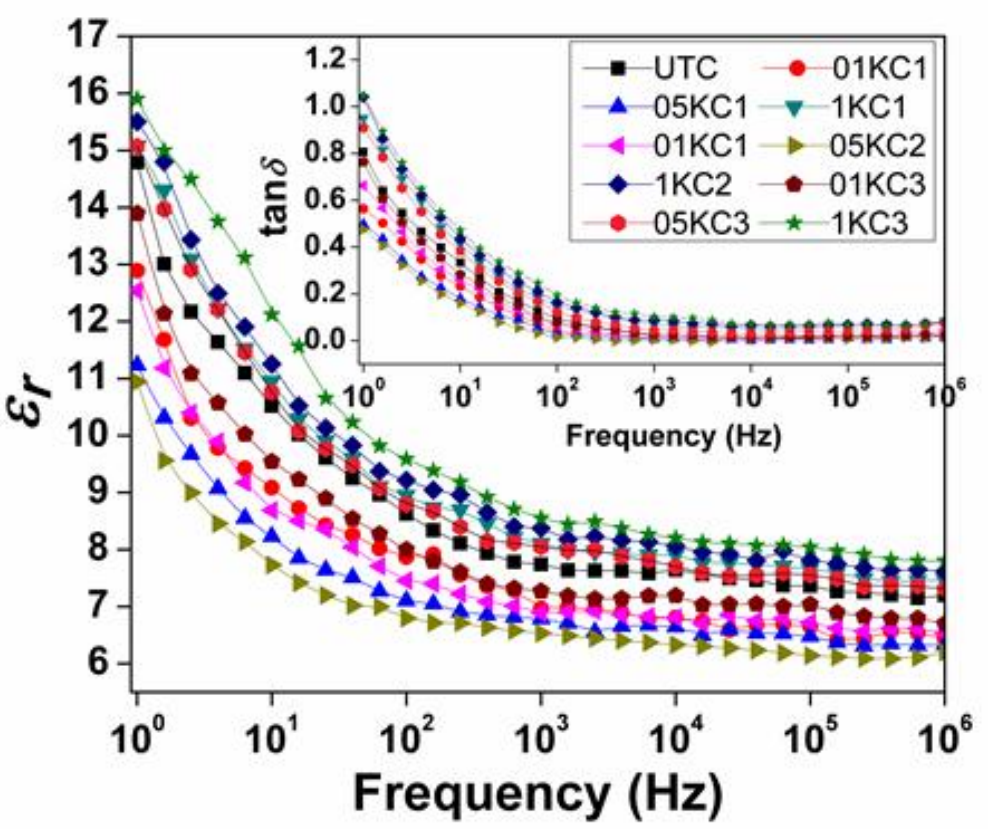

Fig. 5. 12: Variation of ε_r with frequency for UTC and KFREC. **Inset:** Variation of tanδ with frequency for UTC and KFREC.

It is found that with the increase in frequency the value of ε_r as well as tanδ decreases. The values of ε_r and tanδ at lower frequency region is higher than that at

very high frequency. Generally, ε_r and tanδ of a polymeric material depends mainly on interfacial and dipole polarization. The interfacial polarization is prominent in heterogeneous material and is highest at lower frequency. Hence, the higher values of ε_r and tanδ at lower frequency can be explained in terms of interfacial polarization and the free motion of dipoles within the material which is connected to ac conductivity relaxation. It is found that the values of ε_r of the investigated composites follow the following trend 05KC2<05KC1<01KC2<01KC1<01KC3<UTC <05KC3<1KC1<1KC2<1KC3. It may be due to the increase in the degree of crystallinity and hydrophobicity of the fiber because of the removal of non-crystalline part of the fiber. The overall dielectric properties in a polymeric composite are the contribution of both the crystalline and amorphous content of the composite. Amorphous content makes the major contribution to both ε_r and tanδ. As a result, ε_r and $\tan\delta$ decreases with an increasing degree of crystallinity [31]. Therefore 05KC2 has the least values of ε_r and tanδ. However at higher concentration, the value ε_r tends to increase even above the value of ε_r of UTC. It becomes highest for the maximum soaking time at this concentration i.e. at 1KC3. The higher concentration of the $KMnO_4$-acetone solution tries to degrade the strength providing cellulose part in the fiber and hence creating more polar group resulting in higher values ε_r and tanδ.

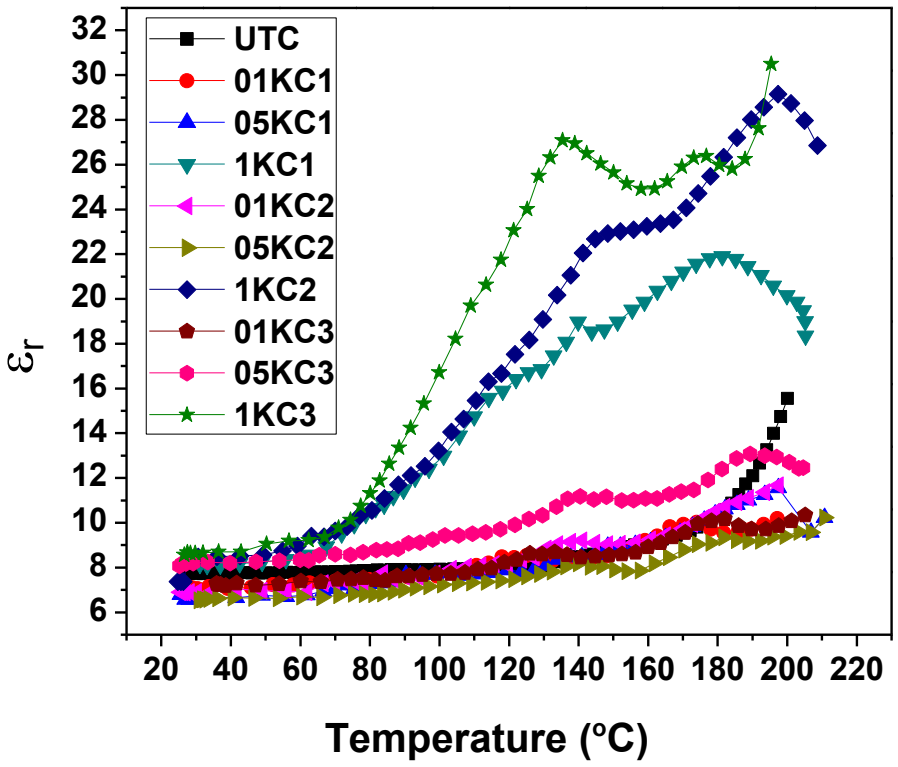

Fig 5.13: Variation of ε_r with temperature for UTC and KFREC.

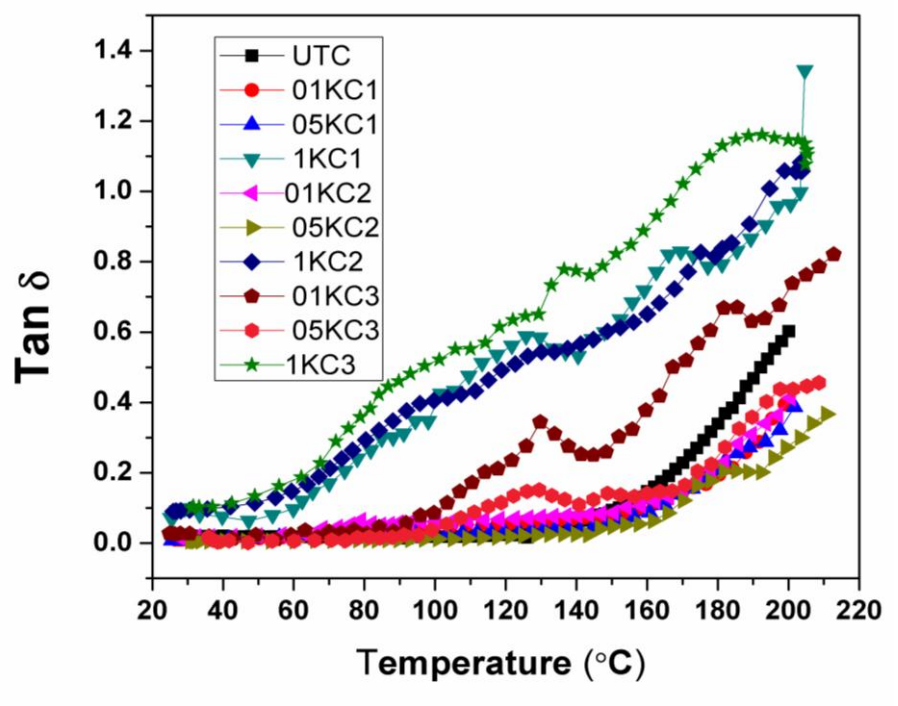

Fig. 5.14: Variation of tanδ with temperature for UTC and KFREC.

The temperature variation of dielectric constant and loss of KFREC at 1 kHz frequency is shown in Fig.5.13 and Fig. 5.14 respectively. It is observed that with rise in temperature ε_r of KFREC increases. The relatively high values of ε_r and tanδ at high temperature is attributed to the enhanced mobility of large parts of the polymer chains and the co-operating contribution of interface polarization (weak Maxwell-Wagner-Sillars (MWS)) effect in the composite systems which arise due to additives, plasticizers etc. in polymer composite.

5.2.7 Electric modulus spectroscopy & Ac conductivity study

It is well known that electrical relaxation effects in polymer matrix composites arise from interfacial effects, phase transitions and polarization or conductivity mechanisms. In the present study, experimental data were analyzed via ac conductivity and electric modulus formalism. The interpretation of relaxation phenomena via the electric modulus formalism offers some advantages upon other method, since large variations in the permittivity and dielectric loss at low frequencies and high temperatures are minimized. Further, difficulties occurring from the electrode nature, the electrode-specimen contact and the injection of space charges and absorbed impurities can also be neglected.

The recorded dielectric data, of all the examined specimens, were first expressed in terms of real and imaginary parts of permittivity and then transformed, to the electric modulus formalism. The use of modulus spectroscopy plot is particularly useful for separating components with similar resistance but different

capacitance. We have adopted the formalism of electric modulus in order to minimize the effect of dc conductivity and to suppress the electrode effect [32].

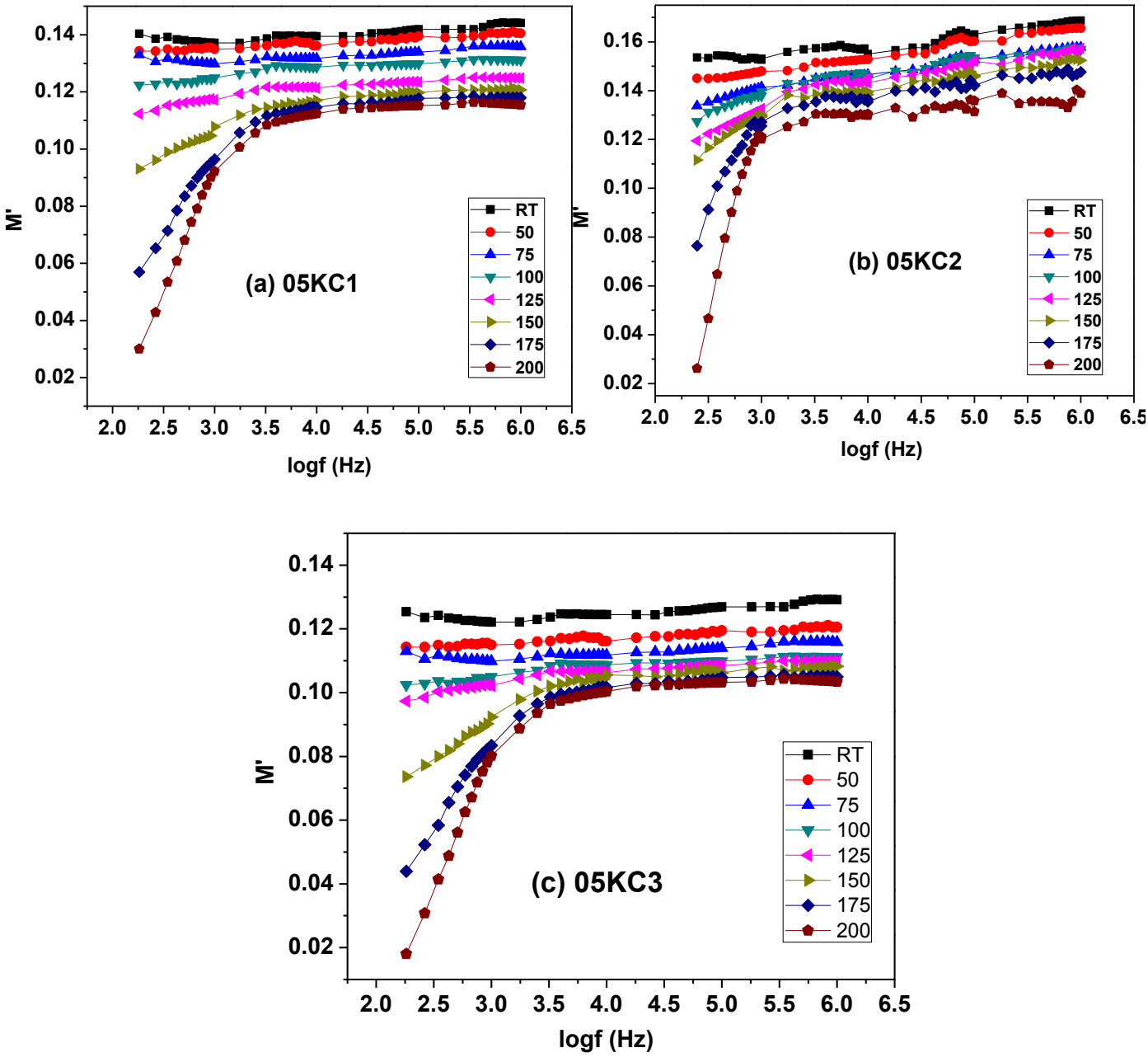

Fig. 5.15: Variation of *M'* as a function frequency for (a) 05KC1, (b) 05KC2 and (c) 05KC3 at different temperatures.

The complex electric modulus (M^*) have been calculated from the impedance data using the following relation:

$$M^* = M' + JM'' = 1/\varepsilon^* = J\omega C_0 Z^* \quad (5.10)$$

Where $M' = \omega C_0 Z''$, $M'' = \omega C_0 Z'$, ω (angular frequency) $= 2\pi f$, C_0 = geometrical capacitance of the sample = $\varepsilon_0 (A/t)$, ε_0 = permittivity of free space, A = area of the electrode surface and t = thickness of the sample.

Figures 5.15 (a-c) and 5.16 (a-c) shows the isothermal scans of the real and imaginary part of electric modulus for the 05KC1, 05KC2, 05KC3 samples at temperatures varying from RT to 200°C, respectively. The existence of a clear 'step-like' transition from low to high values of (M'), at moderate frequencies, is evident in Figures 5.15(a-c). It is found that the values of M′ increased with increase in frequency at a constant temperature and finally reached a constant value. The evolution towards a constant value of M' at the high frequency region is due to the fact that polarization becomes ineffective at higher frequency region because the heavy dipoles cannot follow the high frequency applied field. The existence of a step-like transition from low to high values of (M') is evident in all specimens, at temperatures higher than 100°C. The recorded transitions indicate the presence of a relaxation process, which is accompanied by a loss peak in the imaginary part of electric modulus (M'') versus frequency.

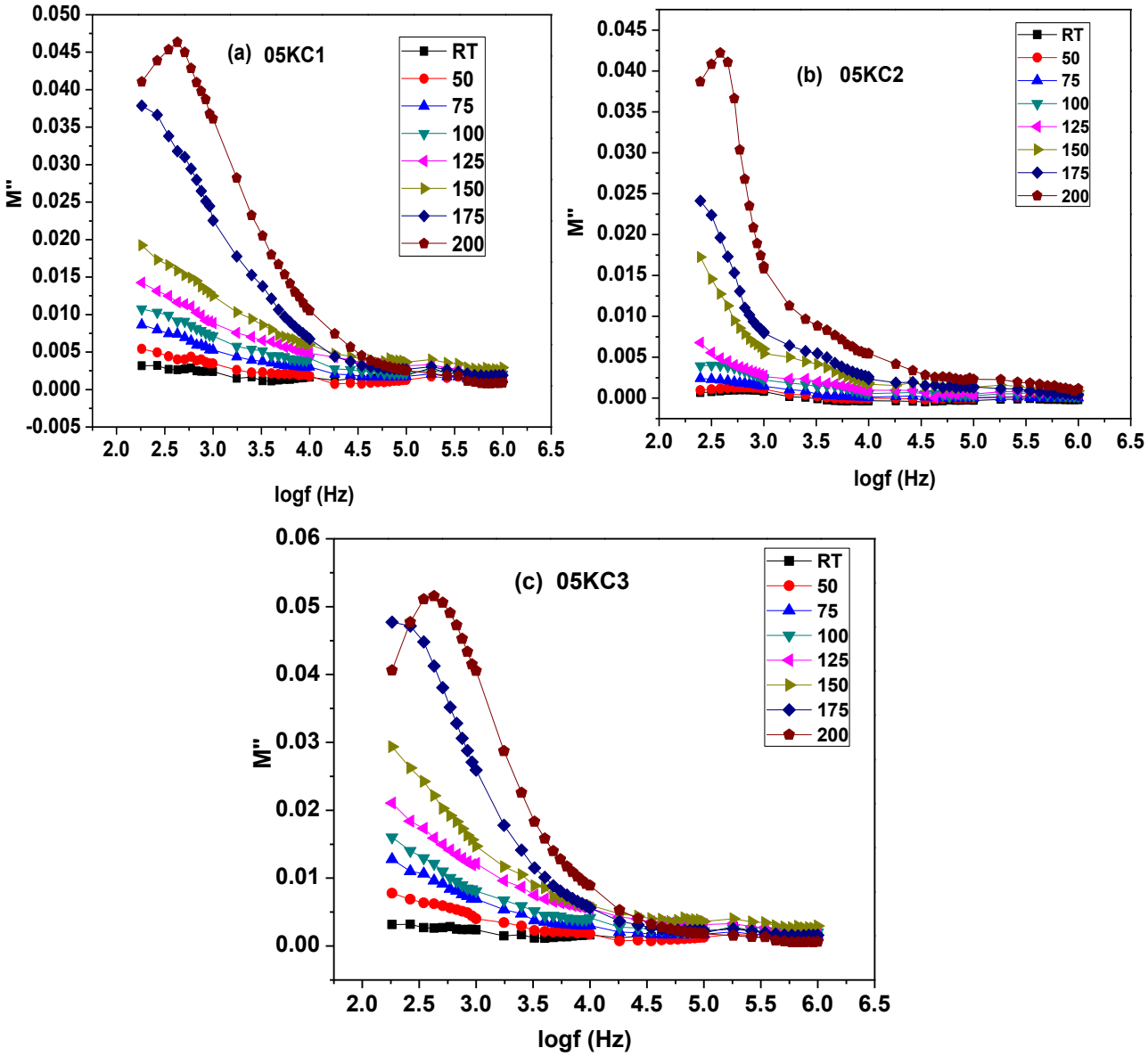

Fig. 5.16: Variation of M'' as a function frequency for (a) 05KC1, (b) 05KC2 and (c) 05KC3 at different temperatures.

The variation of the imaginary part of the electric modulus (M'') of 05KC1, 05KC2 and 05KC3 with frequency at selected temperatures are shown in Figures 5.16 (a-c). The maxima value of M'' (M''_{max}) shifts towards higher frequencies side with rise in temperature indicating the presence of temperature dependent relaxation process.

The shifting of relaxation peaks suggests that there is a spread of relaxation times. The relaxation mechanism at lower temperature and lower frequency is different from higher temperature and higher frequency. The nature of the figures at low frequency region suggest that there are other relaxation peaks also present at frequency lower than 100 Hz.

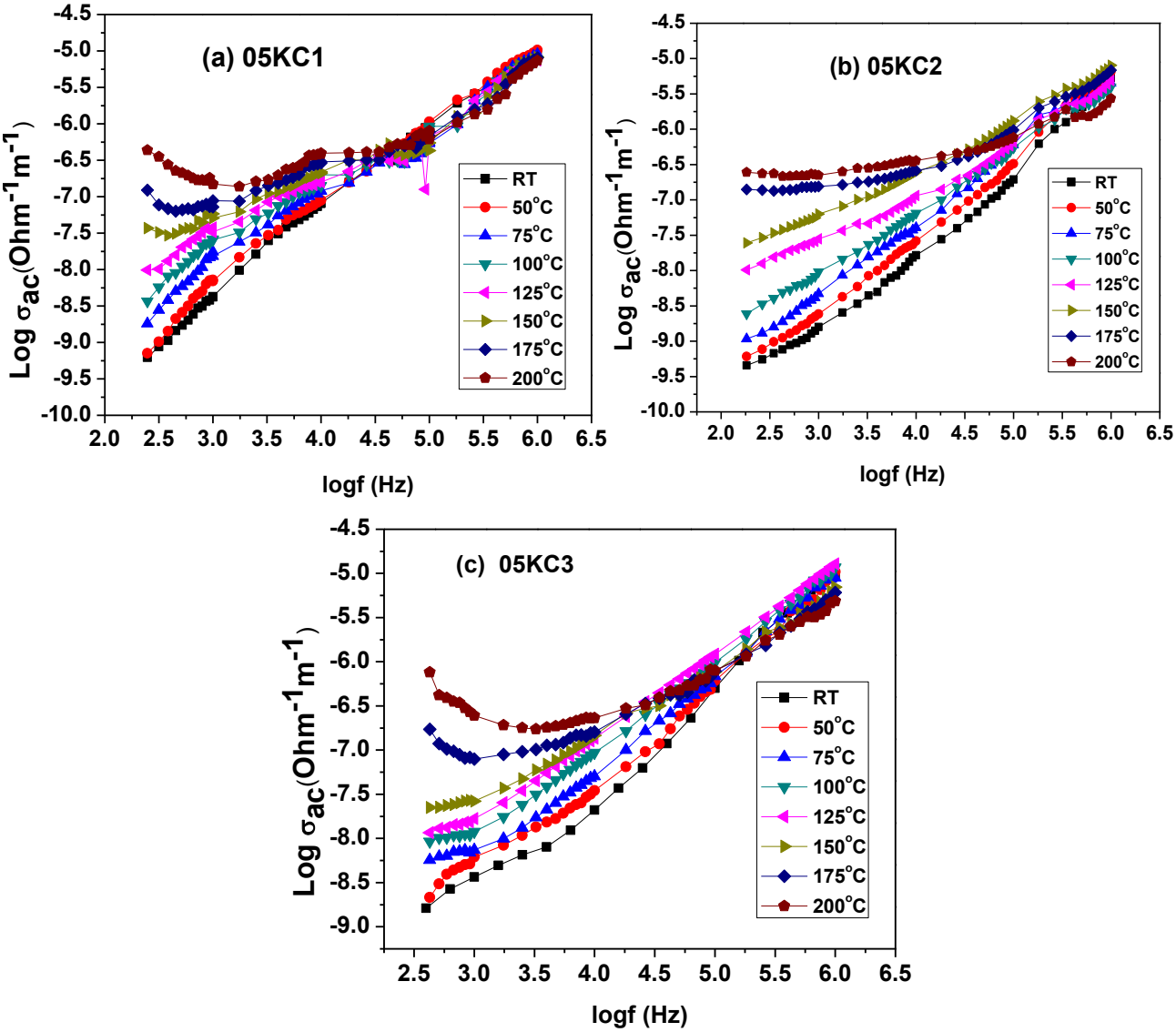

Fig. 5.17: Frequency dependent ac conductivity for the (a) 05KC1 (b) 05KC2 and (c) 05KC3 at different temperatures.

The frequency dependence of ac conductivity (σ_{ac}) of 05KC1, 05KC2 and 05KC3 at different temperatures in wide range of frequencies are shown in Fig. 5.17 (a-c). The σ_{ac} was calculated using an empirical relation i.e. $\sigma_{ac} = \omega\varepsilon_r\varepsilon_0 \tan\delta$, where ε_0 is the permittivity in free space, and ω is the angular frequency. The σ_{ac} patterns show a frequency independent plateau in the low frequency region and exhibits dispersion at higher frequencies. This behavior satisfies the universal power law $\sigma(\omega) = \sigma_0 + A\omega^n$, where σ_0 is the dc conductivity, A is the pre-exponential factor and n is the fractional exponent, whose value lies in between 0 and 1. It is observed that σ_{ac} increases with the increase in temperature and that confirms the negative temperature coefficient of resistance behavior. This behavior also suggests that the electrical conduction in the sample is increasing at the higher temperature which may be due to the increase in the segmental mobility of the polymer molecules. It can also be seen that ac conductivity decreases with decrease in frequency and becomes independent of frequency after a certain limit. Dc conductivity (σ_{dc}) has been calculated by extrapolating this towards the lower frequency side, which follows Arrhenius law given by $\sigma_{dc} = \sigma_0 \exp[-E_a/K_\beta T]$. Where E_a is the activation energy of conduction and T is the absolute temperature. Fig. 5.18 (a-c) shows the variation of logarithmic of dc conductivity ($\log \sigma_{dc}$) against 1000/T. The nature of variation is almost linear over a wide temperature region. The linear least squares fitting to the data gives the values of $E_a \sim 0.48$ eV, 0.60 eV and 0.39 eV, respectively, for 05KC1, 05KC2 and 05KC3. The lower value of activation energy is obtained in case of 05K3 may be due to the decrease in the height of the potential barrier between two orientational conformation states, which can be reached during the molecular motion. Since, the

potential barrier between two orientational conformation states in case of 05KC3 is lower than the other samples, which facilitates the motion of the molecules and increases the value of ε_r, tanδ and conductivity in the sample.

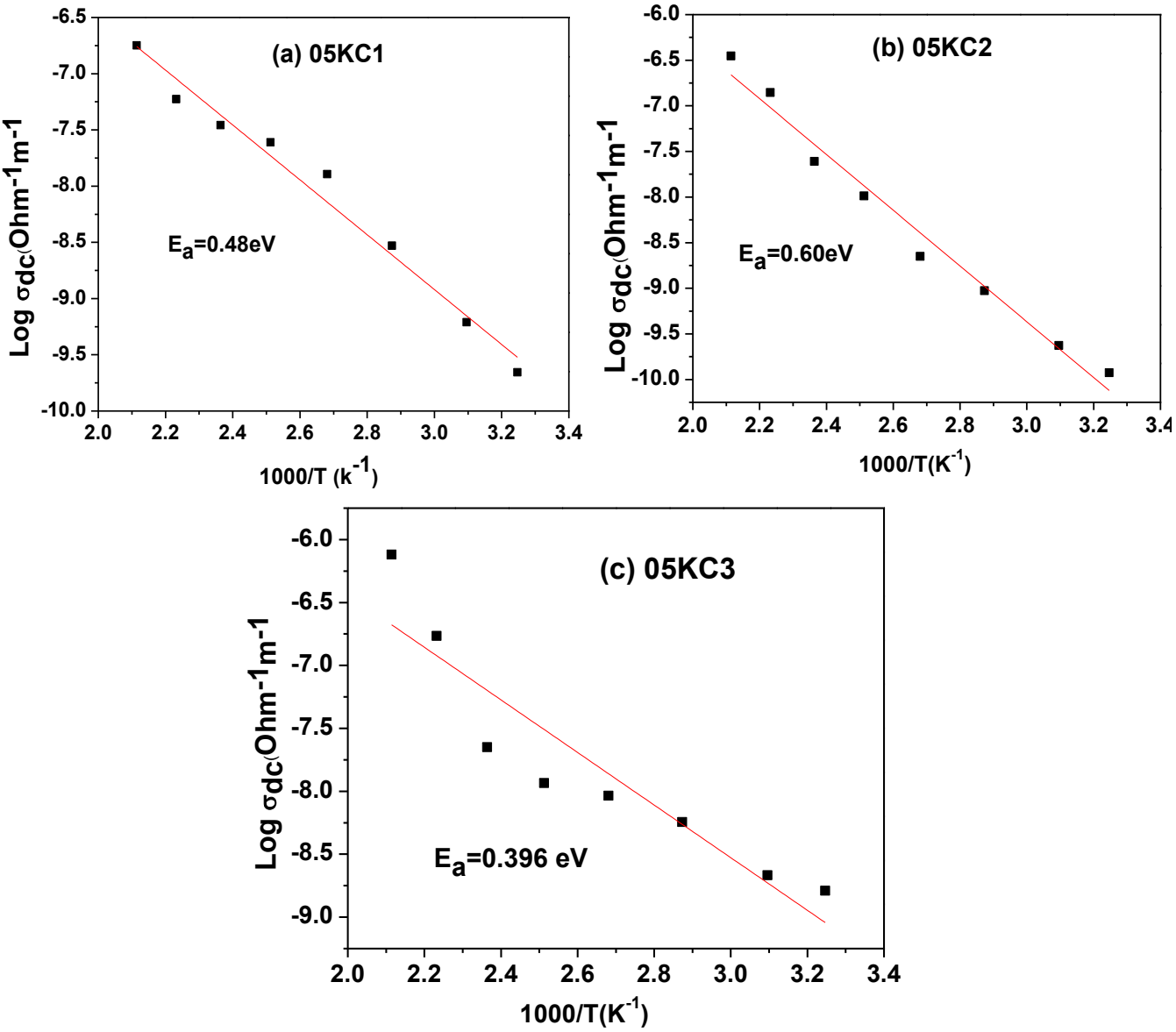

Fig. 5.18: Variation of dc conductivity against 1000/T for the (a) 05KC1, (b) 05KC2 and (c) 05KC3 composites.

5.3 Conclusions

The macromolecular study on the raw and $KMnO_4$ treated sisal fibers by SAXS analysis suggests that 05K2 fiber has less void content showing the least disorderness among all the investigated $KMNO_4$ treated fibers. The degree of crystalinity, crystallite size and bulk density are found to be highest for the above mentioned fiber. Maximum reduction of OH group and lignin content are observed for the 05K2 sample followed by 05K1. Enhancement of the surface roughness and better wetting of 05K2 fibers in the epoxy has been confirmed from the SEM micrograph. The higher mechanical strength i.e. flexural and tensile strength for 05KC2 are due to the better mechanical interlocking of the fiber with the matrix. The lower values of ε_r and tanδ for the above mentioned composite may be due to the reduction of OH group, rigid interface between the fiber and matrix. The higher value of ε_r in case of 1KC3 may be due to the increase in the polar group due to the degradation of the cellulose because of the excessive oxidizing effect of $KMnO_4$ at a higher concentration with higher soaking time. The relaxation mechanism of the sisal fibers are studied with the help of electric modulus and ac conductivity. It is found that with increase in temperature and treatment time ac conductivity increases. The activation energy of the 05KC2 is found to be higher than the 05KC1 and 05KC3. The broadening of the relaxation peak in the imaginary part of modulus indicates the presence of relaxation process in the material. Finally it is concluded that the 0.05% of $KMnO_4$-acteone solution is the best to modify the sisal fiber surface if it is immersed in the solution for 2 min to have a better tensile and flexural strength. It is also found to have lower values of dielectric loss and ε_r.

References:

1. Spinace MAS, Lambert CS, Fermoselli KKG, Paoli MAD. Characterization of lignocllulsic curaua fibre. Carbohydr Polym, 77, (2009) 47-53.
2. Patra A, Bisoyi DK, Dielectric and impendance spectroscopy studies on sisal fibre reinforeced Polyester composite. J Mater Sci, 42, (2010) 5742–5748.
3. Mylsamy K, Rajendran I, Influence of alkali treatment and fibre length on mechanical properties of short Agave fibre reinforced epoxy composites. Mater design, 32, (2011) 4629–4640.
4. Corrales F, Vilaseca F, Llop M, Girones J, Mendez JA, Mutje P, Chemical modification of jute fibers for the production of green composites. J Hazard Mater, 144, (2007) 730–735.
5. Mominul HM, Hasan M, Saiful Islam M, Ershad AM, Physico- mechanical properties of chemically treated palm and coir fiber reinforced polypropyle composites. Bioresour Technol, 100, (2009) 4903–4906.
6. Kalia S, Kaith BS, Kaur I, Pretreatments of natural fibers and their application as reinforcing material. Polym Eng Sci, 49, (2009) 1253-1272.
7. George J, Bhagawan S, Thomas S, Improved interactions in chemically modified pineapple leaf fiber reinforced polyethylene. Compos Interf, 5, (1998) 201-223.
8. Paul PA, Oommen C, Joseph K, Mathew G, Thomas S, The role of interface modification on thermal degradation and crystallization behavior of composites from commingled polypropylene fiber and banana fiber, Polym Composite, 31, (2010) 113–1123.
9. Khan MA, Hassan M, Taslima R, Mustafa AI, Role of pretreatment with potassium permanganate and urea on mechanical and degradable properties of photocured coir (cocos nucifera) fiber with 1, 6-hexanediol diacrylate. J Appl Polym Sci, 100, (2006) 4361– 4368.
10. Paul A, Joseph K, Thomas S, Effect of surface treatments on the electrical properties of low-density polyethylene composites reinforced with short sisal fibers. Compos Sci Technol, 51, (1997) 67-79.

11. Wolfgang G, Martinschitz KJ, Boesecke P, Keckes J, Structural changes during tensile testing of an all-cellulose composite Composites by in situ synchrotron X-ray diffraction, Compos Sci Technol, 66, (2006) 2639–2647.
12. Toki S, Sics I, Ran S, Liu L, Hsiao BS. Molecular orientation and structural development in vulcanized polyisoprene rubbers during uniaxial deformation by in situ synchrotron X-ray diffraction. Polymer, 44, (2003) 6003–6011.
13. Kelarakis A, Yoon K, Sics I, Somani RH, Hsiao BS, Chu B. Uniaxial deformation of an elastomer nanocomposite containing modified carbon nanofibers by in situ synchrotron X-ray diffraction. Polymer, 46, (2005) 5103–5017.
14. Bal S, Behera RC. Analysis of structural parameter of acid and alkali treated polyester fibers using SAXS and other techniques. Indian J Eng Mater Sci, 14, (2007) 240-252.
15. Chand N, Jain D, Effect of sisal fibre orientation on electrical properties of sisal fibre reinforced epoxy composites. Composites: Part A, 36, (2005) 594–602.
16. Hong CK, Wool RP, Development of a bio-based composite material from soybean oil and keratin fibres. J Appl Polym Sci, 95, (2005) 1524–1538.
17. Hong CK, Wool RP, Low dielectric constant material from hollow fiber and plant oil. J Natural Fibres, 1, (2004) 83–92.
18. Patra A, Bisoyi DK, Investigation of the electrical and mechanical properties of shortsisal fiber-reinforced epoxy composite in correlation with structural parameters of the reinforced fiber. J Mater Sci, 46, (2011) 7206–7213.
19. Ruland W, Small-angle scattering of two-phase systems: determination and significance of systematic deviations from porod's law. J Appl Cryst, 4, (1971) 70-73.
20. Khan NMD, Small angle X-ray scattering study of sisal fiber using correlation function. Ph. D Thesis. (1991) 71–72.
21. Vonk CG, A general computer program for the processing of small angle X-ray scattering data. J Appl Cryst, 8, (1975) 340-341.
22. Vilay V, Mariatti M, Mat Taib R, Todo M, Effect of fiber surface treatment and fiber loading on the properties of bagasse fiber–reinforced unsaturated polyester composites. Compos Sci and Technol, 68, (2008) 631–638.

23. Mishra T, Bisoyi DK, Patel T, Patra KC, Patel A, Small angle x-ray study of cellulose in cotton using correlation function Polym J, 20, (1988) 739-749.
24. Prasad N, Patnaik J, Bohidar N, Mishra T, Effect of temperature on Nylon 6 fibers at different denier values and study of macromolecular parameters by SAXS technique. J Appl Poly Sci, 67, (1998) 1753–1759.
25. Segal L, Creely J, Martin JAE, Conrad CM, An empirical method for estimating the degree of crystallinity of native cellulose using the X-ray diffractomerter. Text Res J, 29, (1959) 786-794.
26. Yan L, Chunjing H, Yehong Y, Interfacial studies of sisal fiber reinforced high density polyethylene (HDPE) composites. Compos Part A, 39, (2008) 570–578.
27. Moharana S, Mishra SB, Tripathy SS, Permanganate-initiated graft copolymerization methyl methacrylate onto jute fibers. J Appl Polym Sci, 40, (1990) 354-357.
28. Georgopoulos ST, Tarantili PA, Avgerinos E, Andreopoulos AG, Koukios EG, Thermo plastic polymers reinforced with fibrous agricultural residues. Polym Degrad Stabil, 90, (2005) 303– 312.
29. Franco PJ, Valadez-Gonzalez A, A study of the mechanical properties of short natural fibre reinforced composites. Compos Part B, 36, (2005) 597–608.
30. K. Joseph, S.Thomas, C. Pavithran, Effect of chemical treatment on the tensile properties of short sisal fibre-reinforced polyethylene. Polymer, 37, (1996) 5139-5149.
31. Hanna AA, Ibrahem AA, Heikal SO, Some Electrical Properties of Wood Pulp Treated with Sodium Hydroxide. J Polym Sci Polym Chem Ed, 18, (1980) 1425-1429.
32. Macdonald JR, Impedance Spectroscopy, John Wiley & Sons, New York (1987).

Chapter 6

Influence of Microwave Irradiation

6.1. Introduction

Development of environment friendly product is gaining impressive attention from the last few decades due to the increased awareness about the environmental concerns and the rising interest in buying eco-friendly products. It has gradually shifted the economy towards the toxic alternatives. Due to this, the development on the natural fiber reinforced polymer composite (NFRPC) has become an attractive active research area [1]. Fiber modification by chemical and physical methods are found to be the effective way to deal with the hydrophilicity of the fiber and resulting in good wetting of the fibers with the matrix [2]. Though chemical modifications are suitable in modifying the fiber for its potential applications but the hazardous chemicals that are required to modify the surface are still remain health and environmental concern. Increasing awareness for the environment has given an impetus to research on the non-hazardous method to modify the surface of the natural fiber for total or partial replacement of chemical methods, which has

environment degrading effect. In this regard microwave irradiation on the natural fiber is gaining substantial attention. Microwaves are electromagnetic waves that lie between radio and infrared frequency regions in the electromagnetic spectrum. The majority of the microwaves frequencies are dedicated for communications and radar purposes, while the following frequencies 915 MHz, 2.45 GHz, 5.8 GHz, and 20.2-21.1 GHz are designated for industrial, scientific, and medical uses [3, 4]. Kitchen microwave ovens operate at a frequency of 2.45 GHz frequency due to the fact that the water molecules present in food show good microwave absorption at this frequency. The relative availability of 915 MHz and 2.45 GHz microwave ovens has made it popular in the applications for the processing of materials [3]. Microwaves interact with materials in different ways. Depending on the materials, microwaves are generally reflected, transmitted or absorbed. The ability of certain materials to convert microwaves into heat makes these materials suitable for microwave processing [5]. In conventional heating, the heating elements supply heat to the sample; the majority of heat is concentrated along the surface of the body when compared with the interior of the sample. In microwave heating, the material will absorb microwave energy and then convert it into heat. In recent years many materials are dried and modified under microwave irradiations [6, 7]. Xue et al. [8] have studied the structural and physical properties of microwave irradiated wool fabric. They have found that microwave heating is more efficient than conventional heating. Silk degumming using microwave irradiation was done by Mahmoodi et al. [9]. Their finding supports the potential production of new environment friendly textile fibers using microwave. Microwave irradiation is also found to be suitable for

joining of green composites [10]. Microwave heating of cotton fibers during mercerization reduces the values of concentration of NaOH in the aqueous solution and the time of treatment that are needed for the complete transformation of cellulose lattice type I into cellulose lattice type II without any heating [11]. The above findings show that microwaves irradiation is as an alternative processing method for the fiber as well as composite due to their beneficial effects on processing time, mechanical and thermal properties. However, there is hardly any report on the effect of the microwave irradiation on the macromolecular structure of the sisal fiber.

Dewaxing of the sisal fiber is found to be beneficial from both mechanical and electrical point of view when it is reinforced in epoxy matrix [12]. The present analysis is an attempt to study the effectiveness of the microwave irradiation on the properties of the fiber as well as composite. Special emphasis is made on the study of macromolecular parameters of the raw and microwave treated (MT) sisal fiber.

6.2. Results and discussion

6.2.1 SAXS Analysis

Fig 6.1 exhibits the diffuse scattering curve for the untreated and MT fibers. The background corrected intensities are used for the analysis of the SAXS data. Five background corrected intensities are taken for extrapolation up to x=0 as it is practically impossible to get the scattering curve up to x=0, where x=2$a\theta$ and 2θ is the scattering angle. The extrapolated points are indicated by hollow symbols in the inset graph of Fig. 6.1. The above method of extrapolation does not disturb the position and height of the 1st subsidiary maxima of the one dimensional correlation function $C_1(y)$

[13]. The small but finite positive values of R in table 6.1 evaluated by using the equation (2.3) from the smeared the out intensities indicates that samples are non-ideal two phase system [14].

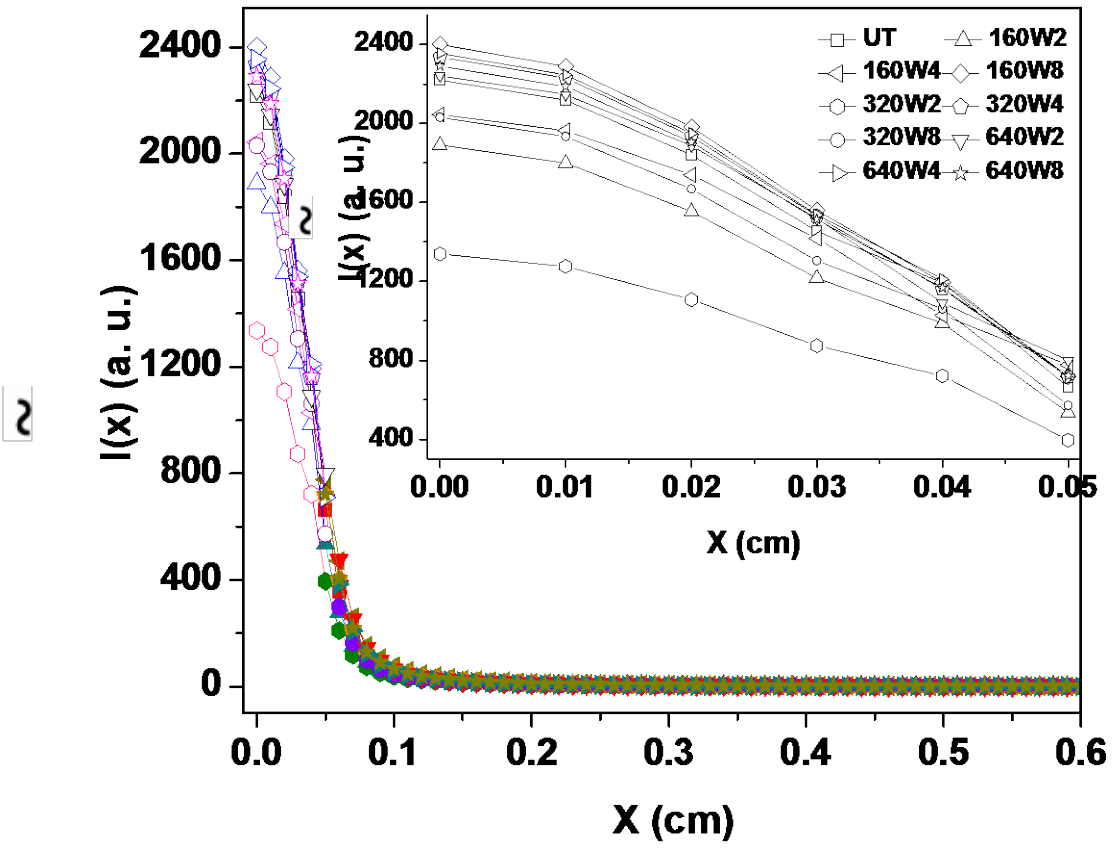

Fig 6.1: Background-corrected, smeared-out scattering curves for raw and MT sisal fibers. **Inset:** Magnified view of the initial scattering curves to show the extrapolated data.

The $C_1(y)$ of all the fibers for various values of y are computed and the plots are given in the Fig. 6.2. Previous works on the lignocellulosic fiber suggest that the areas of cellulose production near the protoplasm are related to each other in some

order. Hence form the cellulose molecules with high degree orientation to each other. This leads to the kind of isotropic lamellar structure [15]. It justifies taking into account of one dimensional correlation function for all the investigated fiber samples [16].

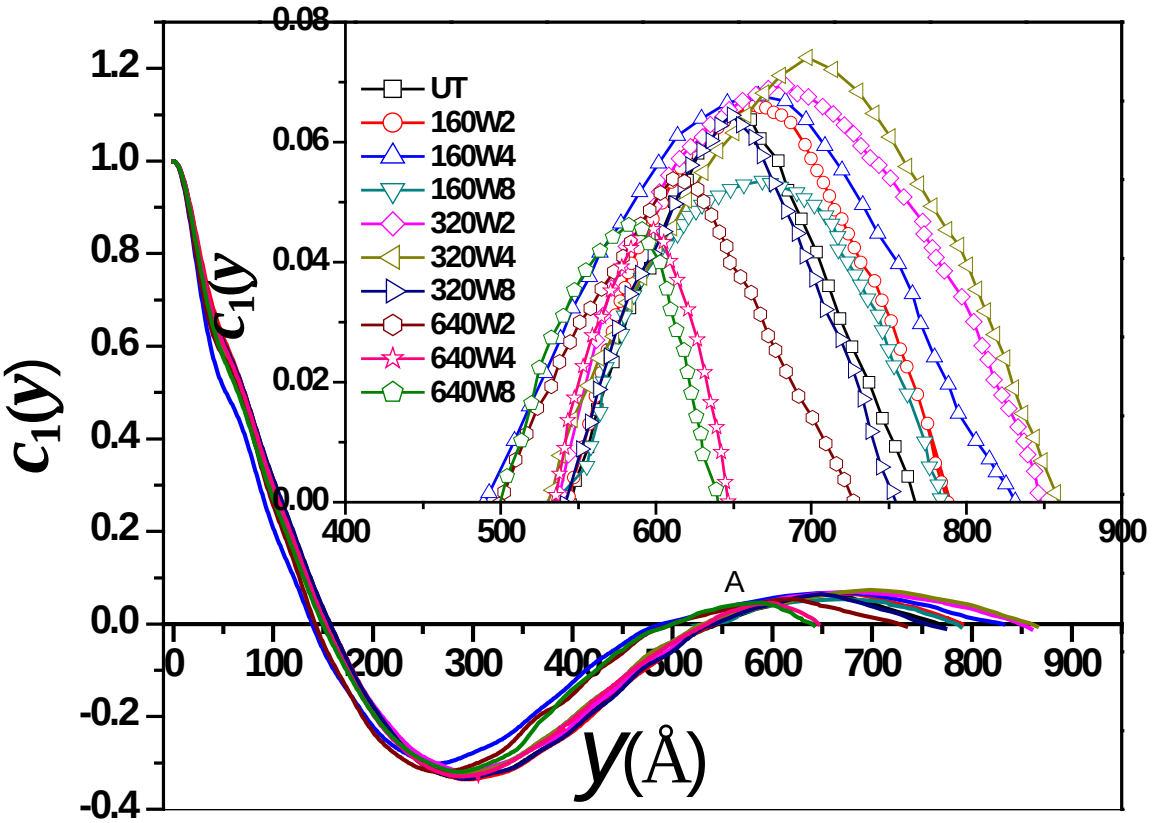

Fig. 6.2: Variation of one dimensional correlation function $C_1(y)$ against y for the raw and MT fibers. **Inset:** First subsidiary maxima of the one-dimensional correlation functions

The observed maximum value of D corresponding to the first subsidiary maxima in the Fig. 6.2 of 320W4 sample, may be due to the sufficient evaporation of water from the fiber surface because of the efficient heating produced by the

microwave irradiation. The microwave rotates the dipoles in the fiber producing the uniform heating [17]. This also leads to the release of residual stress from the fiber. The expansion of matter phase occurs due to heat produced by microwave irradiation within the fiber. This might have caused the expansion of matter phase and compression of void phase.

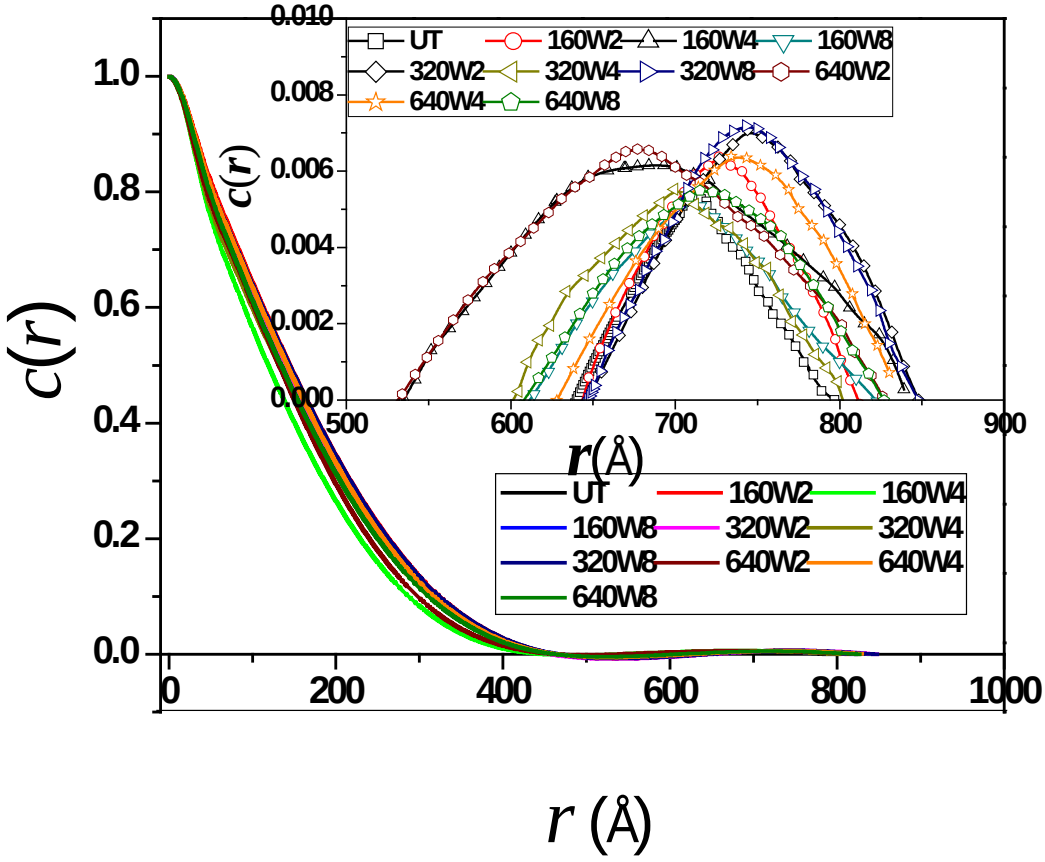

Fig. 6.3: Variation of three dimensional correlation function C(r) against r for raw and MT fibers. **Inset:** First subsidiary maximum of the three-dimensional correlation functions.

It is observed that at the microwave power setting of 160W and 320 W the values of l_1 and ϕ_1 are increased from 2 min to 4 min period of irradiation and

beyond that l_1 and ϕ_1 starts decreasing. However, at a higher power of 640 W, with the increment in irradiation period these parameters are decreased. The values of $\bar{l}_1$ and ϕ_1 are found to be highest for 320W4 which may be due to the rearrangement of cellulose micro fibril, decreasing the volume fraction of the void content.

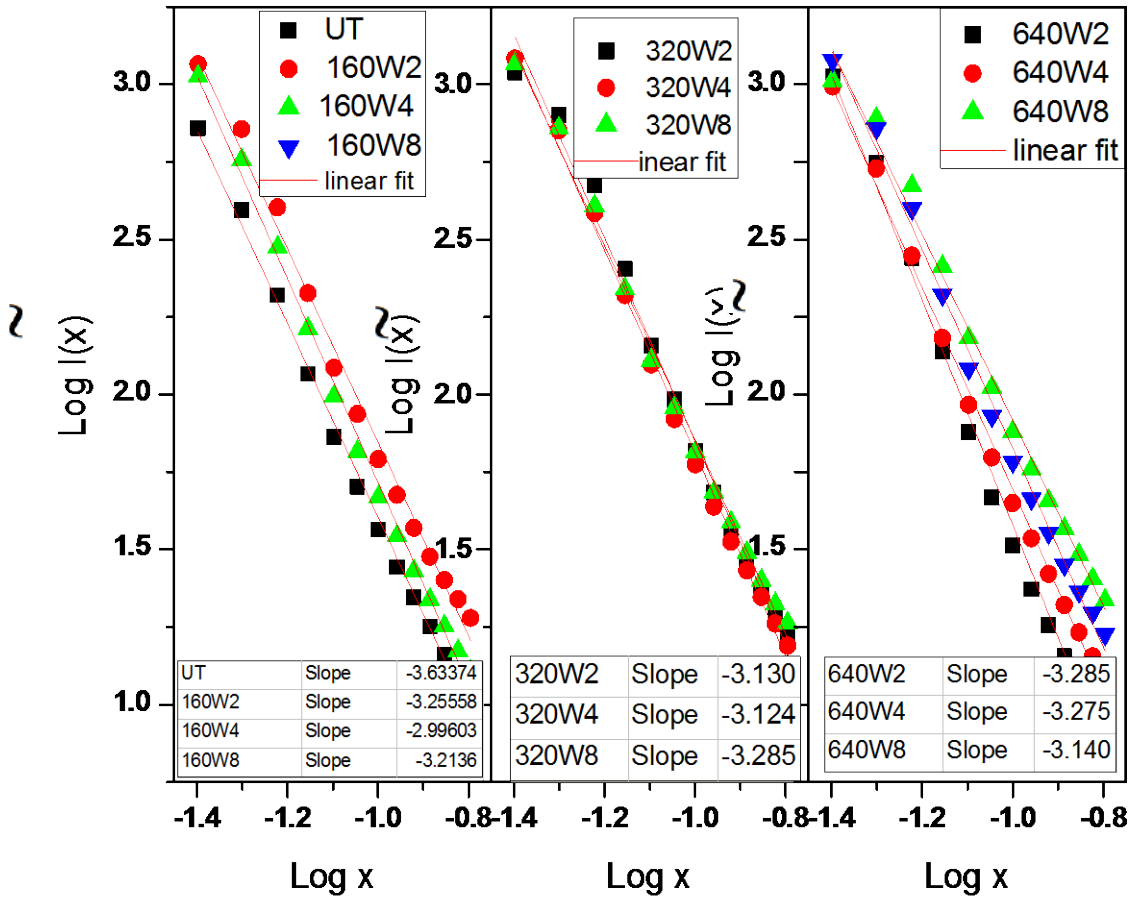

Fig. 6.4: Double logarithmic plots for raw and MT fibers.

The values of $C(r)$ have been computed according to the relation (2.5) are displayed in Fig. 6.3. The curve pattern of $C(r)$ has same nature as that of $C_1(y)$. These computed values of $C(r)$ are used for the subsequent analysis. The slope of $C(r)$ at

different points of *r* has been derived by central difference method taking constant interval of 1Å. The logarithmic plots between the *x* and $\tilde{I}(x)$ for the raw and treated fiber are compiled in Fig. 6.4. The negative slopes of all the plots are ~ -3. This suggests that all the samples are non-ideal two phase systems [18]. In the present study, the widths of transition layers are calculated by two different methods as described by Ruland and Vonk.

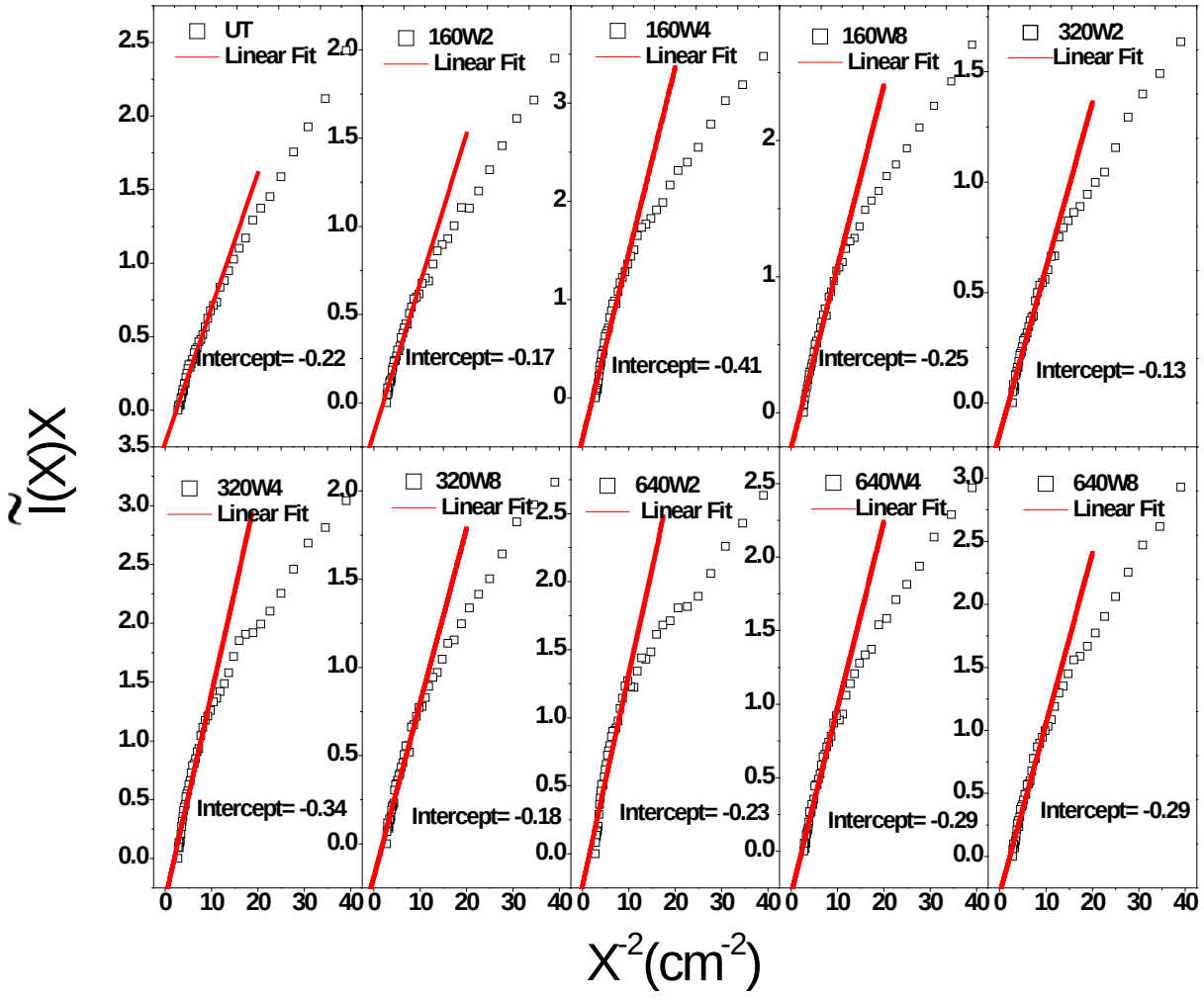

Fig. 6.5: Ruland plots $\tilde{I}(x)x$ Vs x^{-2} for raw and MT sisal fibers.

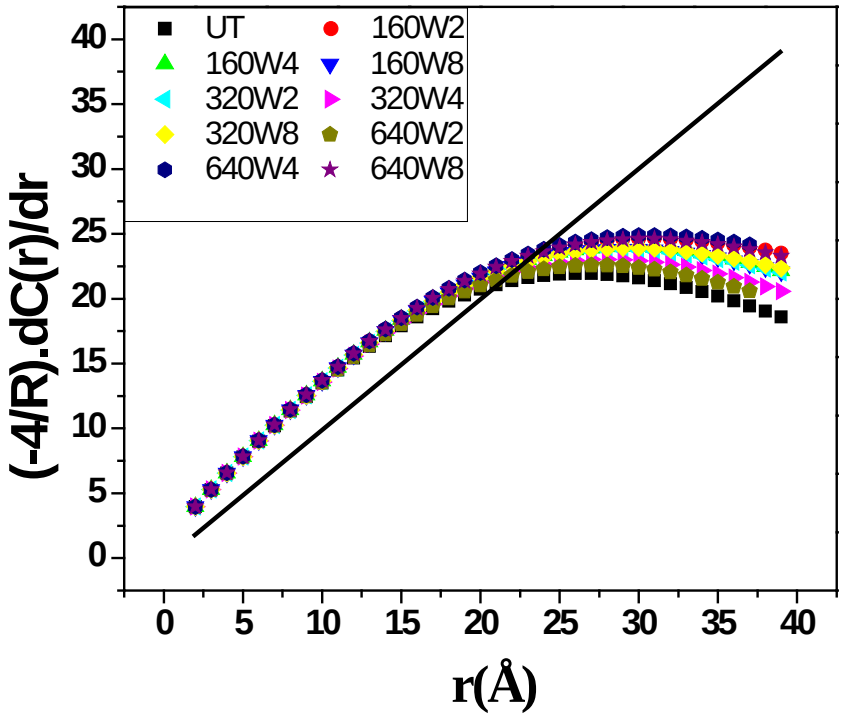

Fig. 6.6: Variation of $\left(-\frac{4}{R}\right)\frac{dC(r)}{dr}$ against r for the raw and MT sisal fibers to find out the E_v of the respective fibers.

Fig. 6.5 displays the typical Ruland plots for all the investigated fibers. The values of E_r can be calculated from the Ruland plot which is a graph of $\tilde{I}(x)x$ vs x^{-2}. The values are found to be 23.293 , 23.011 , 22.844 , 22.778 , 22.07 , 22.902 , 21.788, 23.806, 23.297 Å for 160W2, 160W4, 160W8, 320W2, 320W4, 320W8, 620W2, 640W4, 640W8 fibers respectively. The standard deviations (σ) of the intensities are well within the permissible range showing the accuracy of the data collection. The width of transition layer by Vonk (E_v) method is calculated from the plot between $\left(-\frac{4}{R}\right)\frac{dC(r)}{dr}$ vs r and are shown in Fig. 6.6. The straight line equidistance from both

the axes has been drawn and the point of intersection with the curve gives the value of E_v [19] as 23.293, 23.011, 22.844 , 22.778 , 22.07, 22.902, 21.788, 23.806, 23.297 Å for 160W2, 160W4, 160W8, 320W2, 320W4, 320W8, 620W2, 640W4, 640W8 fibers, respectively. It is found to be in close agreement with E_r justifying the accuracy of our analysis.

Table 6.1: Various Macromolecular parameters of raw and MT sisal fibers derived from SAXS study.

Macro molecular parameters	UT	160W2	160W4	160W8	320W2	320W4	320W8	620W2	640W4	640W8
R(10^{-4}Å^{-2})	8.831	9.576	11.7098	10.575	11.986	12.869	8.567	7.986	6.753	6.132
D(Å)	654	665	675	670	683	698	648	620	598	582
S/V(10^{-3} Å^{-1})	3.058	3.007	2.962	2.985	2.928	2.865	3.086	3.225	3.344	3.436
E_v(Å)	21.081	23.293	23.011	22.844	22.778	22.07	22.902	21.788	23.806	23.297
E_r(Å)	19.792	19.14	19.992	19.802	19.24	19.351	19.358	19.667	18.747	19.258
Φ_1	82.601	83.123	87.001	84.65	87.593	88.201	81.301	80.153	75.132	70.298
Φ_2	17.399	16.877	12.999	15.35	12.407	11.799	18.699	19.847	24.868	29.702
$\bar{l}_1$ (Å)	1080.421	1105.535	1174.513	1134.31	1196.520	1231.285	1053.660	993.8972	898.578	818.268
$\bar{l}_2$ (Å)	227.578	224.464	175.486	205.690	169.479	164.714	242.339	246.102	297.421	345.731
$\bar{l}_r$ (Å)	187.982	186.581	152.675	174.116	148.452	145.279	197.024	197.258	223.458	243.042
l_c	351.097	320.745	279.345	285.678	271.765	260.567	340.43	345.987	350.768	367.598
$2E_v/D$ (%)	6.446	7.005	6.818	6.819	6.669	6.323	7.068	7.028	7.961	8.005
σ	0.013	0.017	0.023	0.011	0.018	0.028	0.024	0.022	0.015	0.021

6.2.2 XRD Study

Fig. 6.7 shows the XRD patterns of the untreated and MT sisal fibers. Microwave irradiation does not change the basic crystalline nature of the cellulose but the crystallinty and crystallite size of the fiber are greatly affected by the microwaves. The highest degree of crystallinty for the 320W4 is shown by maximum increase in the intensity of the crystalline peak at 22.5^0 followed by 320W2 min and is least for 640W8 min.

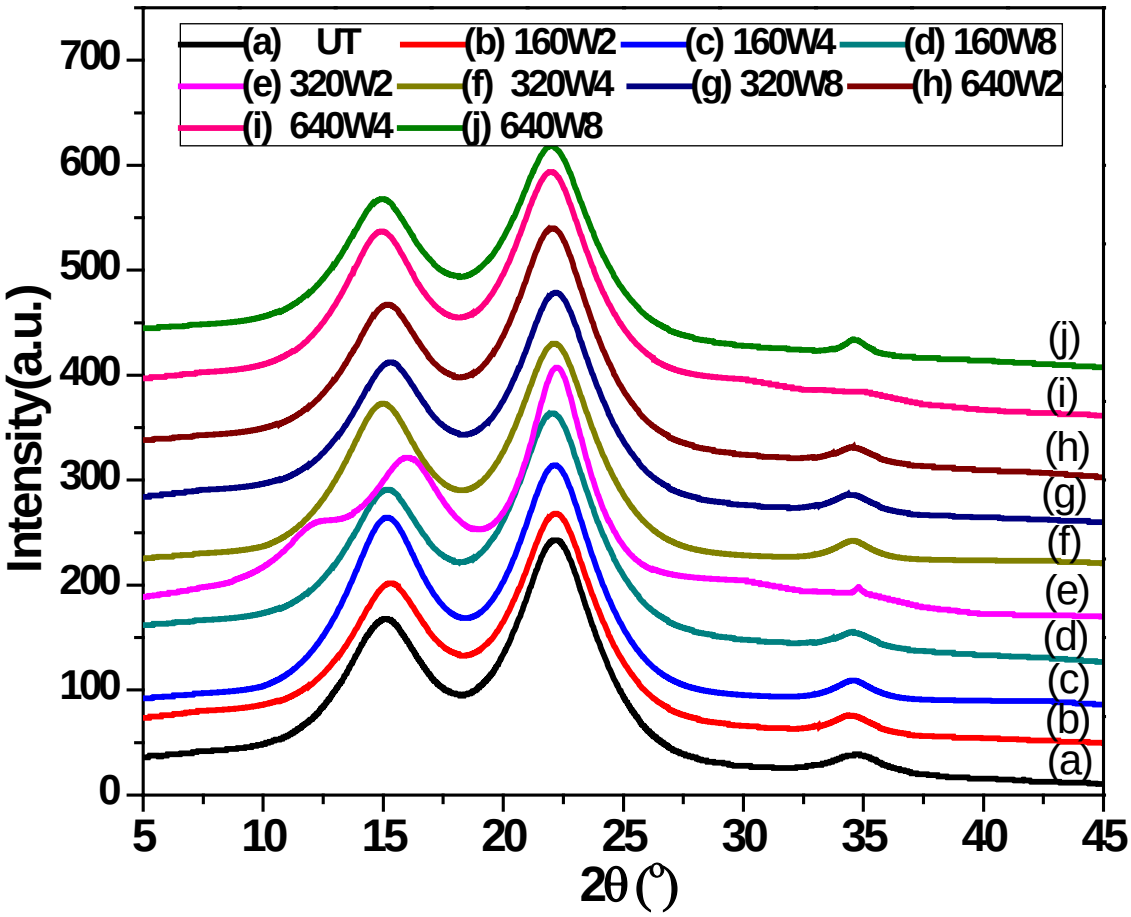

Fig. 6.7: XRD patterns of raw and MT sisal fibers.

The lower and moderate microwave power may have able to effectively release the residual stress from the fiber by the absorption of microwave and rearrangement of the fine structure of the fiber [20]. The increment in the crystallite size and crystallinity may be due to the decrease in crystal distortion and defects in the crystal which is further strengthened by the fact that the 320W4 has least (S/V), specific inner surface area. It also leads to the increment in bulk density of the fiber given in the Table 6.2. Whereas at higher power and higher irradiation period, the degradation of the strength providing cellulose becomes more due to excessive heating. The fiber becomes brittle and turns into black colour. The crystallinity and the crystallite size of these fibers seem to be decreased at higher power and become least for 640W8 which may be due to the rupturing of cellulose particle into new dimensions.

Table 6.2: Crystallographic and physical parameters of the investigated raw and MT sisal fibers.

Fiber	Degree of crystallinity(%)	Crystallite size (Å)	Density(g/cc)
UT	52.11	29.19	1.32
160W2	59.15	35.00	1.45
160W4	61.07	40.17	1.63
160W8	60.15	39.21	1.58
320W2	63.15	43.33	1.70
320W4	65.25	44.09	1.75
320W8	51.00	29.00	1.25
640W2	50.11	28.00	1.34
640W4	48.21	27.12	1.30
640W8	43.35	26.12	1.21

6.2.3 FTIR Study

Fig. 6.8 exhibits the FTIR Spectra of the untreated and MT sisal fibers. The broad absorbance peak at 3200-3400 cm^{-1} corresponds to the O-H stretching of hydrogen bond network [30].

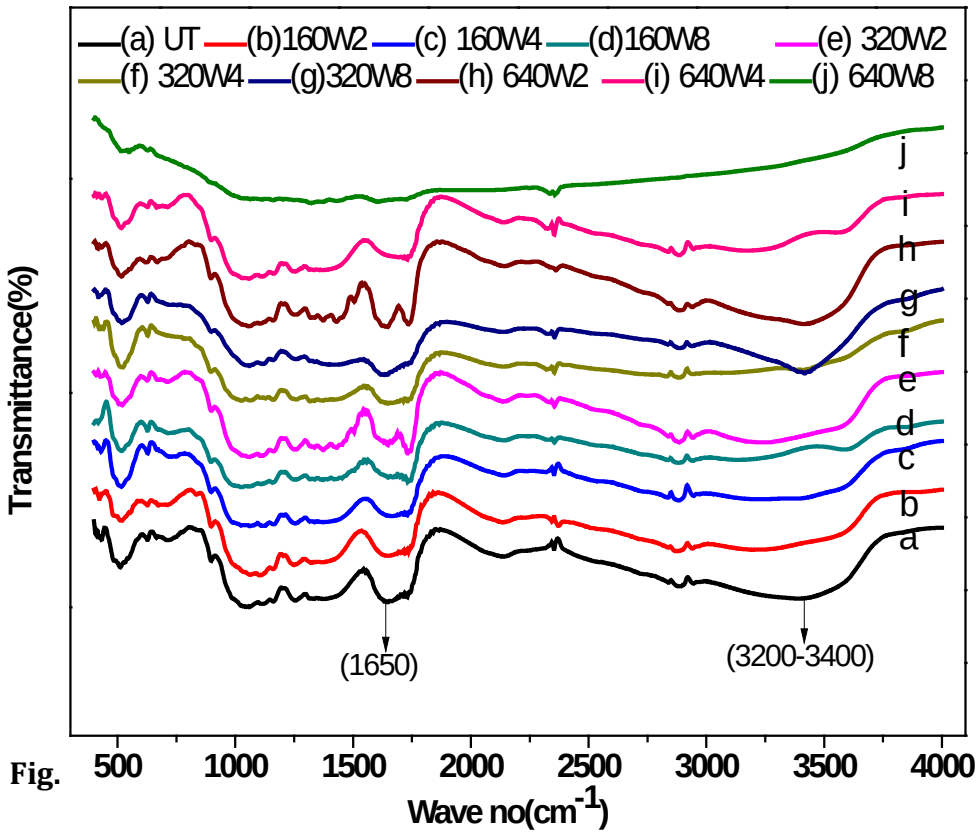

Fig. **6.8:** FTIR spectra of raw and MT sisal fibers.

It shows that hydrogen bond between intermolecular and intra molecular has changed significantly. The absorbance peak tends to decrease remarkably for 320W4 showing the reduction of O-H group. But at a higher treatment power and time, the intensities of O-H group tend to increase because of the degradation of cellulose and incorporation of more polar groups [21]. Hence at 640W8 the O-H group is highest.

The 1650 cm^{-1} band which corresponds to the absorbed water are found to be decreased remarkably at 320W4. Sisal is a porous dielectric medium, which means that sisal has both free and bound water within the cell. Free water can appear as vapour or liquid in the pores. Bound water is captured in the cell matrix. With the absorption of electromagnetic energy, the temperature of the sisal will reach the boiling point of water. As the temperature increases, the internal pressure also increases, causing moisture evaporation that will be forced from the interior towards the surface of the sisal fiber. It seems that these high frequency radio waves are efficient in penetrating the water molecule inside the fiber causing sufficient heat by synchronizing oscillation of water molecule. This causes heat to be generated through inter molecular friction. All other peaks are remains unaffected by the microwave tradition. It suggests that the chemical changes in MT sisal fibers are not significant. It affects the OH group and absorbed water molecules of the fiber. As a result, better hydrophobicity of the fiber is achieved at proper power setting and treatment period.

6.2.4 Morphological Study

SEM micrographs of 160W2, 160W4, 160W8, 320W2, 320W4, 320W8, 620W2, 640W4, 640W8 fibers are shown in Figs. 6.9(a-i). It is observed that with the increase in irradiation period from 2 min to 8 mins keeping the power constant (160W), the surface roughness of the fiber has been increased. At 320W power setting, the etching of the fiber surface continues from 2 min to 4 min period of irradiation. Uniform surface roughness is achieved for the 320W4 fiber sample. Beyond this damaging effect of microwave on the surface of the fiber is observed.

Fibers irradiated at 640W shows serious damaging effect on the surface of the fiber with the increase in irradiation period from 2 min to 8 min. The severity of damage can be estimated from the exposure of inner central lumen of the fiber shown in Fig 6.9 (h) and (i). Longer period of bombardment of the high energy radiation lead to the heavy damage to the surface along with the damage to the strength proving cellulose.

SEM micrographs of the fractured surfaces of the 160WC2, 160WC4, 160WC8, 320WC2, 320WC4, 320WC8, 620WC2, 640WC4, 640WC8 composites are shown in Fig. 6.10(a-i). In case of 320W4 sample, the microwave irradiation leads to the uniform surface roughness of the fiber. This may have led to the better wetting of the epoxy shown in Fig. 6.10 (e). However, longer period of bombardment of the high energy radiation lead to the heavy damage of the surface along with the damage of the strength proving cellulose. It results in the poor wetting of the fibers with the matrix as shown in Fig. 6.10 (h & i).

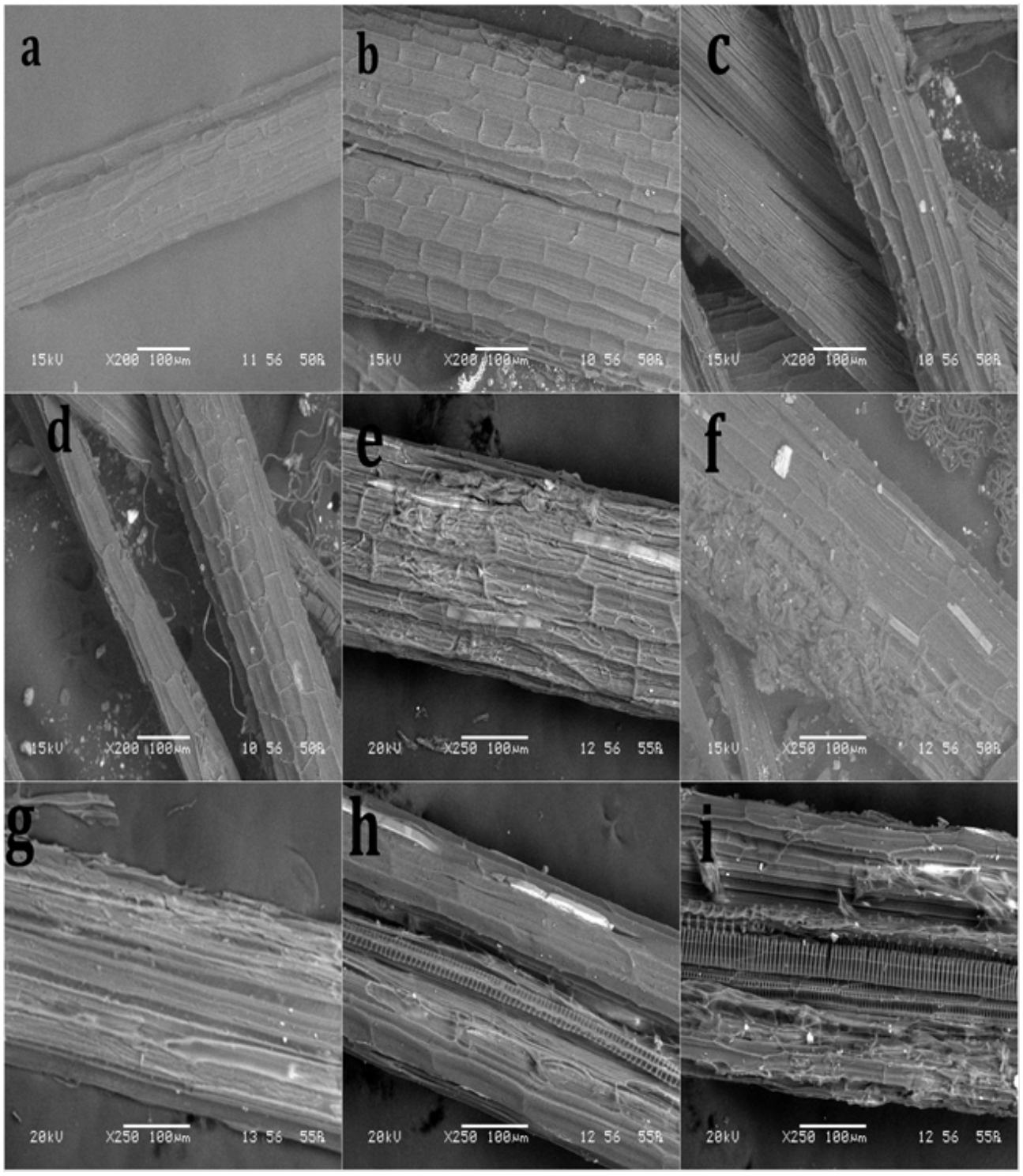

Fig. 6.9.(a-i): Longitudinal morphology of 160W2, 160W4, 160W8, 320W2, 320W4, 320W8, 620W2, 640W4, 640W8 fiber respectively.

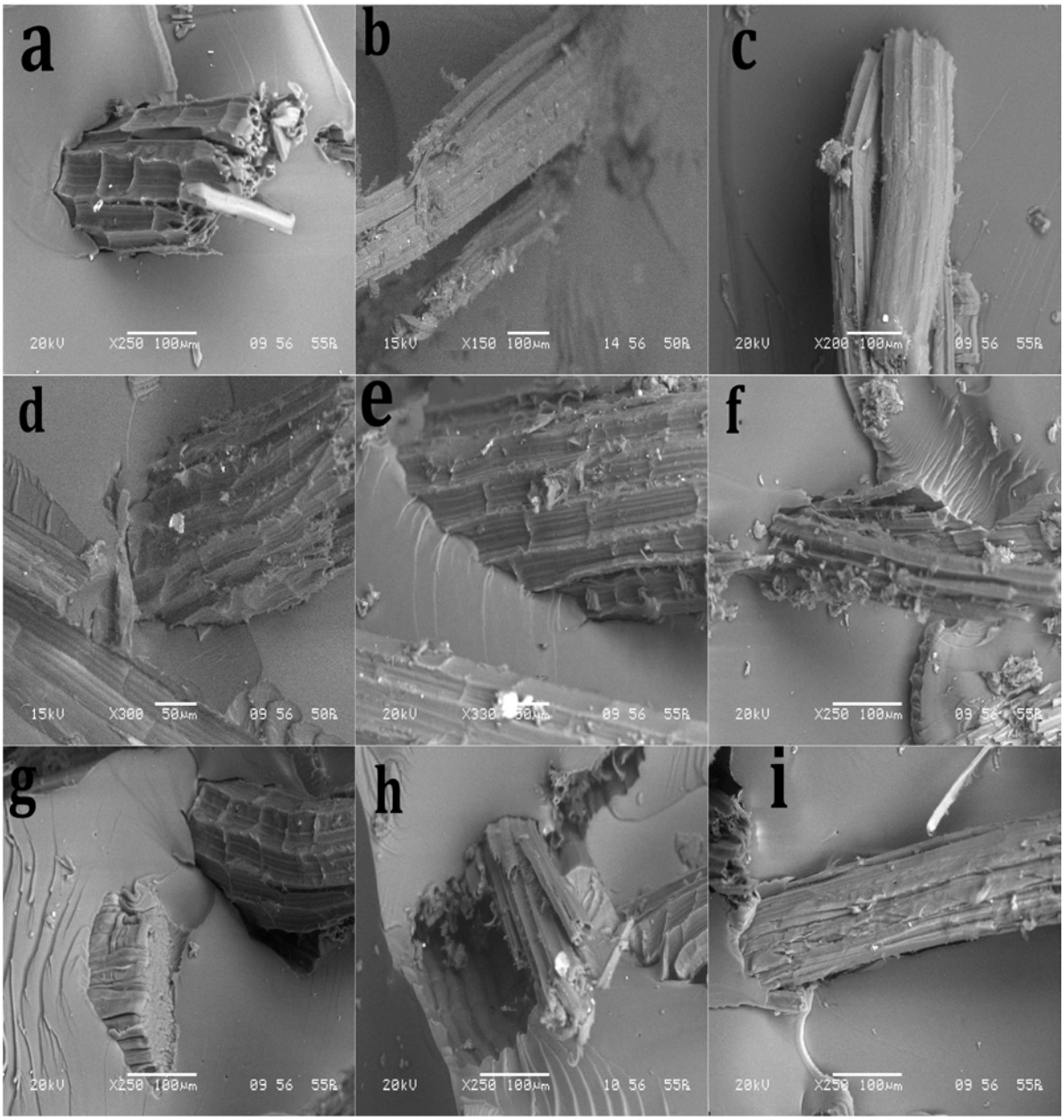

.

Fig. 6.10 (a-i): Fractured surfaces of 160WC2, 160WC4, 160WC8, 320WC2, 320WC4, 320WC8, 620WC2, 640WC4, 640WC8 composites respectively.

6.2.5 Mechanical Study

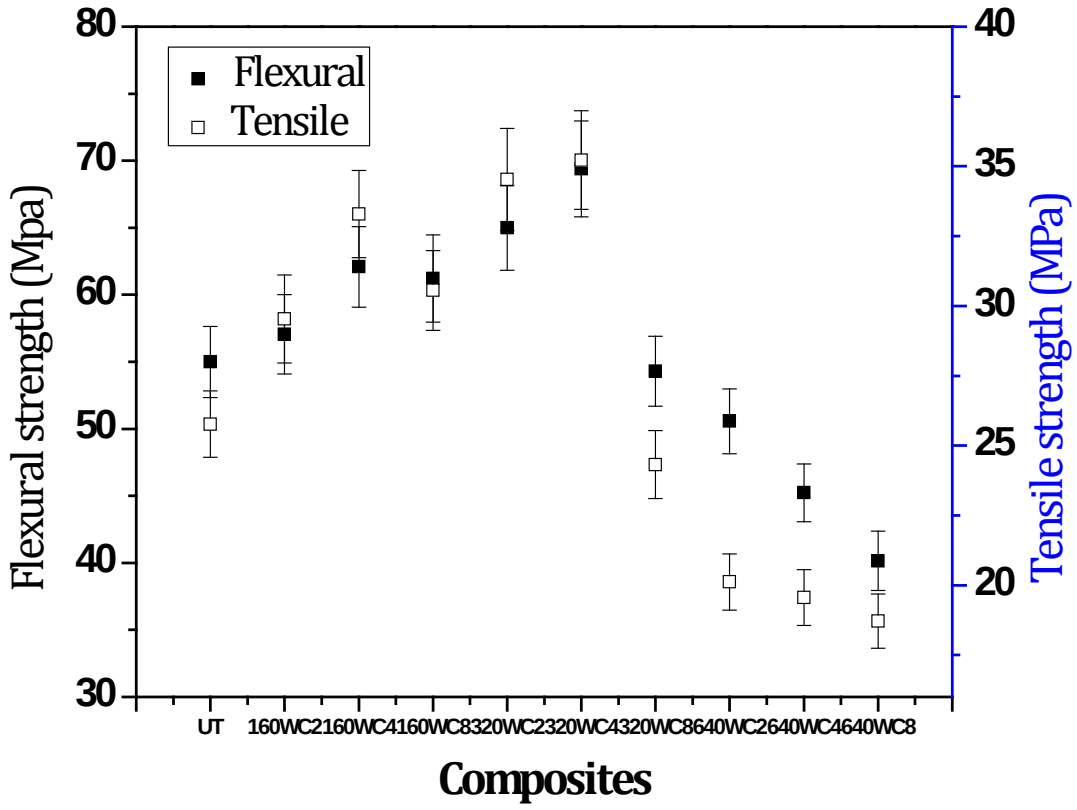

Fig. 6.11: Flexural and tensile strengths of UTC and MFREC.

Fig. 6.11 shows the flexural and tensile strength of the MT sisal fiber reinforced composite in comparison to the untreated composite. Among all the investigated composites, 320WC4 and 320WC4 composite are found to have 25% and 16 % increment in the flexural strength whereas 25% and 21% increase in tensile strength compared to untreated composite. The enhanced bonding of the fibers treated with 2 min and 4 min at moderate microwave power setting i.e. 320W may be the reason for the improvement of the flexural and tensile strength of the composite. The sufficient roughness and hydrophobicity of the fibers without damage of the

strength providing cellulose content in the fibers may have led to the better wetting of the fibers with the matrix. This results in composites with superior mechanical strength. However, 320WC8 sample is shown to have lower flexural and tensile strength. It may be due to the damage occurred to the fibers for longer exposure of microwave irradiation which in turn affects the mechanical strength of the composite. The strength reduction continues and worsens for the composites reinforced with 2 min to 8 min of microwave irradiated fibers at 640W. This might be due to the reinforcement of damaged fibers (shown in fig 6.9 (g-i)) to the matrix, led to the decrement of the mechanical strength of the composite. It may be the possible cause of lower flexural and tensile strength of the 640WC8 sample.

6.2.6 Dielectric Study

Figure 6.12 displays the frequency dependence of dielectric constant (ε_r) of both UTC and MFREC. Inset of the above Figure shows the frequency dependence of dielectric loss ($\tan\delta$). It is found that with the increase in frequency the value of ε_r as well as $\tan\delta$ decreases. The change of ε_r and $\tan\delta$ at lower frequency region is higher than that at very high frequency. Generally, the ε_r and $\tan\delta$ of a polymeric material depends mainly on interfacial and dipole polarization. The interfacial polarization is prominent in heterogeneous material and is highest at lower frequency region. Hence, the higher values of ε_r and $\tan\delta$ at lower frequency can be explained in terms of interfacial polarization and the free motion of dipoles within the material which is connected to ac conductivity relaxation.

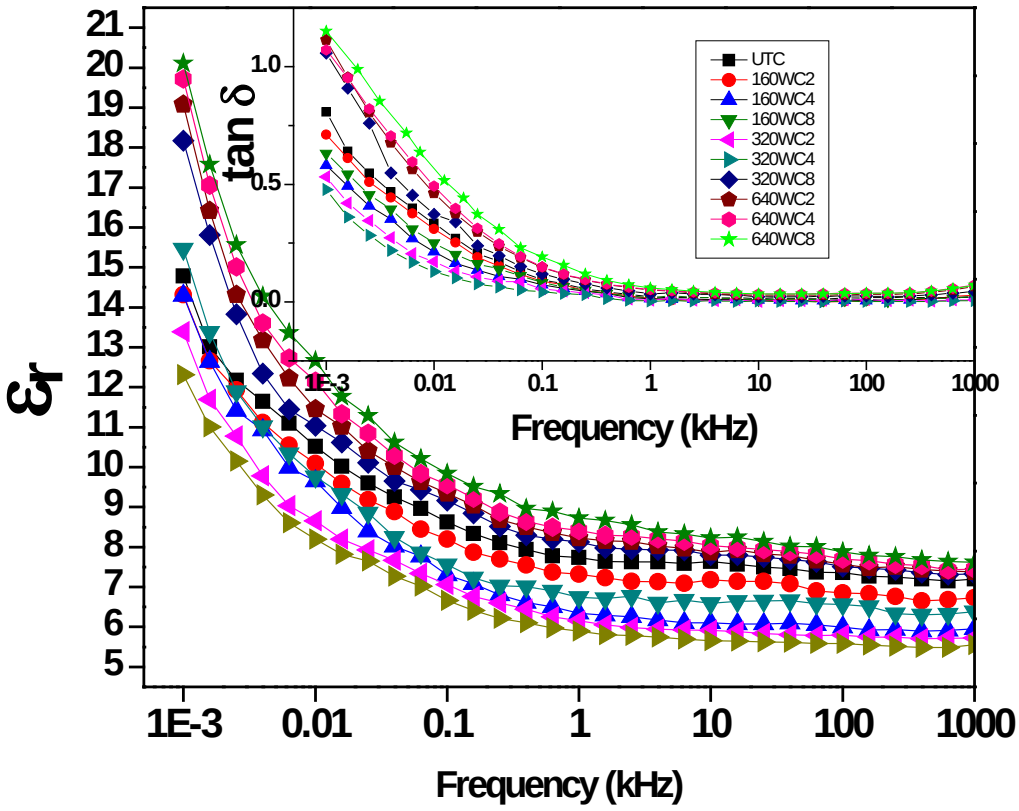

Fig. 6.12: Variation of ε_r with frequency for UTC and MFREC. **Inset:** Variation of $\tan\delta$ with frequency.

It is found that the values of ε_r of the investigated composites follows the trend of 320WC4<320WC2<160WC4<160WC8<160W2<UTC<320W8C<640WC2<640WC4<640WC8. The overall dielectric properties in a polymeric composite are the contribution of both the crystalline and amorphous content of the composite. Amorphous content makes the major contribution to both ε_r and $\tan\delta$. As a result ε_r and $\tan\delta$ value decreases with the increase in degree of crystallinity [22]. 320WC4 sample is found to have lower values of ε_r and $\tan\delta$. It may be due to the increase in the degree of crystallinity of the reinforcing fiber because of the rearrangement of cellulose chains

due to the removal of residual stress and absorbed water molecule from the fiber. However, at higher power the value ε_r tends to increase even above the corresponding ε_r value of UTC. It becomes highest for the maximum irradiation time at 640WC8. The higher irradiation time of the microwave tries to degrade the strength giving cellulose part of the fiber and hence creating more polar groups resulting in higher values ε_r and $\tan\delta$ in the 640WC8 composite.

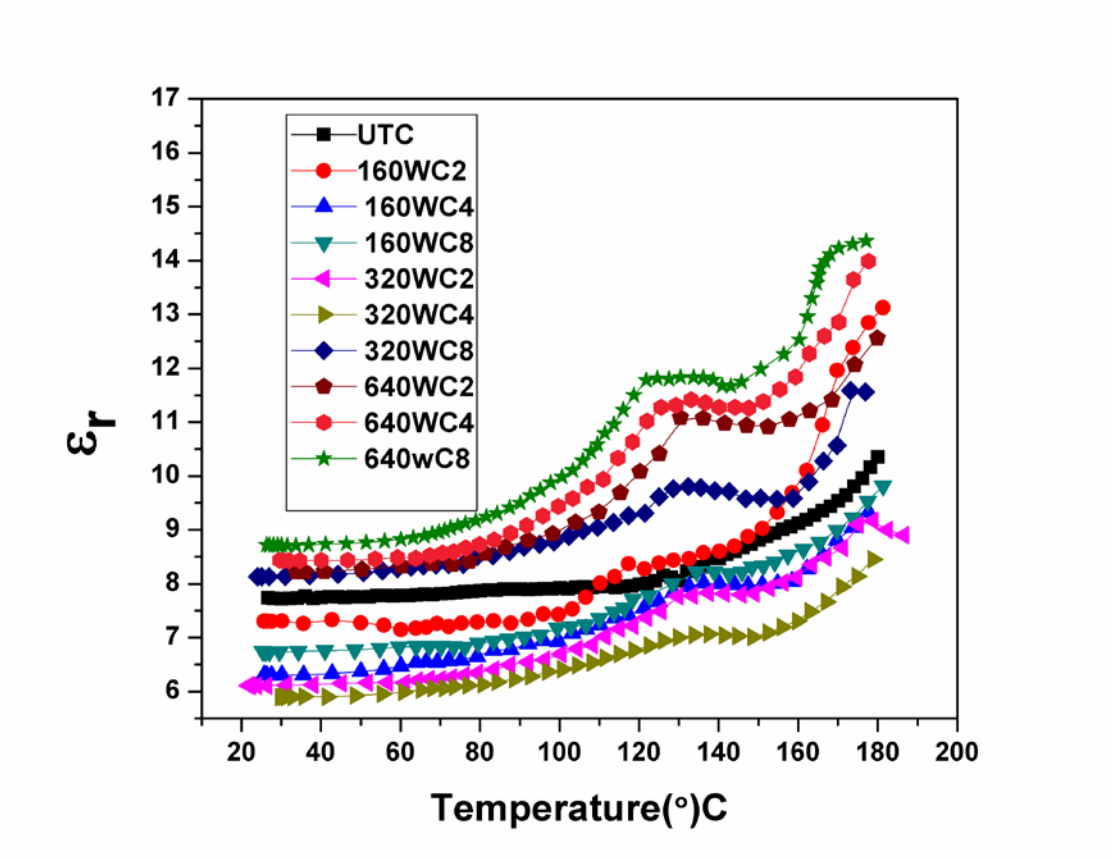

Fig. 6.13: Variation of ε_r with temperature for UTC and MFREC.

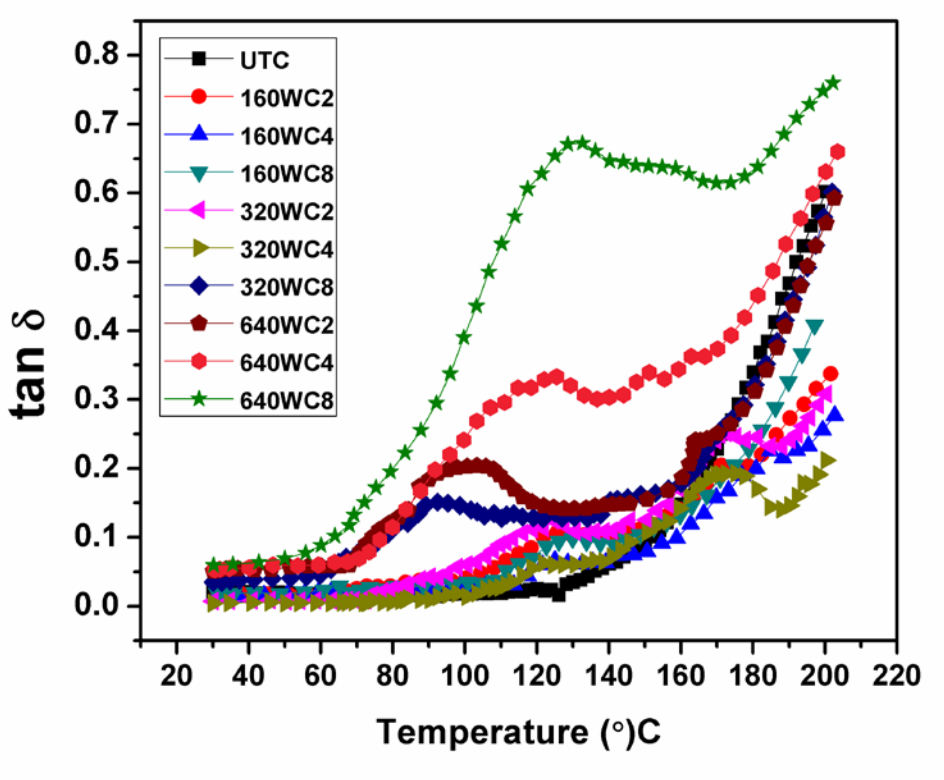

Fig. 6.14: Variation of $\tan\delta$ with temperature for UTC and MFREC.

The temperature dependence of ε_r for UTC and various MFREC has been shown in Fig. 6.13. The value of dielectric constant is found to increase with the increase in temperature up to $\approx 120^0$ C. This is due to the enhanced mobility of the polymer chain and dipolar molecules with the rise in temperature. The first exothermic peak observed ~ 120°C for all the composite samples is related to the removal of water content from the fiber as well as the presence of α relaxation associated with the glass to rubbery transition. Display of α relaxation shoulder on the higher temperature side (~ 135°C) is observed for 320WC4. This may be associated with the rigid interfacial region because of higher cross linking near the fiber which reduced the movement of epoxy chain.

The temperature dependence of $\tan\delta$ for UTC and various MFREC has been shown in Fig 6.14. The microwave treatment on the fiber reduces the relaxation associated with water with the decrease in hydrophilcity of the fiber. Therefore, lower values of $\tan\delta$ is observed for 320WC4 sample. The second exothermic peak associated with all the samples is attributed to the Maxwell wager-seller (MWS) effect. The immobile free charges in the composite get some movement with the increase in temperature. These charges can migrate with the applied electric field and get trapped at the interface of the fiber and matrix because of the different permittivity and conductivity of both the constituents [23].

6.2.6 Electric Modulus and Ac conductivity Studies

The present study focuses towards the ac response of fiber reinforced polymer composites and detailed examination concerning electrical relaxations and characteristics of the above composites. The composite systems can be regarded as stochastic mixtures of the two phases and are prepared by randomly dispersing sisal fibers in an epoxy resin. All the reported data were recorded by means of Dielectric spectroscopy and analyzed by using the formalism of electric modulus, with varying parameters the frequency of the applied field and temperature. The 'electric modulus' formalism, was first introduced by McCrum et al. [24] and intensively used for the investigation of electrical relaxation phenomena by Macedo et al. [25] and Howell et al. [26] in vitreous ionic conductors. Recently, it has been adopted for the investigation of electrical relaxation effects in polymers as well as polymeric composite systems [27, 28]. The use of electric modulus offers some advantages in

interpreting bulk relaxation processes since by its definition, variations in the large values of permittivity and conductivity at low frequencies can be minimized.

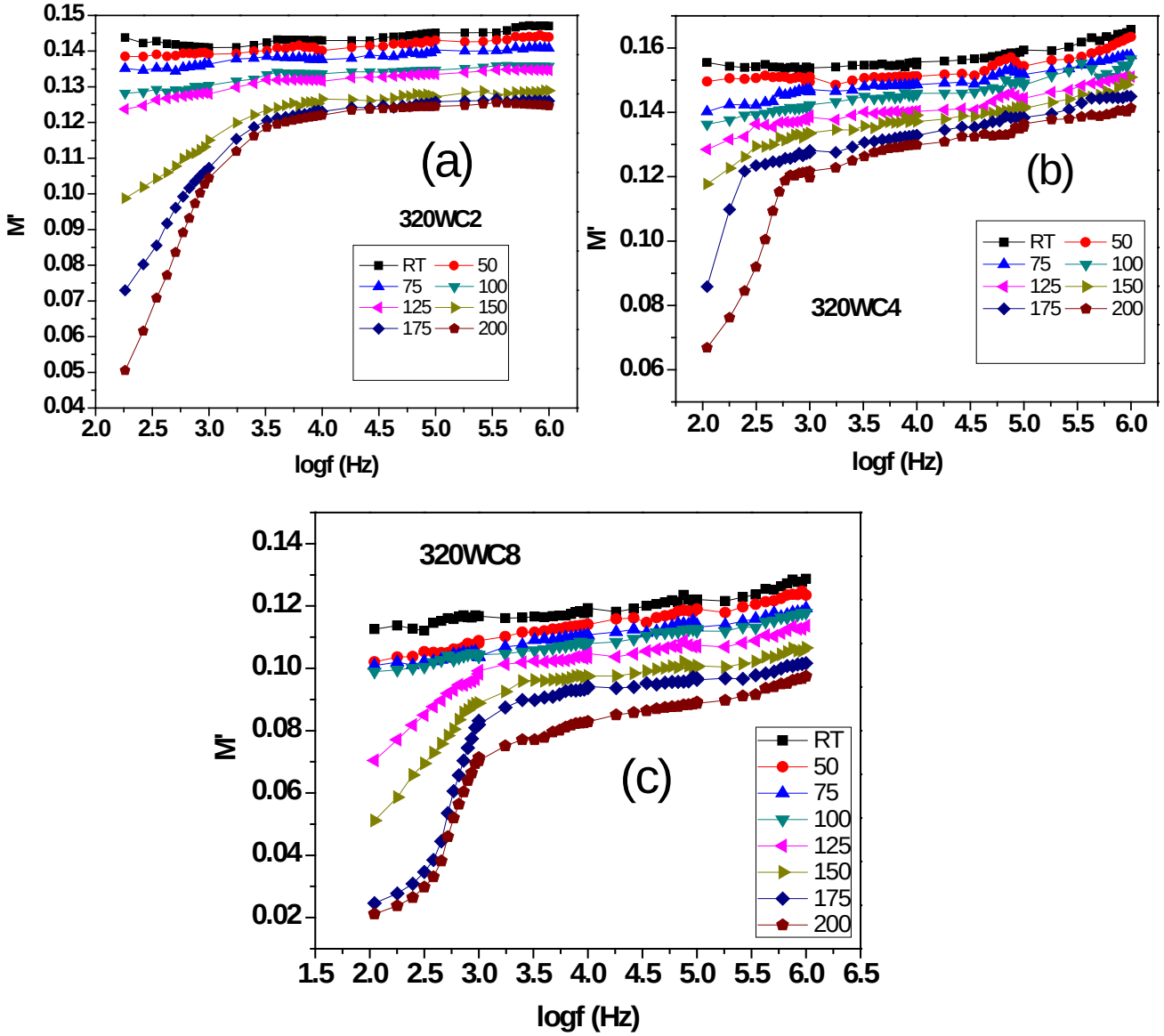

Fig. 6.15: Variation of real part of modulus (M') as a function of frequency at different temperatures for (a) 320WC2 (b) 320WC4 and (c) 320WC8.

Figures 6.15 (a-c) shows the isothermal scans of the real and imaginary part of electric modulus for the 320WC2, 320WC4 and 320WC8 samples at temperatures varying from RT to 200°C. The existence of a clear 'step-like' transition from low to high values of (M'), at moderate frequencies, is evident in all the figures. It can be observed that the values of M' increased with increase in frequency at a constant temperature and finally reached a constant value. The evolution towards a constant value of M' at the high frequency region is due to the inability of the heavy dipoles to follow the high frequency applied field. The existence of a step-like transition from low to high values of (M') is evident in all specimens, at higher temperature. The appearance of this transition implies the presence of a relaxation process. It can be seen that the value of M' decreases with increase in temperature.

The variation of the imaginary part of the electric modulus (M'') of 320WC2, 320WC4 and 320WC8 with frequency at different temperatures are shown in Fig. 6.16 (a, b & c), respectively. It is observed that the maxima of M'' (M''_{max}) shifts towards higher frequency side with rise in temperature indicating the presence of temperature dependent relaxation process in the material. The shifting of relaxation peaks suggests that there is a spread of relaxation times. The relaxation mechanism at lower temperature and lower frequency is different from at higher temperature and higher frequency. The nature of the figures at low frequency region at low temperature suggest that there are other relaxation peaks also present at frequency lower than 100 Hz. The value of M'' found to increase with increase in temperature, which may be due to increase in conductivity in sample.

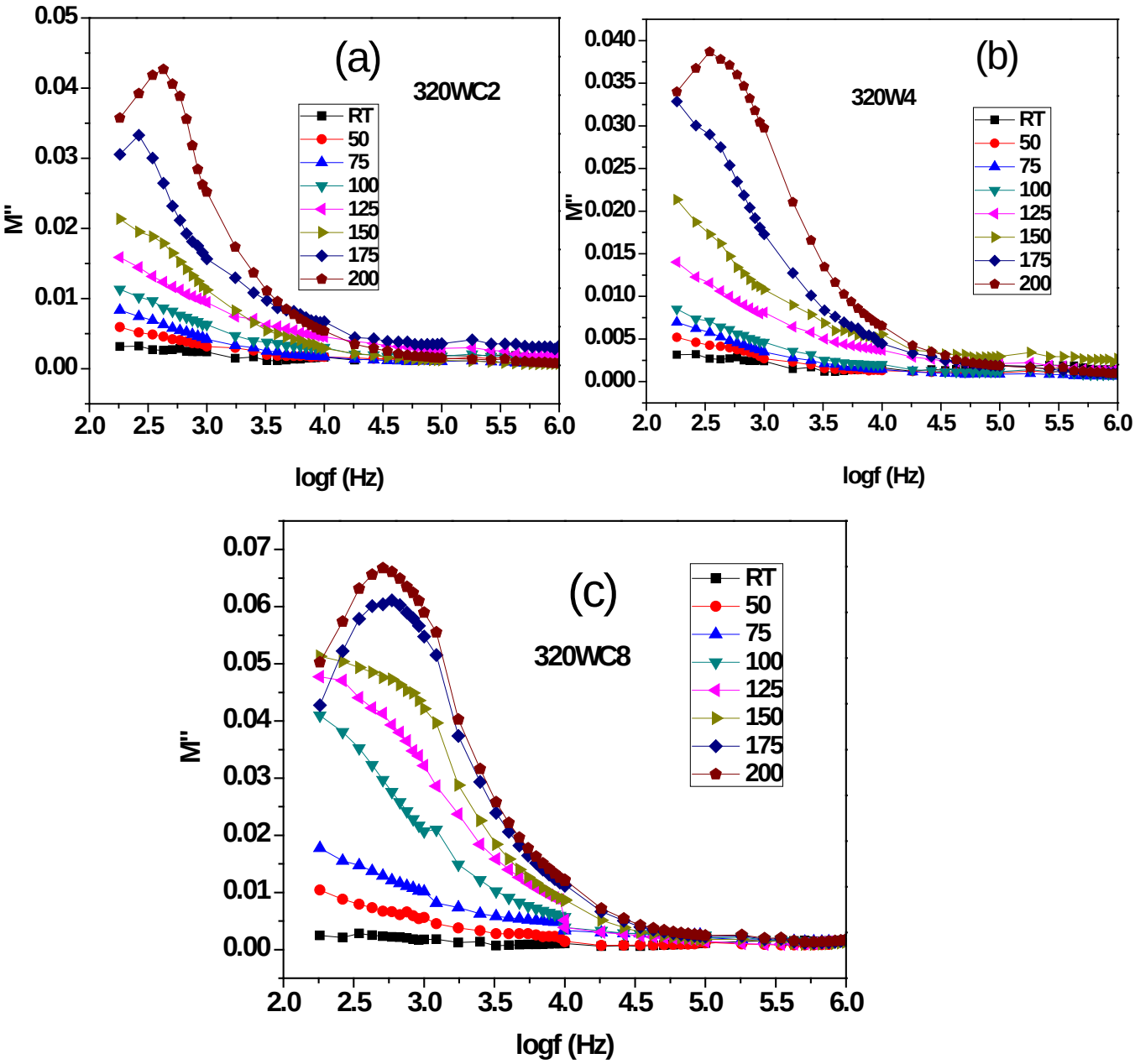

Fig. 6.16: Variation of imaginary part of modulus (*M''*) with frequency at different temperatures for (a) 320WC2 (b) 320WC4 and (c) 320WC8.

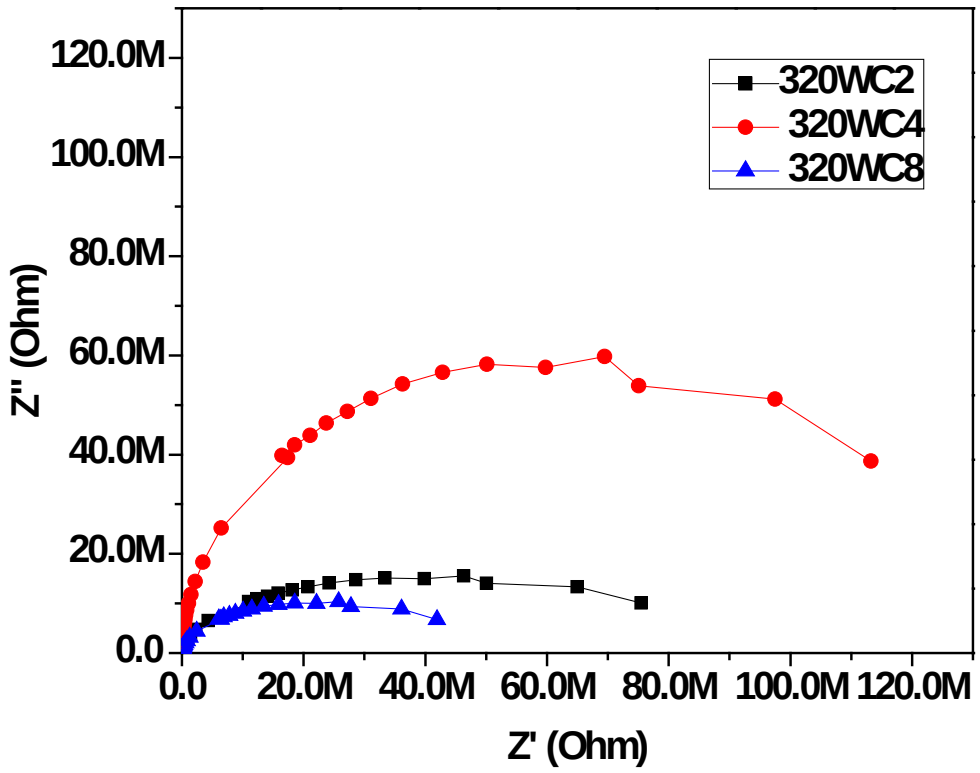

Fig. 6.17: Nyquist plots of 320WC2, 320WC4 and 320WC8 samples at 175°C temperature.

Fig. 6.17 represents the complex impedance spectrum/Nyquist plot (Z' vs. Z'') of 320WC2, 320WC4 and 320WC8 at 175°C temperature. The suppressed semi-circles in the Nyquist plot correspond to the relaxation processes occurring in each of the specimens. A single semi-circle is obtained in all the samples. The intercept of the semicircle with the real axis (Z') at low frequency (end) give rise to the bulk resistance (R_b) of the materials. The value of R_b is found to be high for 320W4.

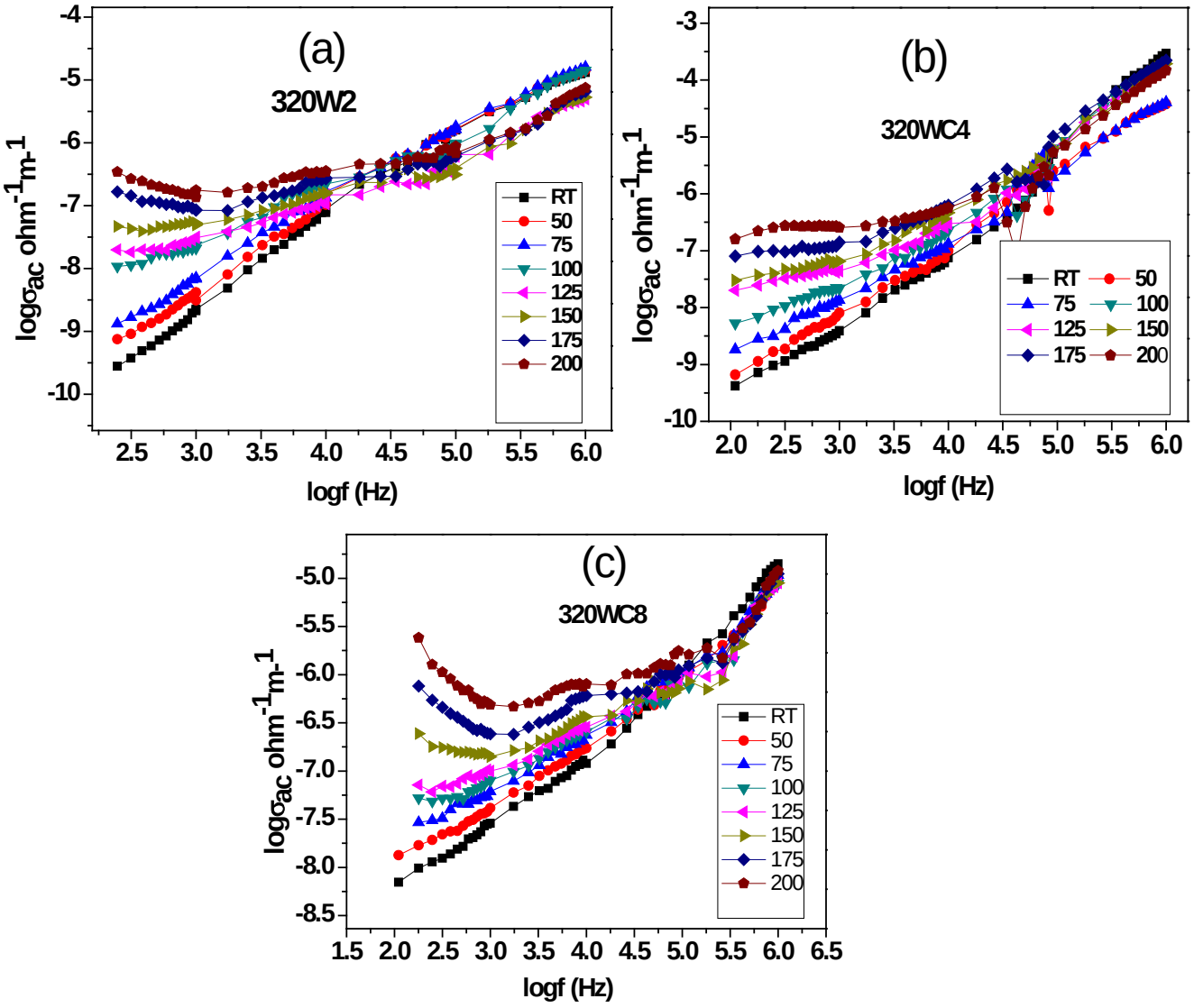

Fig. 6.18: Variation ac conductivity as a function of frequency at different temperatures for (a) 320WC2 (b) 320WC4 and (c) 320WC8 samples.

The frequency dependence of ac conductivity (σ_{ac}) of 320WC2, 320WC4 and 320WC8 at different temperatures in wide range of frequencies are shown in Fig. 6.18 (a-c). The σ_{ac} was calculated using an empirical relation i.e. $\sigma_{ac} = \omega\varepsilon_r\varepsilon_0 \tan\delta$, where ε_0 is the permittivity in free space, and ω is the angular frequency. The σ_{ac} patterns

show a frequency independent plateau in the low frequency region and exhibits dispersion at higher frequencies. This behavior satisfies the universal power law $\sigma(\omega) = \sigma_0 + A\omega^n$, where σ_0 is the dc conductivity, A is the pre-exponential factor and n is the fractional exponent, whose value lies in between 0 and 1. It is observed that σ_{ac} increases with the increase in temperature and that confirms the negative temperature coefficient of resistance behavior. This behavior also suggests that the electrical conduction in the sample is increasing at the higher temperature which may be due to the increase in the segmental mobility of the polymer molecules. It can also be seen that ac conductivity decreases with decrease in frequency and becomes independent of frequency after a certain limit. Dc conductivity (σ_{dc}) has been calculated by extrapolating this towards the lower frequency side, which follows Arrhenius law given by $\sigma_{dc} = \sigma_0 \exp[-E_a/K_\beta T]$. Where E_a is the activation energy of conduction and T is the absolute temperature. Fig. 6.19 (a-c) shows the variation of logarithmic of dc conductivity ($\log \sigma_{dc}$) against 1000/T for all the samples. The nature of variation is almost linear over a wide temperature region. The linear least squares fitting to the data gives the values of $E_a \sim 0.56$, 0.82 and 0.45 eV, respectively, for 320WC2, 320WC4 and 320WC8 respectively. The value of activation energy is found to be high for 320W4, which may be due to the increase in the height of the potential barrier between two orientational conformation states, which can be reached during the molecular motion.

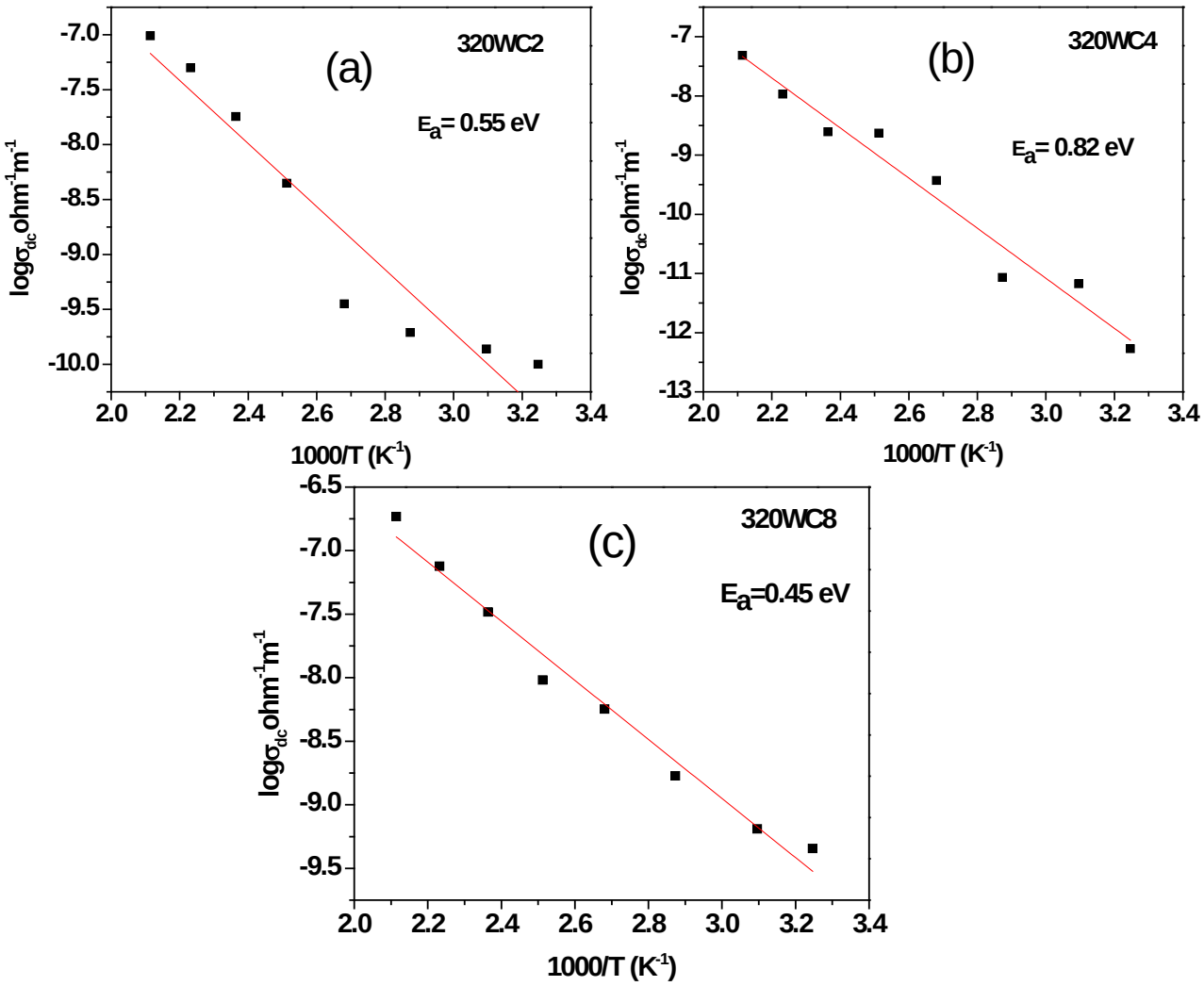

Fig. 6.19: Variation of logarithmic of dc conductivity (log σ_{dc}) against 1000/T for (a) 320WC2 (b) 320W4 and (c) 320W8 samples.

6.3 Conclusions

The suitability and the applicability of the microwave radiation for the modification of sisal fiber have been investigated. Microwave irradiation could affect the macromolecular parameters of the fiber along with crystallographic structures and morphology of the fiber. However, chemical structure of the fiber remained unaffected. Proper treatment time and power of microwave effectively reduced the

absorbed water and OH- group due to the heat generated by water molecule by the synchronizing oscillation with frequency of the microwave. The 320W4 fiber is found to have least disorder and void content with increased degree of crystallinity, crystallite size and density showing the changes in the physical parameters of the fiber. Adequate surface roughness is achieved due to the bombardment of high energy electromagnetic radiation at optimized microwave power and time. The enhanced surface roughness of fibers lead to the better wetting with the matrix resulting in maximum tensile and flexural strength of the 320WC4 composites followed by 320WC2. But excessive radiation leads to the degradation of the fibre and ultimately affecting the strength of the composite. The lowest value of ε_r and $\tan\delta$ was obtained for 320WC4 sample, which may be due to the reduction of OH group and rigid interface between the fiber and matrix. The highest value of ε_r in case of 640WC8 may be due to the increase in the polar group due to the degradation of the cellulose because of excessive heating. It was found that with increase in temperature and irradiation time, ac conductivity increases. The activation energy of the 320WC4 sample is found to be higher than the 320WC2 and 320WC8. The broadening of the relaxation peak in the imaginary part of modulus indicates the presence of relaxation process in the material.

Finally, it can be concluded that microwave irradiation with 320W power for 4 min irradiation period is the best to modify the sisal fiber out of all the MT fiber. This also gives a new insight to the microwave energy as a cleaner and safer modification process for the sisal fiber as compared to the traditional drying which gives non uniform heating.

References:

1. Li X, Tabil LG, Panigrahi S, Chemical treatments of natural fiber for use in natural fiber-reinforced composites: a review. J Polym Environ, 15, (2007), 25–33.
2. Mominul HM, Hasan M, Saiful Islam M, Ershad AM, Physico- mechanical properties of chemically treated palm and coir fiber reinforced polypropylene composites. Bioresour Technol, 100, (2009), 4903–4906.
3. Clark DE, Sutton WH, Microwave processing of materials. Annual Rev Mater Sci, 26, (1996) 299- 331.
4. Katz J, Microwave sintering of ceramics. Annual Rev Mater Sci. 22, (1992) 153–170.
5. Microwave processing of materials. National Academy Press, Washington, D.C. (1994).
6. Murugan R, Senthilkumar M, Ramachandran T, Study on the possibility in the reduction of dying time using micro oven dying technique. Inst Eng (India), Part TX: Text Eng Div, 87, (2007) 23–27.
7. Li JP, Lin H F, Zhao WF, Chen GH, Instant modification of graphite nano sheets by the grafting of a styrene oligomer under microwave radiation. J Appl Polym Sci, 109, (2008) 1377–1380.
8. Xue Z, Xin HJ, Effect of microwave irradiation on the physical properties and structures of wool fabric. J Appl Polym Sci, 119, (2011) 944–952.
9. Mahmoodi NM, Moghimi F, Arami M, Mazaheri F, Silk degumming using microwave irradiation as an environmentally friendly surface modification method. Fiber Polym, 11, (2010) 234–240.
10. Singh I, Bajpai KP, Malik D, Sharma AK, Kumar P, Feasibility study on microwave joining of 'green' composites. Akademeia, 1, (2011), 1–6.
11. Moharram MA, Mahmoud OM, X-ray diffraction methods in the study of the effect of microwave heating on the transformation of cellulose I into cellulose II during mercerization. J Appl Polym Sci, 105, (2007) 2978–2983.

12. Patra A, Bisoyi DK, Investigation of the electrical and mechanical properties of short sisal fiber-reinforced epoxy composite in correlation with structural parameters of the reinforced fiber. J Mater Sci, 46, (2011) 7206–7213.
13. Ruland W, Small-angle scattering of two-phase systems: determination and significance of systematic deviations from porod's law. J Appl Cryst, 4, (1971) 70–73.
14. Vonk CG, A general computer program for the processing of small angle X-ray scattering data. J Appl Cryst, 8, (1975) 340–341.
15. Muhlethaler K, Feinstruktur der Cellulosefaser. Das Papier, 17, (1963) 546–550.
16. Khan NMD, Small angle X-ray scattering study of sisal fiber using correlation function. Ph.D Thesis (1991), 71–72.
17. Katovic D, Microwaves solution for improving woven fabric. Chapter 16. Woven Fabric Engineering. Sciyo, Croatia, 2010.
18. Joseph K, Thomas S, Pavithran C, Effect of chemical treatment on the tensile properties of short sisal fibre-reinforced polyethylene. Polymer, 37, (1996) 5139-5149.
19. Kartky O, Miholic G, Small-angle X-ray investigations with absolute intensity measurements on regenerated, air-swollen cellulose. J Polym Sci C, 2, (1963) 449–476.
20. Tsukada M, Islam S, Arai T, Boschi A, Freddi G, Microwave Irradiation Technique to Enhance Protein Fiber Properties. Autex Res J, 5, (2005) 40–48.
21. Paul A, Joseph K, Thomas S, Effect of surface treatments on the electrical properties of low-density polyethylene composites reinforced with short sisal fibers. Compos Sci Technol, 51, (1997) 67–79.
22. Hanna AA, Atef AI, Salwa O, Heikal SO, Some electrical properties of wood pulp treated with sodium hydroxide, J Polym Sci Polym Chem Ed, 18, (2003) 1425-1429.
23. Arous M, Amor IB, Amor B, Boufi S, Kallel A, Experimental study on dielectric relaxation in alpha fiber reinforced epoxy composite. J Appl Polym Sci, 106, (2007) 3631-3640.

24. McCrum NG, Read BE, Williams G, Anelastic and dielectric effects in polymeric solids. John Wiley, London, (1967), 108–111.
25. Macedo PB, Moynihan CT, Bose R, The role of ionic diffusion in polarization in vitreous ionic conductors. Phys Chem Glasses, 13, (1972) 171–179.
26. Howell FS, Bose RA, Macedo PB, Moynihan CT, Electrical relaxation in a glass-forming molten salt. J Phys Chem, 78, (1975) 639–686.
27. Mudarra M, Belana J, Canadas JC, Diego JA, Sellares J, Diaz-Calleja R, Sanchis MJ, Space charge relaxation in polyetherimides by electric modulus formalism. J Appl Phys, 88, (2000) 4807–4818.
28. Okrasa L, Boiteux G, Ulanski J, Seytre G, Molecular relaxation in anisotropic composites based on (hydroxypropyl)cellulose and acrylic polymer. Polymer, 42, (2001) 3817–3841.

Chapter 7

Influence of Alkali treatment

7.1. Introduction

The efficiency of mechanical and electrical properties of the fiber reinforced composite depends on the properties of interface shared by matrix and the fiber. The main job of the interface is to enhance the stress transfer between fiber to fiber through matrix [1]. But the hydrophilic nature of lignocellulose fiber gives poor compatibility to the hydrophobic matrix like epoxy, polyester etc. Modification of fiber can lead to better compatibility between these essential constituents of the composite system. Some chemical modification like dewaxing, mercerization cleans the surface impurities, waxy layer from the fiber and provides it an enhanced surface area for better mechanical interlocking with the matrix. Mercerization is one of the most popular modifications in the textile fiber industry [2-4]. The nature of alkali and its concentration also affect the properties of the fiber. Out of all the alkali NaOH is popular alkali used for the treatment of natural fiber as Na has the favourable diameter to fit in between pores in the lattice plane that results in higher amount of

swelling and formation of Soda Cellulose. Subsequent rinsing will lead to the thermally stable cellulose II [5, 6]. So in brief alkali treatment converts cellulose I present in the fiber to cellulose II. Hasim et al. [7] presented a systematic study on the mercerization treatment parameter effect on natural fiber reinforced polymer matrix composite. The flexibility of the cotton textile has increased significantly after mercerization [8]. Effect of period of soaking of sisal fiber in 5% of NaOH solution was studied by Chand et al. [9]. They found that the strength of the sisal polyester composite was enhanced for 80-90 hr period of treatment and falls beyond that. Structural, microstructural, macromolecular, morphology of the cotton fiber are greatly affected by the NaOH treatment [9]. Study on the sisal polyester composite shows that at 10% of NaOH solution soaked for 1 hr give weaker fiber because of excess delignification which in turn gives composite of weaker strength [10]. The surface of the sisal fiber becomes smooth when soaked below 2% of NaOH solution where as it becomes rough for more than 6% [11]. According to Yu et al. [12] alkali treatment is an effective surface treatment than the silane treatment for ramie fiber . The effect of alkali treatment on the macromolecular parameters of the natural fiber was also studied by Khan [13]. His finding suggests that the pH of alkali greatly affects the matter phase, periodicity transverse to the layer and also the void content in the fiber.

As the natural fiber composite are gaining attention in the electrical applications, the study of electrical properties is essential. The influence of alkali treatment of the fiber on the electrical properties of the composite was studied by Goud et al. [14]. According to them Alkali-treated fiber composites exhibited a lower

loss tangent and lower dielectric constant than untreated fiber composites. However, these values decreased with increase in frequency. Investigation on the electrical properties of low-density poly-ethylene composites reinforced with short sisal fiber was done by Paul et al. [15]. They confirmed that surface modification greatly affect the electrical properties of the composite. Shinoj et al. [16] did a comparative study on dielectric properties of flax, hemp and oil palm fibers.

From the above literature survey it is concluded that even though there are many reports on the effect of NaOH treatment on the various properties of natural fiber as well as reinforced composites but they are conflicting to each other in many aspects. In addition to this, no systematic attempt has been made to correlate the macromolecular and structural properties of the fiber with the mechanical and electrical properties of the alkali modified sisal fiber reinforced epoxy composite. The present study focuses on the effect of alkali treatment on the macromolecular parameters along with the structural and morphological properties of the fiber. Mechanical and electrical properties of the NaOH treated fiber reinforced epoxy composite have also been studied to evaluate the effectiveness of the surface modification of fiber on the composite properties.

7.2. Results and Discussions

7.2.1 SAXS Analysis

The slit smeared data of SAXS intensities for alkali treated fibers in comparison to the untreated fiber are shown in Fig 7.1. The background corrected

intensities were used for the analysis of the SAXS data. The extrapolated points are indicated by hollow symbols in the inset graph of Fig. 7.1.

The ratio *R* determines the nature of the samples. The values of *R* were evaluated using the equation (2.3) are compiled in table 7.1. The small and positive value of *R* indicates that gradient at the phase boundary of matter and void phases are finite which lead to finite value of *R* for all the fiber samples. Hence the calculation based on smeared out intensities indicates that samples are non-ideal two phase systems [17].

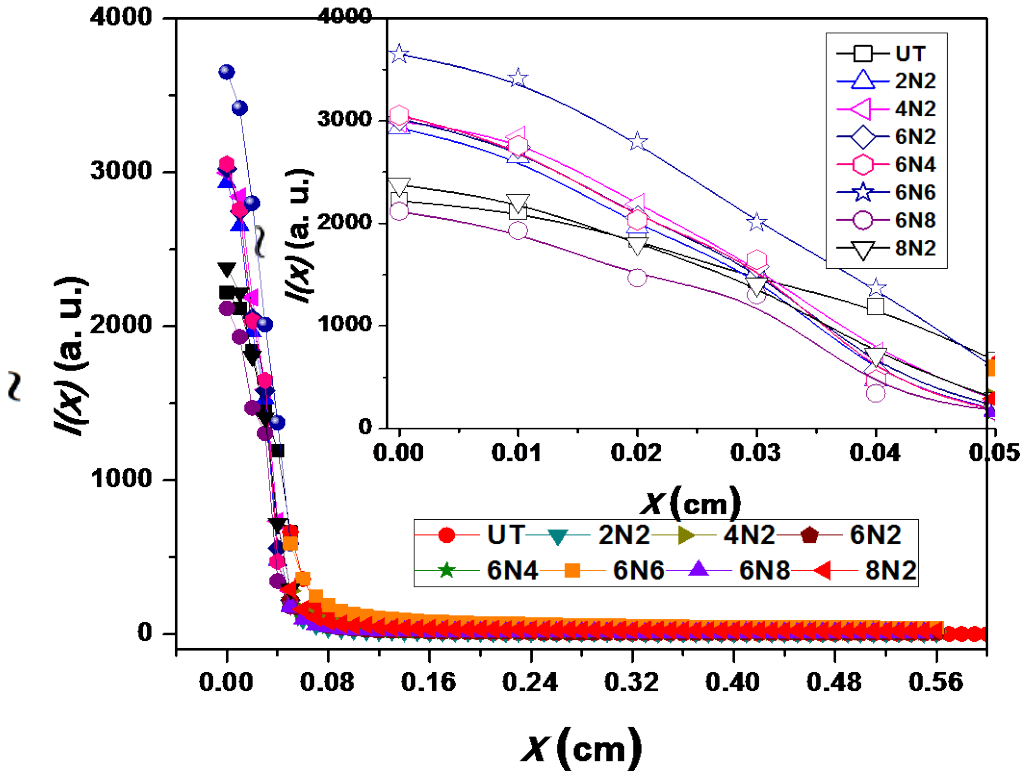

Fig.7.1: Background-corrected, smeared-out scattering curves for raw and alkali treated sisal fibers. **Inset:** Magnified view of the initial scattering curves to show the extrapolated data.

The $C_1(y)$ of all the fibers for various values of y are computed and the plots are given in the Fig. 7.2. (a) and (b). For non-ideal two phase lamellar structure the value of $C_1(y)$ is unity at the origin and as y increases the $C_1(y)$ oscillates between positive and negative values. From this plot the values of D, the periodicity transverse to the layer are calculated from the first subsidiary maxima.

The observed maximum value of D for 6N2 fiber corresponding to the first subsidiary maxima as shown in the Fig.7.2 (a), may be due to the swelling of cellulosic particle [13]. The increment in the values of D is proportional to the concentrations (2% to 6%) of NaOH solution in which fibers were soaked for period of 2 hr. However, decrease in the D value was observed for fibers soaked in 8% NaOH solution.

Hence, the variation of soaking period of sisal fibers in 6% of NaOH was chosen to study the effect of it on the macromolecular and physical parameters of the fibers at this concentration. The soaking period of sisal fibers in 6% of NaOH concentration varied from 2 hr to 8 hr. The values of D continues to increase from 2 hr to 6 hr in 6% NaOH solution(shown in Fig 7.2 (b)) along with the increment in the matter phase(ϕ_1), transverse length to matter phases (l_1) as visible from Table 7.1. This may be due to the readjustments of cellulose chain in the fiber because of the removal of non-cellulosic part of the fibers after the NaOH treatment. Further increment in the soaking period of the fibers led to the decrement in the values of $\bar{l}_1$ and ø_1. The reason for this may be rupture of cellulosic particles in to new particles of different dimensions [13].

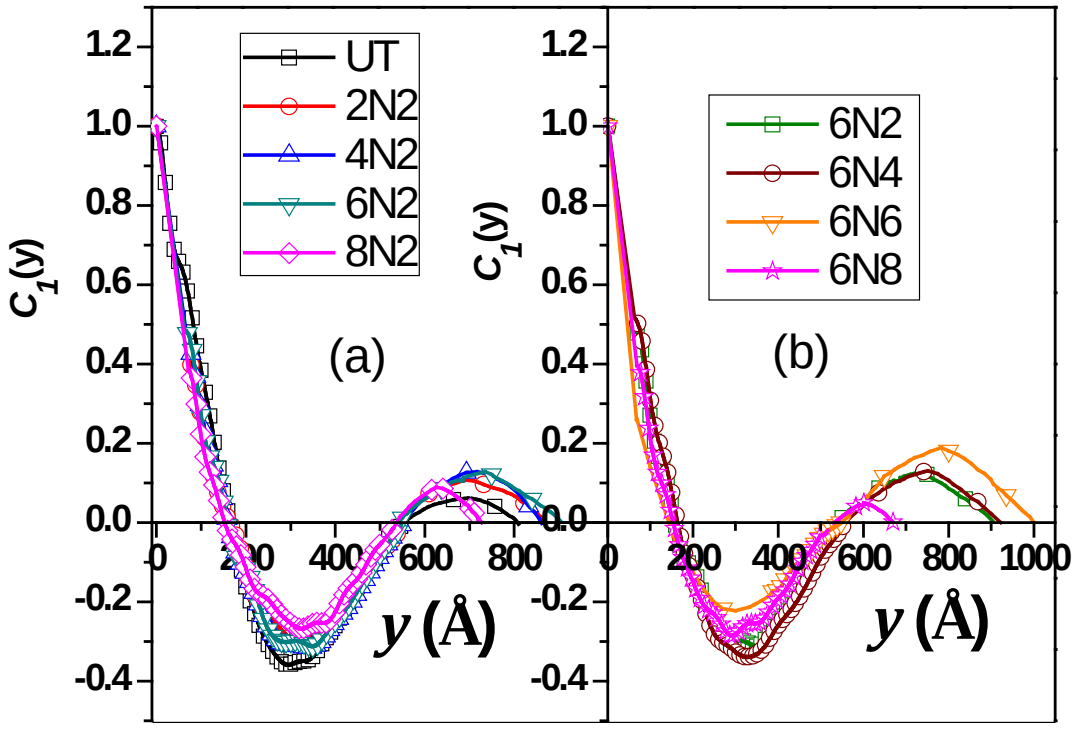

Fig. 7.2: Variation of one dimensional correlation function $C_1(y)$ against y for (a) UT, 2N2, 4N2, 6N2, 8N2 fibers, (b) 6N2, 6N4, 6N6, 6N8 fibers.

The values of $C(r)$ have been computed according to the relation (2.5) are displayed in Fig. 7.3. It represents the probability that a point at a distance 'r' in any arbitrary direction from a given point in the particle will also be in the particle. However, in case of non-ideal two phase system, $C(r)$ tends to unity and for large values of r, it continues to oscillate between positive and negative values tending asymptotically to zero. This behaviour was observed by all the investigated samples in the present study. These computed values of $C(r)$ were used for the subsequent analysis. The slope of $C(r)$ at different points of r had been derived by central difference method taking constant interval of 1 Å.

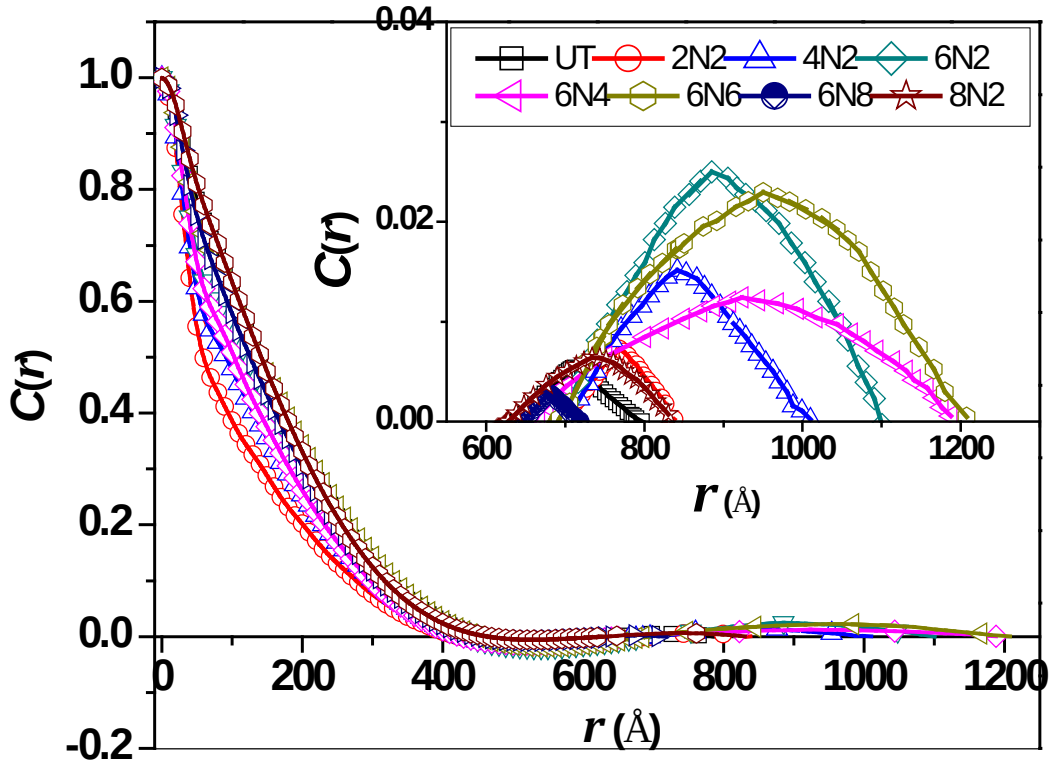

Fig. 7.3: Variation of three dimensional correlation function $C(r)$ against r for raw and alkali treated fibers. **Inset:** First subsidiary maximum of the three-dimensional correlation functions.

The logarithmic plots between x and $\tilde{I}(x)$ for the raw and treated fibers are compiled in Fig. 7.4. The negative slopes of all the plots are ~- 3. This suggests that the all the alkali treated samples are non-ideal two phase system [18]. The phase in the non-ideal two phase system has some corrugation. Here the electron density is non-uniform and may be assumed to vary over certain thickness which is known as width of transition layer. This was calculated by two different methods as described by Ruland and Vonk [19-20].

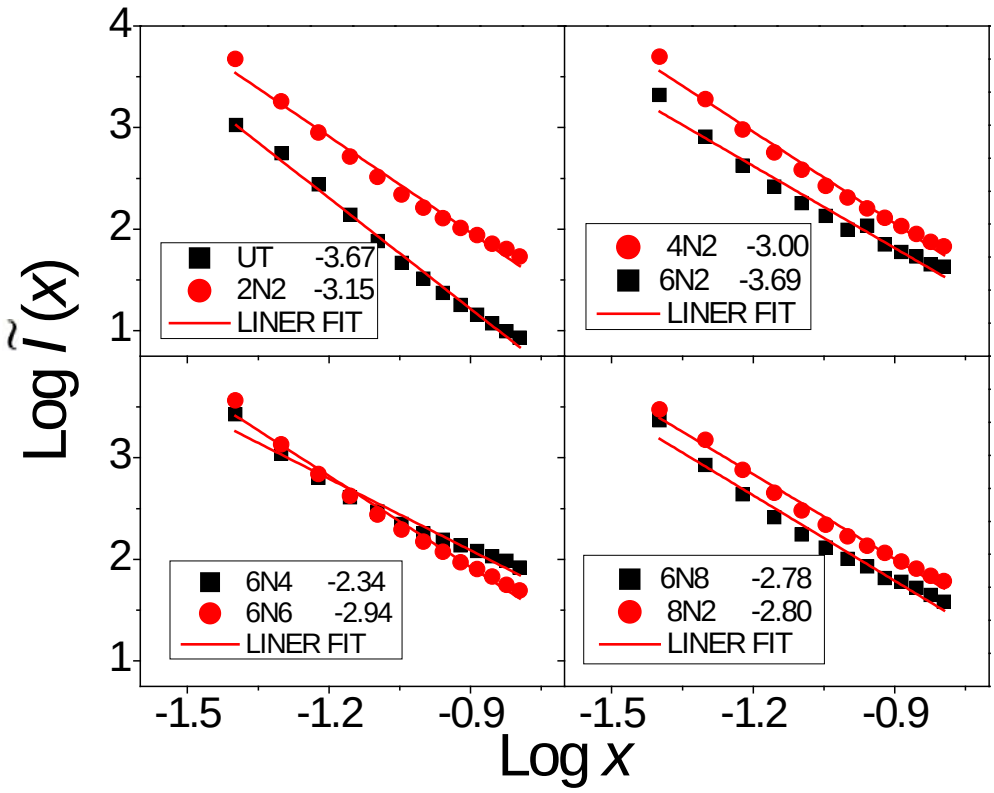

Fig. 7.4: Double logarithmic plots for raw and Alkali treated fibers.

Fig 7.5 displays the typical Ruland plots for all the investigated fibers. The values of E_r can be calculated from the Ruland plot which is a graph of $\tilde{I}(x)x$ vs. x^{-2}. The values of E_r are found to be 21.081Å, 23.7Å, 23.250Å, 22.222Å, 22.040Å, 23.120Å, 23.07Å for UT, 2N2, 4N2, 6N2, 6N4, 6N6, 6N8, 8N2 fibers respectively.

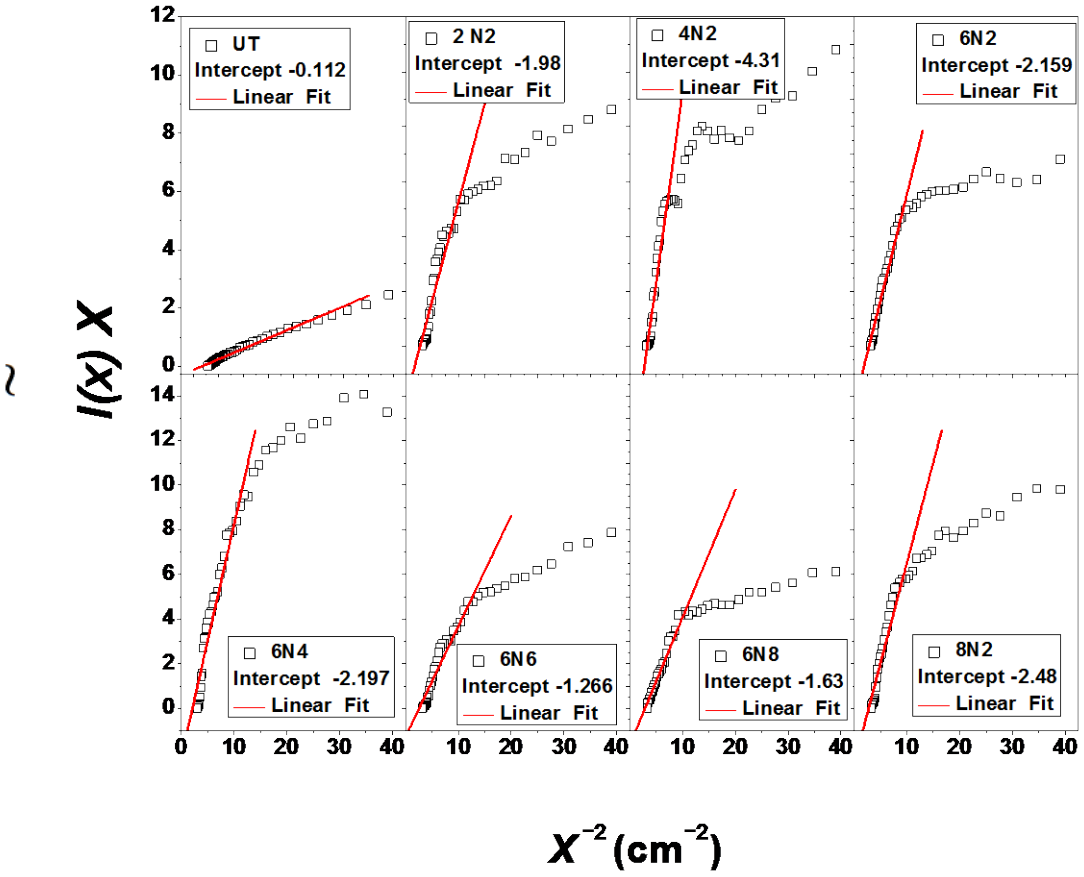

Fig. 7.5: Ruland plots $\tilde{I}(x)x$ Vs x^{-2} for raw and alkali treated sisal fibers.

The standard deviations (σ) of the intensities were well within the permissible range showing the accuracy of the data collection. The width of transition layer (E_v) by Vonk method was calculated from the plot between $\left(-\frac{4}{R}\right)\frac{dC(r)}{dr}$ vs. r and are shown in Fig. 7.6. Negative intercept of the regression line fitting to the 15 extreme points of the tail region of the corresponding scattering curve confirmed the non-ideal two phase nature of the fibers.

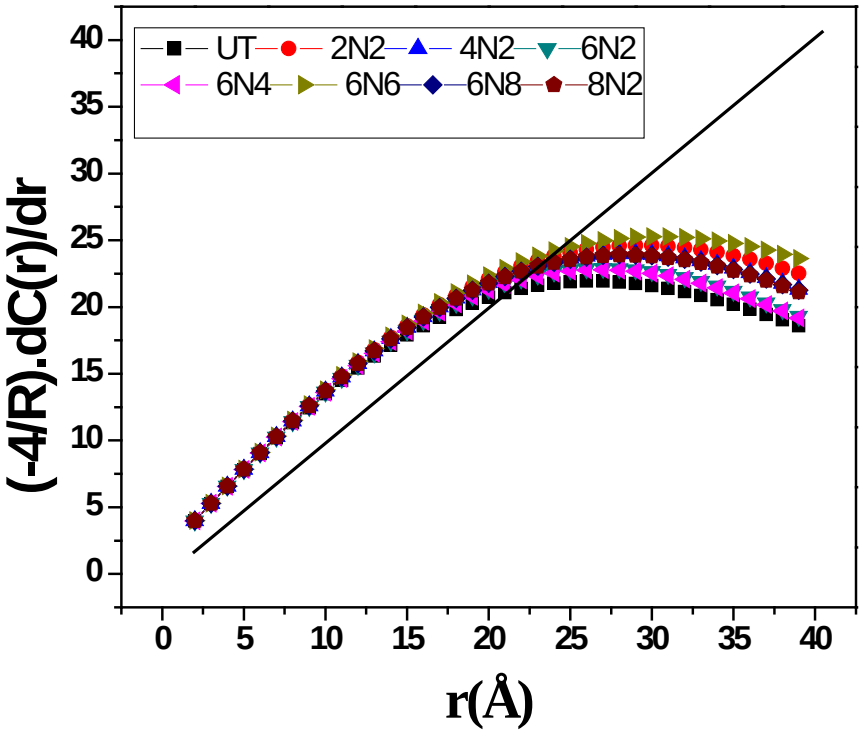

Fig. 7.6: Variation of $\left(-\frac{4}{R}\right)\frac{dC(r)}{dr}$ against *r* for the raw and alkali treated sisal fibers to find out the E_v of the respective fibers.

The straight line equidistance from both the axes has been drawn and the point of intersection with the curve gives the value of E_v as 19.792Å, 21.115Å, 21.226Å, 21.198Å, 21.145Å, 21.616Å, 21.376Å for UT,160W2, 160W4, 160W8, 320W2, 320W4, 320W8, 620W2, 640W4, 640W8 fibers respectively [20]. It is found to be in close agreement with E_r values justifying the accuracy of our analysis.

Table 7.1: Various macromolecular parameters of raw and Alkali treated sisal fibers derived from SAXS study.

Macro molecular parameter	UT	2N2	4N2	6N2	6N4	6N6	6N8	8N2
R(10^{-4}Å^{-2})	8.831	12.3	10.6	21.3	14.3	17.9	14.9	15.321
D(Å)	654	693	720	736	750	785	600	625
S/V(10^{-3} Å^{-1})	3.058	2.886	2.777	2.717	2.666	2.547	3.333	3.2
E_v(Å)	21.081	23.7	23.25	22.222	22.04	22.25	23.12	23.07
E_r(Å)	19.792	21.115	21.226	21.198	21.465	21.145	21.616	21.376
Φ_1	82.601	84.449	86.235	88.401	89.001	89.839	78.003	80.239
Φ_2	17.399	15.551	13.765	11.599	10.999	10.161	21.997	19.761
$\bar{l}_1$ (Å)	1080.421	1224.630	1246.163	1297.942	1345.076	1431.428	1152.204	1221.63
$\bar{l}_2$ (Å)	227.578	151.837	167.957	94.058	130.924	108.752	127.696	176.316
$\bar{l}_r$ (Å)	187.982	135.082	148.006	82.702	119.311	101.072	114.957	154.119
l_c	351.097	333.907	330.126	278.081	316.587	306.041	306.455	347.067
$2E_v/D$ (%)	6.446	6.839	6.458	6.0385	5.877	5.668	7.706	7.382
σ	0.013	0.002	0.009	0.007	0.054	0.014	0.029	0.005

7.2.2 XRD Study

Fig. 7.7 shows the XRD patterns of the alkali treated sisal fiber in comparison to the untreated fiber. The broad peaks at 15.3^o, 22.6^o in the fiber corresponds to the (110) and (020) planes respectively in the lignocellulosic fibers [21]. Lignin contributes to the amorphous part of the fiber. It was observed that with the increase in NaOH concentration in which the fibers were soaked from 2% to 6% the degree of

crystallinity of the fibers were increased. It may be due to the removal of amorphous part, natural wax, impurities of the fibers which increase the percentage of crystalline part in it. However, beyond that the decrease in the degree of crystallinity and crystallite size was achieved which may be due to the degradation of crystalline part at a higher concentration of NaOH solution. The increase in the period of treatment up to 6 hr for the fibers soaked in 6% NaOH solution was found to have increased degree of crystallinity and crystallite size. This may be due to the sufficient removal of non-crystalline part of the fibers which gave the chance of rearrangement of the cellulose chains leading to improved degree of crystallinity in the fibers.

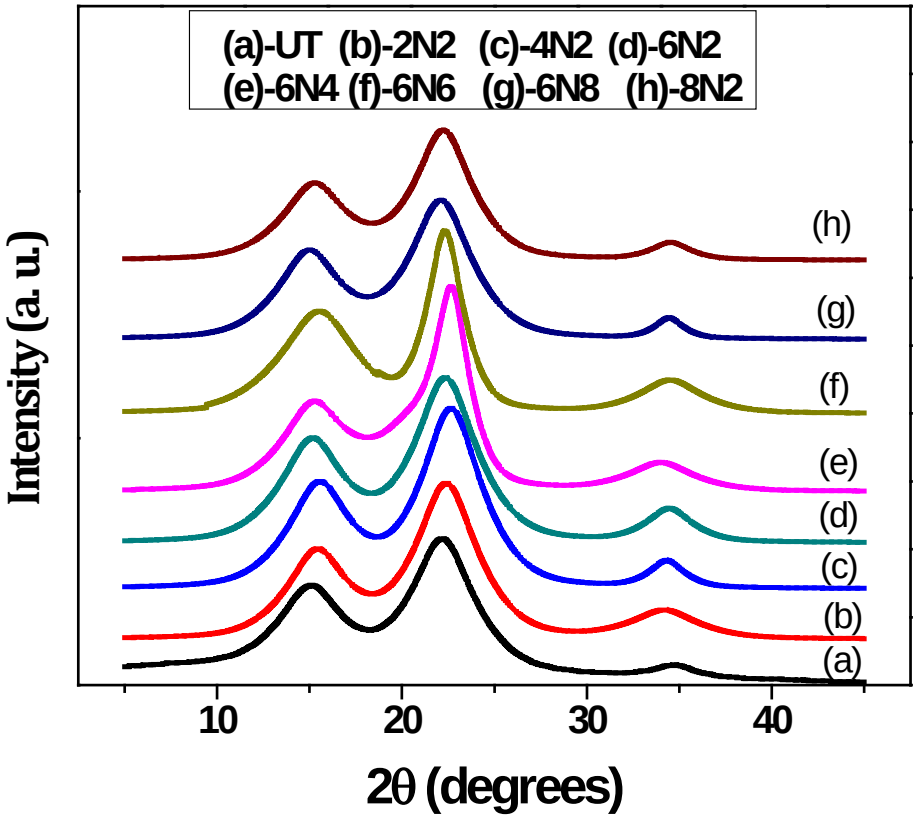

Fig. 7.7: XRD patterns of raw and Alkali treated sisal fibers.

The improved degree of crystallinity for 6N6 fiber can be estimated from the increased cellulose relative peak intensity in the XRD pattern of the same which is shown in Fig. 7.7. The increment in the crystallite size and crystallinity may also be due to the decrease in crystal distortion and defects in the crystal which was further strengthened by the fact that the 6N6 has least specific inner surface area (*S/V*), calculated from SAXS analysis. This led to the increment in bulk density of the fiber given in the Table 7.2. The degree of crystallinity of 6N8 fiber was found to decrease, which could be due to the degradation and delignification of fibers at higher soaking period in the solution [9].

Table 7.2: Various crystallographic and physical parameters of the investigated raw and Alkali treated sisal fibers.

Fiber	**Degree of crystallinity (%)**	**Crystallite size (Å)**	**Density (g/cc)**
UT	52.11	29.19	1.32
2N2	57.52	32.18	1.43
4N2	59.31	35.23	1.47
6N2	60.52	40.01	1.58
6N4	62.12	42.21	1.69
6N6	66.77	44.75	1.77
6N8	51.58	28.99	1.31
8N2	53.15	31.22	1.36

7.2.3 FTIR Study

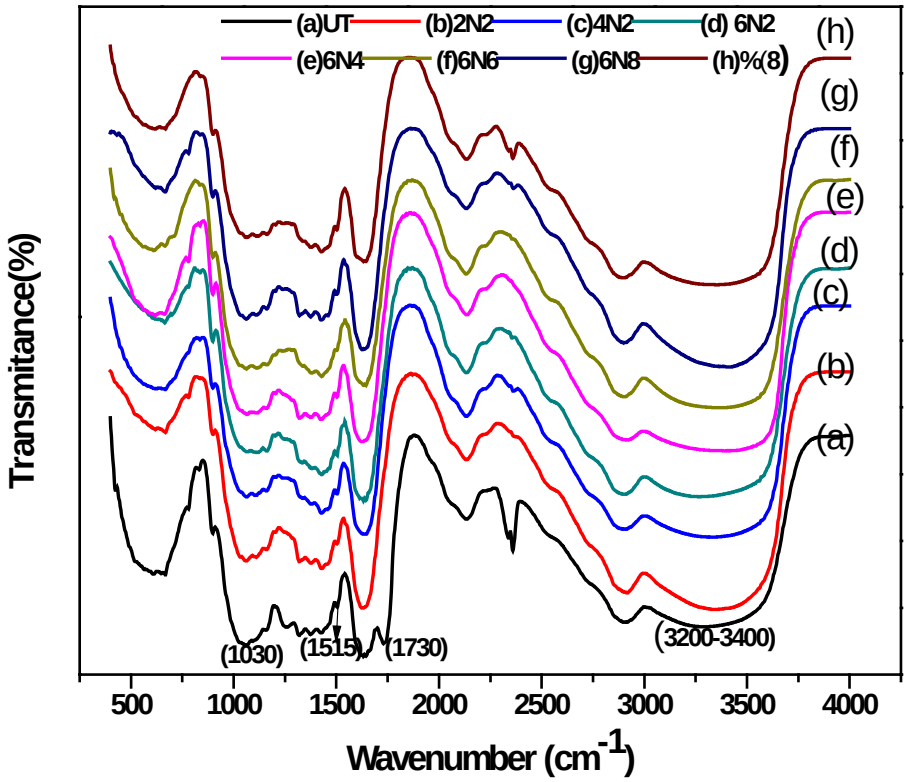

Fig. 7.8: FTIR spectra of raw and alkali treated sisal fibers

Fig. 7.8 exhibits the FTIR Spectra of the untreated and Alkali treated sisal fibers. It can be seen that raw fiber has 1730cm^{-1} band which corresponds to hemicellulose. The disappearance of this peak after NaOH treatment confirmed the removal of hemicellulose part from the fiber which may be due to the removal of acetyl group present in the hemicellulose [22]. This also led to the weight loss of the fiber. The band at 3300-3500 cm^{-1} is the characteristic of the axial vibration of hydroxyls from cellulose (carbons 2, 3 and 6 of the glucose). The broadness of this band increased with NaOH treatment due to change of the inter- and intra-molecular hydrogen bonding in polysaccharides [23, 24]. The band at 1030 cm^{-1} is assigned to

aromatic C-H plane deformation for primary alcohol in lignin which was significantly reduced after alkali treatment compared to the raw fibers. The aromatic ring of lignin band (1505 cm^{-1}) shows a decreased absorbed intensity ratio after alkali treatment which confirms the reduction of lignin content.

7.2.4 Morphological Study

SEM micrographs of UT, 2N2, 4N2, 6N2, 6N4, 6N6, 6N8, 8N2 fibers are shown in Fig. 7.9(a-h). The surface roughness of the fiber was increased with increase in concentration of NaOH solution from 2% to 6% when it was soaked for 2 hr. It may be due to the removal of hemicellulose, lignin and surface impurities from the fiber hence provided a rough surface to the fiber. The soaking of fiber beyond 6% of NaOH solution led to the degradation of fiber. But the improvement in the surface roughness was observed for the increase in soaking period of the fibers at 6% concentration of NaOH solution. Maximum surface roughness was observed for 6N6 fibers which is may be due to the substantial removal of impurities and partial removal of hemicellulose from the fiber. Thus the materials in the interfibrillar region were etched away and the fibrous region became more pronounced. On the other hand, longer duration of soaking period beyond 6 hr led to the degradation of the fiber which may be due to degradation of cellulosic part and over delignification of the fiber. SEM micrographs of the fractured surfaces of the 2NC2, 4NC2, 6NC2, 6NC4, 6NC6, 6NC8, 8NC2 composites are shown in Fig 7.10. As the roughness of the fiber increased with increase in the concentration of NaOH, the wetting of fibers increased with the matrix because of the increase in the area of contact.

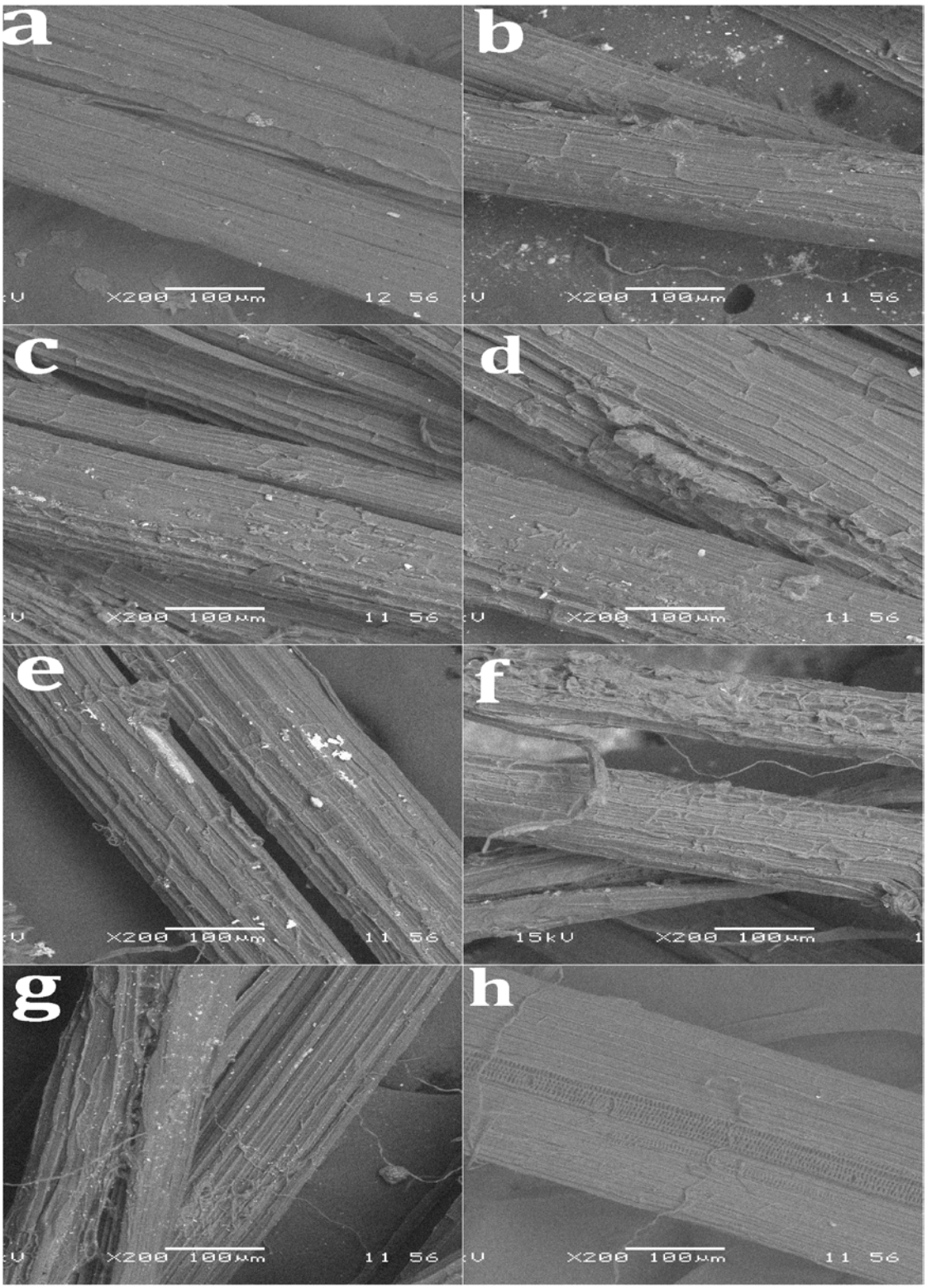

Fig. 7.9(a-h): Longitudinal morphology of UT, 2N2, 4N2, 6N2, 6N4, 6N6, 6N8, 8N2 fiber, respectively.

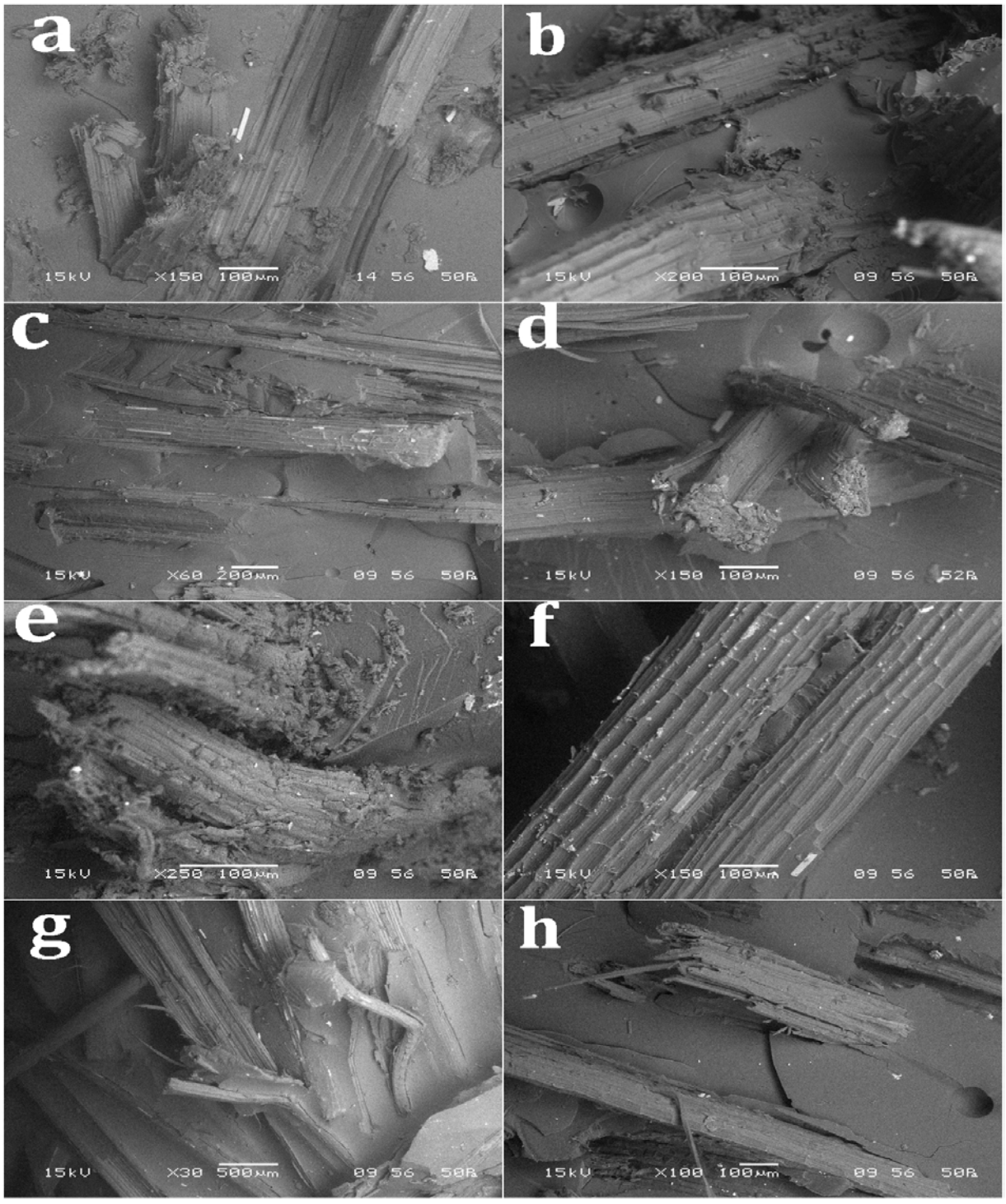

Fig. 7.10 (a-h): Fractured surfaces of 2NC2, 4NC2, 6NC2, 6NC4, 6NC6 (e &f), 6NC8, 8NC2 composites, respectively.

This may have led to the better bonding between the fiber and the epoxy. For 6NC6 composite, epoxy seems to be impregnated between the interfibrillar regions of the fiber as shown in Fig. 7.10 (f). Whereas the fiber soaked for longer period in alkali solution did not have better wetting with the matrix due to the degradation of cellulosic part and excess delignification of the fiber. Hence debonding was observed at the fiber matrix interface for 6NC8 composites.

7.2.5 Mechanical Study

Fig 7.11.(a) shows the variation of flexural strength and tensile strength of the alkali treated sisal fiber reinforced epoxy composite in comparison to the untreated composite as a function concentrations of NaOH.

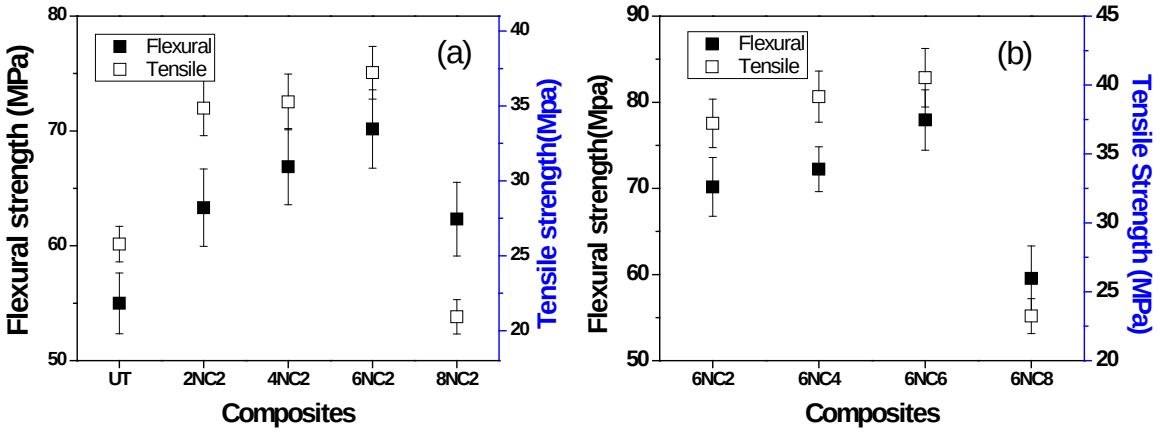

Fig. 7.11: Variation of Flexural and tensile strengths of composite (a) as a function of concentration of NaOH and (b) as a function of soaking period of fibers.

It can be observed that among all the investigated composites, the composite reinforced with sisal fiber soaked in 6% NaOH solution was found to have better

properties. This is due to better wetting of the fiber with the matrix with the removal of natural and artificial impurities and enhanced area of contact between fiber and matrix. However, both the flexural and tensile strength was decreased significantly for 8NC2 composites. Fig. 7.11 (b) shows the variation of flexural and tensile strengths as a function of duration of soaking period of fibers at 6% of NaOH solution. The flexural and tensile strength was found to increase initially with the increase in soaking period up to 6 hr, with further increase in soaking time the properties were degraded. Maximum flexural and tensile strength was obtained for the 6NC6 composite which may be due to the high interfacial friction stress, and stress transfer between fiber and epoxy [25]. 6NC8 and 8NC2 found to have reduced flexural and mechanical strength because of the reinforcement of degraded fibers in the matrix.

7.2.6 Dielectric Study

Fig. 7.12 (a) & (b) shows the frequency dependence of dielectric constant (ε_r) and dielectric loss ($\tan\delta$) of both UTC and ALKC, respectively. It was found that with the increase in frequency the values of ε_r as well as $\tan\delta$ for all the composite decreases which is the typical characteristic of polymeric material. The interfacial polarization is prominent in heterogeneous material and is highest at lower frequency. Hence, the higher values ε_r and $\tan\delta$ at lower frequency can be explained in terms of interfacial polarization.

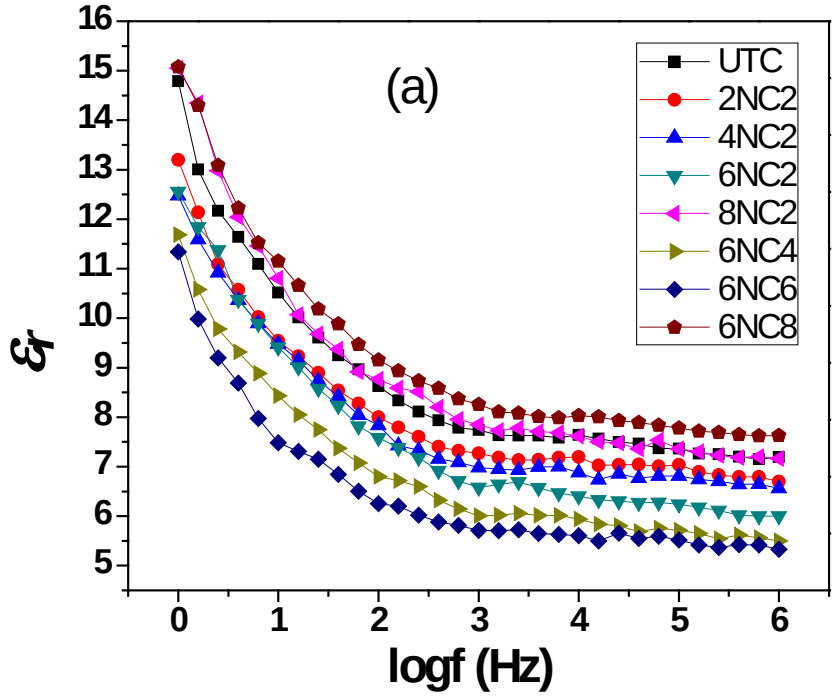

Fig 7.12 (a): Variation of ε_r with frequency for UTC and ALKC.

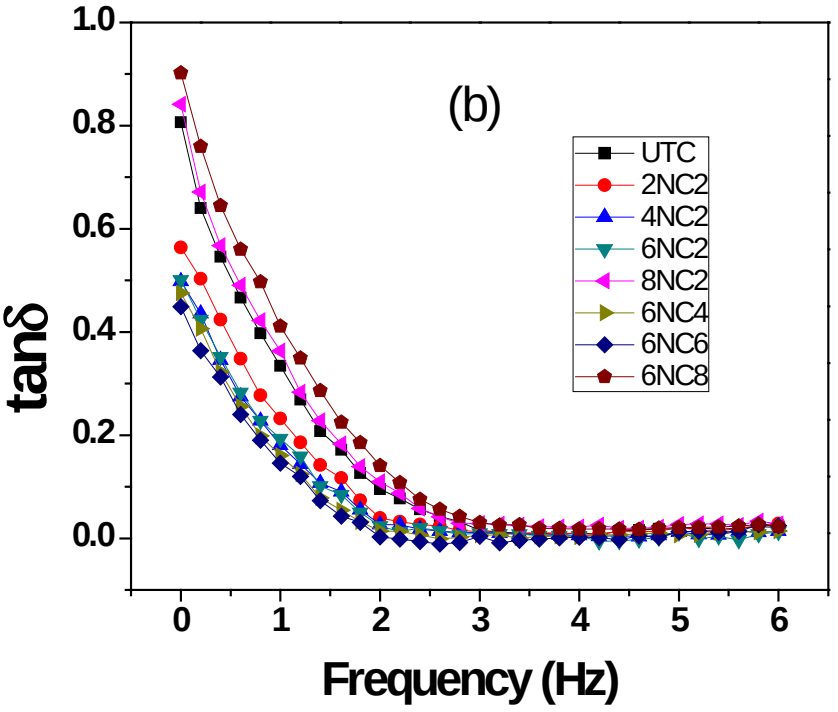

Fig. 7.12 (b): Variation of $\tan\delta$ with frequency for UTC and ALKC.

From Fig. 7.12, it can be clearly seen the effect of alkali treatment decreased the values of ε_r and $\tan\delta$. This may be due to the fact that after alkali treatment the moisture content of the fibers decreased due to the removal of hemicelluloses, lignin and waxy material of the fibers, which in turn reduced the contribution of the orientation polarization on the overall dielectric properties of the material [14]. Again from the XRD study, it is already confirmed that due to alkali treatment on the fiber, the degree of crystallinity increased. The increased crystallinity of the fiber is also another factor for the reduction of ε_r and $\tan\delta$ due to alkali treatment [26]. Lowest values of ε_r and $\tan\delta$ are found for the 6NC6 sample, which may be due to the optimum time and concentration of alkali treatment on the fiber. However the values ε_r and $\tan\delta$ of 6NC8, 8NC2 tend to increase even above the corresponding values of ε_r and $\tan\delta$ of UTC. The poor contact of the fibers with matrix might have led to the absorption of moisture hence resulted in increased dielectric loss and ε_r of the composite.

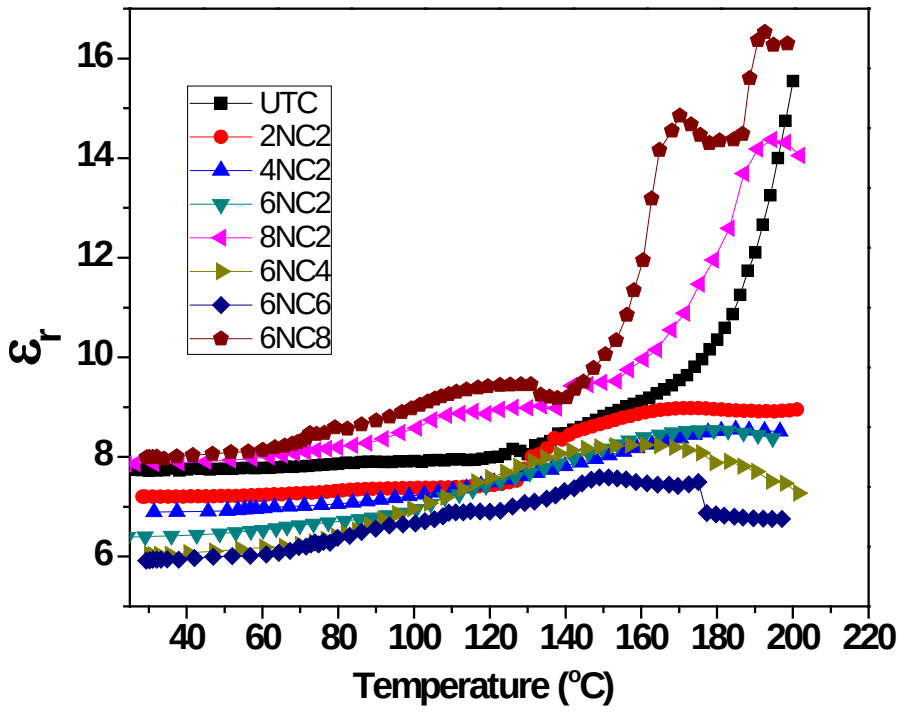

Fig. 7.13: Variation of ε_r with temperature for UTC and ALKC.

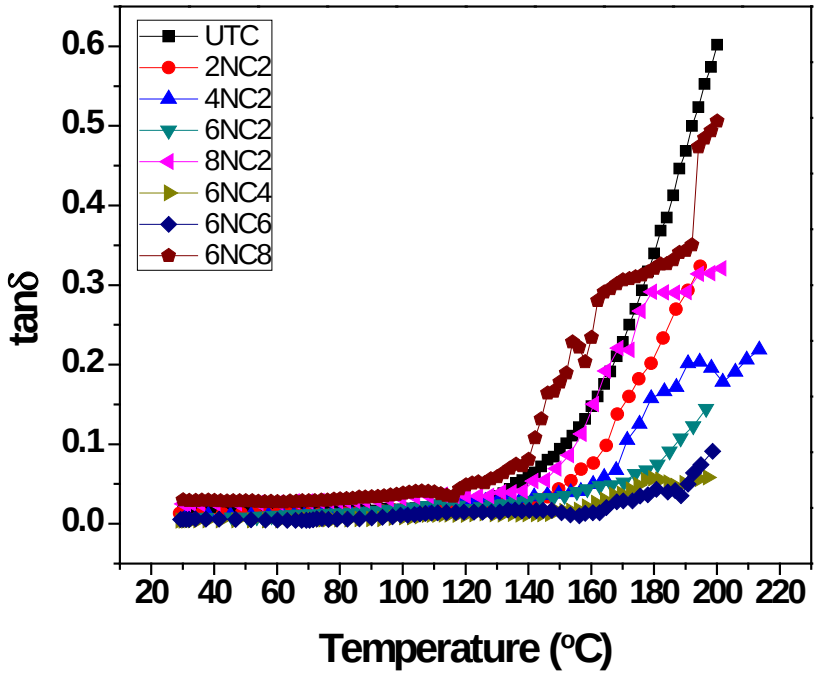

Fig. 7.14: Variation of $\tan\delta$ with temperature for UTC and ALKC.

The temperature dependence of ε_r of all the ALKC samples are shown in Fig 7.13. The values of dielectric constant continue to increase with the increase in temperature up to $\approx 130^0$ C. This is due to the enhance mobility of the polymer chain with the rise in temperature. The exothermic peak observed for all the composite samples around 130^0 C, is the α relaxation which is associated with the glass to rubbery transition of the material. The value of dielectric constant remains very low even at higher temperature in case of 6NC6 sample. The second exothermic peak associated with all the samples is attributed to the Maxwell wager-seller (MWS) effect. The immobile free charges in the composite get some movement with increase in temperature. These charges can migrate with the applied electric field and get trapped at the interface of the fiber and matrix because of the different permittivity and conductivity of both the constituents [27]. The temperature dependence of $\tan\delta$ for all the ALKC are shown in Fig. 7.14. The behaviour of $\tan\delta$ is found to be similar to the behaviour of ε_r i.e., with increase in temperature dielectric loss increases.

7.2.7 Electric Modulus Spectroscopy and Ac conductivity Studies

The present investigation aims to study the ac response of alkali treated sisal fiber reinforced epoxy composites. The composite systems can be regarded as a stochastic mixture of the two phases and are prepared by randomly dispersing sisal fibers in an epoxy resin. All the reported data were recorded by means of dielectric spectroscopy and analysed by using the electric modulus formalism, by varying the frequency of the applied field and temperature. Ac conductivity and electric modulus

study has been carried out for the composites having low as well as high values of dielectric constant and dielectric loss i.e, for 6NC4, 6NC6 and 6NC8 samples.

Figures 7.15 (a-c) shows the isothermal scans of the real and imaginary part of electric modulus for the 6NC4, 6NC6 and 6NC8 samples at temperatures varying from RT to 200°C. Like the $KMnO_4$ and microwave treatment, the existence of a clear 'step-like' transition from low to high values of (M'), at moderate frequencies, is also evident here in all the samples. It can be observed that the values of M' increased with increase in frequency at a constant temperature and finally reached a constant value. The evolution towards a constant value of M' at the high frequency region is due to the inability of the heavy dipoles to follow the applied field. At low temperature, straight line behaviour is observed. The existence of a step-like transition from low to high values of (M') is evident in all specimens, at temperature higher than 100°C. The appearance of this transition implies the presence of a relaxation process. It can be seen that the value of M' decreases with increase in temperature.

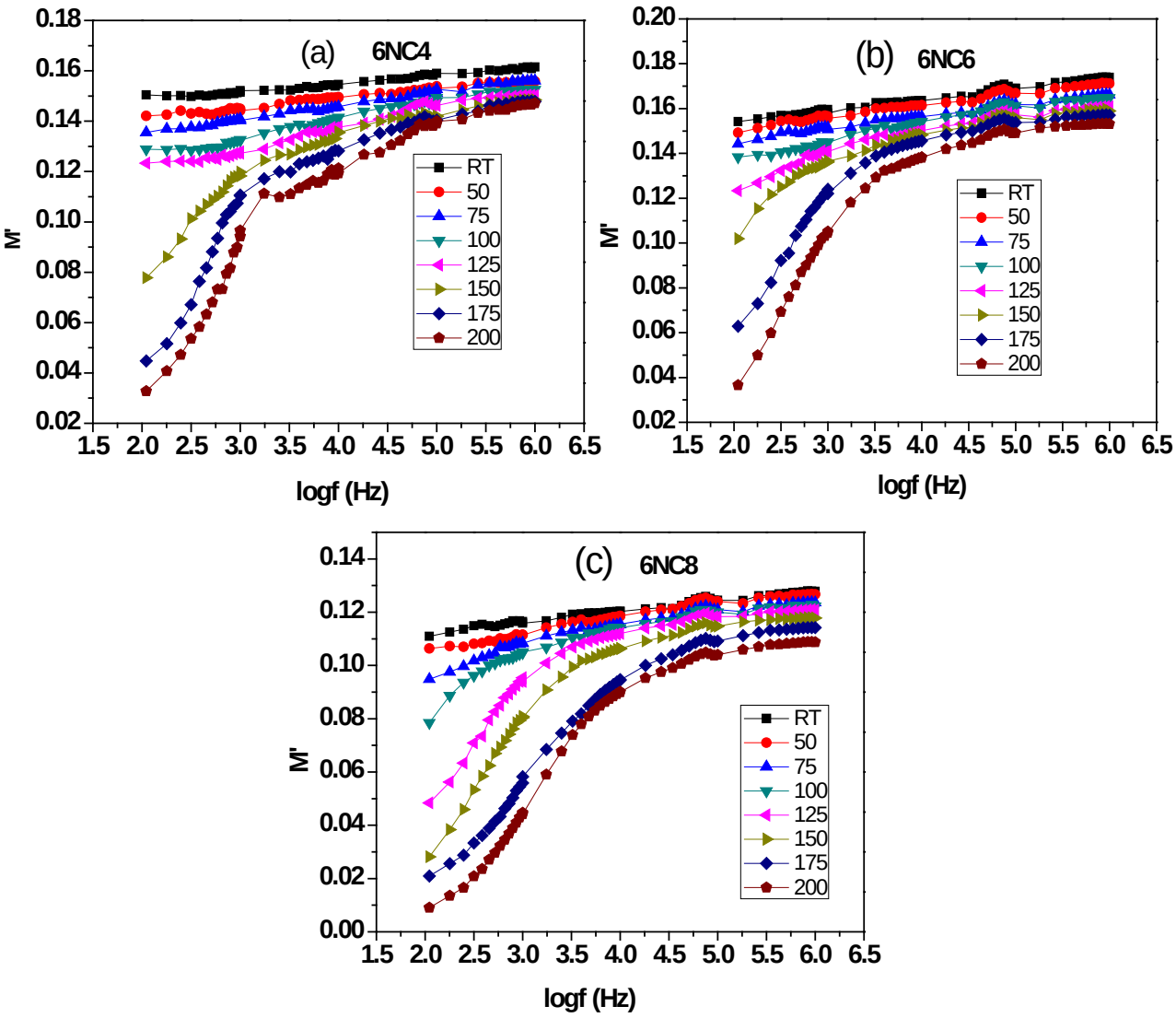

Fig.7.15: Variation of M' as a function of frequency at different temperatures for (a) 6NC4 (b) 6NC6 and (c) 6NC8.

The variation of the imaginary part of the electric modulus (M'') of 6NC4, 6NC6 and 6NC8 with frequency at different temperatures are shown in Figures 7.16a, 7.16b and 7.16c, respectively. It is observed that the maxima of M'' (M''_{max}) shifts towards higher frequency side with rise in temperature indicating the presence of temperature dependent relaxation process in the material.

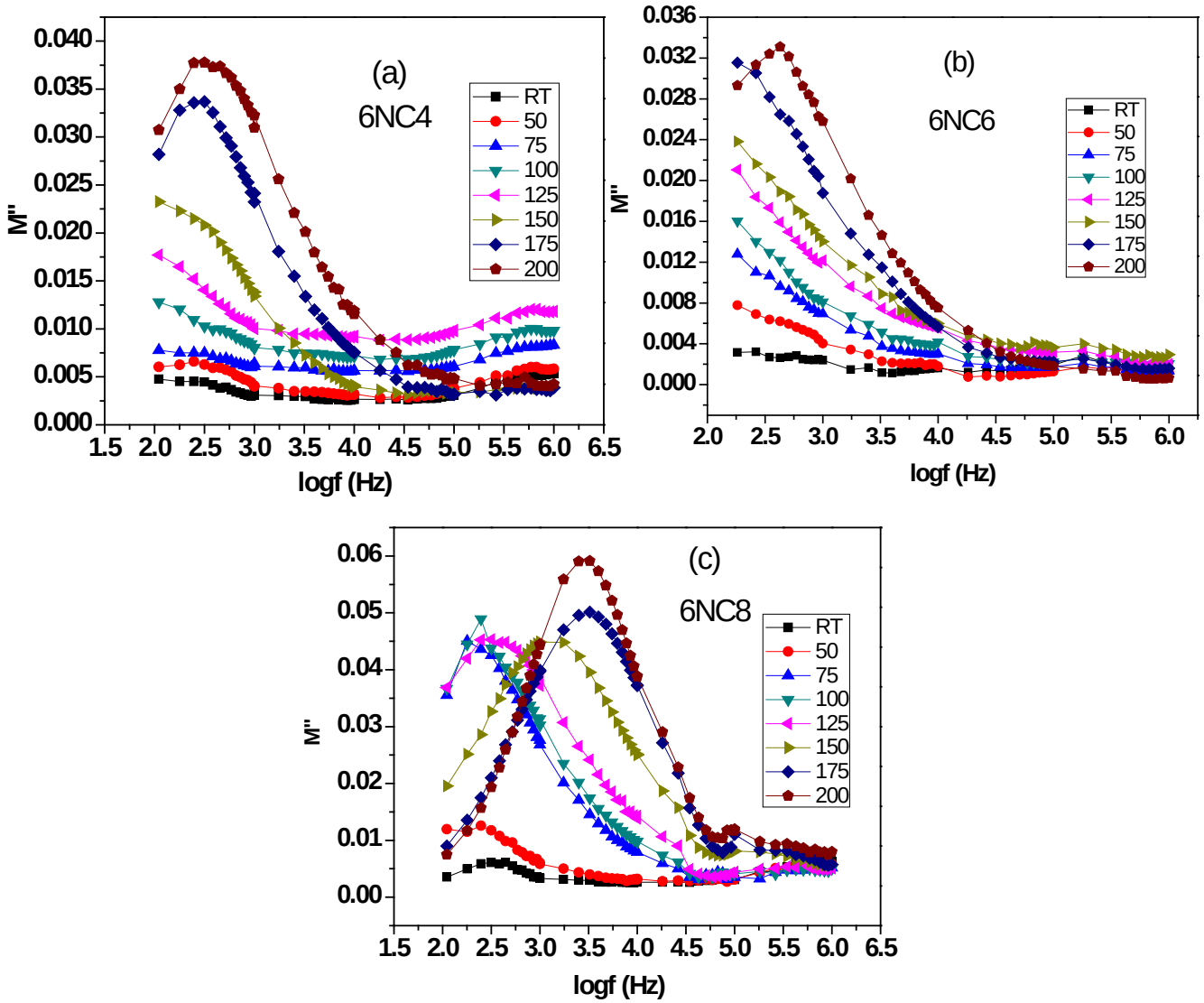

Fig. 7.16: Variation of *M″* as a function of frequency at different temperatures for (a) 6NC4 (b) 6NC6 and (c) 6NC8.

The shifting of relaxation peaks suggests that there is a spread of relaxation times. The nature of the figures at low frequency region at low temperature suggest that there are other relaxation peaks also present at frequency lower than 100 Hz. The values of *M″* increased significantly for 6NC8 sample. It can also be seen that the

relaxation peaks are shifted towards the high frequency region in 6NC8 sample, which may be due to the increase of conductivity in the sample.

The frequency dependence of ac conductivity (σ_{ac}) of 6NC4, 6NC6 and 6NC8 samples at different temperatures are shown in Fig. 7.17(a-c), respectively. The σ_{ac} was calculated using an empirical relation i.e. $\sigma_{ac}=\omega\varepsilon_r\varepsilon_0\tan\delta$, where ε_0 is the permittivity in free space, and ω is the angular frequency. It can be seen that at low frequency region the value of σ_{ac} seems to be constant and dispersion is exhibited at higher frequencies. This behaviour satisfies the universal power law $\sigma(\omega) = \sigma_0 + A\omega^n$, where σ_0 is the dc conductivity, A is the pre-exponential factor and n is the fractional exponent, whose value lies in between 0 and 1 [28]. It is observed that σ_{ac} increases with the increase in temperature and that confirms the negative temperature coefficient of resistance (NTCR) behaviour similar to the semiconductor. This behaviour also suggests that the electrical conduction in the sample is increasing at the higher temperature which may be due to the increase in the segmental mobility of the polymer molecules. It can also be seen that ac conductivity decreases with decrease in frequency and becomes independent of frequency after a certain limit. DC conductivity (σ_{dc}) has been calculated by extrapolating this towards the lower frequency side, which follows Arrhenius law given by $\sigma_{dc}= \sigma_0 \exp[-E_a/K_\beta T]$. Where E_a is the activation energy of conduction and T is the absolute temperature. The ac conductivity is found to be lowest for 6NC6 sample.

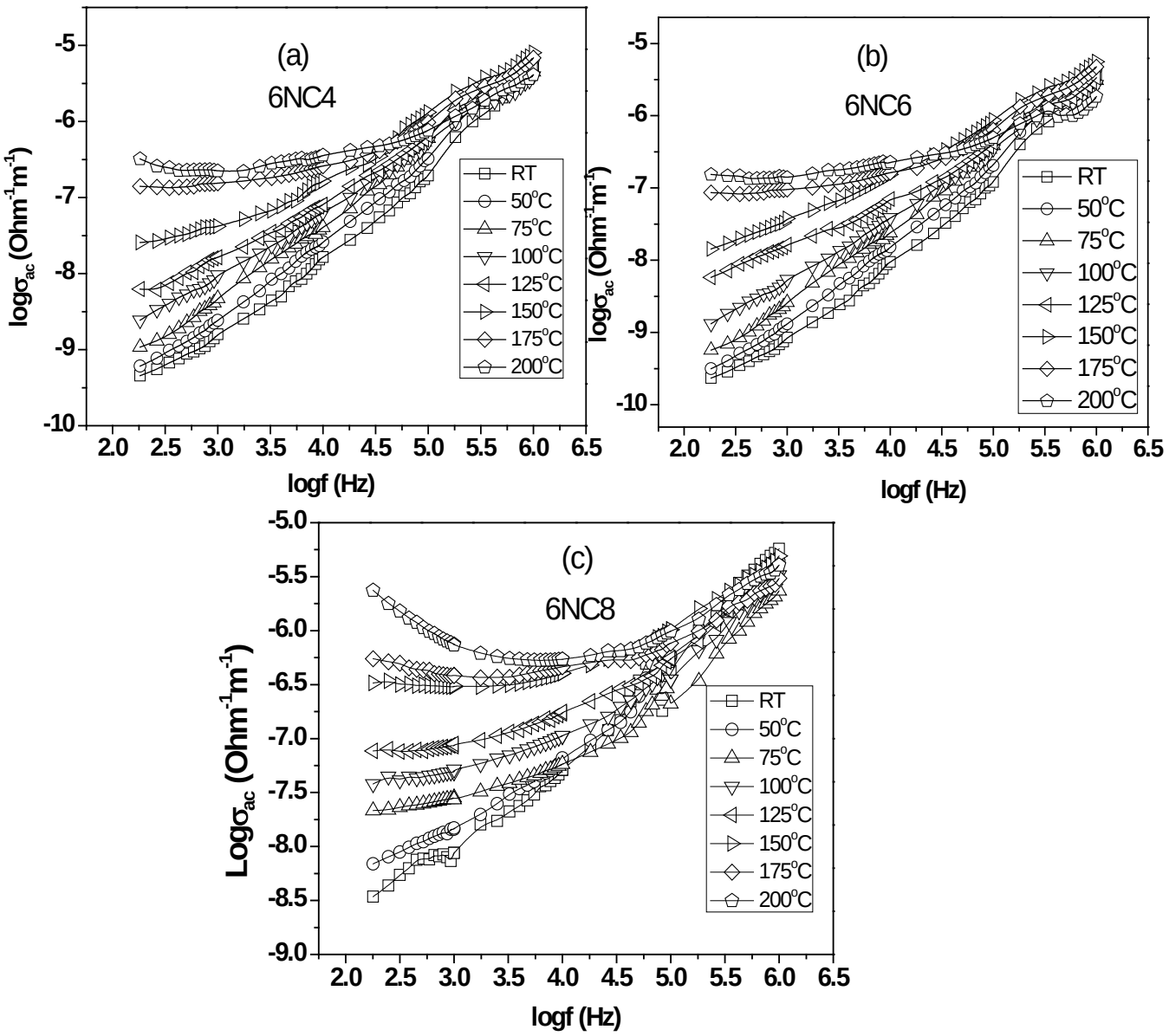

Fig. 7.17: Variation of ac conductivity as a function of frequency at different temperatures for (a) 6NC4 (b) 6NC6 and (c) 6NC8 samples.

Fig. 7.18(a-c) shows the variation of logarithmic plot of dc conductivity (log σ_{dc}) against 1000/T for the 6NC4, 6NC6 and 6NC8 samples. The nature of variation is almost linear over a wide temperature region. The values of E_a for 6NC4, 6NC6 and

6NC8 samples are found to be 0.50, 0.68 and 0.40 eV respectively. The higher activation energy for 6NC6 may be due to the increase in the height of the potential barrier between two orientational conformation states, which can be reached during the molecular motion.

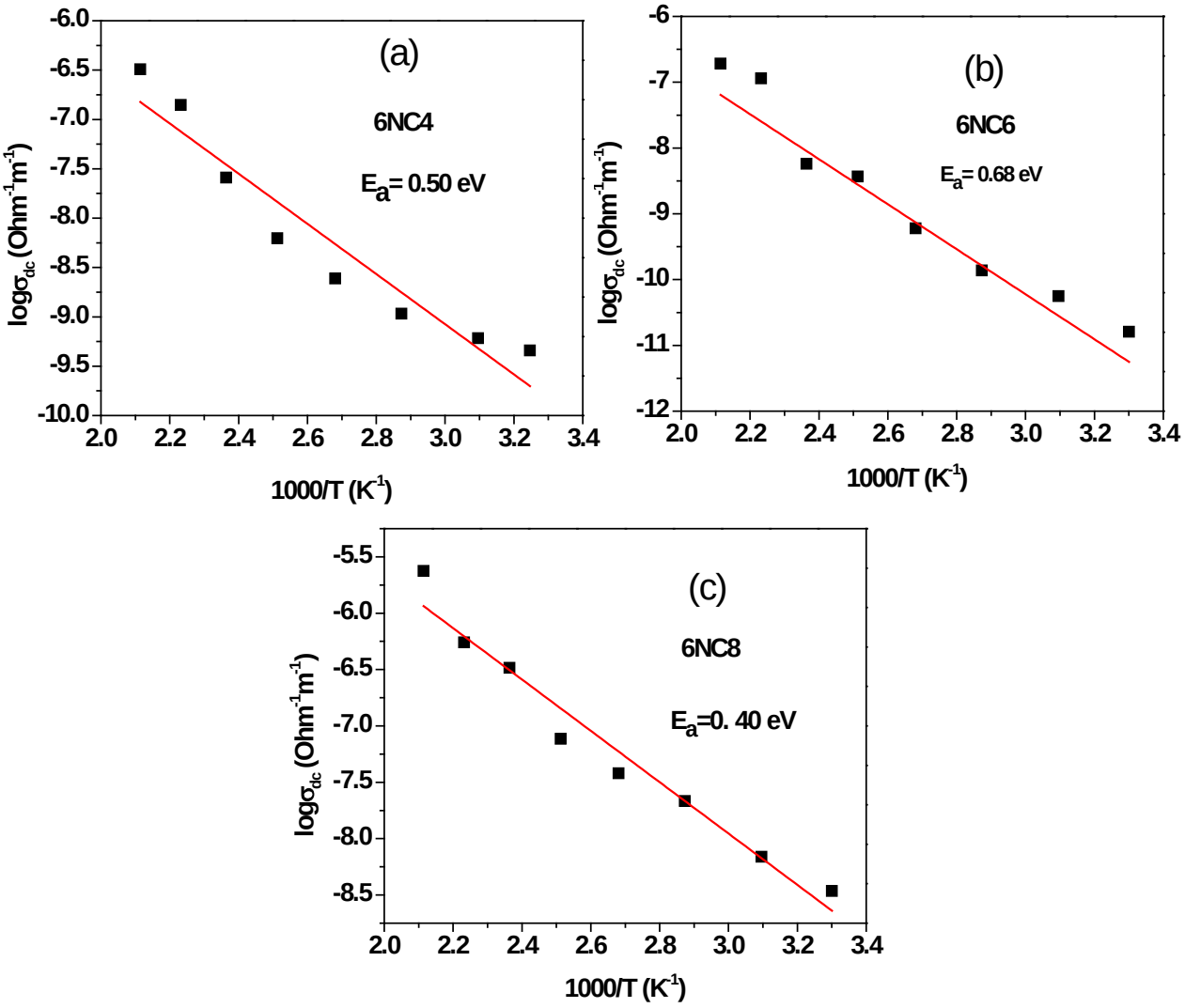

Fig.7. 18: Variation of dc conductivity against 1000/T for (a) 6NC4 (b) 6NC6 and (c) 6NC8 samples.

7.3. Conclusions

Alkali treatment significantly affected the microstructural and surface morphology of the sisal fiber. The reduction of disorderness, increase in the matter phase, and degree of crystallinity was observed for fiber soaked in 6% NaOH solution up to 6 hr. Reduction of the hemicellulose, lignin was confirmed from FTIR spectra. The surface roughness increased after the Alkali treatment. The enhanced surface roughness of fibers led to better wetting with the matrix resulting in maximum tensile and flexural strength for the 6NC6 composites followed by 6NC4 composite. But excessive soaking period at high concentration caused the degradation of the fibre and ultimately affecting the strength of the composite. The dielectric constant and loss reduced for 6NC6 because of the reduction of water uptake the composite and better adhesion between the fiber and matrix. The reduction of OH group, increased degree of crystallinity of fiber, rigid interface between the fiber and matrix are also governing factors for lower values of ε_r and tanδ in 6NC6 composite. The highest value of ε_r in case of 6NC8 may be due to the increase in the polar group due to the degradation of the fiber at a higher soaking time. The relaxation mechanism of the sisal fibers are studied with the help of electric modulus and ac conductivity. The activation energy of the 6NC6 is found to be ~ 0.68 eV which is higher than the other composites. The broadening of the relaxation peak in the imaginary part of modulus indicates the presence of relaxation process in the material.

References:

1. Bisanda ETN, The effect of alkali treatment on the adhesion characteristics of sisal fibres. Appl Compos Mater, 7, (2000) 331–339.
2. George J, Sreekala MS, Thomas S, A review on interface modification and characterization of natural fiber reinforced plastic composites. Polym Eng Sci, 41, (2001) 1471-1485.
3. Bachtiar D, Sapuan SM, Hamdan MM, The effect of alkaline treatment on tensile properties of sugar palm fibre reinforced epoxy composites. Mater Des, 29, (2008) 1285-1290.
4. Islam MS, Pickering KL, Foreman NJ, Influence of alkali treatment on the interfacial and physico-mechanical properties of industrial hemp fibre reinforced polylactic acid composites. Composites Part A, 41, (2010) 596-603.
5. Akil HM, Omar MF, Mazuki AAM, Safiee S, Ishak ZAM, Bakar AA, Kenaf fiber reinforced composites: a review. Mater Des, 32, (2011) 4107-4121.
6. Li X, Tabil LG, Panigrahi S, Chemical treatments of natural fiber for use in natural fiber-reinforced composites: a review. J Polym Environ, 15, (2007) 25-33.
7. Hashim MY, Roslan MN, Amin AM, Zaidi AMA, Ariffin S, Mercerization treatment parameter effect on natural fiber reinforced polymer matrix composite: a brief review. World Academy of Science, Engineering and Technology, 68, (2012) 1638-1644.
8. Kolpak FJ, Blackwell J, Mercerization of cellulose: 2. The morphology of mercerized cotton cellulose. Polymer, 19, (1978) 132–135.
9. Chand, N, Rohatgi PK, Adhesion of sisal fibre-polyester system. Polymer Communications, 27, (1986) 157–160.
10. Mishra S, Mohanty AK, Drzal LT, Misra M, Parija S, Nayak SK, Tripathy SS, Studies on mechanical performance of biofibre/glass reinforced polyester hybrid composites. Compos Sci Technol, 63, (2003) 1377-1385.

11. Sydenstricker THD, Mochnaz S, Amico SC, Pull-out and other evaluations in sisal-reinforced polyester biocomposites. Polymer Testing, 22, (2003) 375-380.
12. Yu T, Ren J, Li S, Yuan H, Li Y, Effect of fiber surface-treatments on the properties of poly(lactic acid)/ramie composites, Composites Part A, 41, (2010) 499-505.
13. Khan NMD. Small angle X-ray scattering study of sisal fiber using correlation function. Ph. D Thesis. (1991).
14. Goud G, Rao RN, The effect of alkali treatment on dielectric properties of roystonea regia/epoxy Composites. International J Polym Anal Charact, 16, (2011) 239–250.
15. Paul A, Joseph K, Thomas S, Effect of surface treatments on the electrical properties of low-density polyethylene composites reinforced with short sisal fibers. Compos Sci Technol, 57, (1997) 67–79.
16. Shinoj S, Visvanathan R, Panigrahi S, Towards industrial utilization of oil palm fibre: Physical and dielectric characterization of linear low density polyethylene composites and comparison with other fibre sources. Biosystems Engg, 106, (2010) 378-388.
17. Vonk CG, A general computer program for the processing of small angle X-ray scattering data. J Appl Cryst, 8, (1975) 340–341.
18. Kartky O, Miholic G, Small-angle X-ray investigations with absolute intensity measurements on regenerated, air-swollen cellulose. J Polym Sci C, 2, (1963) 449–476.
19. Ruland W, Small-angle scattering of two-phase systems: determination and significance of systematic deviations from porod's law. J Appl Cryst, 4, (1971) 70–73.
20. Vonk CG, A general computer program for the processing of small angle X-ray scattering data. J Appl Cryst, 8, (1975) 340–341.
21. Ouajai S, Shanks RA, Composition, structure and thermal degradation of hempcellulose after chemical treatments. Polym Degrad Stabil, 89, (2005) 327–35.

22. Saarkar PB, Mazmudar AK, Note on the Lignin and Hemicellulose of Jute. Text Res J, 12, (1955) 1016.
23. Esmeraldo MA, Barreto ACH, Freitas JEB, Fechine PBA, Sombra ASB, Corradini E, Dwarf-green coconut fibers: a versatile natural renewable raw bioresource.Treatment morphology and physicochemical properties. Bioresources, 5, (2010) 478–501.
24. Barreto ACH, Rosa DS, Fechine PBA, Mazzetto SE, Properties of sisal fibers treated by alkali solution and their application into cardanol-based biocomposites. Composites: Part A, 42, (2011) 492–500.
25. Mylsamy K, Rajendran I, Influence of alkali treatment and fibre length on mechanical properties of short Agave fibre reinforced epoxy composites. Material design B, 32, (2011) 4629–4640.
26. Jacob M, Varughese KT, Thomas S, Dielectric characteristics of sisal–oilpalm hybrid biofibre reinforced natural rubber biocomposites. J Mater Sci, 41, (2006) 5538–5547.
27. Perrier G, Bergert A, Polystyrene–glass bead composites: Maxwell–Wagner–Sillars relaxations and percolation. J Polym Sci B: Polym Phys, 35, (1997) 1349-1359.
28. Jonscher A K, The universal dielectric response. Nature, 267, (1977) 673–679.

Chapter 8

Major Conclusions and Future works

8.1 Conclusions

In search of potential applications of sisal fiber, environment friendly short sisal fiber reinforced epoxy composites have been fabricated by hand layup process. The compatibility of the hydrophilic sisal fiber with the hydrophobic epoxy matrix was enhanced by both chemical and physical treatment. The morphological, vibrational, physical and macromolecular structural parameters have been investigated for the sisal fiber, along with the mechanical and electrical properties of the surface modified sisal fiber reinforced epoxy composites. This work contributes to the research and development of improved sisal fiber properties, which manifests with improved mechanical and electrical properties of the sisal fiber reinforced epoxy composite in the following aspects:

- Short sisal fiber reinforced epoxy composites were made out of unmodified fiber with different volume percentage 5, 10, 15 and 20%.

- The reinforcement of 15 volume percentage of the fiber in epoxy was found to have better flexural, tensile strength along with low dielectric constant and loss out of other. Hence, 15% of volume of fiber was used for composite fabrication for the entire study.
- The fibers were modified by Dewaxing, $KMnO_4$, Microwave and NaOH treatment. Major conclusions drawn from these treatments are given in the following sub headings.

Dewaxing

- Small angle X-ray scattering showed the higher values of D, l_1, ϕ_1 for the Dewaxed sisal fiber in comparison to the untreated one.
- Degree of crystallinity and crystallite size were enhanced for Dewaxed fiber compared to the untreated fiber because of the partial removal of impurities and waxy material from the fiber by ethanol- benzene solution.
- This provides enhanced surface roughness to the fiber that leads to the better wetting of the fiber with the matrix which is confirmed from the SEM study.
- Dewaxed fiber reinforced composite was found to have better flexural and tensile strength than the untreated fiber reinforced epoxy composite.
- Relatively lower values of dielectric loss and dielectric constant was achieved for the Dewaxed fiber reinforced epoxy composite in comparison with its counterpart (i.e. untreated one).

$KMnO_4$ treatment:

- Change in the macromolecular parameters of $KMnO_4$ modified fibers were confirmed by SAXS data analysis.
- Disorderness and void content were found to be reduced for 05K2 fiber followed by 05K1.
- Better wetting of 05K2 fibers in the epoxy had been confirmed from the SEM micrograph.
- The higher mechanical strength, in terms of flexural and tensile strength for 05KC2 might be due to the better mechanical interlocking of the fiber with the matrix.
- The lowest value of ε_r and $\tan\delta$ for the above mentioned composite may be due to the reduction of OH group and rigid interface between the fiber and matrix.
- The higher values of ε_r and $\tan\delta$ in case of 1KC3 may be due to the increase in the polar group, that may be due to the disintegration of the cellulose because of the excessive oxidizing effect of $KMnO_4$ at a higher concentration with higher soaking time.
- The temperature dependent electric modulus study confirms the presence of relaxation process in the material.
- The activation energy (E_a) of 05KC2 was found to be higher than 05KC1 and 05KC3, which may be due to the increased height of the potential barrier between two orientation of the different states.

Microwave treatment

- Microwave irradiation affected the macromolecular parameters of the fiber.
- The 320W4 fiber was found to have lower disorderness, void content with increased degree of crystallinity, crystallite size and density showing the improvement in the physical parameters of the fiber.
- Adequate surface roughness was achieved due to the bombardment of high energy electromagnetic radiation at optimized microwave power and treating time.
- The enhanced surface roughness of fibers led to better wetting with the matrix resulting in maximum tensile and flexural strength of the 320WC4 composites followed by 320WC2. But excessive radiation led to the degradation of the fiber and ultimately reduced the strength of the composite.
- The ε_r and $\tan\delta$ value of 320WC4 was significantly reduced due to the appropriate treatment time and power. The use of microwave also effectively reduced the absorbed water content and O-H group due to heat generated by water molecule by the synchronizing oscillation with the frequency of the microwave.
- The value of ac conductivity was found to be lower for the 320WC4 sample.
- The shifting of relaxation peaks in the temperature dependent modulus plot confirmed the presence of temperature dependent relaxation process in the material.

Alkali treatment

- The reduction of disorderness, increase in the matter phase and degree of crystallinty were observed for the sisal fiber soaked in 6% NaOH solution up to 6 hr.
- Alkali treatment significantly affected the surface morphology of the sisal fiber. The surface roughness of the fiber is enhanced after the alkali treatment.
- Reduction of the hemicellulose, lignin groups in the fiber was confirmed by FTIR spectra after alkali treatment at optimized condition.
- The enhanced surface roughness of fibers manifests for better wetting with the matrix resulting in higher tensile and flexural strength of the 6NC6 composites followed by 6NC4 composite.
- However, excessive soaking period at higher concentration led to the degradation of the fibre and that ultimately affecting the strength of the composite.
- The values of dielectric constant and loss reduced because of the reduction of water uptake capacity of the composite and better adhesion between the fiber and matrix.
- The values of ac conductivity and dielectric loss was found to be lower for 6NC6 sample.

8.2 Future Works

The work presented in this thesis investigates the macromolecular and physical parameters of both treated and untreated sisal fiber. It tries to exploit the fiber for its potential applications in the composite industry by enhancing both mechanical strength and electrical properties of the composite. Further studies on different aspects of surface modification of the sisal fiber, characterization techniques are suggested in the following paragraphs for academic/fundamental interest. This may also open up many windows to predict their potential applications.

- In order to extract more detail information about the structure of the fiber Transmission electron microscope (TEM) measurement must be carried out which is complement to SAXS analysis.
- The electrical properties of the fiber should be measured to manifest direct effect of modification on the fiber properties.
- Sisal fiber is well known for its good fire resistant and sound absorbing capacity. Fire resistant and acoustic impedance studies of this fiber may be helpful for the potential application of it in these fields.
- As synthetic polymers are not completely biodegradable, therefore study must be carried out to develop environment friendly green composites by taking biopolymers as a matrix in place of synthetic counterpart.
- Low frequency electrical study of the fiber as well as composite should be carried out for better understanding of the composite and fiber response to the electric field. Moreover, the relaxation mechanism can be well studied at low frequency.

CURRICULUM VITAE

Name: **Annapurna Patra**
Mothers Name: Mrs. Hiramani Patra
Fathers Name: Late Nilamani Patra
Date of Birth: 15th June, 1982
Gender: Female
Nationality: Indian
Marital Status: Unmarried

Permanent Address:

E-127, Sector-7
Dist – Sundarghara, State - Odisha
INDIA, PIN – 769003
E-mail ID: annapurna.patra@gmail.com

Present Position:

Research Officer (Physics)
Engineering Seismology Division
Central Water and Power Research Station
Khadakwasla, Pune-411024
Maharashtra, India

Educational Qualifications:

• ***Doctor of Philosophy (Ph.D.) (Physics) – (Cont.)***
National Institute of Technology, Rourkela, Odisha, India
• ***Master of Science (M.Sc.) (Physics) – 2007***
First Division, 8.3 CGPA
National Institute of Technology, Rourkela, Odisha, India
• ***Bachelor of Science (B.Sc.) (Physics (Hons)) – 2005***
First Division, 72.25 %
Sampalpur University(SG Women's college,Sec-2. Odisha, India)
• ***Senior Secondary (10+2) (Science) – 1999***
First Division, 62.6 %
C.H.S.E., Odisha (SG Women's college, Sec-2, Odisha, India)
• ***Matriculation (10th) (General) – 1997***
First Division, 83.6 %
B.S.E., Odisha (Ispat High School, Sec-7, Odisha, India)

Research Experiences:

M.Sc. Project Work (July 2006 – July 2007)
National Institute of Technology, Rourkela, Odisha, India
Senior Research Fellow (July 2010 – September 2011)
National Institute of Technology, Rourkela, Odisha, India

Academic Achievements:

Fair & lovely foundation fellowship for women studies (2010)
Jawaharlal Nehru fellowship for Doctoral studies (2011-13)
CSIR SRF fellowship (2012-14)

Reviewer of International Journals:

Journal of applied polymer science. Willey Interscience.
Journal of petroleum and gases. Elsevier.

Symposium/Workshop attended:

1. Industrial summer training, Rourkela Steel Plant, Rourkela, Odisha, India, May 2006-July 2006.
2. Department of Pure & Applied Physics, Guru Ghasidas Central University, Koni, Bilaspur- 495009 Chhattisgarh (INDIA) Jan, 2008.
3. SAXS, A noble scientific approach to nanotechnology. 26-30 May, 2008, Department of Physics, NIT Rourkela. Odisha, India 769008,
4. Defense Metallurgical Research Laboratory. Kanchanbagh, Hyderabad, 500 058/500 258, 2008
5. Contribution of small angle X-ray scattering in nanoscience and nanotechnology. 22-26 May, 2010, Department of Physics, NIT Rourkela. Odisha, India, 769008.

List of Publications

A: In International Journals

1. ***Annapurna Patra****, D.K. Bisoyi.* Dielectric and impendance spectroscopy studies on sisal fiber reinforeced Polyester composite *J. Mater. Sci. 42, (2010), 5742.*
2. ***Annapurna Patra****, D.K. Bisoyi.* Investigation of the electrical and mechanical properties of shortsisal fiber-reinforced epoxy composite in correlation with structural parameters of the reinforced fiber. *J. Mater. Sci. 46, (2011), 7206.*
3. ***Annapurna Patra****, D.K. Bisoyi. P.K Manda, A.K. Singh,* Electrical and mechanical properties of the potassium permanganate treated short sisal fiber reinforced epoxy composite in correlation to the macromolecular structure of the reinforced fiber. *J. Appl. Polym. Sci. (201), DOI: 10.1002/app.38195*
4. ***Annapurna Patra****, D.K. Bisoyi*. *P.K Manda, A.K. Singh* Effect of Microwave Radiation on the Macromolecular, Morphological and Crystallographic Structures Of Sisal Fiber. Applied Physics A. (2012) *DOI 10.1007/s00339-012-7489-y*

B: Papers communicated

1. ***Annapurna Patra****, D.K. Bisoyi.* Impendance and dielctric spectroscopy study of microwave irradiated sisal fiber composite. (Journal of applied polymer science).
2. ***Annapurna Patra***, D.K. Bisoyi. Electrical and mechanical properties of the mercerized sisal fiber epoxy composite in correlation to the macromolecular parameters of the fiber. (Composite Part A).
3. ***Annapurna Patra***, D.K. Bisoyi. Effect of fiber content on the electrical and mechanical properties of short sisal fiber reinforced epoxy composite. (Express Polymer letter).

Paper presented at National/International Conferences:

1. *D.K. Bisoyi,* ***Annapurna Patra*****,** Generalised and realistic approach to macromoleculer structure of polymeric materials by SAS analysis. Presented at RRCAT, Dec 24, 2009, Bardhaman University, west Bengal, India.
2. ***Annapurna Patra,*** *D.K. Bisoyi*, Effect of surface treatment on the structural and electrical properties of sisal. Presented at international conference on recent trends in materials and characterization (RETMAC), February14–15, 2010, National Institute of Technology Karnataka, Surathkal, India.
3. ***Annapurna Patra,*** *D.K. Bisoyi*, Effect of surface treatment on structural and dielectric properties of sisal fiber reinforced epoxy composite. Presented at ISRS, December 20–22, 2010, IIT Madras, India.
4. ***Annapurna Patra,*** *D.K. Bisoyi*, Effect of microwave irradiation on the Structural and Electrical Properties of Sisal Fiber. Presented at ICMF, February 23-25, 2011, The Government Engineering College, Thrissur, India.